MicroRNA Mediated Biological Effects in Response to Bariatric Surgery

Qianxin Wu

Computational and Systems Medicine

Division of Surgery and Cancer

Faculty of Medicine

Imperial College London

Thesis submitted for degree of Doctor of Philosophy of Imperial College London

2014

Declaration of Originality

I declare that all research presented in this thesis is my own.

All other work is referenced.

Copyright Declaration

Abstract

Bariatric surgery offers sustained dramatic weight loss and remission of diabetes, yet the mechanisms of these health benefits are not clear. In the present study, I profiled circulating and colorectal microRNAome in response to bariatric surgery (Roux-en-Y gastric bypass). Indeed, the response of circulating and colorectal microRNA profiles to RYGB were striking and selective. Fourteen circulating microRNA and thirteen colorectal microRNA exhibited significantly alteration post RYGB. Interestingly, circulating miR-122 decreased dramatically (56 fold) post RYGB surgery. The expression of hepatic miR-122 and its metabolic targets were examined both in *in vivo R*YGB surgical model and in an i*n vitro* mechanistic model. Manipulation of microRNA-122 cold induce changes of key enzymes involved in energy metabolism, glucose transport, glycolysis, TCA cycle, pentose phosphate shunt, fatty acid oxidation and gluconeogenesis, suggesting an overall increased energy expenditure status after RYGB. Furthermore, potential mechanisms involved in the control of hepatic miR-122 were investigated, with focus on metabolites (glucose, and fatty acids), hormones (glucocorticoid) and transcription factors (PPARs). Finally, by correlating the circulating microRNAome and metabolome data, we were able to generate a comprehensive landscape of the crosstalk between microRNAs and metabolic pathways. Follow-up studies will allow a detailed understanding of microRNAs responsible for regulating specific metabolic pathways, and conversely identifying metabolites capable of regulating the expression and activity of specific microRNAs.

吾生也有涯，而知也无涯

——庄子（公元前 300 年）

Life is short, while knowledge is boundless and infinite.

—— Zhuang Zhou (300 BC)

Acknowledgements

First, I would like to thank my mentor, Professor Nigel John Gooderham, without his help, encouragement and guidance, I would never begin this wonderful PhD journey, not even mentioning to pursuit my dream of being a scientist. I would also like to acknowledge Professor Elaine Holmes, for her generous help and advice. In particular, I want to thank Dr Jia Li, who is a great teacher, a brilliant scientists and above all, a close friend.

I also want to acknowledge the help from two amazing surgeons, Mr. Hutan Ashrafian and Mr. Florain Seyfried.

During the PhD, I have received countless help, suggestion, encouragement and most importantly, companion from all the previous and current lab members: Dr Costas Koufaris, Dr Reshat Reshat, Dr Corrinne Segal, Dr Nurul Huda Abd Karim, Kuanwei Chen, Dr. Rhiannon David, Abdullah Alkandari, Leanne Harling, Mariana Flores Torres, Saroor Patel, Michael Osborne and Mailk Shahwar. I will always remember Corrinne, who taught me, for the first time, all the experimental techniques in the lab with great patience; Rhiannon, who always gave me good advices and great encouragement; Mariana, who helped me enormously for the next generation sequencing and brought the amazing Mexican spicy food; Leanne, who gave me tremendous help during the most difficult time of my PhD. Finally, Abdullah, a great neighbor who carried endless interesting talks with me, which turned out to be perfect English training sessions in the end.

Last but not least, I am grateful for my parents and my grandma, who always stands on my side and be supportive for all the willful decisions I made. This thesis is dedicated to them.

Table of Contents

List of Figures

List of Tables

List of Abbreviations

11-DHC	11-dehydrocorticosterone
11β-HSD	11β-hydroxysteroid dehydrogenase
3HB	D-3-hydroxybutyrate
5-HT	5-hydroxytryptamine
ACAA2	acetyl-Coenzyme A acyltransferase 2
AcAc	acetone acetate
ACACB	acetyl-Coenzyme A carboxylase 2
ACC	actyl-CoA carboxylase
acetyl CoA	acetyl CoA
ACLY	ATP citrate lyase
ACO	acyl-CoA oxidise
Ago	Argonaute
AgRP/NPY	Agouti-related peptide/neuropeptide Y
ALDOA	aldolase A
AMP	adenosine monophosphate
AMPK	AMP-activated protein kinase
AMPK	AMP-activated protein kinase
ATP	adenosine triphosphate
BCA	bicinchoninic assay
BMI	body mass index
BPD	bilio-pancreatic diversion
C/EBP	CCAAT/enhancer binding protein
CA	Cinnamyl Anthranilate
CNS	central neural system
CPT1	carnitine palmitoyl transferase 1
CS	citrate synthase
Ct	Cycle of threshold
CV	coefficient of variance
CYP	cytochrome P450
db/db	leptin receptor-deficient
DEHA	Dehydroepiandrosterone
DEHP	Diethylhexylphthalate
DIO	diet induced obesity
DJE	duodenal-jejunal exclusion
DMEM	Dulbecco's Modified Eagle's medium
DMSO	dimethylsulphoxide
DNMT	DNA methyltransferases
DTT	Dithiothreitol
EDA	ectodysplasin-A
EDTA	ethylenediaminetetraacetic acid
EGA	enterogastro anastomosis
FA	fatty acid
FABP	fatty acid binding protein

FASN	Fatty acid synthase
FATP	fatty acid binding protein
FBS	fetal bovine serum
FFA	free fatty acid
FFL	feedforward loop
FISH	fluorescence *in situ* hybridization
Foxa	forkhead box protein A
FXR	farnesoid X receptor
G6PC	glucose-6-phosphatase
G6PD	Glucose-6-phosphate dehydrogenase
GABA	γ-aminobutyric acid
GC	glucocorticoid
GI tract	gastrointestinal tract
GK	Glucokinase
GK	Goto-Kakizaki
GLB	gastric lap-band model
Glc6Pase	Glucose 6-phosphatase
GLP-1	glucagon-like peptide-1
GLUT	glucose transporter
GPR	G-protein-coupled receptor
GR	glucocorticoid receptors
GRE	glucocorticoid response elements
GyK	glycerol kinase
GYS	Glycogen synthase
HbA1c	glycosylated hemoglobin
HDL	high density lipoproteins
HK2	hexokinase 2
HNF-4α	hepatocyte nuclear factor 4α
HOMA-IR	homeostatic model assessment of insulin resistance
HRP	horseradish peroxidise
IDH1	isocitrate dehydrogenase 1
IT	ileal transposition
KO	knock out
LAGB	laparoscopic adjustable gastric banding
LDHA	lactate dehydrogenase A
LNA	locked nucleic acid
MEM	minimum essential medium
microRNA	microRNA
MRE	microRNA responsive elements
MTT	Mixed Meal Test
NADPH	Nicotinamide adenine dinucleotide phosphate
NAFLD	non-alcoholic fatty liver disease

NEAA	non- essential amino acids
NOD	non-obese diabetic
ob/ob	leptin deficient obese
OGTT	Oral Glucose Tolerance Test
PBMC	peripheral blood mononuclear cell
PBS	phosphate-buffered saline
PBS-T	phosphate buffered saline - tween-20
PCA	principal component analysis
PD	Parkinson's disease
PDK	phosphoinositide-dependent protein kinase
PDK4	pyruvate dehydrogenase kinase, isozyme 4
PEPCK	Phosphoenolpyruvate carboxykinase
PGC-1α	peroxisome proliferator-activated receptor coactivator-1 α
piRNA	piwi interacting RNA
POMC	Pro-opiomelanocortin
PPAR	peroxisome proliferator-activated receptor
PPRE	peroxisome proliferator hormone response elements
PYY	peptide Y
qRT-PCR	quantitative real-time PCR
RIN	RNA integrity number
RISC	RNA induced-silencing complex
RLC	RISC loading complex
ROS	reactive oxygen species
RXR	retinoid X receptor
RYGB	Roux-en-Y-Gastric bypass
SCFA	short chain fatty acid
SCOT	succinyl CoA-oxoacid transferase
SD	Sprague Dawley
SDS-PAGE	sodium dodecyl sulfate polyacrylamide gel electrophoresis
SIRT1	Sirtuin 1
snoRNAs	Small nucleolar RNAs
SOS	Swedish Obese Subjects Study
SREBP	sterol regulatory element binding proteins
T2DM	type 2 diabetes mellitus
TCA	tricarboxylic acid cycle
TFs	transcriptional factors
TGR-5	G protein-coupled bile acid receptor 1
TLDA	Taqman low density assay cards
TRBP	Tar RNA binding protein
UCO2	uncoupling protein 2
UTR	untranslated region
VGB	vertical banded gastroplasty
XPO-5	Exportin-5

1. Introduction

1.1 Obesity and bariatric surgery

1.1.1 Obesity epidemiology

Obesity is an increasingly important public health issue worldwide. Overweight and obesity are defined as abnormal or excessive fat accumulation that may impair health. Body mass index (BMI), which is an index of weight-to-height that is commonly used to classify overweight and obesity in adults, is defined as a person's weight in kilograms divided by the square of their height in meters (kg/m^2). World Health Organisation (WHO) defines that a BMI greater than or equal to 25 is overweight, whereas a BMI greater than or equal to 30 is obesity. According to WHO statistics, the prevalence of obesity has nearly doubled since 1980. In 2008, more than 1.4 billion adults were overweight. Of these over 200 million men and nearly 300 million women were obese (WHO 2008). In the UK, according to the NHS, nearly a quarter of adults in England were obese in 2008. Just under a third of women (32%) were overweight and 42% of men were overweight (Statistics on obesity, physical activity and diet: England, 2010). It was estimated that by 2040, 60% of men and 50% of women could be clinically obese (Preston ^ *et al*. 2014). Obesity and its co-morbidities, such as type 2 diabetes mellitus (T2DM), sleep apnea, hypertension and hyperlipidaemia, are responsible for a huge health and economic burden worldwide (Yach *et al*. 2006). Multiple factors have been shown to contribute to obesity, such as poor diet, sedentary lifestyle, environmental factors, genetics and disturbed energy balance (Aronne 2002). Treatments for obesity include dietary therapy, exercise and behavioral interventions, weight loss medications and bariatric surgery. Notably, studies have shown that bariatric surgery can provide long term sustained weight loss and place type 2 diabetes in remission within days (Buchwald, Avidor, Braunwald & Jensen 2004a).

1.1.2 Bariatric surgery

1.1.2.1 Bariatric surgery types and procedure

Generally speaking, surgical treatment for morbid obesity falls into three categories: restrictive surgery, malabsorptive surgery and combined restrictive/malabsorptive surgery. The restrictive surgery includes vertical banded gastroplasty (VGB) and laparoscopic adjustable gastric banding (LAGB), which simply restrict the intake of food *via* decreasing the volume of the stomach. The malabsorptive surgery is able to reduce the nutrient absorption *via* altered bile flow. One example of a malabsorptive procedure is bilio-pancreatic diversion (BPD), which diverts bile into the terminal segment of the ileum so that bile and food are only mixed in the final segment of the small bowel. Combined restrictive and malabsorptive gastric bypass (Roux-en-Y-Gastric bypass, RYGB) surgery, involving both the restriction of the stomach and the bypass of the small bowel, is considered the most effective and the gold standard of bariatric surgery techniques. It can induce more rapid and substantial weight loss than the restrictive surgery. It is also the most commonly performed bariatric surgery accounting for 40% of the over 344,000 metabolic operations worldwide in 2008 (Buchwald & Oien 2009). RYGB can lead to a 68%-83% rapid weight loss during the first 12 months to 2 years (Buchwald, Avidor, Braunwald & Jensen 2004a). Furthermore, it is believed that RYGB not only makes people “lighter”, but also makes them “healthier”. The majority of patients with diabetes, hyperlipidemia, hypertension and obstructive sleep apnea that underwent bariatric surgery experienced complete resolution or significant improvement of their health status (Buchwald, Avidor, Braunwald & Jensen 2004a).

During the RYGB procedure, a surgical stapler is used to create a small vertical gastric pouch (Figure 1.1). This 30-50mL small pouch is completely separated from the remnant stomach. The small pouch is anatomised to the jejunum (upper alimentary limb), whereas

the excluded biliary pancreatic limb is anastomosed to the lower alimentary (Roux) limb. After RYGB surgery, the food bypasses about 95% of stomach tissue, the entire duodenum and part of the jejunum. Hence, foods are mainly mixed with bile in the distal jejunum (alimentary limb) and absorption is facilitated through the remaining portion of the small bowel.

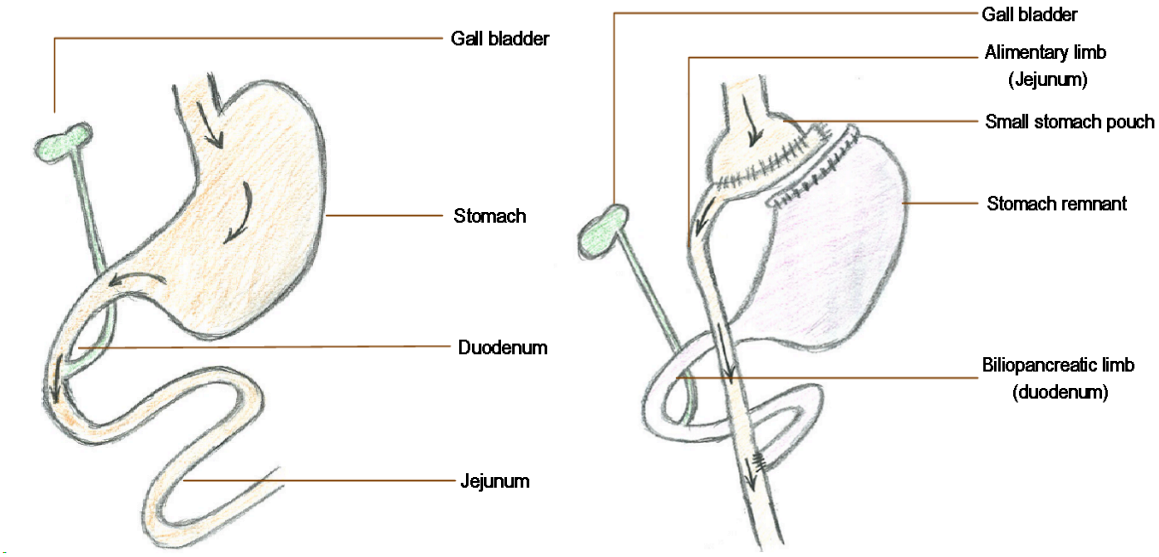

Figure 1-1 The principle of Roux-en-Y-Gastric bypass surgery

(left, normal anatomical gastrointestinal system; right, RYGB surgery)

1.1.2.2 Outcomes of bariatric surgery

Sustained weight loss

In a meta-analysis of the effectiveness of surgical treatment of obesity (Maggard *et al*. 2005), the author systematically assessed 147 studies, 89 of which contributed to the weight loss analysis. In 32 studies comparing RYGB procedures with randomized control, and involving 2,937 patients, average weight loss outcomes for RYGB averaged 43.46kg at 12 months. In 36 months after surgery, 21 studies and 1281 pooled patients showed an average 41.46kg weight loss. Another meta-analysis extracted 22,094 patients' weight loss

information from 136 studies. Similarly, they found 43.48kg absolute weight loss, which accounts for 34.93% of initial weight (Maggard *et al*. 2005). The Swedish Obese Subjects (SOS) study post-operatively follows bariatric surgery patients and matched medically treated controls (Sjostrom *et al*. 2004). At 8 years post-operative, the average weight loss was 20kg among 251 surgically treated patients, whereas the average weight did not change in the medically treated patient cohort. Clearly, effective weight loss was achieved in morbidly obese patients undergoing bariatric surgery and unlike behavior intervention and exercise in the medically treat cohort, bariatric surgery induced weight loss is sustainable in the long term.

Resolution of diabetes

Besides the sustainable long term weight loss, it has been consistently reported that bariatric surgery can induce long-term remission of type 2 diabetes mellitus (T2DM). An analysis of 136 studies that included a total of 22,094 patients who underwent bariatric surgery showed that 84% of bariatric surgery patients showed resolution of T2DM (Maggard *et al*. 2005). The SOS project showed that bariatric surgery patients have a lower incidence of developing diabetes and higher diabetes recovery rate at both 2 years (77%) and 10 years (73%) (Sjostrom *et al*. 2004). Furthermore, two studies, which included patients with T2DM or impaired glucose tolerance showed normalised glycosylated hemoglobin (HbA1c) levels in 89% and 82% of patients after RYGB without any anti-diabetic medication (Pories *et al*. 1995; Schauer *et al*. 2004). Additionally, in a pilot study that examined the effects of gastric bypass surgery in T2DM patients with BMI>35 and T2DM patients with BMI<35, the four year follow-up results show that 90% of patients with BMI<35 and 98% of patients with BMI>35 exhibited normalised glycaemia (Rubino *et al*. 2010).

1.2 Mechanisms of bariatric surgery mediated effects

Different types of bariatric surgery may have different weight loss and anti-diabetic effect. Restrictive procedures control diabetes exclusively through weight-loss induced improvements in peripheral insulin. On the contrary, malabsorptive procedures such as RYGB can ameliorate glycemic control in T2DM within days or weeks after surgery, long before the drastic weight loss (Kashyap *et al*. 2010). Evidence suggests that malabsorptive bariatric surgery related diabetes resolution is more than just decreased body weight and changed food intake. Multiple hypotheses have been proposed to explain the early effect of RYGB surgery on diabetes. Over the past decade, there has been an exponential increase in the analysis of the altered metabolic mechanisms after RYGB surgery, which mainly falls into the following areas (Figure 1.2): 1) altered intestinal and hepatic glucose metabolism, 2) increased gut hormone secretion, 3) shifted gut microbiota, 4) remodelled muscle promoter methylation, 5) changed brain effects, 6) changed bile flow and bile acids composition. Here, I will focus on previous studies in both human and animal models and discuss the above-mentioned mechanisms individually.

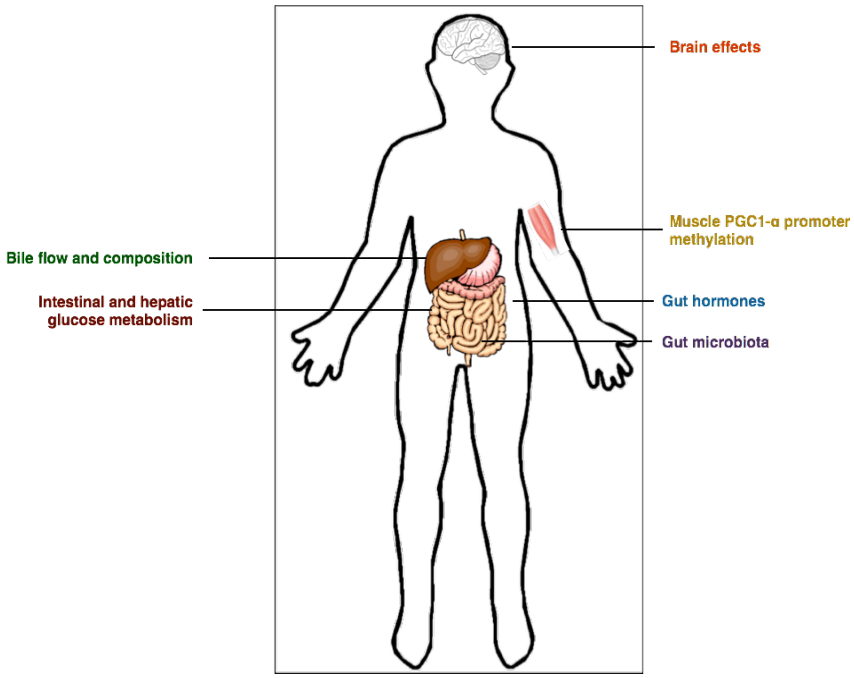

Figure 1-2 Schematic representation of the potential mechanisms that underlie weight loss and glycaemic control after bariatric surgery.

1.2.1 Altered intestinal glucose metabolism

In the past, the gastrointestinal (GI) tract was not often considered in T2DM research. Attention was normally given to the liver, muscle, brown and white adipose tissue and pancreas, which are the essential organs involved in glucose homeostasis control. Here, I'll provide two examples of why bariatric surgery draws attention to the GI tract in treating T2DM and how the GI tract and the liver work together to improve glucose metabolism post RYGB.

In 2008, Troy *et al*. first provided evidence that the beneficial effects of bariatric surgery involves increased intestinal gluconeogenesis and stimulation of hepatoportal glucose sensor (Troy *et al*. 2008). Due to the inability to perform RYGB in mice, their study was based on a RYGB mimic model enterogastro anastomosis (EGA, malabsorptive procedure) and a gastric lap-band model (GLB, restrictive procedure). By comparison to these two models, a better understanding of the two procedures could be achieved independently of body weight loss. They found that the EGA procedure specifically induced a strong inhibition of food intake and quickly improves glucose homeostasis. However, the effects were not observed in GLB pair-fed mice. The key observation was that EGA specifically resulted in induction of both Glucose 6-phosphatase (Glc6Pase) and phosphoenolpyruvate carboxykinase (PEPCK) in the distal jejunum and ileum. Glc6Pase and PEPCK are two of the most important enzymes involved in liver gluconeogenesis, which are also expressed in small intestine. Glc6Pase and PEPCK also proved to be two key triggers for the release of glucose by the small intestine. Indeed, glucose tracer dilution studies showed that this increase in Glc6Pase and PEPCK could translate into a significant glucose release by the small intestine in the post-absorptive situation. Furthermore, hepatoportal vein glucose sensing requires the presence of glucose transporter 2 (GLUT2), since the increased endogenous intestinal gluconeogenesis effects after EGA were abolished in GLUT2 knockout mice (Troy *et al*. 2008).

It should be noted that although EGA is an intervention that is similar to RYGB, it does not completely model RYGB procedure, because there is no intestinal segment that represents the Roux limb. Moreover, contradictory results were shown in two recent reports in both obese diabetic animals and human, in which they did not find the increased intestinal gluconeogenesis post RYGB (Hayes *et al*. 2011; Wolff *et al*. 2009).

In 2013, Saeidi *et al*. demonstrated that intestinal glucose metabolism is reprogrammed after RYGB and this reprogramming is triggered by exposure of the Roux limb to undigested nutrients (Saeidi *et al*. 2013). It was reported that the Roux limb of RYGB surgical rat exhibits up-regulated glucose transporter 1 (GLUT1), an enhanced basolateral glucose uptake and an augmented aerobic glycolysis (Saeidi *et al*. 2013). All these effects were suggested to meet the increased bioenergetic demand in the Roux limb. The above-mentioned effect means that the intestine exhibits the highest rate of glucose uptake and becomes a major tissue for glucose disposal post RYGB. Moreover, the increased intestinal glucose uptake showed a positive correlation with glycemic control post RYGB. To find the reason why the intestine exhibited glucose metabolism reprogramming, the author developed a rat model in which a loop of jejunum is transected and transposed between the oesophagus and the stomach. A similar effect was observed in this transposed jejunum. Hence, the authors argue that undigested nutrients are a major reason for the post RYGB Rous limb glucose reprogramming (Saeidi *et al*. 2013).

I.2.2 Altered hormone secretion

Altered gut hormones are the most widely studied area in metabolic surgery. In the past, the hindgut and foregut hypotheses were proposed to explain the beneficial metabolic effects of bariatric surgery (Cummings *et al*. 2013).

Hindgut theory suggests that diabetes resolution results from more rapid delivery of nutrients to the distal intestine, which could induce the L cells to release hormones such as glucagon-like peptide-1 (GLP-1) and peptide Y (PYY). Both GLP-1 and PYY exhibit anorectic actions and are implicated in mediating the weight loss effect after bariatric surgery. GLP-1 is produced in response to a meal, which could stimulate insulin release in response to nutrient ingestion, increase insulin biosynthesis and inhibit glucagon secretion (Baggio & Drucker 2007). Furthermore, GLP-1 could decrease food intake through its effect on the hypothalamus and brainstem (Baggio & Drucker 2007). Similarly, PYY is also a peptide hormone synthesised by the intestinal L- cells in the distal GI tract in response to food ingestion. PYY was reported to increase energy expenditure and postpone stomach emptying (Baggio & Drucker 2007). The majority of previous studies have shown an increase in GLP-1 and PYY levels post RYGB surgery (Vincent & Le Roux 2008; Borg *et al*. 2006). Furthermore, to rule out weight loss as the contributor of increased GLP-1, a comparison between RYGB and body weight matched controls proved that GLP-1 only increased in RYGB and not in diet induced weight loss controls (Laferrère *et al*. 2008). Also, by using oxctreotide to block PYY release, post RYGB patients could correspondently increase food intake (Le Roux *et al*. 2006). In all, the above evidence suggests that both GLP-1 and PPY play an important role in post-RYGB metabolic benefits.

The foregut theory suggests that exclusion of proximal small intestine could reduce or suppress the secretion of anti-incretin hormones, which could improve blood glucose control. However, support for this theory has been gradually eroded since 1) by assessing the impact of ileal transposition (IT, no foregut anatomical structure) and duodenal-jejunal exclusion (DJE, with foregut anatomical structure), a comparable weight loss, improvement in glucose tolerance and increase in GLP-1 was found (Kindel *et al*. 2009). Furthermore, by administration of GLP1 receptor antagonist, the improved glucose

tolerance in DJE subjects could be abolished (Kindel *et al*. 2009). Hence, gut hormones secreted via distal L-cells are the major factors contributing to improved glucose metabolism post RYGB.

Besides the above-mentioned gut hormones, ghrelin, which is a unique orexigenic hormone secreted from the stomach, was also widely examined post RYGB surgery. Ghrelin is a peptide produced by the X/A-like endocrine cells in the fundus of the stomach during fasting (Date *et al*. 2000). Ghrelin expression has been proven to induce body weight and regulate glucose and energy metabolism (Klok *et al*. 2007). Previous research reported a reduction in circulating ghrelin post-RYGB. The author believed that the empty stomach and bypassed duodenum could generate a continuous stimulatory signal, which could in turn inhibit gherlin secretion *via* “override inhibition” (Cummings *et al*. 2002). On the contrary, other studies reported ghrelin either to be increased or unaltered (Barazzoni *et al*. 2013). This discrepancy may be due to the inconsistency of measurements between labs and ghrelin expression changing with weight loss and the potential fluctuation before establishing the homeostasis point post RYGB.

1.2.3 Shifted gut microbiota

Recent studies have shown that gut microbiota play an important role in obesity by increasing the host’s energy harvesting efficiency. The gut microbiota has been reported to be different between lean and obese individuals (Turnbaugh *et al*. 2006) (Turnbaugh *et al*. 2008) (Ley *et al*. 2005). A shift of gut microbiota colonisation has been observed in multiple studies of bariatric surgery (Li *et al*. 2011a; Paziuk *et al*. 2013a; H. Zhang *et al*. 2009a) and conserved among human, rat and mice. Consistently, a rapid and sustained increase in the γ-proteobacteria (Escherichia) and Verrucomicrobia (Akkermansia) and a significant decrease in Firmicutes was noted (Liou *et al.* 2013b). These changes may be elicited by the changed dietary composition, altered intestinal luminal pH and influenced

bile flow. One remaining question is whether the shifted microbiota is the cause or result of post-RYGB metabolism benefits, such as facilitated weight loss. An elegant study involving transfer of the gut bacteria from RYGB mice to unoperated germ-free mice has been reported. Liou *et al.* found that these faecal transplanted animals exhibited weight loss and decreased fat mass (Liou, Paziuk, Jesus-Mario Luevano, Machineni, Turnbaugh & Kaplan 2013b). It suggested that change in gut microbiota might lead to, rather than be the consequence of, weight loss after RYGB. However, colonising RYGB microbiota in recipient mice for 2 weeks only elicited about 5% weight loss compared to 30-40% in 2 week post RYGB surgery in rats. It suggested that shifted microbiota is not the sole reason of facilitated weight loss post RYGB. Nevertheless, faecal transplant still provides a novel and promising method of obesity treatment in the near future.

1.2.4 Remodeled muscle promoter methylation

Skeletal muscle is widely recognised as the most important organ involved in the development of insulin resistance in T2DM. Epigenetic factors, such as DNA methylation, appear to play a vital role in controlling environmentally induced transcriptional response, which could further regulate metabolism. In 2009, Barres *et al.* found that peroxisome proliferator-activated receptorγ (PPARγ) coactivator-1 α (PGC-1α) is hypermethylated and PGC-1α mRNA is decreased in T2DM patients, concomitant with reduced mitochondrial content in type 2 diabetic patients (Barrès *et al*. 2009). Following this study, in 2013, *Barres et al.* (Barrès *et al*. 2013) showed that the metabolic benefits post-RYGB may be caused *via* epigenetic regulation, such as promoter methylation. The author found that post-RYGB there was an increase in PGC-1α mRNA expression and a decrease in PDK4 mRNA expression in skeletal muscle. Furthermore, these mRNA alterations are strongly inversely correlated with their promoter methylation levels (Barrès *et al*. 2013). Hence, changes in DNA methylation and metabolic gene transcription may contribute to the post-RYGB metabolism and insulin regulation.

1.2.5 Changed brain effects

More and more attention has been drawn to brain mediated mechanisms in regulating energy metabolism. For RYGB surgery, three aspects of brain related/mediated effects have been described, 1) reduced appetite and changed food preference, 2) influenced hypothalamic signalling and 3) changed vagal mediated effects.

1.2.5.1 Reduced appetite and changed food preference

Conventional low calorie diet treatment for obesity showed an 80%-90% failure rate (Ayyad & Andersen 2000). The reason may be due to the robust compensatory mechanism, whereby low calorie diet leads to an increase in hunger, a decrease in satiety and a decrease in energy expenditure after initial weight loss. Unlike natural weight loss, patients undergoing RYGB surgery, on the other hand, reported reduced hunger, a faster satiation during meals and exhibit an increased energy expenditure (Roux *et al*. 2006) (Dixon *et al*. 2005). In addition to appetite, it has been increasingly recognised that RYGB may alter food intake through shifted taste preference. For example, patients showed a preference for high-fat diet over low fat diet before surgery, but this reversed after RYGB surgery (Thirlby *et al*. 2006). Additionally, many post RYGB patients experienced nausea, vomiting and abdominal pain after intake of fat and milk products, such as ice cream (Kenler *et al*. 1990). Furthermore, animal experiments also clearly demonstrated that post RYGB rats showed a decreased acceptance for a high-fat diet compared to the sham operated rat, and the effect could be increased with time post surgery (Zheng *et al*. 2009). In all, both the reduced appetite and shifted food preference towards healthy food may contribute to the restricted calorie intake post RYGB surgery.

1.2.5.2 Influenced hypothalamic signaling

In the brain, many anatomical regions are recognised to play roles in metabolism homeostasis. However, the hypothalamus is a particularly crucial region in sensing and

integrating signals from the periphery and effecting physiological changes in order to maintain energy homeostasis (Schwartz 2006). The hypothalamic arcuate nucleus contains two populations of neurons with opposing effects, specifically the orexigenic AgRP/NPY neurons and anorexigenic POMC neurons (Hahn *et al*. 1998). It was shown that leptin inhibits AgRP/NPY neurons and excites POMC neurons (Cone 2005). Furthermore, the effect of serotonin (5-hydroxytryptamine, 5-HT) is also mediated by the POMC expressed 5-hydroxytryptamine 2C receptors (Y. Xu *et al*. 2008). Both leptin and 5HT have been reported to be altered post RYGB surgery, possibly stimulating the hypothalamus POMC neuron while inhibiting the AgRP/NPY neuron to achieve the reduced appetite effects. AgRP/NPY neuron can synthesise neuropeptide Y and γ-aminobutyric acid (GABA). Interestingly, GABA expression was shown to be increased in post-RYGB faecal samples and the increased expression was believed to be derived from microbial processing of putrescine (J. V. Li *et al*. 2011a). There are no studies investigating whether the gut microbiota generated GABA contribute to brain GABA levels.

Additionally, there is an established cross-talk between the hypothalamus and peripheral organs in controlling glucose homeostasis. For example, glucose sensing POMC neurone has been reported to control systemic blood glucose. High-fat diet induced obese mice exhibited an impaired uncoupling protein 2 mediated glucose sensing in POMC neuron (Parton *et al*. 2007). Furthermore, Osundiji *et al* showed that hypothalamic glucose sensors may also play an important role in controlling insulin secretion from the pancreas (Osundiji *et al*. 2012).

1.2.5.3 Vagal mediated effects.

The vagus is an important signaling relay system which sends signals between the gut and the brain. The vagal nerve has been proven to play a key role in the regulation of food intake, body weight control and release of gastrointestinal hormones, such as gastrin and

secretin. The vagal mediated effect post RYGB is still controversial. One study showed that vagal dissection during gastric bypass surgery could contribute to the early weight loss effect (Yong Wang & Liu 2009). However, another study showed that the preservation of vagal nerves during surgery was associated with greater and more sustained weight loss post RYGB (Seyfried *et al*. 2011). In all, the vagal mediated effects post RYGB surgery are still unclear and further studies should be carried out using vagatomy surgery.

1.2.6 Changed bile flow and bile acids composition

Bile acids are derived from hepatic cholesterol and oxysterols. Bile acids are known to regulate lipid and glucose metabolism *via* nuclear receptor farnesoid X receptor (FXR) and a G-protein family receptor TGR-5 (Fiorucci *et al*. 2010). Furthermore, bile acids could stimulate GLP-1 secretion through TGR5 activation in mice (Katsuma *et al*. 2005). Multiple studies have shown that circulating bile acid levels are more than 2 times higher post RYGB surgery compared to non-surgical controls (Simonen *et al*. 2012; Kohli *et al*. 2013). This increase could be mediated by an increased activity of hepatic CYP27A1, indicating a favoured acidic bile acid synthesis pathway. However, the most interesting finding of RYGB elicited bile acid alteration is not the increased total bile acid, but the decreased taurine-conjugated bile acids (Simonen *et al*. 2012). It was showed that decreased taurine-conjugated bile acid after RYGB rather than increased serum total bile acids is highly correlated with the decreased respiratory quotient (RQ, stands for energy expenditure) (Simonen *et al*. 2012). Furthermore, increased lipid oxidation and decreased glucose oxidation after RYGB was only observed in those individuals who had a decrease in the levels of taurine-conjugated bile acids (Simonen *et al*. 2012). There is still an absence of detailed information following this intriguing observation. Nevertheless, the role of bile acid provides another alternative mechanism of weight loss and glycaemic control post RYGB surgery.

1.3 MicroRNA

MicroRNAs (microRNAs) are 18-25 nucleotides long non-coding RNAs that can silence or repress potentially thousands of genes at the post transcriptional level (L. He & Hannon 2004). The first microRNA (lin-4) was discovered in 1993 in *C elegans* (R. C. Lee *et al*. 1993). Seven years later, the second highly conserved microRNA let-7 was discovered (Reinhart *et al*. 2000). Since then many new microRNAs have been identified. There were 1028 human microRNA sequences annotated on September 2010. Four years later, there are currently 1872 known *homo sapien* microRNAs according to miRBase (http://www.mirbase.org). MicroRNAs are estimated to regulate the expression of more than 60% of protein-coding genes (Friedman *et al*. 2009). MicroRNAs are not only involved in multiple biological processes, but also play important roles in various diseases.

1.3.1 MicroRNA biogenesis

The biogenesis of microRNA takes place through multiple-steps, which include RNAse enzymes Drosha and Dicer, and ultimately results in the production of mature 22 nucleotide microRNA. MicroRNA biogenesis is initiated by RNA polymerase (pol) II or RNA pol III, which can help to form hairpin-shaped primary microRNA transcripts (pri-microRNA). Pri-microRNA is then cleaved by the nuclear RNase III enzyme (Drosha) and DGCR8 (Pasha) to release the 70 nt precursor of microRNA (pre-microRNA) (Han *et al*. 2004). After nuclear processing, pre-microRNAs are exported to the cytoplasm by Exportin-5 (XPO-5) in complex with Ran-GTP (Bohnsack *et al*. 2004). Cytoplasmic pre-microRNAs are then processed and multi-protein RNA induced-silencing complex (RISC) is assembled mediated by the RISC loading complex (RLC), which is a multi-protein complex composed of cytoplasmic RNase III (Dicer), double stranded Tar RNA binding protein (TRBP), protein activator of PKR (PACT) and core component Argonaute-2 (Ago2) (Tomari *et al*. 2004; MacRae *et al*. 2008). The loop of the pre-microRNA is cleaved by

Dicer to produce an approximately 22 nucleotide double stranded microRNA duplex. Finally, one strand of the dicer duplex is bound by Argonaute to form an miRNA-induced silencing complex (miRISC), which targets mRNAs for regulation. The other strand, which is often called the star strand (miRNA*), is degraded. (Fig.1.3)

Traditionally, it was believed that microRNA repress protein production *via* decreasing translational efficiency or facilitating mRNA degradation by de-adenylation. However, a recent study using ribosome profiling shows that the lowered mRNA levels account for the majority (84%) of decreased target protein production (H. Guo *et al*. 2010). Interestingly, microRNA inhibits its target's expression first by translation repression, followed by mRNA degradation.

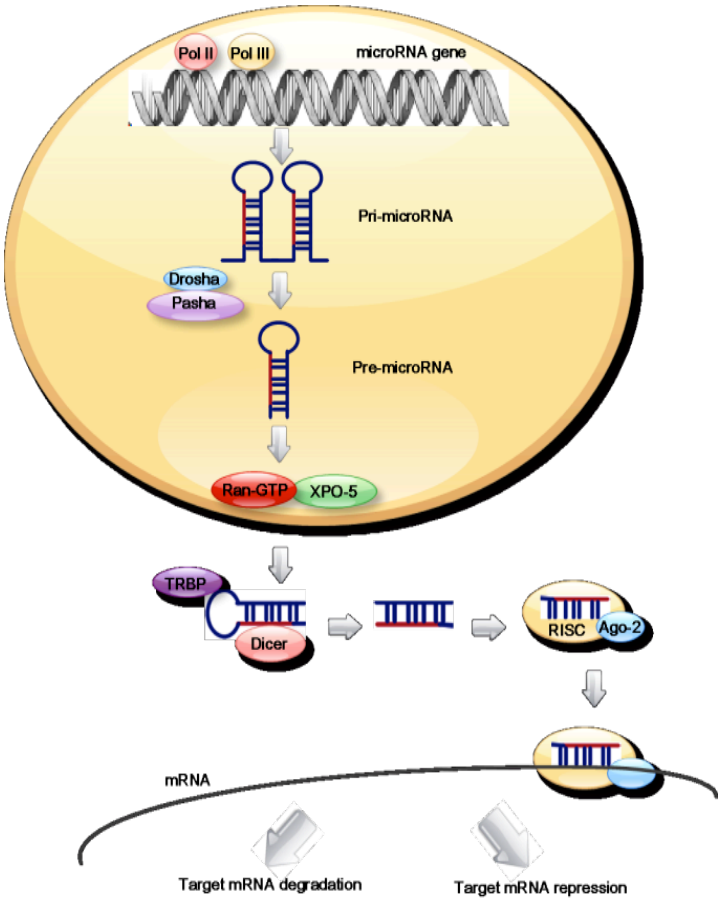

Figure 1-3 The biogenesis of microRNA

1.3.2 microRNA and metabolism

Diabetes is a worldwide chronic disease defined as a metabolic disorder of multiple aetiologies. It is characterised by hyperglycaemia with disturbances of carbohydrate, fat and protein metabolism resulting from defects in insulin secretion, insulin action, or both (Alberti & Zimmet 1998). MicroRNA plays an important role in insulin production, secretion and pancreatic development. Recent data have also shown that microRNAs have a different expression pattern in hyperglycaemic status (Heneghan *et al*. 2010).

1.3.2.1 MicroRNAs in regulating glucose metabolism

The first insulin production and secretion related microRNA, miR-375, was reported in 2004, and is a pancreatic islet-specific microRNA (Poy *et al*. 2004). The over-expression of miR-375 suppressed glucose-induced insulin secretion, and conversely, inhibition of endogenous miR-375 enhanced insulin secretion (Poy *et al*. 2004). El Quaamari A *et al*. have shown that miR-375 is involved in regulation of insulin gene expression thorough 3'-phosphoinositide-dependent protein kinase-1 (PDK1). PDK1 has a central role in the regulation of cell growth and organ development, and the ablation of PDK1 in beta-cells could induce diabetes after a reduction in beta-cell mass (Rintelen *et al*. 2001; Hashimoto *et al*. 2006). MiR-375 directly targets PDK1 and reduces its protein expression resulting in decreased glucose-stimulatory action on insulin gene expression and DNA synthesis. Poy and colleagues also provide evidence that miR-375 is essential for glucose homeostasis, pancreatic alpha and beta cell turnover and adaptive beta-cell expansion in response to increasing insulin demand in insulin resistance (Poy *et al*. 2009). Moreover, by knocking out miR-375, mice suffered hyperglycaemia and glucose intolerance, which is associated with impaired gluconeogenesis (Poy *et al*. 2009). In summary, miR-375 plays a key role in regulating glucose metabolism not only *via* regulating insulin secretion, but also by regulating pancreatic cell development.

There is also some evidence that other microRNAs are also involved in regulating insulin secretion and islet development. Plaisance *et al*. have shown that over-expression of miR-9 in insulin-secreting cells could cause a reduction in exocytosis elicited by glucose (Plaisance *et al*. 2006)13, and Lovis *et al*. showed that miR-124a and miR-96 modulate the expression of proteins involved in insulin exocytosis and affect the insulin secretion of the beta-cell line MIN6B1 (Lovis, *et al*. 2008a). Additionally, Foxa2 has been described as a main regulator of pancreatic development and is also involved in glucose metabolism and insulin secretion and miR-124a plays a key role in pancreatic development through the regulation of Foxa2 expression (Baroukh *et al*. 2007).

More recently, several studies have monitored the microRNA expression changes between normoglycaemic and hyperglycaemic exposure or diabetes both *in vitro* and *in vivo*. MiR-30d (X. Tang *et al*. 2009), miR-125a (Herrera *et al*. 2009), miR-133a (Fred *et al*. 2010) and miR-126 (Zampetaki *et al*. 2010) all showed differences in levels of expression between normal and abnormal glucose levels, which indicates that they may be involved in insulin gene expression or diabetes progress.

1.3.2.2 microRNA in regulating lipid metabolism

Lipids don't only act as energy stores, but are also an important class of signalling molecule. MiR-33 and miR-122 are two of the most well-studied lipid homeostasis related microRNAs.

For miR-33, an interesting miR-33-SREBP (sterol regulatory element binding proteins) regulatory circuit has been established (Rayner *et al*. 2010). SREBP is an important class of transcriptional factor that controls the expression of numerous genes involved in fatty acid and cholesterol metabolism and the production of phospholipids and triglycerides (Horton *et al*. 2002). The conservative miR-33a is embedded in the intron of SREBP-2 on

chromosome 22, whereas the miR-33b is located in the intron of SREBP-1 on chromosome 17. The intron microRNAs are normally co-expressed with the host genes, hence the co-expression pattern of SREBP and miR-33 has been found in multiple tissue types, including liver, brain, heart, muscle, spleen, kidney and lung (Najafi-Shoushtari *et al*. 2010; Rayner *et al*. 2010). The activation of SREBP-1 induces the expression of genes involved in fatty acid, phospholipid and triglyceride synthesis, whereas SREBP-2 activates genes that control cholesterol synthesis and uptake (Ye & DeBose-Boyd 2011). Interestingly, miR-33a and miR-33b could inhibit fatty acid degradation and cholesterol flux through their targets adenosine triphosphate–binding cassette transporter A1 (ABCA1) and carnitine palmitoyltransferase 1A (CPT1A) (Najafi-Shoushtari *et al*. 2010; Rayner *et al*. 2010). This suggests that miR-33 and its host gene SREBP could coordinate with each other to achieve, and more efficiently control, lipid and cholesterol homeostasis.

MiR-122 is another well-studied hepatic microRNA regulating lipid metabolism. The discovery of miR-122 dates back to 2002 (Lagos-Quintana *et al*. 2002) and has been identified as the most abundant microRNA in the liver, and accounts for around 70% of all hepatic microRNA (Chang *et al*. 2004). Multiple studies have revealed the important roles of miR-122 in regulating lipid metabolism. By inhibiting miR-122 using antisense locked nucleic acid, decreased plasma cholesterol and triglyceride levels are observed, which is associated with increased fatty acid oxidation and changed cholesterol biosynthesis (Esau *et al*. 2006). On the contrary, adenoviral overexpression of miR-122 leads to increased cholesterol biosynthesis (Krutzfeldt *et al*. 2005).

Besides the aforementioned miR-33 and miR-122, other microRNAs have also been related to lipid metabolism. For example, miR-14 and miR-278 have been shown to regulate fat metabolism in *Drosophila melanogaster* (Telernan & Cohen 2006; P. Xu *et al*. 2003). By knocking out miR-14 *in vivo*, flies showed increased levels of triglycerides and

diacylglycerol (P. Xu *et al*. 2003). In addition, miR-14-null flies had significantly increased lipid droplet accumulation in adipose tissue. MiR-278 mutants showed elevated insulin production and a lean phenotype *via* a reduction in whole body fat levels (Telernan & Cohen 2006). Previous studies have also shown that miR-103 and miR-107 (Wilfred *et al*. 2007), the miR-143 clusters (Esau *et al*. 2004) and the miR-17-92 clusters (Qiang Wang *et al*. 2008) are all involved in regulating fatty acid metabolism.

1.3.2.3 microRNA in metabolic syndrome

Metabolic syndrome is defined as a combination of medical disorders which could increase the risk of developing cardiovascular diseases and diabetes (Alberti *et al*. 2006). According to the National Cholesterol Education Program's Adult Treatment Panel III report (ATP III), there are 6 components of metabolic syndrome: abdominal obesity, atherogenic dyslipidemia, raised blood pressure, insulin resistance and glucose intolerance, a pro inflammatory state, and a prothrombotic state (the abnormal tendency of developing blood clots) (Grundy *et al*. 2004). MicroRNA have been implicated as key regulators of metabolic homeostasis. It is not surprising that under an abnormal metabolic environment, such as obesity and diabetes, the expression of microRNAs is altered. The result of this change could either be beneficial, in that it helps to maintain normal metabolic homeostasis, or detrimental, facilitating the abnormal metabolic process.

Numerous studies have addressed the microRNA dysregulation in diabetes and obesity using various animal models and in patients. For example, in non-obese diabetic (NOD) mice, the miR-29 family, miR-21, and miR-34a showed up-regulation in pancreatic islet cells (Roggli *et al*. 2010). In leptin receptor-deficient (db/db) mice, miR-34a and miR-146, expressed in pancreatic islet cells, were up-regulated (Lovis, Roggli, *et al*. 2008b). In leptin deficient obese (ob/ob) mice and diet induced obesity (DIO) mice, miR-143 and miR-802 are increased in the liver (Jordan *et al*. 2011; Kornfeld *et al*. 2013), while miR-103 and

miR-107 is altered in the white adipose tissue (Wilfred *et al*. 2007). Inconsistent results have been published for miR-375; Bolmeson *et al.* showed miR-375 merely changed in human diabetic subjects' islet cells (Bolmeson *et al*. 2011), whereas Zhao *et al*. reported that miR-375 is up-regulated in the islets of T2DM (Zhao *et al*. 2010).

Recent studies also suggest that extracellular circulating microRNA could be considered as biomarkers of diabetes and obesity. By using a cohort of 80 patients, a group of microRNAs were found to be correlated with T2DM, including decreased miR-20b, miR-21, miR-24, miR-15a, miR-126, miR-191, miR-197, miR-223, miR-320, and miR-486 expression and elevated miR-28-3p expression (Zampetaki *et al*. 2010). Kong *et al*. reported that 7 microRNAs could be linked with diabetes including miR-9, miR-29a, miR-30d, miR-34a, miR-124a, miR-146a and miR-375 (Kong *et al*. 2011). A more recent study profiled circulating microRNAs in 32 men after surgery-induced weight loss and in 6 morbidly obese patients and identified a microRNA signature of obesity (Ortega *et al*. 2013). The result was cross-validated in 80 men and 22 surgery-induced weight loss patients. It was suggested that morbidly obese patients showed a marked increase of miR-140-5p, miR-142-3p, miR-222 and decreased levels of miR-532-5p, miR-125b, miR-130b, miR-221, miR-15a, miR-423-5p and miR-520-3p. Bariatric surgery-induced weight loss leads to a significant decrease in miR-140-5p, miR-122, miR-193-5p and miR-16-1 and up-regulation of miR-221 and miR-199-3p (Ortega *et al*. 2013).

1.3.3 Circulating microRNAs

Blood containing RNA has long been considered as a promising biomarker for disease diagnosis. The phenomenon that circulating RNA can stably survive in RNase-rich plasma dated back to 2004 (El-Hefnawy *et al*. 2004). The important features and functions of circulating microRNA are summarised and presented below.

1.3.3.1 Circulating microRNAs stability

Circulating microRNAs have been consistently reported to remain stable in serum, which contains high levels of ribonuclease enzymes, which degrade RNA. However, microRNA combined proteins or packaged particles may function to protect circulating microRNAs from being digested by RNase. Moreover, circulating RNA has been shown to withstand high temperatures, extreme pH levels, multiple freeze-thaw cycles, prolonged incubation at room temperature (24 hours) (Tewari *et al*., 2008) and even 10 years storage (Zhu *et al*., 2009).

1.3.3.2 Detecting circulating microRNA

Since circulating microRNAs are present at much lower concentration than other tissues, detecting and analysing them is a real challenge. There are several technologies available for circulating microRNA profiling, such as deep sequencing, microRNA microarray and quantitative real-time PCR (qRT-PCR). The most widely used is qRT-PCR, which has a high specificity and sensitivity; for example a previous study has shown that 220 microRNAs can be detected in a single cell (Tang *et al*., 2006). Technology development makes the detection of low level circulating RNA possible. Nonetheless, conflicting data have been published due to differences in blood collection and serum separation protocols, the use of various microRNA profiling methods and a lack of a universally accepted method of normalisation. In solid tissue samples, microRNA expression is always normalised with internal consistently expressed reference RNAs, for example 18S, 5S ribosome RNA and small nuclear RNAs. For circulating microRNA, the expression stability of the above mentioned reference RNAs needs to be examined before using them to normalise the data. Synthetic *C elegans* microRNAs, cel-miR-39, cel-miR-54 and cel-miR-238, have been used as internal standards and have proved to be an alternative useful normalisation tool (Mitchell *et al*. 2008). Different normalisation methods need to be

examined and compared before drawing any conclusion related to circulating microRNA expression level.

1.3.3.3 Circulating microRNAs secretion and function

Based on recent findings, there are at least four ways that microRNAs can be combined with protein or packaged and transported into the bloodstream. MicroRNAs can be packaged into exosomes or microparticles and secreted into circulating blood. Both exosomes and microparticles are membrane-bound small particles with different sizes. Exosomes originate from endosome-derived intracellular multivesicular bodies, with range from 30 to 100 nm, whereas microparticles, also called microvesicles, are larger (100-1500 nm) and are shed directly from the cell membrane (Ratajczak *et al*., 2006). Both exosome and microparticles have been reported as physiological carriers of microRNA (Zhang *et al*., 2010, Hunter *et al*., 2008). Likewise, cellular microRNA can be exported in conjunction with high density lipoprotein (HDL) (Vickers *et al*., 2011) and 96 KDa argonaute protein 2 (Ago-2) (Turchinovich *et al*., 2011, Arroyo *et al*., 2011). Jason D. Arroyo and colleagues elegantly demonstrated that at least two forms of circulating microRNA exist in plasma or serum, vesicle-associated and non-membrane bound forms. Surprisingly, approximately 90% of microRNAs in circulation are present in the latter non-membrane bound form (Arroyo *et al*., 2011). Vickers *et al*. found that plasma-derived high density lipoproteins (HDL) contain microRNAs. Furthermore, these HDL can transport endogenous microRNA to recipient cells with functional abilities (Vickers *et al*., 2011). This evidence suggests that circulating microRNA may function as communicators between cells, yet little is known about how these circulating microRNAs are secreted into the circulation and what functional differences there are between the above-mentioned vesicle-associated and non-membrane bound microRNAs.

1.4 Hypothesis

The aims of this project were 1) to examine whether RYGB surgery influences circulating and colorectal microRNA profiles 2) to determine whether the microRNAs are involved with the altered metabolic effects post RYGB surgery and 3) to assess the causes of RYGB induced microRNA dysregulation.

2. Materials and Methods

2.1 Animal experiment and tissue collection

2.1.1 Design of the animal study

The animal experiment was carried out under a UK home office license (PL 70-6669). Thirteen male Sprague Dawley (SD) rats were individually housed and kept under a 12h/12h light/dark cycle at room temperature. All rats were acclimatized and fed on high fat diet (Altromin C 1090 - 60 obesity-inducing diet) for 1 week prior to the experiment. Animals were randomly divided into two groups: RYGB (n=8) and sham (n=5). The antibiotic combination amoxicillin/flucoxacillin was administrated to all rats at a dose of 12.5 mg each, pre-surgery.

The sham procedure was carried out including a 7 mm gastrotomy on the anterior wall of the stomach with subsequent closure (interrupted prolene 5-0 sutures) and a 7 mm jejunotomy with subsequent closure (running prolene 6-0 suture). For the RYGB procedure, the proximal jejunum was divided 15 cm distal to the pylorus to create a biliopancreatic limb. After identification of the cecum, the ileum was then followed proximally to create a common channel of 25 cm. Here, a 7 mm side-to-side Jejuno-Jejunostomy (running prolene 7-0 suture) between the biliopancreatic limb and the common channel was performed. The gastric pouch and alimentary limb were anastomosed end-to-side using a running prolene 7-0 suture. The gastric remnant was closed with interrupted prolene 5-0 sutures. The complete bypass procedure lasted approximately 60 minutes and the abdominal wall was closed in layers using 4-0 and 5-0 prolene sutures. Approximately 20 minutes before the anticipated end of general anesthesia, all rats were injected with 0.1 ml of 0.3% buprenorphine subcutaneously to minimize postoperative discomfort. Immediately after abdominal closure, all rats were

injected subcutaneously with 5 ml of normal saline to compensate for intra-operative fluid loss. After 24 hours of wet diet (normal chow soaked in tap water), regular chow was offered on postoperative day 2 and throughout the remaining experiment period.

2.1.2 Tissue collection method

Tissues, including liver (left lobe), pancreas, spleen, heart, white fat, duodenum (biliopancreatic limb if RYBG), jejunum (alimentary if RYBG), ileum (common channel if RYBG) and colon were collected 53 days after surgery. Approximately 5ml of the whole blood was taken from the heart, 2.5 ml of which was transferred into an EDTA-containing tube (BD Bioscience) for Taqman low density assay cards (TLDA) and the remaining to a sodium heparin-coated tube (BD Bioscience) for metabonomics analysis. After a gentle shake, blood with anti-coagulant reagents was immediately centrifuged at 6000 rpm at room temperature for 10 minutes. The plasma samples obtained using the anticoagulants were then transferred into two 1.5ml RNase-free Eppendorf tubes, separately. All samples were immediately snap-frozen in liquid nitrogen and stored at -80ºC.

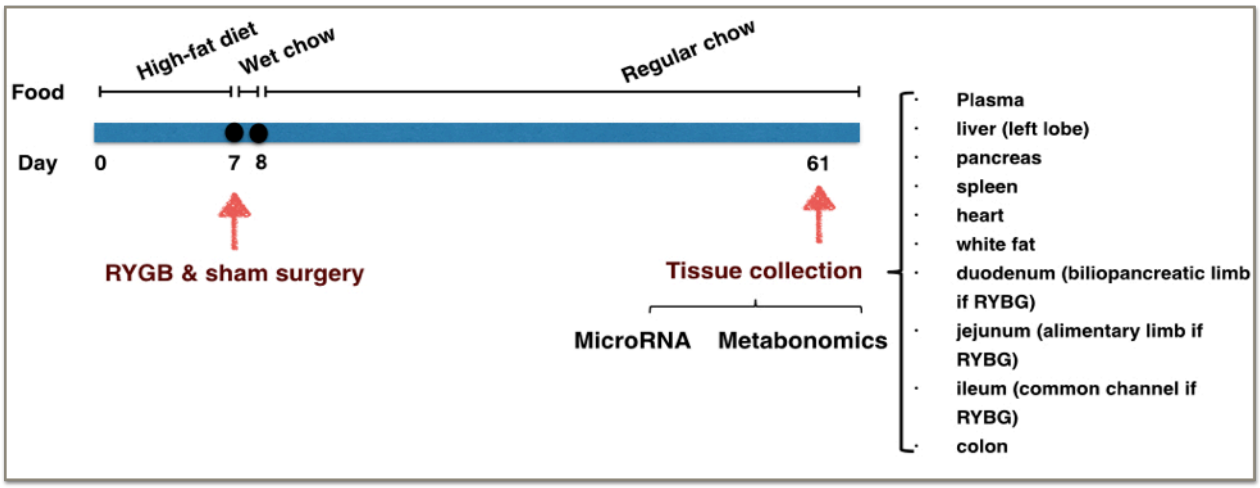

Figure 2-1 Experiment outline for rat with RYGB and sham-operated surgery

2.2 Tissue culture

All cell culture reagents were supplied by Invitrogen (Life Technology), unless otherwise stated, and Corning standard tissue culture plated plasticware was used for all cultures.

2.2.1 Cell resuscitation

In order to resuscitate a cell line, a vial of frozen cells was removed from liquid nitrogen storage. Cells were allowed to reach room temperature for 1-2 minutes, warmed gently in a water bath (37ºC) until partially thawed. Approximately 0.5mL pre-warmed media was then added into the vial and the mixture was then centrifuged at 1000g for 1minute. The DMSO containing freeze media was removed and cells were re-suspended in 1mL complete media. Cells were cultured in T25 flasks under standard culture conditions (37ºC, 5%CO_2 and 95% air). After reaching confluence, cells were transferred into T75 flasks for routine culturing and experiments.

2.2.2 Cell passaging

Cells were routinely maintained in T75 flasks in approximately 15mL complete media. Cells were subcultured after reaching approximately 80% confluence. To sub the adherent cells, the cell monolayer was first rinsed with sterile phosphate-buffered saline (PBS) and then incubated with 0.05% trypsin-EDTA (ethylenediaminetetraacetic acid) until suspension. Cells were gentle shaken and pipetted up and down to minimise the trypsinisation time. Trypsinisation was terminated by adding an equal volume of complete media. The media-trypsin cell mixture was then centrifuged at 1000g for five minutes. The supernatant was removed and the pellet re-suspended in fresh media and seeded into new flasks at 1:3 to 1:6 dilutions depending on the different cell lines.

2.2.3 Cell count

Cells were manually counted using haemocytometer and Trypan Blue reagent was used to determine cell viability. Trypan Blue dye is taken up by dead cells, due to permeabilisation of their cell membrane, allowing differentiation between live and dead cells. Generally, an aliquot of the cell suspension (10µL) was added to an equal volume of 0.4% Trypan Blue (10µL). The cells and Trypan Blue were mixed with a pipette and then incubated at room temperature for 1-2 minutes. Approximately 8µL of the mixture was then loaded onto a haemocytometer. Non-blue cells (live population) were counted in at least 9 squares, averaged, and the total number of live cells determined by the equation below. Generally cells are diluted 1:1 (vol:vol) with Trypan Blue, thus there is a dilution factor of 2 in the equation. Furthermore, the number of cells in the Trypan Blue suspension are in an area of 1mm x 1mm x 0.1mm (or $0.1mm^3$), hence to calculate cells/mL need to multiply by 10^4 in the equation.

Cell number = cell count (per square) * 2 *10^4

2.2.4 Cell freezing

In order to preserve the cell line, cells were frozen and stored in liquid nitrogen. To prepare stock, cells from early passage were pelleted and resuspended in 95% media and 5% of dimethylsulphoxide (DMSO). Cells were then frozen at -80ºC for 24 hours before finally transferred into a liquid nitrogen dewer.

2.2.5 FAO cell line culture condition

FAO (rat hepatocarcinoma) were routinely cultured in complete media consisting of phenol red-free MEM (minimum essential medium, Invitrogen) supplemented with 10% v/v FBS (fetal bovine serum), 1% v/v NEAA (non- essential amino acids), 2mM L-glutamine and 1%

Penicillin/Streptomycin (100U/mL, 100µg/mL respectively) to prevent the growth of bacteria.

2.2.6 B13(H) cell line culture condition

B13 (pancreatic progenitor cell line) were routinely cultured in complete media consisting of DMEM (Dulbecco's Modified Eagle Medium) supplemented with 10% v/v FBS (fetal bovine serum) and 1% Penicillin/Streptomycin (100U/mL, 100µg/mL respectively) to prevent the growth of bacteria. After reaching the required number, B13 cells can be induced to differentiate by synthetic glucocorticoid dexamethasone (10nM) (Shen *et al*. 2000), which was dissolved in ethanol.

2.2.7 Glucose treatment experiment

Glucose treatments were carried out in 6 well plates. Cells (5 X 10^5 / well) were seeded with 2.5mL normal FAO complete media (MEM, 10%FBS, 1% Pen/Strep, 2mM L-glutamine and 1%NEAA) at two days before treatment. FAO cells were given 24 hours (37ºC, 5% CO_2) to attach to the plastic substrate in the normal media. After which, the media was aspirated, cells were carefully washed with warm PBS and an equivalent volume (2.5mL) of experimental media (glucose-free MEM without serum and antibiotics) added. After 24 hours incubation, media was aspirated and cells were replenished with 2.4mL fresh experimental media. In the meantime, α-D-Glucose (Sigma-Aldrich, 180.16 g/mol) was dissolved in experimental media to 625mM, 375mM and 125mM and sterilised using a 0.2µM filter (Millipore). Glucose solution (100µL) was added into each 6 well plate with an equal amount of media added as controls. Hence the final glucose treatment concentrations in each well were 25mM, 15mM and 5mM. All experiments were done with at least three biological replicates and FAO cells were harvested after 2 hour and 8 hour incubation at 37ºC, 5% CO_2. All cells were washed with cold PBS before harvesting with 1mL Trizol.

2.2.8 Dexamethasone treatment

Dexamethasone treatments were carried out in 6 well plates. Similar to the glucose treatment experiment, FAO cells (5 X 10^5 / well) were seeded with 2.5mL complete FAO culture media (phenol red-free MEM, 10% v/v FBS (foetal bovine serum), 1% v/v NEAA, 2mM L-glutamine and 1% Penicillin/Streptomycin) two days before treatment. Old media was removed and a serum-free media was added into cells 24 hours later. On treatment day, old media was replaced with fresh serum free media and ethanol dissolved dexamethasone (treatment concentration 10nM) was added. Dexamethasone stock solution was 1mM. A serial dilution was applied with 1:100 (v:v) and then 1:1000 (v:v) which made the final treatment concentration 10nM in cell culture media. Two sets of experiments were carried out. For 24 hour treatment, 3 biological replicates were used and cells were maintained in same dexamethasone contained media for the whole 24 hours. For 96 hour treatment experiment, 6 biological replicates were used and the experimental dexamethasone containing media was replaced with fresh at 48 hours. All cells were incubated at 37ºC, 5% CO_2 and cells were washed with cold PBS before harvesting with 1mL Trizol.

2.2.9 PPARα (fenofibrate) and PPARγ (rosiglitazone) treatment

PPARα and PPARγ agonist treatment experiments were carried out in B13H cell line. Generally, B13 cells were seeded into 6 well plate in 2.5mL normal B13 media (DMEM, 10%FBS and 1% Pen/Strep) with 5X10^5 cells in each well. Treatment with dexamethasone (10nM, dissolved in ethanol, prepared and preserved in glass, used within 1 month) was applied for two weeks to allow pancreas to liver transdifferentiation. Cells were replenished with fresh B13 media and dexamethasone every 2 days. At day 15, all B13 media with dexamethasone was removed and the transdifferentiated hepatocyte-like B13H cells were washed with 1mL warm PBS. Then, 2.5mL experimental media (DMEM, no FBS, Pen/step

and no dexamethasone) was added to each well. Fenofibrate (306.84g/mol, Abcam) was dissolved in ethanol to final concentrations of 10mM, 30mM and 50mM (0.0180g fenofibrate in 1mL ethanol). Rosiglitazone (357.43g/mol, Abcam) was dissolved in DMSO to final concentrations of 10mM, 30mM and 50mM (0.0179g rosiglitazone in 1mL DMSO). To treat the B13H cells, 2.5µL fenofibrate/ rosiglitazone solution was added into each well, which made the final fenofibrat/ rosigalitazone treatment concentrations 10µM, 20µM and 50µM. For fenofibrate control wells, 2.5µL ethanol vehicle was added, while 2.5µL DMSO vehicle was added for rosiglitazone control wells. All treatments were done with 3 biological replicates. The treated cells were harvested after 24h incubation in 37ºC, 5% CO_2. All cells were washed with cold PBS before harvesting with 1mL Trizol.

2.2.10 Fatty acid (arachidonic acid) treatment

2.2.10.1 Arachidonic acid treatment for 1 hour

Arachidonic acid treatment experiment was carried out in B13H cell line. As before, $5X10^5$ B13 cells were seeded into wells of 6 well plates in 2.5 mL normal B13 media (DMEM, 10%FBS and 1% Pen/Strep). Treatment with dexamethasone (10nM, dissolved in ethanol, prepared and preserved in glass , used within 1 month) were applied for two weeks to allow pancreas to liver transdifferentiation. Cells were replenished with fresh B13 media and dexamethasone every 2 days. At day 15, B13 media with dexamethasone was removed and the transdifferentiated hepatocyte-like B13H cells were washed with 1mL warm PBS. Then, 2.5mL experimental media (DMEM, no FBS, no Pen/step and no dexamethasone) were added to each well. Arachidonic acid (purchased from Sigma-Aldrich, liquid, 250mg/mL = 780mM) was diluted to 300mM (1:2.6 dilution), 100mM (1:7.8 dilution) and 30mM (1:26 dilution) in ethanol. To treat the B13H cells, 2.5µL arachidonic acid solution was added into each well, which made the final arachidonic acid treatment concentrations 30µM, 100µM and 300µM. For control wells, 2.5µL ethanol vehicle was

added. All treatments were done with at least 3 biological replicates. The treated cells were harvested after 1 hour incubation in 37ºC, 5% CO_2. All cells were washed with cold PBS before harvesting with 1mL Trizol.

2.2.10.2 Arachidonic acid treatment for 10 minutes, 1 hour, 4 hour and 10 hour

Arachidonic acid treatment experiment was carried out in B13H cell line. B13 cells ($2.5X10^5$) were seeded into 12 well plate in 1mL normal B13 media (DMEM, 10%FBS and 1% Pen/Strep). Treatment with dexamethasone (10nM, dissolved in ethanol, prepared and preserved in glass, used within 1 month) was applied for two weeks to allow pancreas to liver transdifferentiation. Cells were replenished with fresh B13 media and dexamethasone every 2 days. At day 15, all B13 media with dexamethasone was removed and the transdifferentiated hepatocyte-like B13H cells were washed with 0.5 mL warm PBS. Then, 1mL experimental media (DMEM, no FBS, Pen/step and dexamethasone) was added to each well. Arachidonic acid (purchased from Sigma-Aldrich, liquid, 250mg/mL = 780mM) was diluted to 150mM (1:5.2 dilution), 100mM (1:7.8 dilution) and 50mM (1:15.6 dilution) in ethanol. To treat the B13H cells, 1µL arachidonic acid solution was added into each well, which made the final arachidonic acid treatment concentrations 50µM, 100µM and 150µM. For control wells, 1µL ethanol vehicle was added. All treatments were done with at least 3 biological replicates in each time points. The treated cells were harvested after 10 minutes, 1 hour, 4 hour and 10 hour incubation in 37ºC, 5% CO2. All cells were carefully washed with cold PBS before harvesting with 0.5mL Trizol.

2.2.11 microRNA inhibitor/mimic transfection

MiRDIAN miR-122 mimic (C-320349-05-0005) and scrambled microRNA negative mimic control (CN-001000-01-05) were purchased from Thermo Scientific. Pancreatic derived B13 cells were plated $1x10^5$ in 24 well plates and dexamethasone (10nM) was used to transdifferentiate the cells into hepatocytes for 2 weeks as described before (Marek *et al*.

2003). Dexmethasone was removed 24 hours before transfection. Before transfection, all cells were changed into the serum/antibiotics-free OPTI-MEM media (Invitrogen). Cells were transfected using Lipofectamine 2000 (Invitrogen) for 96 hours. Transfection complex was prepared according to manufacture's description. MiR-122 mimic and scramble control were dissolved with siRNA buffer to the concentration of 20μM. To treat the cells with 20nM, mimics and control were further diluted in Opti-MEM (invitrogen) (1:100). Lipofectamine was diluted 6:100 (v:v, lipo:opti-MEM). Both reagents were incubated 5 minutes at room temperature and then mixed together with gentle pipetting. Mixtures were incubated at room temperature for exactly 20 minutes. Finally, the complete 100μl mixture was added to assigned 24 well plate wells with cells and 400μL opti-MEM. Cells were harvested 96 hours later with PBS wash before harvesting.

2.3 RNA isolation and quantification

2.3.1 Circulating RNA extraction and optimisation

Isolation of plasma total RNA was performed using the mirVANA PARIS isolation kit (Ambion, Applied Biosystems Inc.) following the manufacturer's instructions with minor modifications. Plasma total RNA extraction method was optimised by comparing mirVANA microRNA isolation kit, TRIzol reagent (Invitrogen) and mirVANA PARIS kit (Ambion, Applied Biosystems Inc.). MirVANA PARIS kit was found to be the best-performing and all plasma samples in this study were examined using this method.

Working as an extraction normalizer, synthetic *Caenorhabditis elegans cel-mir-39* (cel-miR-39) was added to the mixture of plasma and denature buffer. In order to analyse the protein denaturation time, the plasma sample was divided into three and incubated with 2 X denature buffer for 0 minute, 5 minutes and 20 minutes with multiple concentrations of cel-miR-39s (25fmol, 50fmol, 250fmol and 500fmol). The result suggested 5 minutes incubation time with 250fmol spike-in cel-miR-39 was optimal. All of the plasma samples were then extracted using the conditions described above.

As shown in Figure 2.2 below, plasma (100µL) was diluted with 100 µL cell disruption buffer (provided by miRVANA PARIS kit) and then an equal volume of 2 X denature solution (miRVANA PARIS kit) was added. The dilution of plasma is crucial for achieving successful RNA isolation since plasma contains a large amount of protein which could not be completely separated if inappropriately diluted. Synthetic Caenorhabditis elegans *cel-mir-39* was added to the mixture of diluted plasma and denature solution. By adding equal amount (400µL) of acid phenol:chloroform solution, RNA was separated as supernatant. The RNA was then purified using filter cartridge containing a glass-fiber filter which immobilizes the RNA by washing with solution I and II as per manufacturer's instruction.

Finally, RNAs were eluted by 100 µL 95ºC DNase, RNase-free water. All of the samples were stored at -80ºC until use.

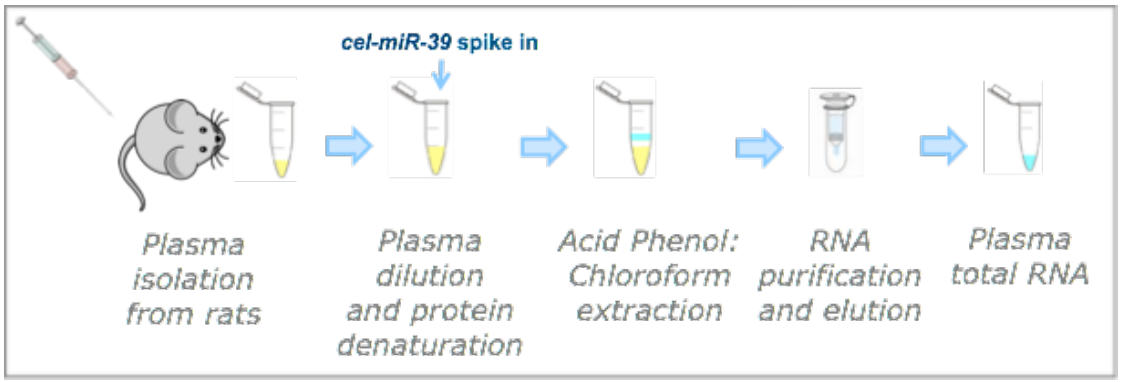

Figure 2-2 Plasma total RNA extraction procedure

The plasma isolated from rats was diluted with cell disruption buffer (supplied with the miRVANA PARIS kit) and spiked with synthetic cel-miR-39. The plasma/disruption buffer mixture was then mixed with acid phenol:chloroform and RNA was purified with filter cartridge and eluted using 100µl water.

2.3.2 Tissue/ cell total RNA extraction

Total tissue and cells containing RNA was extracted from the liver/ colon tissue and cell culture collection using Trizol (Invitrogen) following the manufacturer's instructions. RNA Zap (Ambion) was used to clean surfaces to remove potential RNases. To minimise RNA degradation, frozen liver/colon were cut frozen and transferred into Trizol immediately. Approximately 50mg tissue sample and one T75 flask of cells were extracted using 1ml of Trizol. Following homogenisation at room temperature, the insoluble material was removed by centrifugation at 12000g for 10 minutes. Chloroform (200µL, Sigma) was then added to each sample and the samples were shaken vigorously for 15 seconds and centrifuged at 4ºC at 12000g for 15 minutes to achieve phase separation. The top aqueous phase which contains RNA was then transferred into a new EP tube. Total RNA, which includes ribosomal RNA, mRNA, transfer RNA, microRNA *etc*., was then precipitated with 0.5mL isopropanol at room temperature for 10 minutes. Samples were centrifuged at 12000rpm for 10 minutes to pellet the RNA. The RNA pellet was then washed with 75% ethanol 1-2

times, air-dried, and dissolved in RNA-free water. The solution containing pure RNA was aliquoted, and stored at -80ºC.

2.3.3 Tissue RNA quality control (Agilent bioanalyzer)

In order to assess the purity and integrity of the RNA samples, Agilent Bioanalyser and Eukaryote total RNA Nano kit were used to determine the RNA integrity number (RIN) which indicates the extent of RNA degradation and purity. Generally, a RIN score bigger than 8 is considered as good quality RNA, which could be further processed with deep sequencing/ microRNA array/ TLDA experiments. The Agilent bioanalyser produces an electropherogram and gel-like image which allows users to visualise RNA degradation. A typical Agilent bioanalyser report is shown below (Figure 2.3).

The Bioanalyser protocol was followed as per the manufacturer's protocol and conducted at the Genomics Laboratory in the Medical Research Council Center at Hammersmith Hospital.

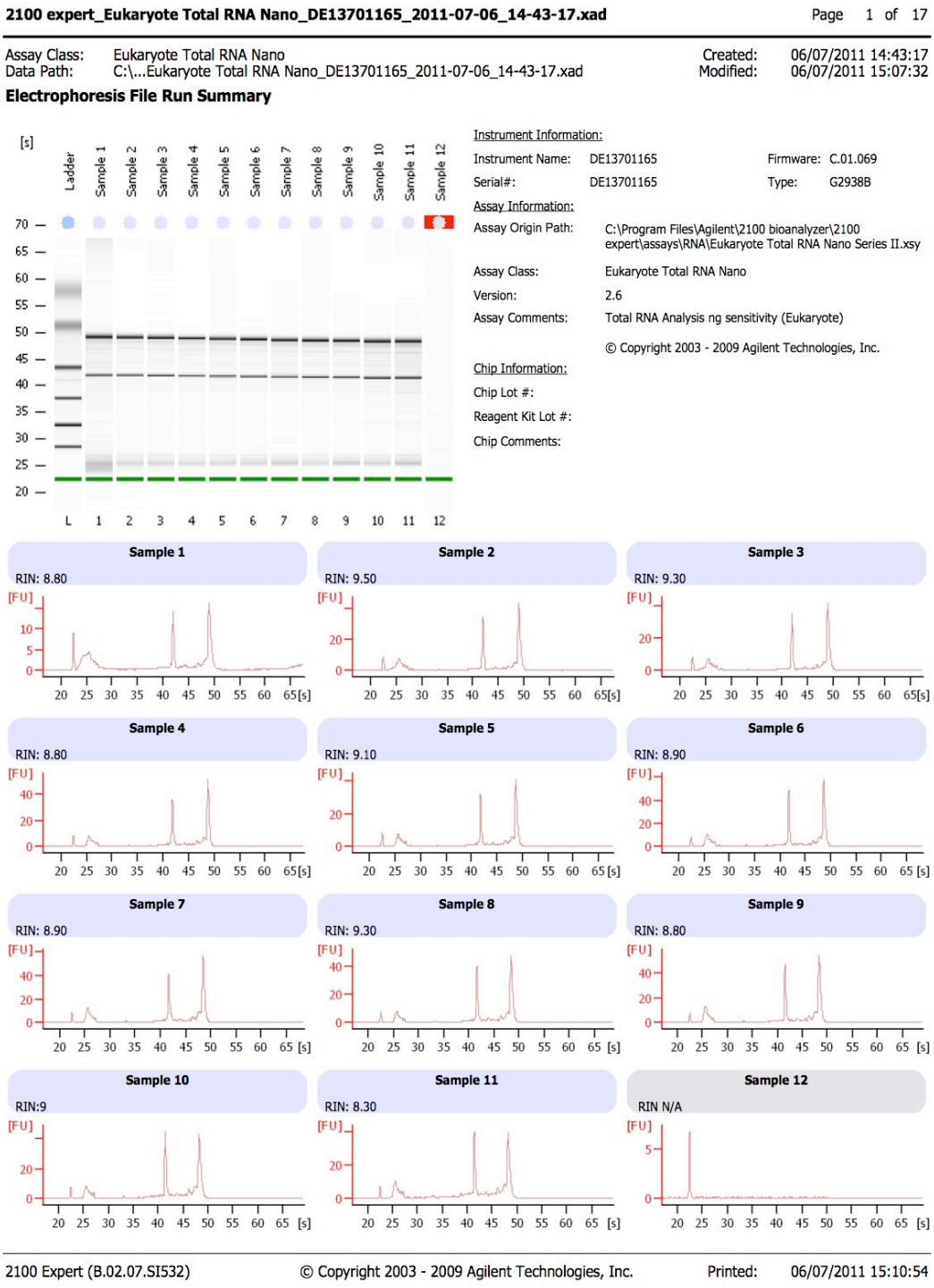

Figure 2-3 Example of Agilent bioanalyzer result

The X axis has units of seconds (s) whilst the Y axis is fluorescence units (FU). Sample 1-11 (rat liver and colon total RNAs) `+have RIN greater than 8. For sample 12 (rat total plasma RNA), the RIN cannot be detected. The two major peaks in sample 1-11 are the ribosome RNA 18s and 28s, respectively. In sample 12, due to the existence of RNase, there is no ribosome RNA detected.

2.3.4 Tissue RNA quantification (Nanodrop)

To measure the RNA concentration, a Nanodrop, micro-volume ultraviolet-visible spectrophotometer (Thermo Scientific, Germany), was used. Nanodrop measures the absorbance spectrum from 220nm to 350nm using 1-3 µL of the sample. RNA has maximum absorbance at 260nm and pure RNA has a 260:280 ratio of 2.0-2.1. Hence low 260:280 and 260:230 absorbance ratios indicate the presence of impurities in the samples. Generally, RNA could be defined as good quality with a 260:280 and 260:230 absorbance ratio ranging from 1.8 to 2.0. A low 260:230 ratio may be the result of residual phenol and guanine and further purification step should be added to increase the ratio.

2.4 PCR

2.4.1 Taqman the low density array card (TLDA)

In order to increase the small quantity of cDNA, the RT products were preamplified. A fixed amount of 2.5 µL RT product was combined with 12.5 µL Taqman PreAmp Master Mix (2×) and 2.5 µL Megaplex™ PreAmp Primers (10×) to generate a final 25 µL preamplification PCR mix. Preamplification was carried out by following the manufacture's instruction. The 10µL preamplification PCR product was diluted with 30µL 0.1XTE pH 8.0. The diluted preamplification PCR product was stored at -20ºC until required.

Diluted preamplification product (9µL) was combined with 450 µL Taqman universal PCR Master Mix (no AmpErase UNG, 2X) and 441µL RNase/DNase free water. QPCR reaction mix (100 µL) was loaded into each port of the TaqMan MicroRNA Array. The array card was centrifuged and then mechanically sealed with Applied Biosystems 7900HT upgrade kit. qRT-PCR reaction was carried out using an Applied Biosystems 7900HT thermocycler according to the manufacture's recommended conditions.

2.4.2 Taqman single microRNA/ mRNA qPCR

In order to detect individual microRNAs, Taqman microRNA assay was used. A fixed volume of 5µL of RNA solution from 100µL elute was used as input into each reverse transcription reaction. Since 100µL plasma was extracted and finally eluted with 100 µL RNase/DNase free water, 5 µL of RNA solution represents the RNA corresponding to 5 µL of plasma. For tissue/ cell extracted RNA samples, RNA were diluted to 2ng/µl. The RNA was reverse transcribed by Taqman microRNA reverse transcription (RT) kit and Taqman microRNA stem loop primers (Applied biosystems). Generally, a master RT master mix was made using 100mM dNTP, Multiscribe TM Reverse transcriptase, 10X Transcription

buffer, RNase inhibitor and DNase-RNase free water. The master mix differed between mRNA and microRNA. The master mix components are listed below (Table 2.1).

Table 2-1 Mix of Taqman qPCR for mRNA and microRNA

	mRNA RT mix (μL)	microRNA RT mix (μL)
10Xbuffer	2	0.75
dNTP	0.8	0.075
RT-primer	2	1.5
Reverse transcriptase	1	0.5
RNase inhibitor	1	0.08
Water	3.2	2.08
cDNA/ reverse transcribed RNA	10	2.5
Total reaction volume	20	7

RT product (2.4 μL) was then combined with 17.25 μL TaqMan® Fast Universal PCR Master Mix II (2×), no UNG, 1.725 μL TaqMan® Small RNA Assay (20×)/ Taqman mRNA Assay (20X) and 13.23 μL water to generate final 34.4 μL volume. Each qPCR plate well was loaded with 10μL mixture and all experiments were done in triplicate using an Applied Biosystem 7500HT fast system.

2.4.3 Semi-quantitative PCR

Traditional semi-quantitative PCR was performed for detecting PPAR downstream genes. A two step RT-PCR reaction was applied here. Both the reverse transcription step and PCR amplification step were carried out using a MJ Research Peltier PTC-200 thermocycler.

mRNA was reverse-transcribed (RT) into cDNA using MMLV reverse transcriptase (SuperScript II Reverse Transcriptase, Invitrogen). For a 25.5μL reaction, a total amount of 14μL RNA (500ng) was mixed with random hexamers, heated at 65ºC for 5 minutes and then placed on ice. RT master mix was then prepared with 1μL dNTP (10mM), 5μL first strand buffer, 2μL Dithiothreitol (DTT, to stabilise the enzyme) and 0.5μL MMLV superscript II. The mixture was gently mixed and run on the thermal cycler with program shown below (Table 2.2).

Table 2-2 Reverse transcript PCR program for mRNA expression

Temperature	Time
25ºC	10 minutes
42ºC	90 minutes
70ºC	15 minutes

In the PCR amplification step, a total amount of 18μL PCR master mix was made containing 0.5μL Tfi polymerase (Invitrogen), 4μL PCR reaction buffer, 1.2μL $MgCl_2$ (50mM), 0.4μL dNTp (10mM), 0.5μL PCR primer (both reverse strand and forward strand) and 11μL DNase-RNase free water. The solution was then mixed with 2μL cDNA and PCR reaction was then performed in the thermal cycler. An initial denaturation step was applied at 94ºC for 2 minutes. Thirty cycles of PCR were then performed with denaturing at 94ºC for 30 seconds, annealing (with different temperature for different genes) for 30 seconds, and elongation for one minute. After the completion of the designated number of cycles the protocol was completed by 5 minutes of extension at 72ºC.

Different genes require specific annealing and elongation time. The primers and PCR program of tested genes are listed below (Table 2.3). All primers were synthesised by

Sigma-Aldrich.

Table 2-3 Primer, Tm and product size of β-actin, ACO, Cyp4a1 and Fabp

Gene	Forward primer sequence	Reverse primer sequence	Annealing temperature	Product size
Beta-actin	cctctatgccaacacagt	agccaccaatccacacag	55ºC	125bp
ACO	attcggtgttgtaagtgc	ttggtgggtgggtgttga	55ºC	417bp
CYP4A1	caggccattgggaacttgaa	ggtccaggtgatcccaggtaa	57ºC	448bp
FABP	gcgatgggtctgcctgag	cacggactttatgcctttgaa	57ºC	243bp

Finally, PCR products were examined using electrophoresis through 2% agarose gels. Gels were made by adding agarose powder to 1xTBE buffer, made up from 10x TAE stock (Sigma-Aldrich), and heating it in a microwave oven to dissolve. Ethidium bromide (1μL in 50mL TBE agarose mixture) was added to the gels to allow visualisation of PCR products. Gels were then allowed to set in a tank for 30 minutes. For a 20 well gel, a total amount of 1.5μL PCR product was mixed with 7.5μL loading dye. Electrophoresis was setup at 100V for 30-60 minutes and PCR products were visualised by exposure to UV light using BioRad transilluminator. All PCR product quantification was performed using the Kodak Imaging Station 4000MM.

2.5 Illumina deep sequencing

MicroRNA library was prepared using Illumina TruSeq Small RNA sample preparation kit (Illumina) following the official preparation guide. Briefly, 1μg of total RNA was used for library construction. Firstly, both 3' and 5' adaptors were attached to the ends of the small RNAs and then the template was constructed by RT reaction and PCR amplification with a specific primer to tag each sample. The PCR amplification program is shown below (Table 2.4). To enrich and purify the construct, PCR product was fractionated using polyacrylamide gene electrophoresis and the bands between 145 to 160 bp were cut for further purification. All cDNA construct was assessed using Agilent bioanalyzer with Agilent High sensitive DNA kit (Agilent Technologies).

Table 2-4 PCR program for small RNA enrichment

Temperature	Time	Cycle
98ºC	30 seconds	1
98ºC	10 seconds	11
60ºC	30 seconds	
72ºC	15 seconds	
72ºC	10 minutes	1
4ºC	∞	1

MicroRNA-seq constructs were then run on the Illumina HiSeq machine at Genomics Lab, Hammersmith Campus, Imperial College London. The raw data was processed to demultiplex (separate the treatment by index) using CASAVA 1.8.2. Cutadapt 1.2.1 was then applied to trim the 3' adaptors and filter the sequence by size which left the sequence between 15 to 25 bp. FastQX (Babraham Institute) was then used to assess the quality control of the reads and Extract and Count Tool was applied to condense the reads into a text file only containing the nucleotide sequence and the number of times it occurred. All

text files were then analysed using miRanalyzer V0.2 (http://bioinfo5.ugr.es/miRanalyzer/miRanalyzer.php) which was used to generate a list of differential expressed microRNAs and all potential novel non-coding RNAs.

2.6 Protein extraction and quantification

2.6.1 Tissue protein extraction us RIPA buffer

Whole liver extract was prepared using RIPA buffer (SIGMA-Aldrich). Approximately 50mg of liver tissue was homogenized with 500 µL RIPA buffer containing 1% protease inhibitor cocktail (SIGMA-Aldrich). Samples were centrifuged at 12,000 rpm for 5 minutes. The aqueous phase protein was collected and immediately frozen at 80ºC.

2.6.2 BCA assay for protein quantification

Protein concentrations were determined using the bicinchoninic assay (BCA, Thermo Scientific). Briefly, protein samples and pre-diluted standard proteins were measured simultaneously. Twenty five µL of a protein sample was placed into a well of a 96 well plate with 200µL working solution (containing 100µL A and 100µL B solution). Protein samples/standards were mixed with working solution gently and then incubated at 37ºC for 30 minutes. Protein concentration was then determined by measuring the absorbance at 560nM on a FluoStar micro plate reader. Protein concentrations were determined through a standard curve. The protein samples used in this study were extracted from two batches. Both sets of BCA standard curve are shown below (Figure 2.4).

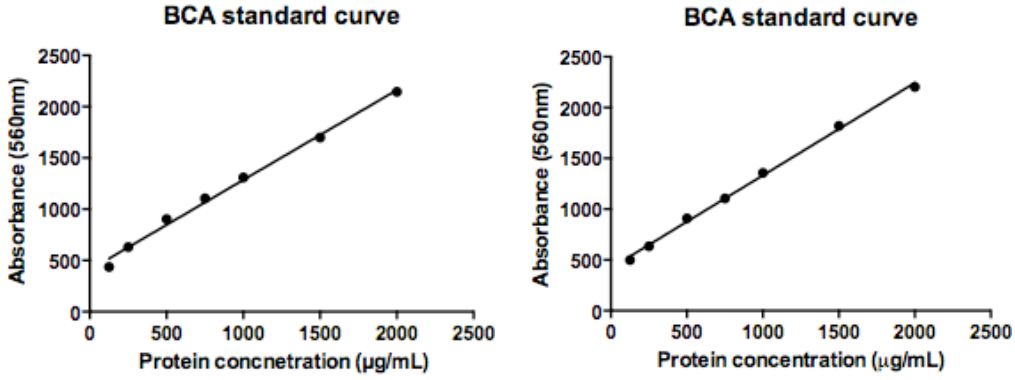

Figure 2-4 BCA standard curve.

The x axis is the protein concentration, and the y axis is the absorbance at 560nm.

2.7 Immunoblot

Briefly, 20 µg of protein was separated by 10% SDS-PAGE gel. The protein was then electro-transferred onto wet nitrocellulose membrane. The nonspecific binding sites were blocked for 1 hour and incubated with primary & secondary antibodies. Membranes were washed and visualised by chemiluminescent regent (Merck Millipore) with BioRad imaging system.

2.7.1 Protein sample preparation

Protein samples were diluted to 20µl (20µg) with water. All protein samples, chemiluninescent ladder (5µl, Cell signalling) and Novex Sharp Pre-Stained Protein Standards (5µL, Invitrogen) were mixed with loading buffer prepared on day of use (66mM Tris pH6.8, 26%w/v glycerol, 2.1%w/v SDS, 0.01%w/v bromophenol blue and 5%v/v β-mercaptoethanol) and heated to 95°C for 5 minutes to allow denaturation. Following denaturation, all samples and ladders were centrifuged at 10000 rpm for 5 minutes and the supernatants were loaded on to a SDS polyacrylamide gel.

2.7.2 SDS-PAGE gel eletrophorse

All samples and ladders were electrophoresed at 60v in stacking gel composed of 5%w/v acrylamide, clean water, 0.07%w/v fresh ammonium persulphate and 1x SDS stacking gel buffer composed of 0.125M Tris pH6.8 and 0.1%w/v SDS until all samples were properly lined up. A voltage of 100v was then applied to allow sufficient separation in resolving gel (10%w/v acrylamide, water, 0.07%w/v fresh ammonium persulphate and 1x SDS resolving gel buffer composed of 0.6M Tris pH8.8 and 0.16%w/v SDS). 2.7.3 Protein transfer

Briefly, a transfer sandwich was made with two sponges, two filter cards and a nitrocellulose membrane. Wet transfer (with transferring buffer) was used in all experiments. Transfer was performed in 1x transfer buffer at 150V, 400mA for 75 mins. An ice block was inserted into the tank in order to maintain a cool transferring temperature. The result of protein transfer was confirmed with ponceau red staining (0.1% Ponceau S w/v in 5% v/v acetic acid, Sigma Aldrich). Ponceau red was washed with PBS-T (1x phosphate buffered saline and 0.1%v/v Tween-20) three times after visualisation.

2.7.4 Blocking and antibody incubation

All blots were incubated with blocking buffer (PBS-T plus 5%w/v semi- skimmed milk powder) for 1 hour at room temperature. Blots were then incubated with primary antibodies (dilutions are shown below, table 2.5) overnight at 4ºC. Blots were then washed with PBS-T 3 times and incubated with secondary horseradish peroxidise (HRP) conjugated antibody (dilutions are shown below, table 2.5) for 1 hour at room temperature. All blots were washed with PBS-T 3 times and stained with 5mL Lunminata Forte Western HRP Substrate (Millipore). All blots were visualised and quantified with Kodak IS4000MM station.

The following primary antibodies were used with all dilution listed below (Table 2.5): citrate synthase (Abcam, ab129095), uncoupling protein 2 (Abcam, ab67241), AMP-activated protein kinase beta1 (Abcam, ab32112), Phospho-AMPKβ1 (Ser108) Antibody (4181, New England Biolabs) and anti-β actin antibody (Sigma-Aldrich). Secondary anti-mouse and anti-rabbit antibodies were all purchased from Abcam.

Table 2-5 Immunoblot antibody dilution ratio

Antibodies	Dilution of primary antibody	Secondary antibody	Dilution of secondary antibody
CS	1:1000	anti-rabbit	1:10000
UCP2	1:500	anti-mouse	1:2500
AMPKβ1	1:1000	anti-rabbit	1:1000
phospho-AMPKβ1	1:1000	anti-rabbit	1:1000
β-actin	1:1000	anti-mouse	1:10000

3. Effect of Roux-en-Y gastric bypass surgery on rat microRNAome

3.1 Introduction

Obesity and its co-morbidities including cardiovascular disease and type 2 diabetes have become one of the biggest socioeconomic problems worldwide. Currently, bariatric surgery is the most effective treatment strategy for morbidly obese patients. The “gold standard” Roux-en-Y gastric bypass (RYGB) is the most widely used procedure (Maggard *et al*. 2005). Surprisingly, RYGB surgery not only provides sustained long-term weight loss, but also resolves type 2 diabetes within days after surgery (Buchwald, Avidor, Braunwald, Jensen, *et al*. 2004b). These intriguing post-surgery effects have led to a rising number of research studies, which mainly focused on the alteration of gut hormones, postoperative metabolism and the shift of gut microbial composition. However, the fundamental molecular mechanisms, which could explain these changes, have not yet been completely clarified.

As described in the introduction chapter, microRNAs have begun to emerge as key metabolic regulators. MicroRNAs are controlled by metabolic stimuli, such as food borne nutrients or hormones (Dumortier *et al*. 2013). At the same time, microRNAs control metabolic processes by regulating their targets. This bidirectional crosstalk has led to an interesting hypothesis that microRNA behavior is a link between metabolic stimuli and the host energy homeostasis. For patients undergoing RYGB surgery, it is likely energy homeostasis is altered by the drastic anatomical changes and that a novel metabolic balance could be subsequently established. The molecules, which are involved in these processes, may also contribute to the various post surgery benefits. Here, plasma and

colonic tissue were used to investigate the impact of RYGB surgery on circulating and local microRNAome, respectively.

In this chapter, the global circulating and colonic microRNA expression from RYGB- and SHAM-operated healthy male Sprague Dawley (SD) rats was profiled at 8 weeks post surgery, using microRNA Taqman low density array card (TLDA) and Illumina deep sequencing platform, respectively.

3.2 Methods

1. Roux-en-Y gastric bypass surgery is described in 2.1.1
2. Tissue samples collection is described in 2.1.2
3. Tissue total RNA extraction is described in 2.3.2
4. Tissue RNA quantification and quality assessment is described in 2.3.3
5. Taqman low density array card preparation is described 2.4.1
6. Taqman single microRNA assay is described 2.4.2
7. Illumina deep sequencing procedure is described 2.5

3.3 Result with discussion

3.3.1 Clinical effects of RYGB surgery on rats

Data relevant to the effects in post RYGB surgery rats are presented in Figure 3.1. The daily body weight and gut hormone level of all animals were determined by Dr. Florian Seyfried and are presented here to profile the overall post surgery changes. The RYGB surgery induced a reduction of 22.0% of pre-surgical body weight (BW) in SD rats (n=8) over 52 days (pre-surgery BW=467.9±12.9g, post-surgery BW=377.75±33.9g), whereas sham animals (n=5) maintained an average of body weight of 573.2 g. Similar to previously reported observations by others (Roux *et al*. 2006), we also observed altered plasma concentrations of gut hormones, e.g., GLP-1 and PYY were significantly elevated following RYGB surgery (GLP-1RYGB=71.5±11.7 pmol/L, GLP-1SHAM=10.5±3.3 pmol/L, p<0.001; PYYRYGB=26.2±5.6 pmol/L, PYYSHAM=10.4±4.8 pmol/L, p<0.001).

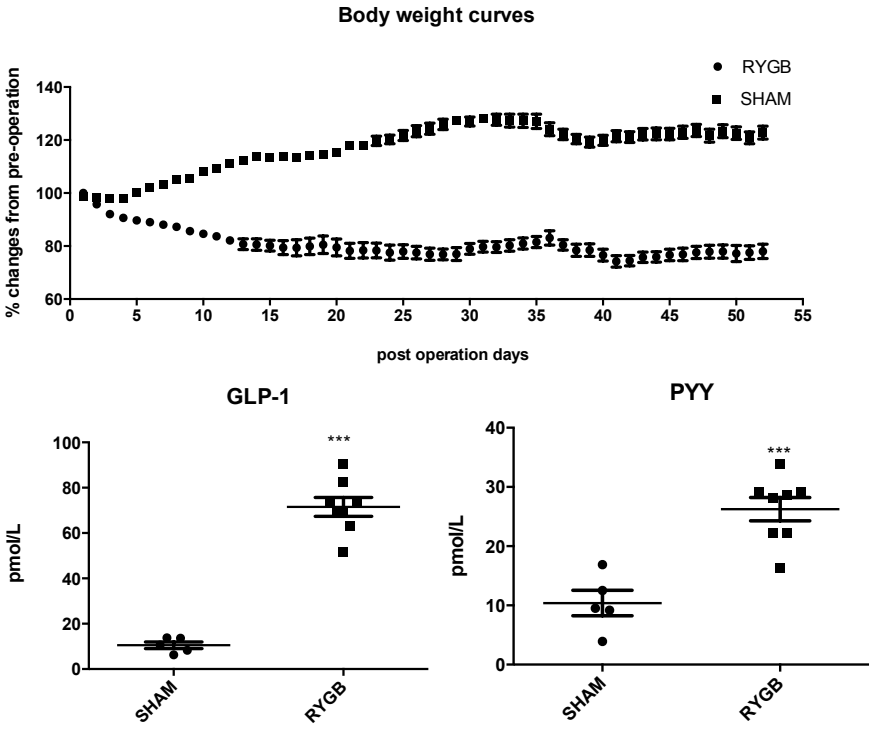

Figure 3-1 Body weight and gut hormone of RYGB and SHAM operated rats

(A) Daily body weight and circulating gut hormones expression

The body weights were measured daily and data presented as body weight alteration ± SD compared to day 0 (surgical day). (RYGB n=8 and SHAM n=5)

(B) Gut hormones (GLP-1 and PYY)

Data are expressed as mean with SEM. **and*** stands for p<0.01 and p<0.0001 of RYGB vs SHAM operated, using a student t test.

3.3.2 Circulating microRNA profiles after RYGB surgery

3.3.2.1 Circulating microRNA isolation, spike-in optimisation and profiling method selection

Plasma total RNA extraction method was optimised by comparing the mirVANA microRNA isolation kit (Ambion, Applied Biosystems Inc.), TRIzol reagent (Invitrogen) and mirVANA PARIS kit (Ambion, Applied Biosystems Inc.). MirVANA PARIS kit was found to be the most robust extraction approach and was selected for examination of all plasma samples in the current study. As previous studies suggested (Mitchell *et al*. 2008), synthetic *Caenorhabditis elegans* cel-mir-39 (5 fmol/µl cel-miR-39) was added to the solution of the plasma and denature solution mixture (100µl plasma diluted with 100µl cell disruption buffer and 200µl denature solution), as an internal standard. In order to find the optimal protein denaturation time, the pooled plasma sample was divided into three aliquots and incubated with 2 X denature buffer for 0 minute, 5 minutes and 20 minutes with multiple concentration of cel-miR-39 (e.g., 25 fmol, 50 fmol, 250 fmol and 500 fmol). The quantitative PCR results suggested 5-minutes incubation time with 250 fmol spike-in cel-miR-39 was optimal. Hence, all of the plasma samples were extracted as described above.

Since microRNAs are present at much lower concentrations in plasma compared with that in other tissues, detecting and analyzing them are a real challenge. There are several technologies available for circulating microRNA profiling, such as deep sequencing, microRNA microarray and quantitative real-time PCR (qRT-PCR). Illumina microRNA deep sequencing and Agilent microRNA microarray methods require good quality total RNA (Agilent Bioanalyzer RNA integrity number higher than 8) and a minimum RNA loading amount of 200 ng/µl (5µl) and 150ng/µl (5µl), respectively. However, the Bioanalyzer quality indicator (RNA integrity number, RIN) uses ribosomal RNA as internal control and

the lack of ribosomal RNA in plasma means that successful RIN determination is not possible. Thus, total circulating RNAs cannot achieve the required quantity and quality metrics. In fact, typical concentrations of plasma RNAs are only around 2.5 ng/mL plasma (RYKOVA *et al*. 2006). Therefore, it is technically difficult to profile circulating microRNAs by microarray or deep sequencing methods unless the volume of the plasma sample being examined is greater than 50mL. The most widely used circulating microRNA profiling tool is qRT-PCR which has the highest specificity and sensitivity. A previous study showed that qRT-PCR is sensitive enough to detect as little as 8 copies of a target RNA in the sample and 220 microRNAs can be detected even in a single cell (F. Tang *et al*. 2006). Hence, I used TLDA card, which is essentially parallel qRT-PCR for all detectable expressed microRNAs in rats, to profile the microRNAome of 4 post RYGB and 4 sham-operated SD rats.

Firstly, to assess the efficiency of plasma total RNA extraction and evaluate the quality and quantity of RNA samples, constitutively expressed miR-16 was examined using single Taqman microRNA RT-qPCR. As shown in Table 3.1, all 8 samples (4 RYGB and 4SHAM) exhibited measureable and consistent amounts of circulating miR-16 levels (Ct value of 23 approximates 10,000 copies of microRNA). Four biological replicated were profiled here, while all the results were confirmed with 13 rats. This data indicates a successful extraction of plasma RNAs and relatively similar extraction efficiency.

Table 3-1 Quality control miR-16 expression pre-test in all TLDA tested samples

	RYGB operated rat				SHAM operated rat			
Circulating miR-16 Ct	23.25	23.5	23.24	23.11	23.49	23.65	23.25	23.2

MiR-16 was detected by Taqman microRNA RT-qPCR (Probe No. 000391). Technical triplicates were loaded in qPCR plates. Negative control was set with qPCR master mix without reverse transcribed microRNA. All amplification curves were adjusted using auto-baseline correction and fix threshold of 0.2. Data presented here is the raw cycle of threshold (Ct) value.

3.3.2.2 Pre-processing the raw data of microRNA low density array card

Taqman Array Rodent Card is able to detect 373 microRNAs expressed in the rat base Sanger miRBase V15 (The current miRBase records 728 mature Rattus norvegicus microRNAs). Each complete assay contains two sets of cards (Card A and B). Card A detects well-characterized microRNAs, which tend to be functionally defined or highly expressed, while Card B detects most of the recently discovered, less functionally defined and narrowly or low expressed microRNAs. The raw data from microRNA TLDA card was first processed by Applied Biosystems commercial software SDS V2.4. Cycle threshold (Ct) value was calculated by SDS V2.4 with an automatic baseline correction and fixed threshold of 0.2. The optimised plots of ΔRn vs cycle of all microRNAs are presented below (Figure 3.2).

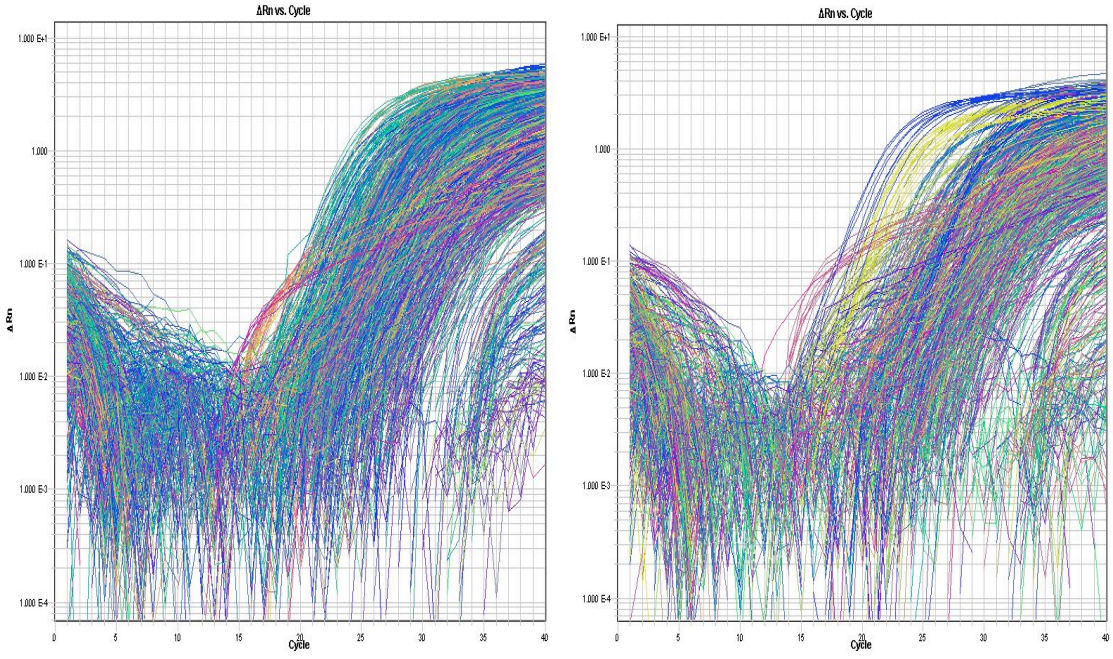

Figure 3-2 ΔRn vs Cycle plot for Taqman ® Array Rodent Card (A+B)

With automatic baseline correction, fixed threshold of 0.2 (Rn is the fluorescence of the reporter dye divided by the fluorescence of a passive reference dye and ΔRn is Rn minus the baseline

Mammalian U6 non-coding RNA was set by TLDA as a quality control and both A and B cards contain 4 wells to evaluate U6 expression. As seen in Table 3.2, the raw U6 Ct values for each of the samples were relatively consistent and stable across all cards, with no obvious outliers.

Table 3-2 TLDA Quality control U6 expression

Mamm U6 Ct Value	Card A (4 replicates)				Card B (4 replicates)			
RYGB 1	24.46	24.51	24.72	25.13	25.07	24.95	25.08	25.05
RYGB 2	24.56	24.39	25.23	25.89	25.68	25.78	25.79	25.43
RYGB 3	25.37	24.86	25.06	24.96	25.37	25.30	25.69	25.47
RYGB 4	23.62	23.12	23.16	23.47	23.35	23.00	23.18	23.35
SHAM 1	25.27	25.29	25.00	25.28	24.71	25.42	25.50	25.45
SHAM 2	25.33	25.31	25.34	24.93	26.41	26.69	26.56	26.74
SHAM 3	26.59	26.72	26.59	26.43	27.09	27.23	27.28	27.03
SHAM 4	26.23	25.98	26.04	25.88	27.03	27.10	26.57	26.73

Raw U6 Ct values were extracted using Invitrogen TLDA software SDS V2.4. All amplification curves were adjusted using auto-baseline correction and fix threshold of 0.2. Data presented here is the raw cycle threshold (Ct) value.

Boxplots were then constructed based on all microRNA adjusted Ct values with all 8 samples using automatic baseline correction and a fixed threshold of 0.2. The minimum and maximum number of all data within the box included the first quartile (the middle number between the smallest number and the median of the data) and third quartile (the middle value between the median and the highest value of the data). Overall, the raw data exhibited a comparable distribution crossing all samples.

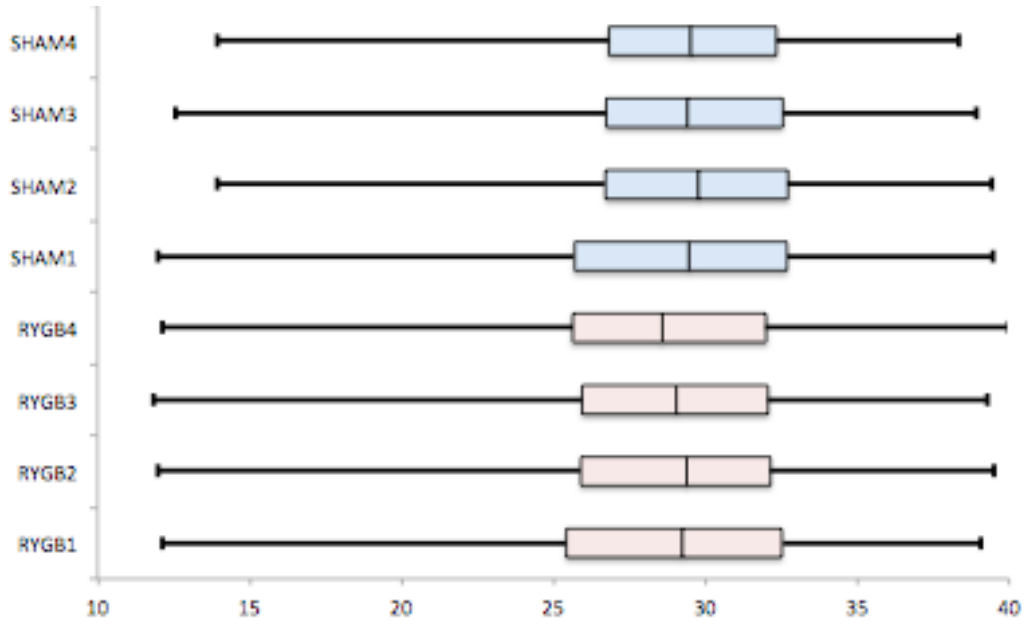

Figure 3-3 Boxplot of adjusted Ct values with all TLDA tested samples

Plot displays the 25th percentile (left end of box), 75th percentile (right end of box), and median (line in the middle of box). Whiskers contain the1.5 interquartile.

3.3.2.3 Normalization method comparison

There are two sources of variation in microRNA expression analysis, biological variation and technical variation. The aim of normalization is to reduce the technical variation to better show biological difference. A Ct value of 35 means there is one copy of the target microRNA in a sample. According to the manufacture's recommendation, a Ct value of 32 (8 copies of target) is used as a threshold and microRNA Ct value less than 32 is defined as expressed. Only expressed microRNA targets (Ct<32) were included in analysis. Although there are a few studies published on plasma/serum circulating microRNAs, there is still no consensus on the most appropriate method of normalization. Thus, we tested four widely used normalization methods including *C.elegans* spike-in, global, U6 and multiple endogenous microRNAs normalization (Y. Zhang *et al*. 2010; X. Chen *et al*. 2008).

In order to select appropriate endogenous microRNAs for normalization, the stability of potential endogenous microRNA normalizers were first checked. The U6 small nuclear RNA (Mamm-U6) is the most frequently used reference gene. There are four detection wells in both A and B Taqman microRNA rodent cards and average expression are presented as Mamm-U6-01 and Mamm-U6-02. Both were included as normalizer candidates. MiR-16 has been widely used as plasma/serum reference gene and was identified as consistently expressed in previous research (Resnick *et al*. 2009). MiR-223 and miR-1937b were found to be well expressed and relatively consistent in our data across all eight rats. Thus, these five microRNAs were selected as normalizers. The Ct value for these five microRNAs ranged from 19.99 to 26.84 and the average Ct values were 20.91, 21.80, 23.85, 24.89 and 25.56 for mmu-miR-1937b, mmu-miR-16, mmu-miR-223, Mamm-U6-02 and Mamm-U6-01, respectively (Figure 3.4). The expression levels of these five endogenous microRNA shared a similar pattern and were consistent across all of our samples.

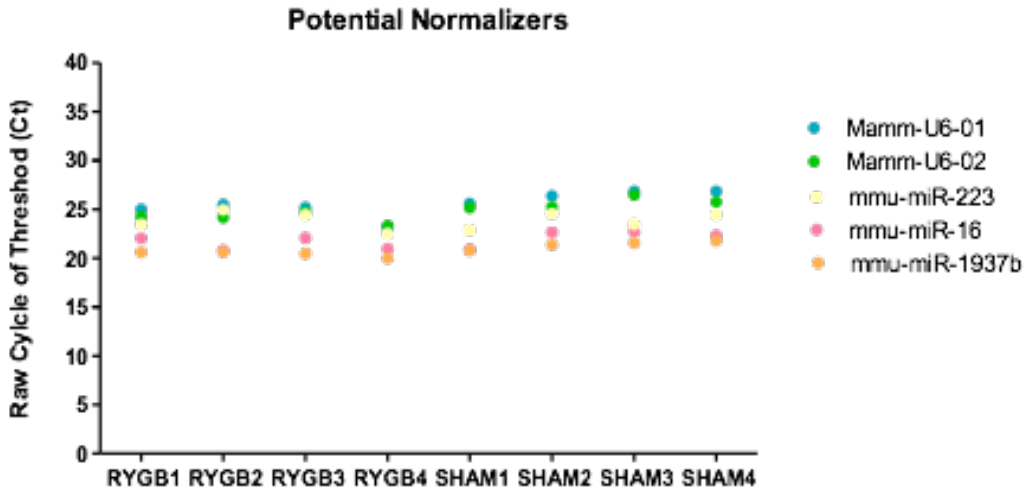

Figure 3-4 Raw Ct value of 5 endogenously expressed normalizer microRNAs

Plot displays the non-normalized raw Ct values of 5 endogenous microRNA normalizer candidates. Ct values were calculated using auto-baseline correction and fixed threshold of 0.2.

The coefficient of variance (CV) of normalized RQ (fold change) for each expressed individual microRNA was then calculated. Calculation details are presented below (Figure 3.5). All four methods were analyzed and the cumulative distribution of RQ CV with four normalization method and un-normalized data were ranked and plotted to select the best one.

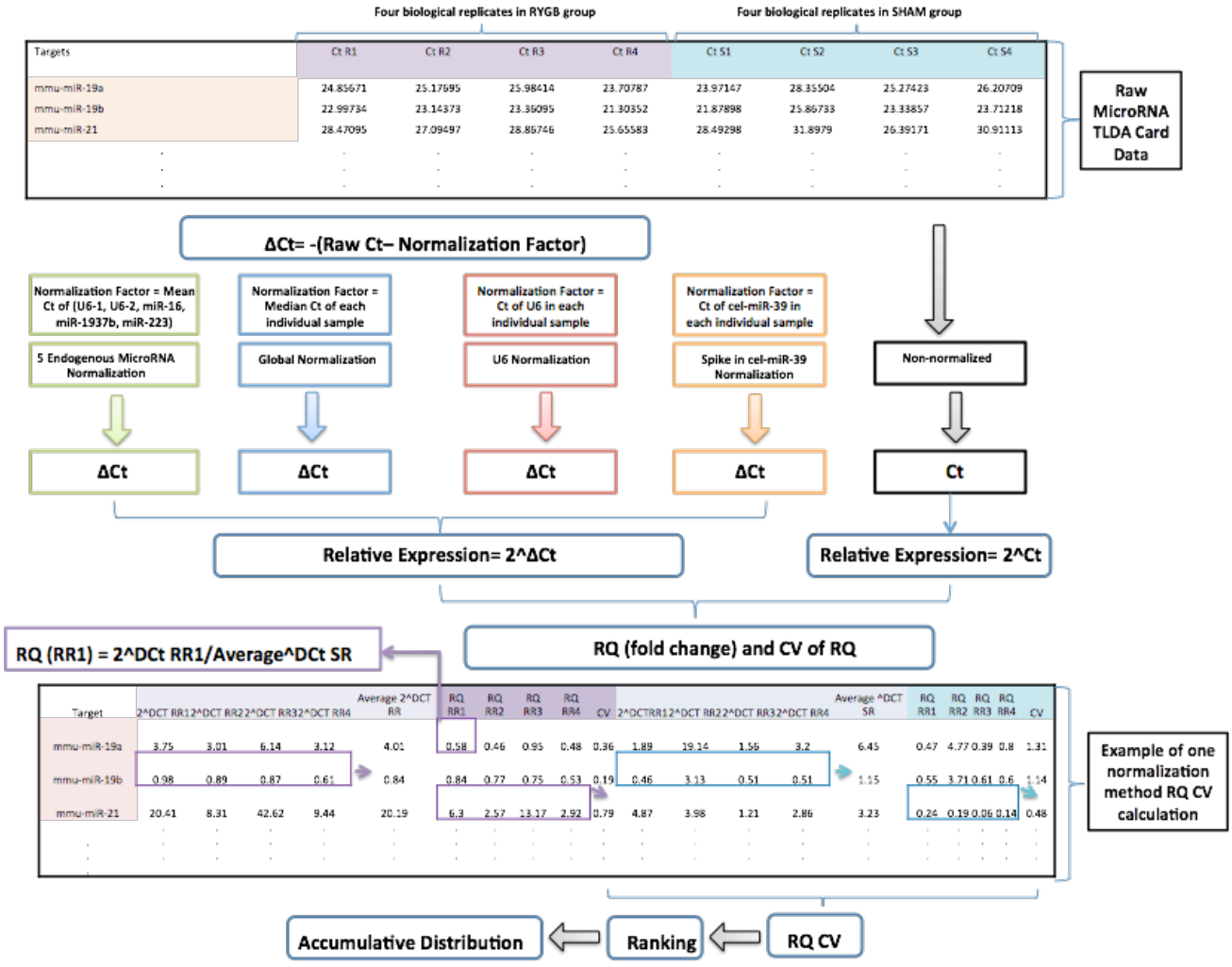

Figure 3-5 The cumulative distribution calculation method of the coefficient of variance (CV) of normalized RQ (fold change)

Four different normalizers were calculated first based on four different normalization methods. All raw Ct values were normalized by the normalizers and non-normalized Ct was used for comparison. Normalized Cts were anti-log2 transformed to acquire relative microRNA expression value. Fold changes (RQ) of RYGB/SHAM were then calculated for all microRNAs. The coefficient of variance (CV) values were finally ranked and plotted in order to visualize the result.

RQ CV of the data was compared using the different normalization methods (Figure 3.6). Normalization using global and U6 clearly result in decreased CV values, but normalizing with the 5 endogenous microRNAs significantly reduced the overall CV values. The widely used spiked-in cel-miR-39 normalization method, on the other hand, led to a more variable data set than the non-normalized one. It may be due to the fact that synthesis of single strand cel-miR-39 RNA is not as stable as plasma microRNAs, which are bound with AGO protein. Although multiple optimization experiments were carried out to choose optimal spike-in amounts and time points, cel-miR-39 could still be partially degraded, which led to the large variance of the normalized data. Hence, the 5 endogenous microRNAs normalization was determined as the optimal method and, therefore, selected for all downstream analysis.

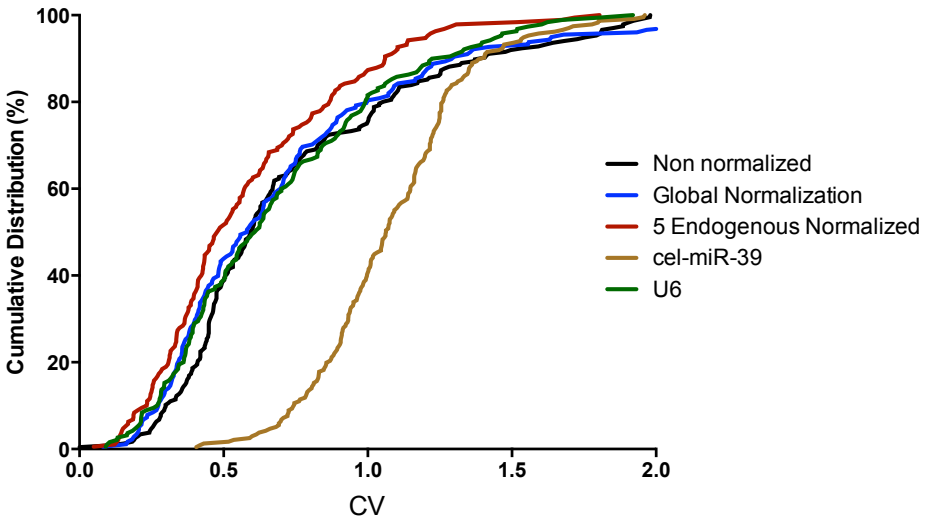

Figure 3-6 Cumulative distribution with four normalization method of microRNA RQ (fold change) verses coefficient of variation (CV) values

3.3.2.4 Overall circulating microRNA profile

The circulating microRNA profile of the RYGB and SHAM operated rats were analysed using the 5 endogenous microRNAs normalization method. MicroRNAs were defined as expressed only if it could be detected in three out of four biological replicates which belong to the same biological group. As shown in Figure 3.7, 113 microRNAs were present in RYGB surgical rats, while 92 microRNAs were detected in SHAM operated ones. Among these expressed microRNAs, 88 of them were detected in both RYGB and SHAM operated rats, while 25 and 4 of them were only expressed in RYGB and SHAM rats, respectively. The list of these detectable microRNAs can be found in Table 3.3.

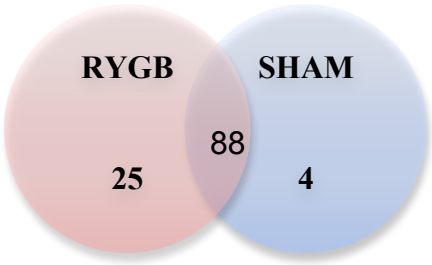

Figure 3-7 Detectable circulating microRNA number in TLDA tested samples

Table 3-3 All detectable circulating microRNAs in RYGB and SHAM operated rats

only in RYGB	Only in SHAM	Common	
hsa-miR-206	mmu-miR-122	hsa-miR-140-3p	mmu-miR-1971
hsa-miR-421	mmu-miR-130a	hsa-miR-200c	mmu-miR-19a
mmu-miR-1188	mmu-miR-197	hsa-miR-214	mmu-miR-19b
mmu-miR-15b	mmu-miR-222	hsa-miR-223	mmu-miR-20a
mmu-miR-1928		hsa-miR-30a-3p	mmu-miR-2134
mmu-miR-194		hsa-miR-30e-3p	mmu-miR-2138
mmu-miR-1961		hsa-miR-93*	mmu-miR-21
mmu-miR-203		Mamm U6	mmu-miR-215
mmu-miR-2146		mmu-let-7c	mmu-miR-223
mmu-miR-2183		mmu-miR-106a	mmu-miR-24
mmu-miR-218		mmu-miR-106b	mmu-miR-25
mmu-miR-30d		mmu-miR-125b-5p	mmu-miR-26a
mmu-miR-34b-3p		mmu-miR-126-3p	mmu-miR-26b
mmu-miR-34c*		mmu-miR-126-5p	mmu-miR-27a
mmu-miR-363		mmu-miR-1274a	mmu-miR-27b
mmu-miR-434-3p		mmu-miR-1-2	mmu-miR-29a
mmu-miR-463*		mmu-miR-133a	mmu-miR-29b*
mmu-miR-467b		mmu-miR-138	mmu-miR-29c
mmu-miR-532-3p		mmu-miR-139-5p	mmu-miR-301a
mmu-miR-685		mmu-miR-140	mmu-miR-30a
mmu-miR-694		mmu-miR-142-3p	mmu-miR-30b
mmu-miR-712		mmu-miR-1	mmu-miR-30c
mmu-miR-721		mmu-miR-145	mmu-miR-30e
mmu-miR-877*		mmu-miR-146a	mmu-miR-31
rno-miR-190b		mmu-miR-148a	mmu-miR-320
		mmu-miR-150	mmu-miR-328
		mmu-miR-152	mmu-miR-335-3p
		mmu-miR-155	mmu-miR-342-3p
		mmu-miR-16	mmu-miR-375
		mmu-miR-17	mmu-miR-451
		mmu-miR-186	mmu-miR-463
		mmu-miR-188-5p	mmu-miR-465C
		mmu-miR-1894-3p	mmu-miR-466k
		mmu-miR-1896	mmu-miR-652
		mmu-miR-1897-5p	mmu-miR-673
		mmu-miR-1904	mmu-miR-720
		mmu-miR-191	mmu-miR-744
		mmu-miR-192	mmu-miR-872
		mmu-miR-1937b	mmu-miR-92a
		mmu-miR-1937c	rno-miR-1
		mmu-miR-193b	rno-miR-146B
		mmu-miR-1951	rno-miR-632
		mmu-miR-195	rno-miR-664
		mmu-miR-1969	rno-miR-7*

3.3.2.5 Clustering analysis of microRNAs

We then generated an overall view of microRNA expression profiles using principal component analysis (PCA). PCA, an unsupervised method which is a linear rearrangement of the original variables, is widely used to analyse massive data sets such as gene express data, which contain much larger numbers of variables than observations (Yeung & Ruzzo 2001). PCA was performed here to find combinations of microRNAs differentiating between RYGB and SHAM operated rats. Figure 3.8 shows the PCA scores plot of all microRNA expression including both the expressed and non-expressed ones. Clear separation can be seen between RYGB group (red) and SHAM group (blue), which indicates alterations in rat circulating microRNAome after RYGB surgery.

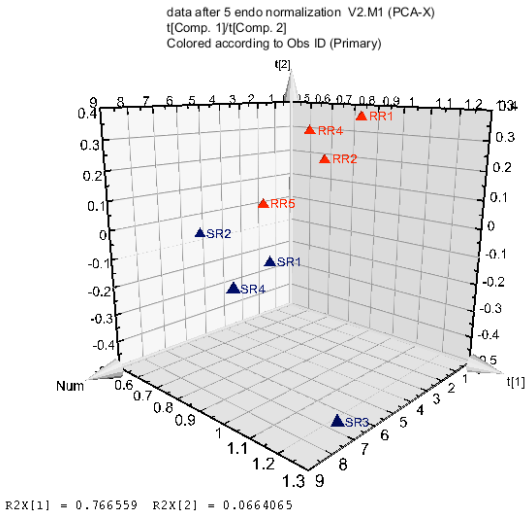

Figure 3-8 PCA of normalised microRNA expression in 8 TLDA tested samples

Each symbol represents one biological sample, with its colour indicating the group to which it belongs to (Blue=SHAM, Red=RYGB)

3.3.2.6 Identification of differentially expressed microRNAs

A two-tailed Student's t-test was carried out on the normalized circulating microRNA data to determine the statistically differentially expressed microRNAs between RYGB and SHAM operated group. Fourteen microRNAs were found to be differentially expressed at a significance level of 0.05 (Figure 3.9). Eleven of the altered microRNAs were significantly down-regulated (e.g. miR-122, miR-93*, miR-872*, miR-7*, miR-146a, miR-342-3p, miR-150, miR-139-5p, miR-30a-3p, miR-30e and miR-320), whereas 3 microRNAs, namely, miR-463*, miR-34c* and miR-1188, were up-regulated in the RYGB group. Compared to sham-operated rats, these RYGB-altered microRNAs vary within a range of 1.5 to 6 fold change with the exception of miR-122, which exhibited a 56-fold down-regulation in RYGB animals. MiR-122 is a liver-enriched microRNA which is highly active in a number of metabolic processes, e.g. cholesterol synthesis and fatty acid beta-oxidation (Esau *et al*. 2006; Elmen *et al*. 2008). Due to its dramatic change and important metabolic function, I subsequently focused on validation and metabolic function examination of miR-122 after bariatric surgery in Chapter 4.

Besides miR-122, a few other microRNAs, which were found here to be differentially expressed, have also exhibited interesting metabolic function, reported in previous studies. For instance, the expression of miR-146a was significantly decreased in PBMCs from type 2 diabetes patients compared to control subjects (Balasubramanyam *et al*. 2011). Additionally, the reduced miR-146a level in PBMC was highly associated with insulin resistance, poor glycemic control and the concentration of several circulating pro-inflammatory cytokines (TNFa and IL6) (Balasubramanyam *et al*. 2011). MiR-320 is another well-studied microRNA, which has been linked with insulin resistance. MiR-320 can inhibit insulin–PI3-K signalling in adipocytes, resulting in insulin resistance (Ling *et al*.

2009). Moreover, miR-320 targets p85, which plays a critical role in cell growth by increasing Akt phosphorylation and thus the level of Glut4 (Ling *et al*. 2009). The decreased miR-320 in our study may also be associated with improved insulin resistance post RYGB. Finally, circulating miR-1188 was found to be down-regulated 1.7 fold in newly diagnosed diabetic cats, together with 45 fold up-regulation of miR-122 (Fleischhacker, Bauersachs, Wehner, Hartmann & Weber 2013b). The up-regulated miR-1188 and significant down-regulation of miR-122 in my study is consistent with an anti-diabetic effect of RYGB.

Another interesting finding is that among 11 differentially expressed microRNAs, 7 are reverse strand microRNA labeled with "*" or "-3p". As mentioned in the introduction, microRNA synthesis generates equal amounts of microRNA duplexes, but their individual strand accumulation is mostly asymmetric at the steady state. The most abundant strand is referred as forward strand microRNA (-5p), whereas the less abundant strand is referred as passenger strand/ reverse strand (*/3p). An siRNA study revealed that the relative thermodynamic stability of the ends of the duplex determines which strand is to be selected (Petri *et al*. 2011). Interestingly, another quantification experiment demonstrated that although the presence of microRNA* strand is universal, specific accumulation was found with certain microRNA species (Kuchenbauer *et al*. 2011). Here, the multiple reverse strand microRNAs were found to be differentially expressed, highlighting the importance of these long ignored microRNAs and also sheds some light on their potential metabolic related functions

microRNAs	Fold change	p value
miR-93*	-3.34	0.0008
miR-463*	5.74	0.0028
miR-146a	-3.63	0.0029
miR-122	-56.81	0.0095
miR-34c*	11.19	0.01
miR-872*	-1.84	0.0103
miR-30a-3p	-1.81	0.0153
miR-150	-1.92	0.0162
miR-7*	-3.42	0.0164
miR-139-5p	-2.17	0.0179
miR-30e	-1.62	0.0219
miR-320	-3.33	0.0249
miR-342-3p	-3.65	0.0374
miR-1188	5.39	0.0377

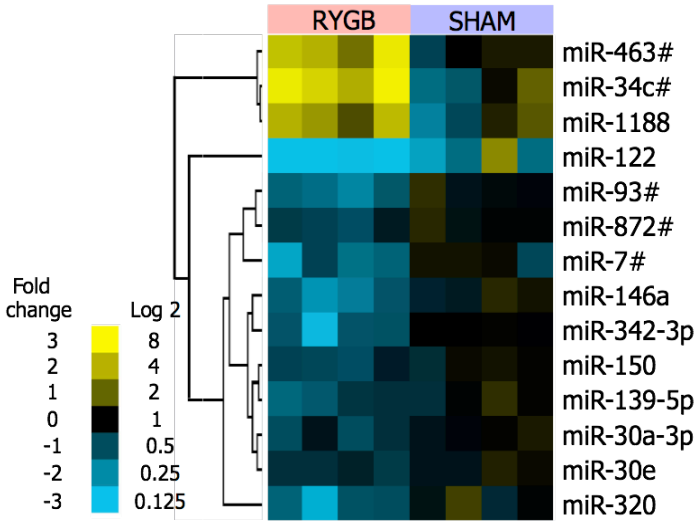

Figure 3-9 Differentially expressed circulating microRNA after RYGB

A. Differentially expressed circulating microRNAs

Fold change is the microRNA expression ratio between the two experimental conditions: positive/yellow means that microRNA is up- regulated at RYGB compared with SHAM; negative/blue means repressed in RYGB. p-value was calculated by unpaired student t test.

B. Clustering heat map of differentially expressed microRNAs

Heatmap and clustering of significantly changed plasma microRNAs in RYGB operated and SHAM operated group. The calculated value are log2 transformed microRNA fold change (RYGB/SHAM). Samples were clustered using Spearman's correlation. Yellow colour means up regulated in RYGB group, while blue means down-regulated in RYGB.

3.3.2.7 MicroRNAs-metabolite correlation

In addition to the microRNA target prediction based on the their nucleotide compositions, three data sets, i.e. metabolite profiles, microRNA expression profiles and the peptide gut hormones were statistically integrated in order to probe transgenomic-metabolic interactions following RYGB surgery. A correlation map was generated by Dr. Jia Li (Collaborator, Imperial College London) in order to aid understanding of post surgical metabolic alteration and the relationship with microRNAs (Fig 3.12).

MicroRNAs are linked to cellular metabolism *via* two directions: (1) microRNAs can be regulated by the cellular metabolic status including oxidative stress, glucose levels and hypoxia; and (2) microRNAs can modulate transcriptional and posttranscriptional processes to directly or indirectly impact on metabolic pathways (Singh *et al.* 2012). MicroRNA-metabolite communication is beginning to be examined, but the complexity of these interactions is not fully understood. As an exploratory step, a heat map was used to visualize the global association between circulating microRNAs and metabolites in the plasma, urine and liver. A number of distinctive sets of microRNAs were found to be correlated with lipids, TCA cycle intermediates, host-gut microbial co-metabolites, and liver and plasma energy metabolites. Down-regulated miR-342-3p and up-regulated miR-34c* in RYGB-operated rats demonstrate broad correlation with metabolites, indicating their extensive involvement in many metabolic processes (Figure 3.12). MiR-206, miR-1188, miR-1971 and miR-34c* are reversely correlated with plasma lipid fractions observed in NMR profiles, whereas miR-320 and miR-342-3p, together with miR-7* to a lesser extent, exhibit a positive correlation (Figure 3.12). TCA cycle intermediates including citrate, succinate, 2-oxoglutarate and fumarate are positively correlated with miR-143, miR-126-3p, miR-146a, miR-150 and miR-155, which are also inversely correlated with urinary host-

microbial co-metabolites such as *p-cresyl* glucuronide, *p-cresyl* sulphate and phenylacetylglycine (PAG) (Figure 3.12). In addition, miR-872*, miR463*, miR-30e, miR-2183, miR-1971, miR-150, miR-146a, miR-1188 and miR-93* all potentially relate to liver energy metabolism such as glycolysis and glycogenesis involving glucose, glycogen and lactate.

Very few metabolic related mechanistic studies of the above-mentioned microRNAs have been reported. Interestingly, most of the above-mentioned microRNAs are reported to be dysregulated in either diabetes or obesity development processes. For example, in rodent models, miR-143 was up-regulated in the liver of obese mice (Jordan *et al*. 2011), whereas the newly discovered miR-1188 and miR-1971 were down-regulated in diabetic cats' blood (Fleischhacker, Bauersachs, Wehner, Hartmann & Weber 2013a). In human studies, miR-206 was significantly reduced in diabetes patient's muscle (Gallagher *et al.* 2010). Circulating miR-126-3p, miR-155 miR-342-3p, miR-30e, miR-146a, miR-320 family and miR-150 have all been reported to be dysregulated in T2DM patients, but the direction of change was not consistent (Zampetaki *et al.* 2010). These previous profiling studies indicated that these microRNAs, which strongly correlated with certain metabolites, are highly likely to be involved in energy metabolism.

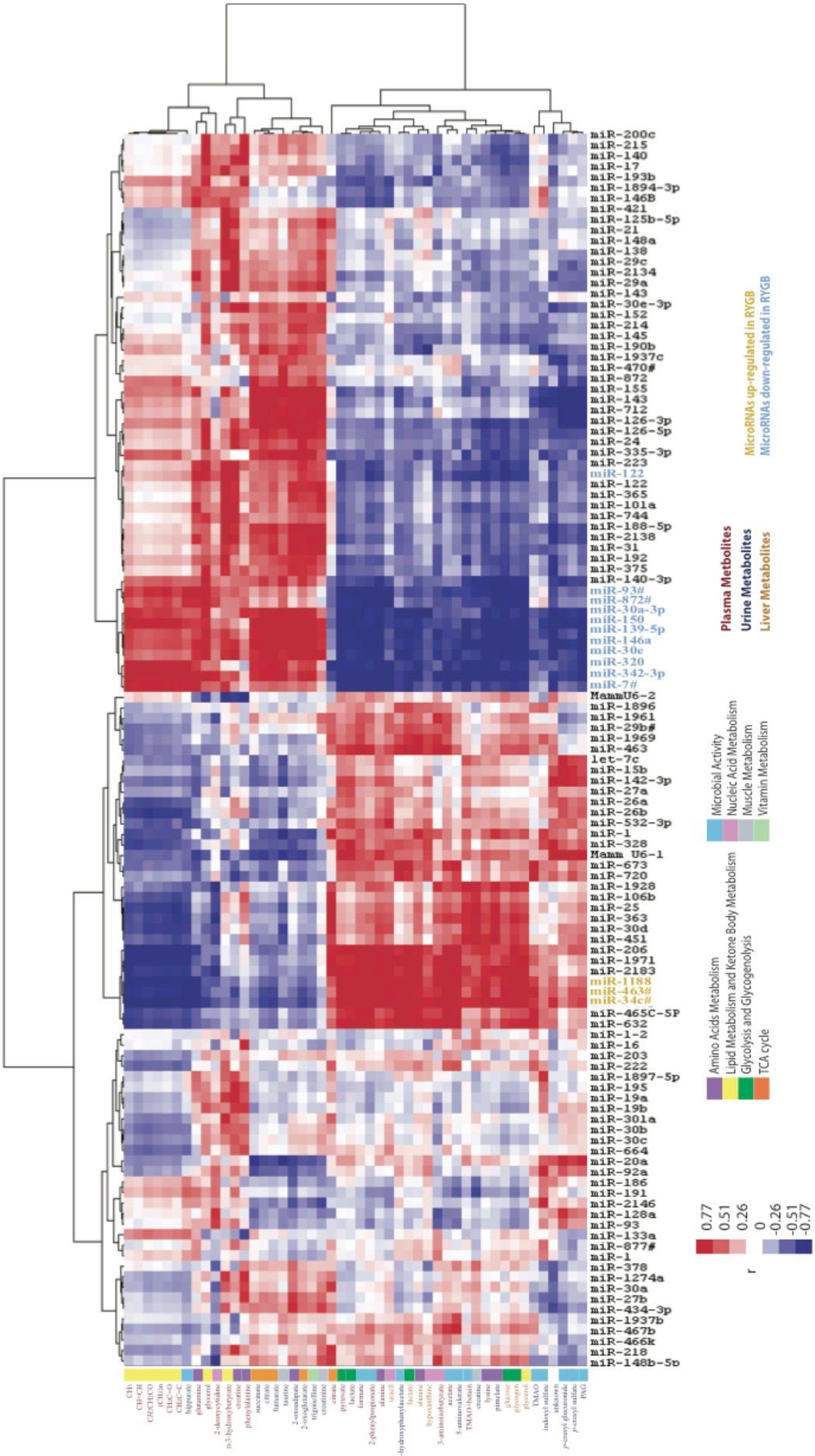
miR-200c
miR-215
miR-140
miR-17
miR-193b
miR-1894-3p
miR-146B
miR-421
miR-125b-5p
miR-21
miR-148a
miR-138
miR-29c
miR-2134
miR-29a
miR-143
miR-30e-3p
miR-152
miR-214
miR-145
miR-190b
miR-1937c
miR-470#
miR-872
miR-155
miR-143
miR-712
miR-126-3p
miR-126-5p
miR-24
miR-335-3p
miR-223
miR-122
miR-122
miR-365
miR-101a
miR-744
miR-188-5p
miR-2138
miR-31
miR-192
miR-375
miR-140-3p
miR-93#
miR-872#
miR-30a-3p
miR-150
miR-139-5p
miR-146a
miR-30e
miR-320
miR-342-3p
miR-7#
MammU6-2
miR-1896
miR-1961
miR-29b#
miR-1969
miR-463
let-7c
miR-15b
miR-142-3p
miR-27a
miR-26a
miR-26b
miR-532-3p
miR-1
miR-328
Mamm U6-1
miR-673
miR-720
miR-1928
miR-106b
miR-25
miR-363
miR-30d
miR-451
miR-206
miR-1971
miR-2183
miR-1188
miR-463#
miR-34c#
miR-465C-5P
miR-632
miR-1-2
miR-16
miR-203
miR-222
miR-1897-5p
miR-195
miR-19a
miR-19b
miR-301a
miR-30b
miR-30c
miR-664
miR-20a
miR-92a
miR-186
miR-191
miR-2146
miR-128a
miR-93
miR-133a
miR-877#
miR-1
miR-378
miR-1274a
miR-30a
miR-27b
miR-434-3p
miR-1937b
miR-467b
miR-466k
miR-218
miR-148b-5p
MicroRNAs up-regulated in RYGB
MicroRNAs down-regulated in RYGB
Plasma Metbolites
Urine Metabolites
Liver Metabolites
Microbial Activity
Nucleic Acid Metabolism
Muscle Metabolism
Vitamin Metabolism
Amino Acids Metabolism
Lipid Metabolism and Ketone Body Metabolism
Glycolysis and Glycogenolysis
TCA cycle
0.77
0.51
0.26
0
-0.26
-0.51
-0.77
r

Figure 3-10 Metabolites-microRNA correlation heat map

Correlation between miRNome and metabolic profiles. The heat map is generated from the Pearson correlation coefficient values between circulating microRNA expression and metabolite levels using a two-way clustering method. The horizontal axis shows all detectable circulating microRNAs while the vertical axis exhibits altered plasma, urinary and hepatic metabolites following RYGB. The color bar next to the metabolites indicates metabolic functions (amino acid metabolism, lipid metabolism and ketone body metabolism, glycolysis and glycogenolysis, TCA cycles, microbial activity, nucleic acid metabolism, muscle metabolism, and vitamin metabolism) of the metabolites. MicroRNAs, which are significantly altered by RYGB surgery, are shown in yellow (up-regulated) and blue (down-regulated), respectively. SHAM n=4, RYGB n=4. Keys: PAG, phenylacetylglycine; TMAO, trimethyalmine-*N*-oxide; TCA, tricarboxylic acid.

3.3.2.8 Correlation of altered miR-122 expression and metabolites — An energy requirement hypothesis

Among the fourteen significantly changed microRNAs post RYGB surgery, miR-122 was affected most (Figure 3.9). Pearson correlation indicated that miR-122 expression is highly positively correlated with D-3-hydroxybutyrate (3HB) and acetoacetate (AcAc) (Figure 3.12). Ketone bodies exist in plasma and the expression level is determined by glucose and insulin levels. A significant elevated ketone body level was observed in diabetes patients' plasma (Laffel 1999). To understand the altered ketone levels, we need to consider the metabolism of ketone bodies from two process, ketogenesis and ketolysis. **For ketogenesis**, blood derived free fatty acid can be taken up by hepatocytes and enter mitochondria. Fatty acid is then metabolised to acetyl CoA which could either enter the TCA cycle or divert to form ketone bodies. Under normal conditions, glycolysis can generate adequate amounts of oxaloacetate, which is essential for leading acetyl CoA into the TCA cycle. However, under extreme metabolic conditions such as long time fasting and diabetes, the glycolysis rate falls to a very low level, oxaloacetate is therefore not available to condense with acetyl CoA so that acetyl CoA diverted from the TCA cycle gets into ketone body synthesis (Laffel 1999). **For ketolysis**, liver-produced ketone bodies can be transferred into other organs, such as heart, brain and kidney, and generate acetoacetyl CoA by the enzyme succinyl CoA-oxoacid transferase (SCOT). During

starvation, the rate determining SCOT is down-regulated (Laffel 1999). Hence, circulating levels of ketone bodies are significantly increased by both favored ketogenesis and inhibited ketolysis. The balance between ketogenesis and ketolysis determines the final circulating ketone body concentration.

In the current study, the RYGB-operated rats had significantly lower circulating levels of miR-122 and ketone bodies (3HB and AcAc) (Table 3.4, metabonomics data acquired by Dr Jia Li), suggest that the ketogenesis process had been significantly inhibited in the liver. In fact, inhibition of miR-122 has been shown to increase fatty acid oxidation, which should theoretically lead to an increased acetyl CoA production. Acetyl CoA could then either get into TCA cycle or divert to form ketones (Figure 3.13). The metabolic profiling data obtained here shows 1) an increased whole body TCA cycle metabolism, evidenced by decreased urinary citrate, succinate, 2-oxoglutarate and fumarate, 2) increased glycolysis in the liver, supported by elevated concentrations of pyruvate, alanine and lactate in the liver and plasma and 3) inhibited ketonegenesis or increased ketolysis, evidenced by reduced circulating ketone levels. Therefore, it appears that the β-oxidation product acetyl CoA could preferably enter into TCA cycle instead of diverting to synthesise ketone bodies (Figure 3.13). Furthermore, the tendency toward glycolysis in the liver also supports the hypothesis because adequate amounts of oxaloactete are needed with acetyl CoA for the TCA cycle. Interestingly, two key metabolic enzymes citrate synthase (CS) and aldolase A (ALDOA), regulating TCA cycle and glycolysis respectively, are validated miR-122 targets (Boutz *et al*. 2011). Since circulating miR-122 exhibited a significant 56 fold decrease, it is very likely that the post RYGB rat hepatic miR-122 expression also is inhibited. Hence, the hepatic miR-122 mediated CS and ALDOA inhibition could then be relieved, which would result in increased glycolysis and TCA cycle in liver. As a consequence, the fatty acid

metabolised acetyl CoA would be more likely to go into TCA cycle to generate energy instead of ketone body production to store energy and reduced expression of miR-122 and ketone levels in blood. This hypothesis will be experimentally examined in chapter 4.

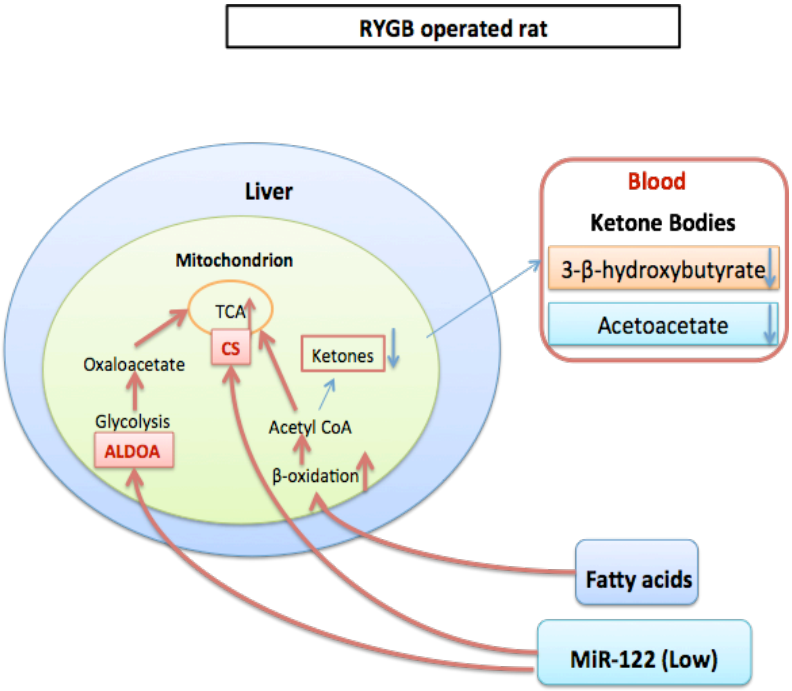

Figure 3-11 Role of miR-122 in RYGB operated rats

CS (citrate synthase); ALDOA (aldolase A, fructose-bisphosphate); TCA(tricarboxylic acid cycle)

Compared with SHAM rats, red arrow stands for a favored process/up-regulation in RYGB, whereas blue arrow means inhibited process/ decreased expression.

Table 3-4 Plasma, urinary and hepatic aqueous metabolites

	An OPLS-DA model of plasma CPMG spectral data (Q^2Y=0.83; R^2X=33.5%)			
Plasma Metabolite	**Change in RYGB**	**Diagnostic peak (δ ^{1}H)**	**p**	**q**
CH_3	-	0.87	0.002	0.025
(CH_2)n	-	1.266	0.005	0.03
CH_2CH_2CO	-	1.562	0.006	0.03
CH_2C=C	-	2.036	0.002	0.02
CH_2C=O	-	2.227	0.004	0.03
C*H*=C*H*	-	5.3	0.007	0.03
pyruvate	+	2.357	0.006	0.03
lactate	+	4.107	0.004	0.03
D-3-hydroxybutyrate	-	1.178	0.09	0.14
glutamine	-	2.426	0.003	0.03
citrate	+	2.664	0.02	0.06
creatine	-	3.023	0.004	0.03
TMAO+Betaine	-	3.252	0.004	0.03
glycerol	-	3.566	<0.001	0.01
2-deoxycytidine	-	6.04	<0.001	0.02
formate	+	8.443	<0.001	0.003
phenylalanine	-	7.407	0.004	0.03
acetate	+	1.904	0.03	0.06
2-phenylpropionate*	+	1.425	<0.001	0.005
alanine	+	1.471	<0.001	0.005
lysine	+	1.892	<0.001	0.006
3-aminoisobutyrate*	+	1.2	0.004	0.03

	An OPLS-DA model of urinary spectra (Q^2Y=0.93; R^2X=36.8%)			
Urinary Metabolite		**Peak (ppm)**	**p**	**q**
succinate	-	2.413	<0.001	<0.001
2-oxoglutarate	-	2.448	<0.001	<0.001
citrate	-	2.548	<0.001	<0.001
fumarate	-	5.528	<0.001	<0.001
2-oxoadipate	+	1.824	<0.001	0.002
5-aminovalerate	+	1.645	0.05	0.06
pimelate	+	1.31	0.004	0.01
TMAO	+	3.273	0.002	0.007
taurine	-	3.433	0.002	0.006
creatine	+	3.933	0.1	0.09
creatinine	-	4.054	<0.001	0.003
4-hydroxyphenylacetate	+	3.454	0.001	0.004
un	+	3.523	0.002	0.006
p-cresyl glucuronide	+	2.301	0.002	0.005
p-cresyl sulfate	+	2.346	0.002	0.007
PAG	+	3.757	<0.001	<0.001
hippurate	-	3.974	0.009	0.02
trigonelline	-	4.436	<0.001	<0.001
indoxyl sulfate	+	7.714	<0.001	0.002

	An OPLS-DA model of liver aqueous extract (Q^2Y=0.81; R^2X=45.6%)			
Liver Metabolite		**Peak (ppm)**	**p**	**q**
lactate	+	1.339	0.001	0.005
alanine	+	1.479	0.01	0.02
glucose	+	5.238	<0.001	0.002
glycogen	+	5.415	<0.001	0.002
glycerol	+	3.78	<0.001	0.001
uracil	+	5.803	0.03	0.05
hypoxanthine	+	8.2	0.006	0.02

Plasma, urinary and hepatic aqueous metabolites found to be altered between RYGB- and SHAM-operated rats based on O-PLS-DA models. R^2X represents the variation in ^{1}H NMR spectral data explained by the O-PLS-DA model. Q^2Y indicates the level of significance of the metabolic differences between two classes. The p and q values in the table represent the significance of the metabolite changes and false discovery rate-adjusted p values, respectively. The "+" or "-" represents the increased or decreased trend of metabolites in RYGB-operated rats compared with SHAM controls. Data provided by Dr Jia Li, Imperial College London.

3.3.2.9 TLDA method validation by qPCR

A number of differentially expressed microRNAs in the TLDA data was further validated using RT-qPCR (quantitative real-time reverse transcriptase polymerase chain reaction). RT-qPCR is a two-step method, which employs the enzyme for reverse transcriptase to generate complementary DNA (cDNA) and followed by PCR amplification (process including denaturation, annealing and extension). The measurement is taken in the exponential phase as this phase exhibits the least variability without saturation of amplification. RT-qPCR is considered to be the "gold standard" for detecting gene expression. Here, to validate the circulation TLDA data, I selected three microRNAs, namely miR-122, miR-34c-3p and miR-1188, to examine their expression across tested SHAM and RYGB rats. As shown in figure 3.14, miR-122 and miR-1188 exhibited similar fold change with TLDA derived data. MiR-122 was shown to be down-regulated 56 fold in TLDA and 155.3 fold in qPCR. MiR-1188 exhibited 5.39 fold up-regulation in RYGB by TLDA and 7.7 fold increase by qPCR. In fact, by using RT-qPCR, miR-122 was only detected in one RYGB animal and miR-1188 was not detected in any SHAM operated animal (a Ct value of 40 was assumed in order to calculate the relative expression using delta/delta Ct method). MiR-34c*, on the other hand, showed 11 fold up-regulation in TLDA data set, but 1.2 fold marginal up-regulation in by qPCR. This inconsistency may be due to the pre-amplification procedure required for TLDA. Pre-amplification step is introduced due to the very low concentrations of RNA in plasma. However, pre-amplification itself has the potential to introduce bias due to the uneven RNA amplification/degradation rate. Therefore, the validation results supported the most significant changes detected by TLDA, for example, when no microRNA exist at all or relatively abundant microRNAs were expressed. However, microRNAs detected by TLDA

with relatively low expression need to be firstly validated before carrying out any downstream analysis.

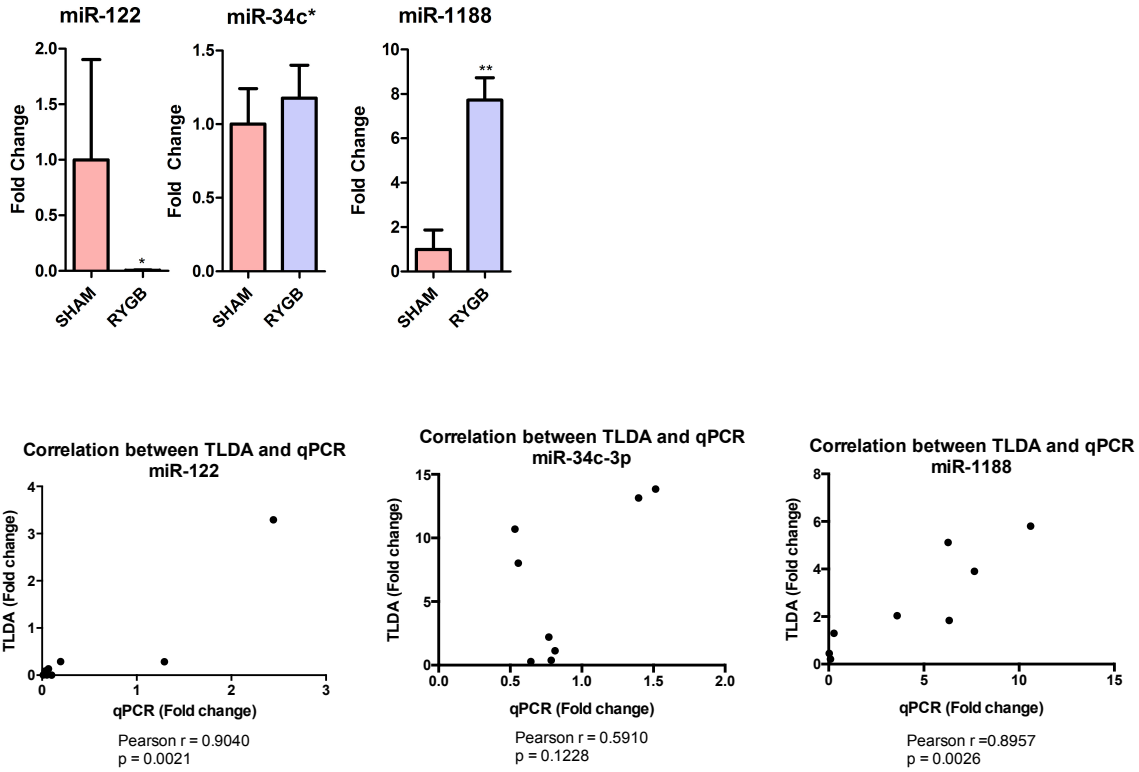

Figure 3-12 Circulating microRNA expression validation by RT-qPCR and correlation analysis

Determined by qRT-PCR of the same samples used for TLDA (4RYGB and 4SHAM animals). Data are expressed as mean with SEM error bars

3.4 Colon microRNA profiling after RYGB surgery

3.4.1 Sequence method data process procedure

Colon microRNAs were sequenced by Illumina microRNA deep sequencing platform after removing both side-attached adapters. The length of the sequenced RNAs varied between 15 and 35 nucleotides. Original sequencing data were processed with Cutadapt (http://code.google.com/p/cutadapt/) to trim both of the side adapters to filter the sequencing size (greater than 15-nucleotide long). CLC genomic workbench was then used to select the sequence between 15 and 35-nucleotide long and count the copy number and the length of these sequences. (This part of the work was done in collaboration with Mariana Flores, Imperial College London.)

All detectable colorectal microRNAs are mapped into the following read length distribution figure (Figure 3.15), which shows three peaks at 21,22 and 23. This result is consistent with other non-coding RNA sequencing system results (Schulte *et al.* 2010) and indicated successful microRNA deep sequencing. These three nucleotide peaks around 22 nucleotides suggest that samples contain enriched mature microRNAs.

Interestingly, besides the peaks around 22, nucleotide length 30 also exhibited a significant enrichment of reads. It perhaps represents the newly discovered RNA class, namely piwi interacting RNA (piRNA). In 2006, four groups independently isolated 30nt length small RNA from testis(Lau *et al*. 2006; Kim 2006; Aravin *et al*. 2006; Girard *et al*. 2006). Small non-coding RNAs exhibit their function by combining with the evolutionarily conserved protein family piwi/argonaute (PAZ-PIWI or PPD), which can be divided into AGO and PIWI subfamilies. AGO proteins bind to siRNAs and microRNAs, whereas PIWI

proteins bind to PIWI-interacting RNAs (Siomi *et al*. 2011). The study of piwi protein was initially on germ cells with functions in meiosis, spermiogenesis, and transposon silencing (Thomson & H. Lin 2009). Despite the common belief that PIWI proteins only have germline-restricted functions, the role of PIWI/piRNA in somatic tissues has recently been explored (Malone *et al*. 2009). However, it is still not clear about the biological function of piRNAs and what role that PIWI proteins play in biogenesis of piRNAs. The expression and function of this 30nt piRNA is certainly worth exploring in future.

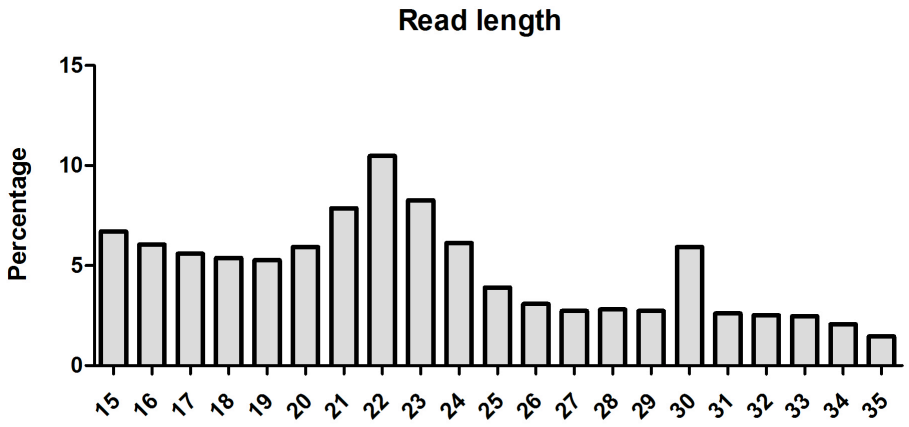

Figure 3-13 Read length distribution of deep sequencing reads

As seen in Table 3.5, each sample mapped mature microRNA and the numbers varied from 256 to 340. The total detectable microRNA number is 372 (the detectable rat colon mature microRNA list is presented in Appendix 1). Among these microRNAs, the most highly expressed microRNAs are rno-miR-143-3p (on average account for 38.7% of total microRNAs) and rno-miR-192-5p (average 11.73%) followed by less expressed rno-miR-10a-5p and rno-miR-22a-3p (Figure 3.16). Interestingly, our result is consistent with a previous study in human, which also reported that miR-10a-5p, miR-21-5p, miR-22a-3p, miR-143-3p and miR-192-5p are the top five most abundant microRNAs and represent

54% of all microRNAs in colorectal cancer patients (Schee *et al*. 2013). The result demonstrated microRNA's conservative feature across species and also suggested that our result in rats may be translatable to human.

Table 3-5 Mapped microRNA number in deep sequenced colorectal samples

	RYGB1	RYGB2	RYGB3	RYGB4	SHAM1	SHAM2	SHAM3	SHAM4
Mapped mature microRNA number	340	268	256	256	288	302	256	317

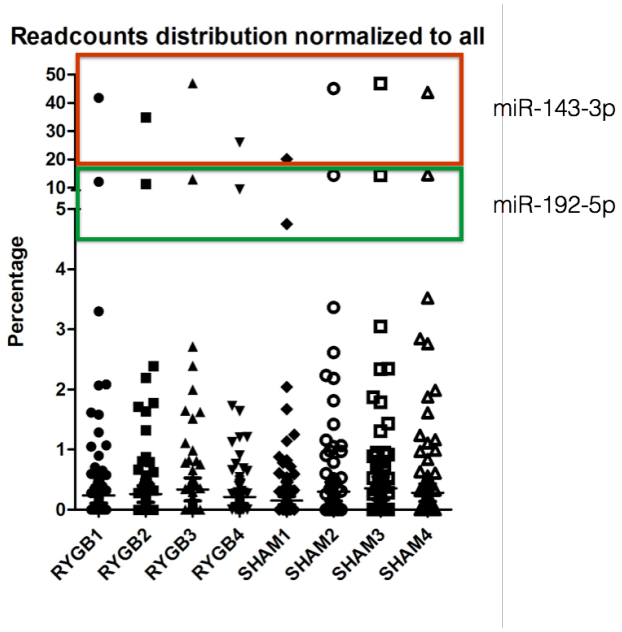

Figure 3-14 Read counts distribution of all microRNAs

The x axis shows 8 deep sequencedsamples. Y axis is the expression percentage of certain microRNA within total microRNA. Read counts are normalized to all reads, includes both mapped and unmapped reads.

3.4.2 Overall colon data comparison

PCA analysis was performed to generate an overall view of the microRNAome between RYGB- and SHAM-operated groups. As seen in Figure 3.17, the two groups were separated along the second principal component. The corresponding loading plot (Figure 3.17) shows that the first component is mainly driven by the most abundant microRNAs

(miR-143-3p and miR-192-5p), whereas the second component is contributed by the most of the differently expressed colonic microRNAs between two groups (such as miR-181a-5p, miR-150-5p and miR-142-5p etc).

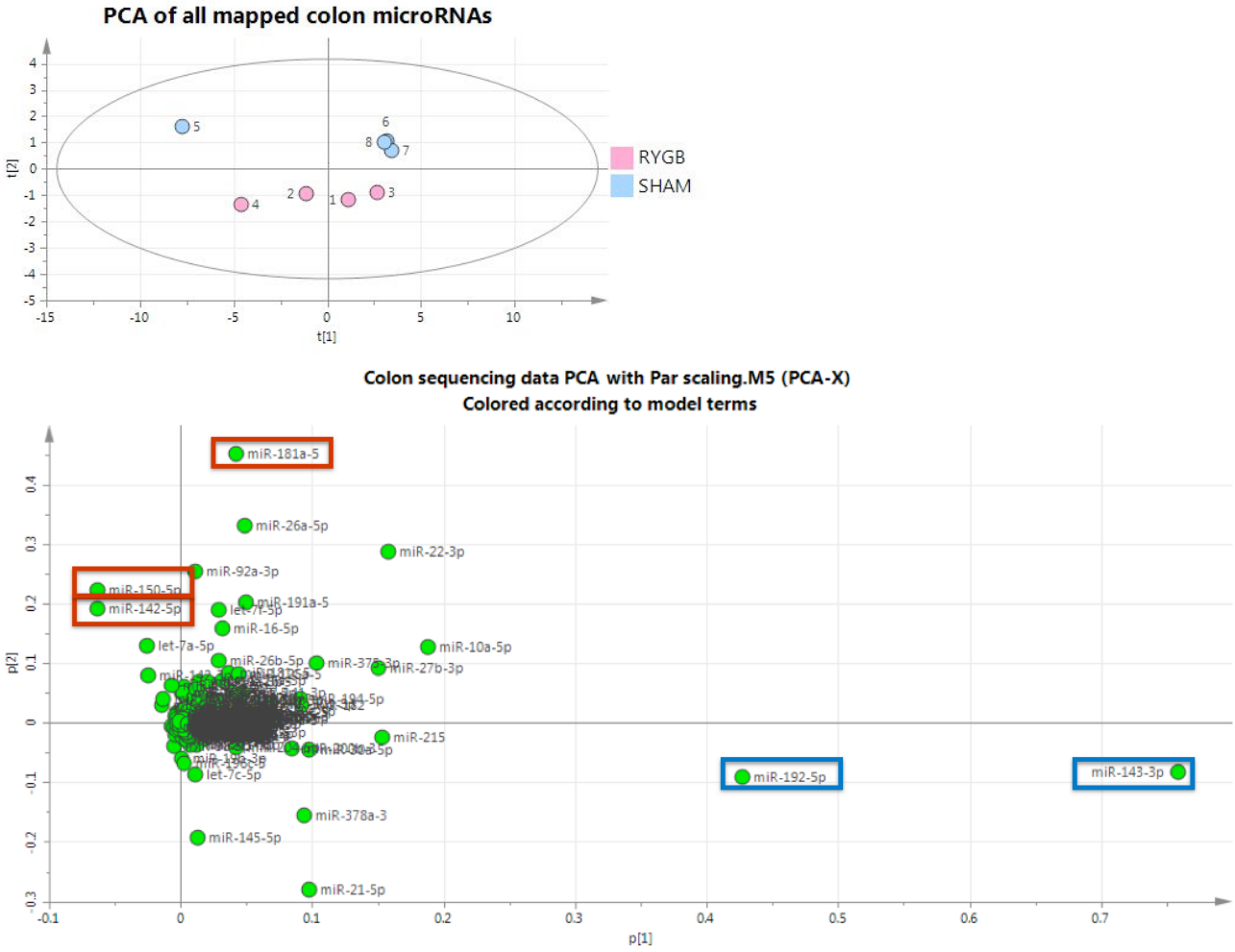

Figure 3-15 PCA and loading plot of colorectal microRNA expression in 8 deep sequenced samples

Each symbol represents a biological sample, with its colour indicating the group to which it belongs to (Blue=SHAM, Red=RYGB)

3.4.3 Altered mature known colonic microRNAs

DESeq is a method developed by Anders *et.al.* to perform differential expression analysis on RNA sequence count data (Anders & Huber 2010). The package DESeq provides methods to test for differential expression by use of the negative binomial distribution

which allow less restrictive variance assumptions than Possion distribution (Anders & Huber 2010). As seen in Figure 3.18 below, 13 colonic microRNAs are significantly different between RYGB- and SHAM-operated groups. Among them, three microRNA families (miR-216 family, miR-19 family, and miR-142 family) exist and hierarchical clustering grouped microRNAs from the same family together. It is expected that microRNAs belonging to the same family would be correlated across all samples. Indeed, as Figure 3.19 shows, we observed a high correlation within each microRNA family (R^2>0.99). This suggested that 1) microRNAs from same family are likely to be regulated by the same promoter and 2) the deep sequencing method is robust and generated a good quality data.

Among these 13 microRNAs, most of them showed 2 to 10 fold change, except for rno-miR-216 family (Figure 3.18), which was calculated as infinite because all four SHAM operated rats do not contain any miR-216 members and three out of four RYGB operated rats expressed of miR-216 family members. Colon expressed miR-216 family has not yet been well studied. Two studies have suggested that the liver miR-216 and miR-217 may be associated with lipid metabolism (Hoekstra *et al*. 2012) (Yin *et al*. 2012). Hepatic miR-216 was markedly decreased in mice fed a western-type high fat diet, but up-regulated in response to fasting (Hoekstra *et al*. 2012). Another paper showed that chronic ethanol exposure up-regulated miR-217 and its increase promotes ethanol-induced fat accumulation by down regulating hepatic sirtuin 1 (SIRT1) (Yin *et al*. 2012). These results indicate that miR-216 family expression may be regulated by the cell's energy state and its alteration may in turn control the cellular metabolic state. However, it is still not clear whether colonic miR-216 family shares a similar function as hepatic miR-216. It would be interesting to explore the consequences of post RYGB miR-216 family alteration. It will

also be important to mimic some of the RYGB-induced benefits by manipulating this "RYGB specific" microRNA in the colon.

In addition to miR-216 family, other microRNAs have also previously been reported to be involved in metabolism. For example, miR-142 family (miR-142-5p and miR-142-3p) in adipose tissue showed up-regulation in mice fed on high-fat diet for 5 months (Chartoumpekis *et al*. 2012). More interestingly, Francisco *et al.* revealed a close positive correlation between circulating miR-142-3p level and the extent of obesity (BMI) (Ortega *et al*. 2013). The significance of their result is further demonstrated by a decreased miR-142-3p upon weight loss (Ortega *et al*. 2013). It would be important to investigate the function of colonic miR-142-3p and miR-142-5p in response to RYGB surgery in future. A microRNA-target based functional analysis will be discussed in the next section in order to generate an overall picture of which communal targets these microRNA may regulate and what the potentially involved biological pathways are.

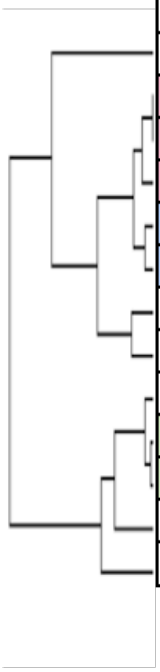

	Fold change (RYGB/SHAM)	Adjusted P value	Location
rno-miR-6215	-6.802721088	3.97E-10	Chromosome 5: 158,393,606-158,397,672
rno-miR-217-5p	Inf	4.35E-44	Chromosome 14: 109,671,480-109,675,584
rno-miR-216a-5p	Inf	3.76E-24	Chromosome 14: 109,664,081-109,668,186
rno-miR-216b-5p	Inf	1.09E-05	Chromosome 14: 109,653,043-109,657,144
rno-miR-19b-3p	2.37	2.19E-06	Chromosome 15: 99,852,320-99,856,406
rno-miR-19a-3p	2.71	3.25E-05	Chromosome 15: 99,852,018-99,856,099
rno-miR-196c-5p	2.24	0.0143	Chromosome 10: 84,993,948-84,998,027
rno-miR-541-5p	2.67	0.0344	Chromosome 6: 134,421,740-134,425,829
rno-miR-150-5p	-7.710100231	2.89E-29	Chromosome 1: 95,594,077-95,598,161
rno-miR-142-5p	-4.51059991	3.15E-12	Chromosome 10: 76,047,280-76,051,366
rno-miR-142-3p	-3.721622627	6.34E-05	Chromosome 10: 76,047,280-76,051,366
rno-miR-342-3p	-4.317789292	0.0002	Chromosome 6: 132,988,797-132,992,895
rno-miR-181a-5p	-1.99880072	0.0002	Chromosome 3: 18,648,904-18,653,020

Figure 3-16 Differentially expressed colorectal microRNAs

Fold change is the microRNA expression ratio between the two experimental conditions (RYGB:SHAM). Positive means that microRNA is up- regulated at RYGB compared with SHAM; negative means repressed in RYGB. P-value was calculated by unpaired student t test with Bonferroni adjustment. Three microRNA families are labelled with red (miR-216 family), blue (miR-19 family) and green (miR-142 family), respectively.

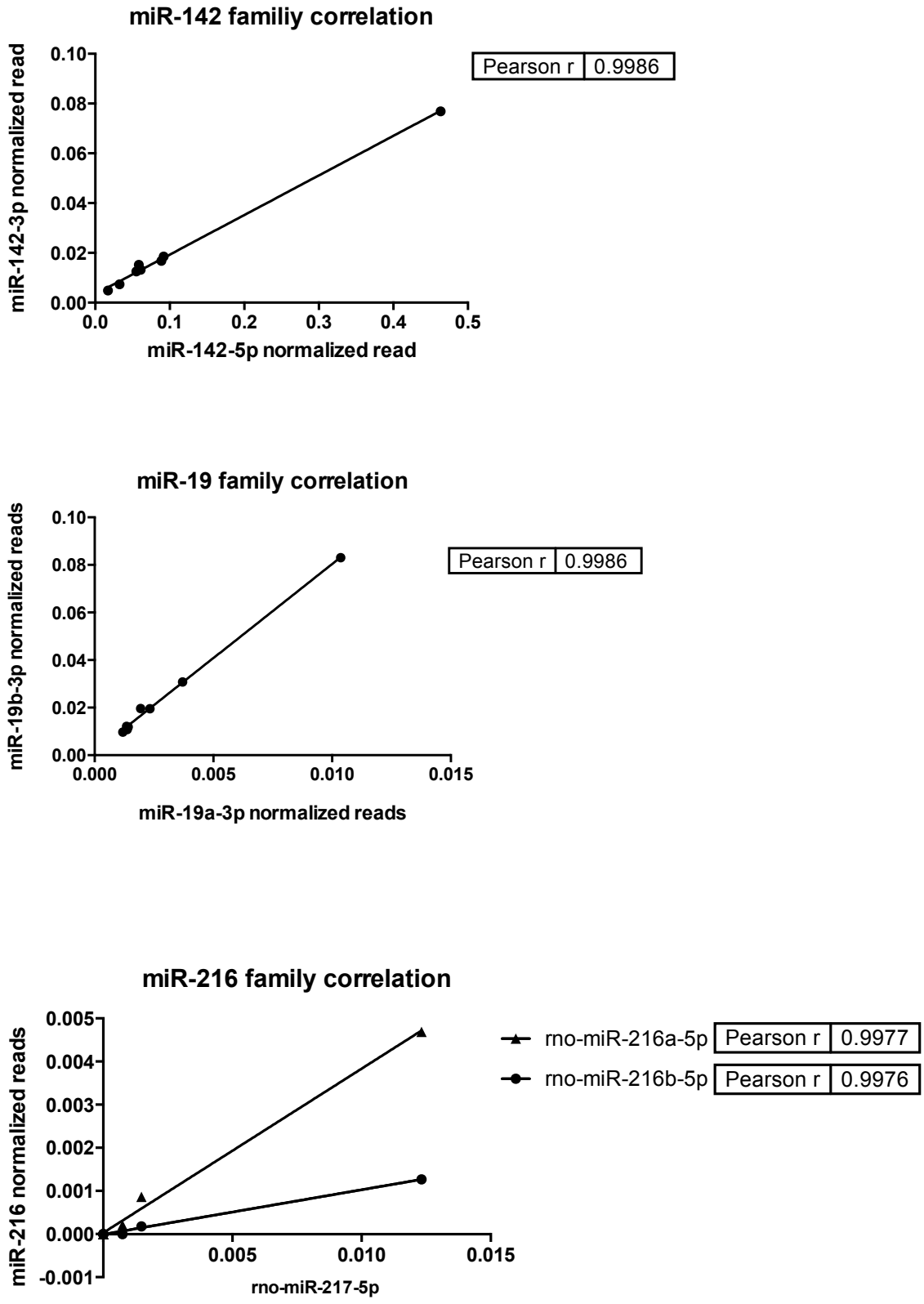

Figure 3-17 microRNA family members correlation between samples;

Pearson correlation. The p value of all correlation tests <0.0001.

3.4.4 Unknown novel colonic microRNA examination

Using a machine learning-based technique, miRanalyzer generated a putative microRNA list based on the mature and precursor sequences, and their folding/binding kinetics (Hackenberg *et al*. 2009). In general, around 50 novel microRNAs were detected in each biological sample. However, most of them were mapped into chromosome unknown (ChrUN), which contains clone contigs that cannot be confidently placed on a specific chromosome. These candidates, which mapped to ChrUN, were filtered out and the rest of thirteen novel microRNA candidates were listed in Table 3.7. A final step for examination of a putative novel microRNA is to determine if it is conserved across species (Martin *et al*. 2007). By applying UCSC genome browser (https://genome.ucsc.edu), conservation across rat, mouse, human, dog and cow could be accessed. Among these thirteen novel microRNA candidates, two of them are conservative across species (Figure 3.20) and are highlighted with red in Table 3.7.

Candidate 1 locates on chromosome X (88,278,172 - 88,378,290). This microRNA has a mature sequence similar to mmu-miR-676-3p (mmu-miR-676) and hsa-miR-676-3p (hsa-miR-676). Hence, here we name it as rno-miR-676-3p (rno-miR-676). There are currently very few studies focusing on the biological function of miR-676-3p in other species. One study showed that mmu-miR-676 was up-regulated in the liver of leptin deficient db/db mice (Kaur *et al*. 2011). Additionally, rno-miR-676-3p locates within ectodysplasin-A (EDA) gene. EDA protein belongs to the tumour necrosis factor family, acts as a homotrimer and may be involved in cell-cell signalling during the development of ectodermal organs (Kere *et al*. 1996). However, there is currently no literature to suggest EDA has any colorectal or metabolic function. Interestingly, rno-miR-676-3p is an intronic microRNA located on chormosome X, which has highly enriched microRNAs compared to autosomes, whereas

surprisingly, Y chromosome has no detectable microRNAs at all (X. Guo *et al*. 2009). The contribution of X chromosome microRNAs to the gender difference for cancer, immune and metabolic diseases has not yet been explored. Previous reports have shown that the cancer protective effects of bariatric surgery is strongest for female obesity-related tumours (Ashrafian *et al*. 2011). Hence, it would be interesting to explore that whether this chromosome X microRNA contributed to these sex specific post-operative benefits in the future.

Candidate 2 locates on chromosome 10 (34,069,743-34,069,860). By mapping the sequence with other species, candidate 2 was found to be similar to the mouse non-coding RNA snoRNA U95 (snord95). Small nucleolar RNAs (snoRNAs) are a class of small RNAs which may guide chemical modification (such as methylation and pseudoridylation) of other RNAs, mainly ribosome RNAs, transfer RNAs and small nuclear RNAs (Kiss 2001). It has been commonly used as a microRNA expression normalizer (Mestdagh *et al*. 2009). My data suggested that, not only mice, but also rats express this small non-coding RNA. The function and expression of rat snord95 needs to be further explored in the future.

Table 3-6 Predicted novel colorectal non-coding RNAs

chromo-some	chrom-Start	chrom-End	strand	sequence	log2 fold change	p value	conserved	microRNA in other species	Chromosome location
chrX	88,378,172	88,378,290	+	CCGTCCTGAGCTTGTCGAGCTA	-2.7	0.0661	yes	mmu-/hsa-miR-676	EDA intron 2
chr7	10,394,873	10,395,011	-	TCTGACCCTATGTCCCCCACAG	-2.3	0.0955	no		
chr2	191,051,916	191,052,042	+	AGTTTCCTGGTTGTGACCG	-1.1	0.1207	no		
chr2	191,045,392	191,045,518	-	AGTTTCCTGGTTGTGACCG	-1.1	0.1207	no		
chr10	34,069,743	34,069,860	+	CAGAGGCTGTTTCTGAGC	-1.3	0.1235	yes	mus snord95	GNB2L1
chr1	131,079,820	131,079,950	+	CATAAGTGTAGAGAGTCTGTAGT	-1.3	0.1335	no		
chr17	62,933,441	62,933,523	-	GGGCCCTTCCCGTGGATCGCCC	2.1	0.1397	no		
chr20	6,853,008	6,853,148	-	CTACTGAGCCACATTCCCAGCCC	-1.7	0.1487	no		
chr5	24,497,507	24,497,593	+	GGGGCGGGGTCCGCCGGCCT	1.1	0.1665	no		
chr4	152,578,763	152,578,853	-	CAACCCGGTCAGCCCCCTCCCG	2.5	0.2093	no		
chr10	43,941,461	43,941,557	-	GTCAGGATGGCCGAGTGGTCTAAGGC	-0.8	0.7585	no		

Candidate1, Chromosome X, 88,378,172 to 88,378,290

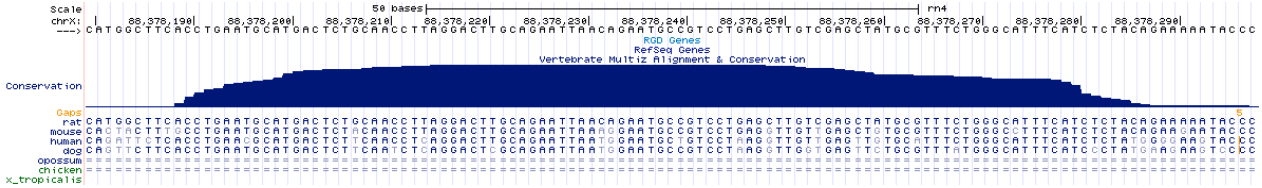

Candidate2, Chromosome 10, 34,069,743 to 34,069,860

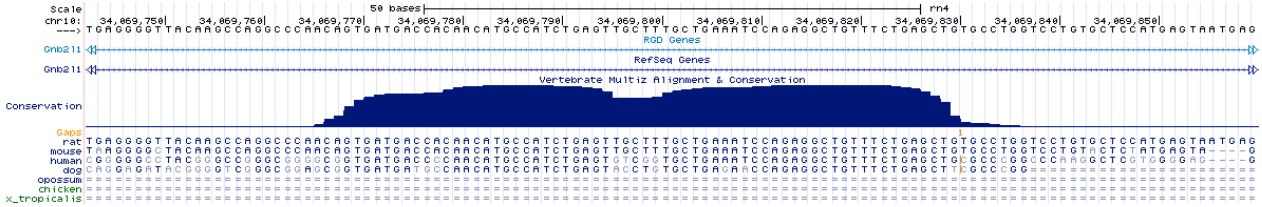

Figure 3-18 The highly conserved colorectal novel non-coding RNAs

The horizontal axis are the RNA sequence of rat, mouse, human dog and cow. The vertical block suggests the conservation of the particular nucleotide.

3.5 Chapter Discussion

3.5.1 Bioinformatics based functional analysis of altered circulating microRNAs

The discovery of microRNAs adds another layer of complexity to epigenetic regulation. Subtle change of a single microRNA has the potential to fine tune multiple biological processes. Although microRNAs remain a young research theme, it has become increasingly clear that a set of microRNAs could influence the metabolic behavior of biological systems by regulating multiple targets in a pathway. To investigate this, we first predict the mRNA targets of each significantly changed microRNA using ten available databases, namely, miRWALK, DIANA-mt, miRanda, miRDB, RNAhybrid, PICTAR4, PICTAR5, PITA, RNA22 and Targetscan (miRWALK database can summarise all targets from different databases . http://www.umm.uni-heidelberg.de/apps/zmf/mirwalk/micrornapredictedtarget.html). With the focus on microRNA target prediction, databases can be classified into two categories: established on the basis of the use or non-use of conservation comparison, a feature that significantly influences an outcome list of targets by narrowing the results (Yue *et al*. 2009). The algorithms based on conservation criteria include: miRanda, PicTar, TargetScan, DIANA-mt; in contrast PITA and RNA22 employ algorithms using other parameters, such as free energy of binding or secondary structures of mRNA 3'UTRs that can promote or prevent microRNA binding. More detailed information can be found in a comprehensive review, which compares various publicly available microRNA target prediction databases (Witkos *et al*. 2011). Here I first used all of these algorithms to predict microRNA targets, but only included targets that are predicted by more than two databases, to increase the accuracy and confidence of the prediction results.

By summarizing the predicted mRNA targets, a pathway map was produced using PANTHER compare gene list tool. This expression overrepresentation tool is based conceptually on statistic binomial test described previously (Mi *et al*. 2013). An input list is divided into groups based on PANTHER classification (either molecular function, biological process, or pathway; here we used pathway, due to its specificity). A maximum of four lists can be uploaded for each analysis at the same time. A reference list, which usually contains all the genes/ proteins, is divided into groups in the same way. The output of the tool is a list of p values for under- or over- representation of each functional category in each of the input lists. A typical output webpage is presented below in Figure 3.10.

	Rattus norvegicus (REF)	miR-122 target.txt			
Pathways	#	#	expected	+/-	▲ P value
Unclassified	20188	728	853.88	-	1.19E-27
EGF receptor signaling pathway	127	21	5.37	+	4.03E-05
Ras Pathway	77	15	3.26	+	3.00E-04
PDGF signaling pathway	133	19	5.63	+	1.19E-03
Angiogenesis	156	20	6.60	+	3.20E-03
Gonadotropin releasing hormone receptor pathway	237	25	10.02	+	7.69E-03
T cell activation	88	13	3.72	+	2.34E-02
FGF signaling pathway	118	15	4.99	+	3.74E-02
B cell activation	69	11	2.92	+	3.99E-02
Endothelin signaling pathway	82	12	3.47	+	4.56E-02
Heterotrimeric G-protein signaling pathway-Gi alpha and Gs alpha mediated pathway	135	16	5.71	+	5.05E-02
Wnt signaling pathway	292	26	12.35	+	7.53E-02
Inflammation mediated by chemokine and cytokine signaling pathway	241	22	10.19	+	1.47E-01
Ionotropic glutamate receptor pathway	47	8	1.99	+	1.84E-01
Dopamine receptor mediated signaling pathway	59	9	2.50	+	1.95E-01
Heterotrimeric G-protein signaling pathway-Gq alpha and Go alpha mediated pathway	112	13	4.74	+	2.17E-01
Synaptic vesicle trafficking	28	6	1.18	+	2.46E-01
Alzheimer disease-amyloid secretase pathway	62	9	2.62	+	2.74E-01
p38 MAPK pathway	40	7	1.69	+	3.19E-01
Angiotensin II-stimulated signaling through G proteins and beta-arrestin	40	7	1.69	+	3.19E-01
Parkinson disease	105	12	4.44	+	3.73E-01
TGF-beta signaling pathway	95	11	4.02	+	5.08E-01
Leucine biosynthesis	2	2	.08	+	5.98E-01
Alanine biosynthesis	2	2	.08	+	5.98E-01
Muscarinic acetylcholine receptor 1 and 3 signaling pathway	45	7	1.90	+	6.09E-01
Cytoskeletal regulation by Rho GTPase	84	10	3.55	+	6.38E-01
VEGF signaling pathway	60	8	2.54	+	8.09E-01
Nicotine pharmacodynamics pathway	36	6	1.52	+	8.40E-01

Figure 3-19 Gene expression data from Compared gene lists tool viewed on PANTHER web site.

The results from Compare gene lists tool. One sample lists (miR-122) were uploaded to the tool. The NCBI rat gene list was used as the reference list.

The predicted pathways, that are likely to be affected by RYGB surgery, were then ranked according to the number of microRNAs involved in each pathway (Figure 3.11), with four major related aspects including G protein signaling, neurodegenerative disease, inflammation, and growth/apoptosis. I shall discuss each of these pathways here.

A) G protein signalling

Increasing evidence indicates that the gut microbiota could influence the intestinal expression of short chain fatty acid (SCFA) receptors (Samuel *et al*. 2008) and the secretion of gut peptides such as PYY and GLP-1 via G-protein-coupled receptors including GPR41 and GPR43 (Bindels, Dewulf & Delzenne 2013a). A substantial shift in microbial phyla towards *Gammaproteobacteria* has been reported in RYGB-operated rats and human (J. V. Li *et al*. 2011a; H. Zhang *et al*. 2009a), together with elevated levels of faecal SCFAs (e.g. acetate, propionate, formate) and decreased levels of oligosaccharides (J. V. Li *et al*. 2011a). These results suggest that following RYGB surgery, GPR43 could be activated by higher levels of SCFAs and stimulate enteroendocrine L cells to release PYY and GLP-1 (Bindels, Dewulf & Delzenne 2013b) with a regulatory effect of the involved microRNAs. Multiple G-protein coupled pathways may be strongly influenced by differentially expressed microRNA, for example, miR-150 is indeed predicted to target GPR43 by miRANDA algorithm.

B) Neurological related

As seen in Figure 3.11, these 14 altered microRNAs, particularly miR-342-3p, miR-320, miR-139-5p and miR-146a, are predicted to be involved in multiple neurological transmitter and receptor-related pathways, as well as two major neurodegenerative diseases (e.g. Parkinson's and Huntington disease), suggesting that RYGB surgery may modulate neurological activity through a microRNA-mediated gut-brain axis. MicroRNAs are abundant in the brain and they act as effectors of neurological development and phenotype. Saba *et al.* have previously reported that miR-342-3p, miR-320, miR-139-5p and miR-146a, which are all down-regulated in the plasma of RYGB-group in our study, exhibited >2.5-fold up-regulation in mouse brain tissue infected with mouse-adapted scrapie (prion induced nerodegeneration) (Saba *et al.* 2008). Interestingly, nine out of these 14 RYGB-related microRNAs are associated with Parkinson's disease (PD) patients, who commonly experience unintended weight loss (H. Chen *et al.* 2003). The overlap in microRNA profiles between bariatric surgery and PD suggest that surgery-induced weight loss may share partial mechanism pathways with unintended weight loss in PD. The reason for weight loss in PD remains unclear, but factors including reduced food intake due to dysphagia, increased resting energy expenditure and potential peptide hormones such as ghrelin could account for the underlying mechanisms (Pfeiffer 2003). Furthermore, glutamate receptor group III pathway is also likely to be regulated by eight gastric bypass-altered microRNAs (Figure 3.11). In fact, previous studies showed that mice with knock-down glutamate receptor group III member, mGluR8, exhibited increased levels of anxiety and body weight compared to their wild type (Duvoisin *et al*. 2005). These multiple connections between metabolic abnormality and the pathogenesis of neurodegenerative diseases pose fascinating possibilities for research on the microRNA mediated post RYGB neurological alteration.

C) Wnt signalling pathway

Most of these microRNA expression changes, such as miR-122, miR-150, miR342-3p and miR139-5p, are strongly predicted to target Wnt signaling pathway and inflammation-related pathways mediated by chemokine and cytokine signaling. Wnt signaling pathway has long been linked to metabolic syndrome due to its function in regulating adipose tissue differentiation and pancreatic cell mass and function (Ross *et al.* 2000; Rulifson *et al.* 2007). The canonical WNT signaling cascade converges on the transcriptional regulator β-catenin. In the absence of WNTs, cytoplasmic β-catenin is recruited to a degradation complex formed by axin and adenomatous polyposis coli (APC), protein phosphatase 2A (PP2A), glycogen synthase kinase 3 (GSK3) and casein kinase 1α (CK1α) (MacDonald, Tamai & He 2009a). The complex could initiate β-catenin ubiquitination and proteasomal degradation(X. He *et al.* 2004). Inactivation of the degradation complex results in hypophosphorylation of β-catenin and its translocation to the nucleus to activate WNT target genes (MacDonald, Tamai & He 2009b). The activation of Wnt signalling pathway can increase cells sensitivity to insulin, in particular Wnt10b, which increases this sensitivity in skeletal muscle cells (Christodoulides *et al.* 2009). Furthermore, to support this, mutation of wnt10b leads to obesity by inactivation of canonical WNT signaling and block of adipogenesis (Christodoulides *et al.* 2006). Interestingly, in the present study, among the differentially expressed microRNAs between RYGB and SHAM animals, miR-122, miR-139-5p, miR-146a, miR-150, miR-320, miR-343-3p are all predicted to target Wnt10b, which potentially indicates their crucial link to the activation of Wnt signalling pathway and the post RYGB anti-diabetic effects.

With network features and relatively high expression in cells, microRNAs are believed to confer biological system robustness under condition of disturbance (Ebert & Sharp 2012).

Multiple sets of microRNAs and their targeted pathways appeared to be affected by RYGB surgery in the current study, suggesting that following a major anatomic alteration in the gastrointestinal track, the biological system is re-building a new metabolic balance by altering these microRNAs. Further studies need to be carried out to identify the commonly regulated crucial molecules and their relationship with the altered microRNAs.

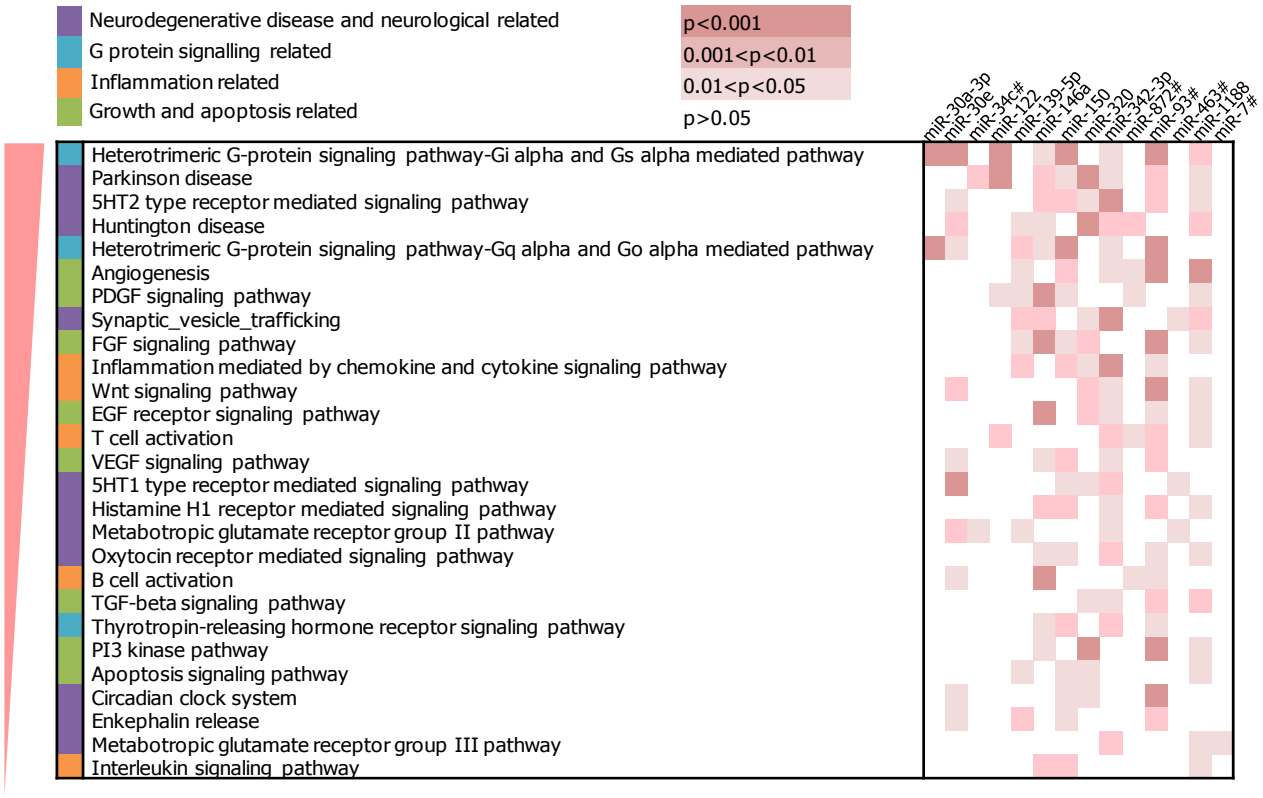

Figure 3-20The predicted most likely altered pathways after RYGB (plasma analysis)

The pathways are ranked according to the number of potentially involved microRNAs. The significant ranges are presented by the different red colours; those more likely to be regulated have a deeper colour. All pathways are classified into four biological process, with colour code on the left side of the table.

3.5.2 Bioinformatics-based functional analysis of altered colonic microRNAs

Similar to the functional analysis of the liver microRNA targets, we first predict the mRNA targets of each significantly changed microRNA using miRWalk. Again, only the targets

that are predicted by more than two databases were included to increase the accuracy and confidence of the prediction results. After summarising all of the predicted mRNA targets, a pathway map was then produced using Panther compare gene list tool (Mi and Thomas, 2009). These predicted pathways, which are likely to be affected by RYGB surgery, are ranked according to the number of microRNAs involved in each pathway and listed in Table 3.6. Interestingly, three classes of neurotransmitter-related pathways (glutamate receptor, 5HT receptor and opioid related pathway) were again (like the plasma analysis) among the most likely regulated biological pathway list. Previously, these neurotransmitter-related pathways were mainly studied in central neural system (CNS). However, recent findings showed that all three neurotransmitter systems (glutamate, 5HT and opioid) exist in the gastrointestinal tract (GI tract) (SANGER 2008) (Glass *et al*. 1999). Two possible mechanisms could be deduced from the altered microRNAs and potentially changed neurological pathways. 1) MicroRNAs could be involved in altered colorectal motility after RYGB. All three neurotransmitter- related pathways have been reported to be able to regulate the motility of gut (Talley 1992) (Toyomasu *et al*. 2010) (Porreca *et al*. 1986). Furthermore, previous studies also showed that bariatric surgery could influence the intestinal motility (Suzuki *et al*. 2005). 2) These altered microRNA may relate to RYGB-induced loss of appetite *via* glutamate receptor pathways. Studies suggest that altered gut hormones, such as ghrelin, PYY and GLP-1, and changed vagal nerve activity could be responsible for inhibited appetite after surgery (Tadross & Le Roux 2009). However, the specific neurotransmitter, which would be involved in mediating this interesting effect and detailed underlying molecular mechanisms, has not yet been explained. It is clear that signals from the gut are crucial for controlling appetite, regulating energy balance and glucose homeostasis. The peripheral and central vagus system could sense both mechanical distention and chemical stimulation by different nutrients (Näslund & Hellström

2007). By response to these vagus stimuli, intestinal L-cells could secrete higher levels of GLP-1 and PYY (Rocca & Brubaker 1999). Evidence suggests that glutamate is the primary afferent neurotransmitter of the vagus nerve conveying information from the gut to the brain (Hornby 2001). Here, three glutamate receptor pathways, both inotropic and metabotropic, were among the top ranking microRNA regulated pathway list. Therefore, it is possible that changed glutamate level/ glutamate receptor activity is responsible for altered vagus activity and subsequently leads to the increased secretion of gut hormones, which contribute to the post-operative effects on the brain, such as reduced appetite and shifted food preference.

Table 3-7 The predicted most likely altered pathways after RYGB (colon)

Pathway	Number of microRNA involved
Ionotropic glutamate receptor pathway	7
5HT1 type receptor mediated signaling pathway	7
EGF receptor signaling pathway	7
Metabotropic glutamate receptor group III pathway	6
Opioid proopiomelanocortin pathway	6
Opioid proenkephalin pathway	6
Metabotropic glutamate receptor group II pathway	6
Dopamine receptor mediated signaling pathway	6
Gonadotropin releasing hormone receptor pathway	6
5HT3 type receptor mediated signaling pathway	6
Angiogenesis	5
TGF-beta signaling pathway	5
Adrenaline and noradrenaline biosynthesis	5

3.5.3 General Discussion

World-wide obesity epidemics have led to severe economic and health burdens. Bariatric surgery has previously been reported to be the only long-term effective treatment for morbid obesity and resolves type 2 diabetes mellitus within days after surgery. From 2010, numerous studies have been undertaken to investigate the mechanism of post bariatric surgery benefits, mainly focused on changed gut hormones and leptin, shifted gut microbiota and altered metabolic profiles. However, the molecular mechanisms, which underline all of these effects, have not been clarified. Here, the function of microRNAs as links mediating metabolic alteration after RYGB surgery has been addressed.

Three principal methods are used to measure microRNA expression: real-time quantitative PCR, microarray hybridization and next generation deep sequencing. Generally, microarray is considered as the most cost-effective standardised high-throughput assay. The merit of deep sequencing is its ability to accurately assess expression and to identify novel microRNAs. However, both microarray and deep sequencing require pre-processing manipulation, such as annealing, RNA ligation, PCR amplification and recovery. These steps may induce inherent bias to the assay. Therefore, real time qPCR is often considered as a gold standard for microRNA detection. Microarray and deep sequencing approaches require at least 100ng of total RNA with good quality. Hence, I profiled the RYGB and SHAM operated rat plasma microRNAs using the most sensitive method available, Taqman TLDA cards, which is essentially real time qPCR. Sample size was less of a problem for colonic tissue so colonic microRNAome was examined using Illumina next generation deep sequencing platform.

The first interesting finding of this study was that RYGB surgery altered both plasma and colonic microRNA profiles at 8 weeks post surgery. A previous study has reported

perturbation in circulating microRNA profiles of morbid obesity patients and after RYGB surgery (Ortega *et al*. 2013). However, using the animal model in this study allows a) examination of the non-obesity related and pure RYGB surgical effects on normal SD rats, b) exploration of the potential metabolic mechanisms behind this altered circulating microRNA profile.

The second key finding was the 56-fold reduction of circulating miR-122 determined using TLDA cards. The result has been separately validated by qPCR. MiR-122 was first discovered in mouse liver in 2003. It was then widely studied across different species, including *Homo sapiens, Bos Taurus , Sus scrofa , Mus musculus* , and *Rattusnor-vegicus,* and was found to be highly conserved (Bartel & C.-Z. Chen 2004). MiR-122 was reported to be highly and specifically expressed in liver and accounts for 70% total hepatic-expressed microRNAs (Chang *et al*. 2004). The function of miR-122 was found to contribute to hepatocarcinogenesis and hepatitis C virus RNA replication (Jopling *et al*. 2005). Most interestingly, Christine Esau *et al*. elegantly proved that miR-122 plays very important roles in regulating lipid and cholesterol metabolism. By inhibiting the liver-expressed miR-122 using 2'-O-methoxyethyl phosphorothioate antisense oligonucleotide, plasma cholesterol level was reduced, hepatic fatty-acid oxidation was increased and the hepatic fatty-acid and cholesterol synthesis rates were inhibited (Esau *et al*. 2006). Although hepatic miR-122 was well studied in the past, it was only recently that blood-circulating miR-122 was detected (Starkey Lewis *et al*. 2011). By correlating my microRNAome profile with metabonomics data generated by Dr. Jia Li, it is hypothesised that the surgically induced miR-122 changes may be responsible for reduced ketone body generation after RYGB via increasing citrate synthase and aldoase expression in liver. In

chapter 4, I will further explore the metabolic function of hepatic miR-122 in the RYGB surgery model.

The third interesting find is the potential brain related functional alterations predicted by changed microRNAs. A total of 14 circulating microRNA and 12 colonic microRNAs were statistically differently expressed between RYGB and SHAM operated groups. It is noteworthy that by predicting biological function of these altered microRNAs with their computational putative targets, both circulating and colonic microRNAs may have the ability to regulate neurodegenerative or neurotransmitter related pathways. My data highlight the potential connection between dramatic metabolic alterations and brain functional changes, which has been referenced as the "gut-brain axis" (Heijboer *et al*. 2006). The gut-brain axis comprises both hormonal pathways (including hormones such as PYY and GLP-1, cytokines and neuropeptides) and neurological pathways (such as the enteric nervous system, sympathetic and spinal nerves and vagus). I shall refer to one example to demonstrate the potential multi-dimensional cooperative regulation mechanism among microRNAs, hormones and neurological systems.

GLP-1, which is the most well studied "gut-brain" hormone, is secreted by intestinal L-cell and beneficial for glucose homeostasis and food intake control . As shown in Figure 3.21, gut microbiota produced (Gutzwiller *et al*. 1999) SCFAs can stimulate GLP-1 secretion via G-protein coupled receptor 2 (FFAR2/GPR43) (Maslowski *et al*. 2009). Additionally, serotonin (5-HT), which is an appetite and hedonic control neurotransmitter, also mediates physiological effects of SCFAs by activating GPR43 (Karaki *et al*. 2006). It has been shown by both by my current study and previous studies that RYGB surgery could influence gut microbiota, SCFA levels and gut hormones (J. V. Li *et al*. 2011a). Panther pathway analysis suggested that both 5-HT1 and 5-HT3 receptor types of pathways might

be influenced by altered colonic microRNAs. It could be possible that microbiota, GPR43, 5HT and GLP-1 are working together as a link between the gut and brain after RYGB surgery, which contributed to reduced appetite. As a facilitator, the inhibition of miR-150 (both in plasma and colon) could lead to up-regulation of colonic GPR-43 since it is a predicted target of miR-150 (predicted by miRANDA algorithm). A few questions should be further explored in future. For instance, is it possible that decreased miR-150 is able to stimulate GPR-43, which leads to an active secretion of GLP-1 and 5HT? Does the gut microbiota or changed SCFAs influence colon miR-150 expression either directly or through transcriptional factors? Do any other colonic microRNAs behave similarly as messengers between the gut and the brain?

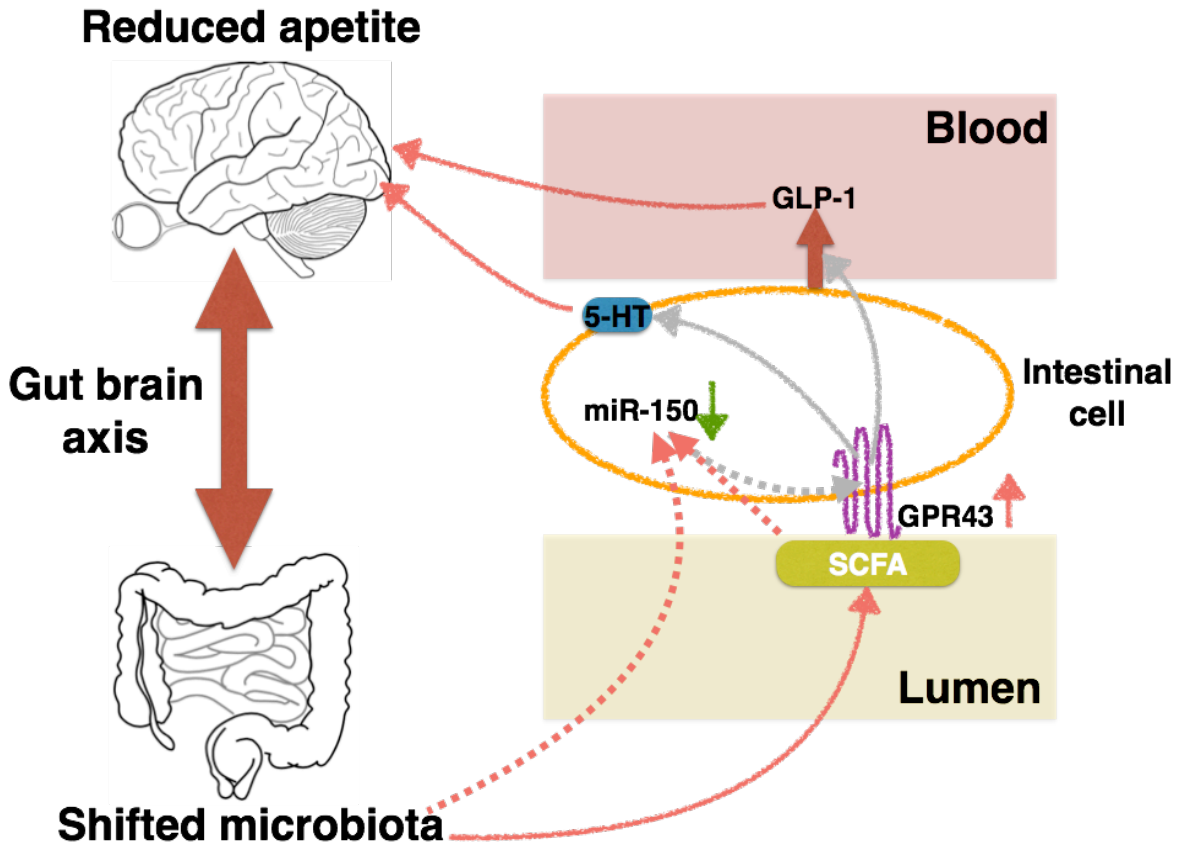

Figure 3-21 Potential mechanism of microRNA mediated crosstalk between gut-brain axis

In conclusion, the current study has shown that circulating and colonic microRNAome is fundamentally different between RYGB and SHAM operated rats. These findings here may shed some light on the mechanisms of microRNAs as metabolic regulators mediating post RYGB surgery benefits. Clearly, more work needs to be carried out to examine the underlying molecular functions of these altered microRNAs. Some of these points will be further investigated in Chapter 4, with a focus on the role of miR-122 in the rat RYGB model.

4. Functionality of Hepatic MiR-122 in Rat RYGB Model

4.1 Introduction

A group of circulating and colonic microRNAs, which are dysregulated post RYGB surgery, are described in Chapter 3. In this chapter, the focus will be placed on miR-122, which exhibits the greatest change among all altered circulating microRNAs, regarding its hepatic expression and metabolic function in RYGB surgery using both *in vivo* and *in vitro* experiments.

The liver is a vital organ, which plays critical roles in regulating energy homeostasis *via* controlling carbohydrate, lipid and protein metabolism. Liver receives blood from the intestinal tract, which contains the products of digestion and absorption. Depending on feeding or fasting conditions, the liver either stores carbohydrate as glycogen or mobilises it to contribute to blood glucose. Furthermore, glucose in liver can also be produced from other substrates, a process named gluconeogenesis. The liver can also oxidise fatty acids and produces smaller and water-soluble ketone bodies, which can be exported to other tissues. By investigating whether the liver function is influenced by altered microRNAs after bariatric surgery, we can understand the rationale behind the post-surgery benefits.

In 2003, systematic cloning and sequencing of small non-coding RNAs led to the discovery of miR-122 in mouse liver (Lagos-Quintana *et al*. 2003). It locates on chromosome 18 intergenic region, from 61,512,747 to 61,512,831 (chromosome location). The structure detail and seed region of miR-122 is shown in Figure 4.1. MiR-122 was also identified as the most abundant microRNA in the liver, which reaches around 70% of total hepatic microRNAs (Lagos-Quintana *et al*. 2002). In 2004, Chang *et al.* detected, in

embryonic and new born mouse, that miR-122 increased from day 12, reaching a plateau level just before birth and continued to increase, but with a much slower rate after birth (Chang *et al*. 2004). This study built the primary link between the liver developmental process and the accumulation of miR-122. Subsequently, functional research considered the contribution of miR-122 to a) hepatocarcinogenesis (Kutay *et al*. 2006), b) hepatitis C virus amplification (Jopling *et al*. 2005) and c) energy metabolism (Elmen *et al*. 2008). Here in this chapter, we focused on the metabolic function of miR-122 after RYGB surgery.

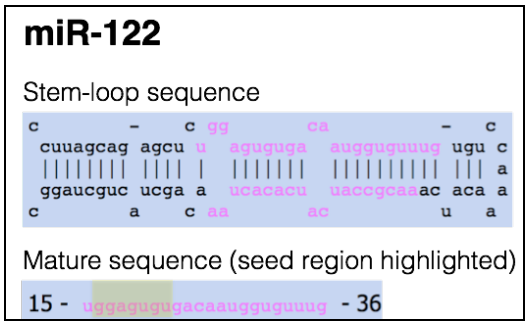

Figure 4-1 The stem-loop structure and mature sequence of miR-122 (seed region highlighted)

Interestingly, most of the liver metabolic pathways are under circadian control. By inducing mutation of the circadian *Clock* gene, mice developed metabolic syndrome with hyperleptinemia, hyperlipidemia, hepatic steatosis, hyperglycemia, and hypoinsulinemia (Turek 2005). Interestingly, both pri-miR-122 and pre-miR-122 are transcribed in a cyclic circadian fashion *via* a circadian nuclear receptor REV-ERBα (Gatfield *et al*. 2009). The expression level of miR-122 has been linked to the energy expenditure rate in previous studies (Elmén *et al*. 2008). It is possible that the oscillation of miR-122 across the day could damp the fluctuation of energy intake and expenditure between daytime and nighttime. Moreover, as shown in Table 4.1, a handful of metabolically related targets of miR-122 have been either experimentally validated or computationally predicted. These targets (Shown in Table 4.1) belong to multiple metabolic pathways, such as glycolysis

(*Aldoa*), gluconeogenesis (*G6pc, G6pc3*), glycogenesis (*Gys1*), pentose phosphate pathway (*G6pd*), fatty acid synthesis (*Fasn*) and TCA cycle (*Cs*). Some of the targets behave as important metabolic regulators, for instance, two (α and β/δ) peroxisome proliferation-activated receptors (*Ppar*) and PPARγ co-activator a (*Pgc1α*) are among either validated or putative miR-122 target lists. PPARs are a group of nuclear receptors that function as transcription factors regulating various metabolic processes *via* heterodimers with retinoid X receptor (RXR) and binding to the promoter region's peroxisome proliferator hormone response elements (PPRE). PPARs play important roles in obesity-related metabolic diseases such as hyperlipidemia, insulin resistance, and coronary artery disease (Evans *et al*. 2004). Besides PPARs, cellular energy sensor AMP-activated protein kinase (AMPK, coded by *Prkab1* and *Prkab2*) are also predicted as targets of miR-122. AMPK acts as a sensitive cellular energy switch. Under energy deficient status (high AMP:ATP ratio), AMPK can switch off ATP-consuming biosynthesis pathways, such as fatty acid synthesis, cholesterol synthesis and gluconeogenesis, and switch on ATP-producing catabolic pathways, for example, fatty acid oxidation and glycolysis in multiple tissues (Hardie 2008).

Table 4-1 MiR-122 predicted and validated metabolic related targets

Validated and putative miR-122 metabolic enzyme/ receptor targets					
Validated targets	SLC7A1	ALDOA	GYS1	PKM2	GK
	IDH1	G6PD	G6PC	G6PC3	FASN
	LDHA	PGC1α	ACLY	CS	
Putative targets	HK2	UCP2	AMPKβ1	AMPKβ2	PPARβδ
	PPARα				

The large number of crucial metabolic targets and circadian expression of miR-122 supports its metabolic importance. Additionally, as described in the Introduction Chapter, the inhibition of miR-122 leads to decreased circulating cholesterol level and increased hepatic fatty acid oxidation rate. Furthermore, miR-122 is the most dramatic altered circulation microRNA (decreased 56 fold) after RYGB surgery (see chapter 3.3.2.6). Therefore, in this chapter, the expression of hepatic miR-122 and its metabolic targets are examined both in *in vivo R*YGB surgical model and in an i*n vitro* mechanistic model.

4.2 Methods and experiment outline

1. Tissue total RNA extraction is described in 2.3.2
2. Taqman single microRNA assay is described in 2.4.2
3. Taqman mRNA qPCR assay is described in 2.4.2
4. Tissue protein extraction and quantification is described in 2.6.1 and 2.6.2
5. Immunoblot is described in 2.7
6. FAO and B13H cell line culture condition is described in 2.2.5 and 2.2.6
7. MicroRNA mimic/ inhibitor transfection is described in 2.2.11

4.3 Results with discussion

4.3.1 Hepatic miR-122 expression in RYGB- and SHAM- operated rat

Similar to circulating miR-122, hepatic miR-122 expression is significantly inhibited (41%) in RYGB operated rats (n=8) compared with SHAM operated rats (n=5) (student's t-test, p=0.0295), but to a much lesser extent (Figure 4.2). Stably expressed endogenous non-coding RNA U6 was applied as a normalisation control and the result is presented as fold change (RYGB/SHAM) using 2-[delta][delta]Ct method (Livak & Schmittgen 2001). The result suggests that the liver, where miR-122 is believed to be synthesised, appears to produce less miR-122 with presumably less being released into the blood stream. Alternatively, in RYGB animals, the liver-secreted miR-122 is transported more to/ taken up into other organs as a hormone, which leads to a moderated suppression in liver but a dramatically decrease in blood. Interestingly, unlike liver, they found brain miR-122 was up-regulated after RYGB surgery. The drastic alteration of miR-122 in circulation compared to liver and its increased level of expression in brain highlights the exciting potential of circulating microRNAs to behave as paracrine hormones.

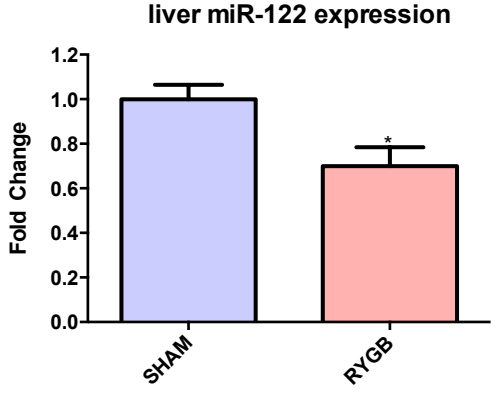

Figure 4-2 Hepatic miR-122 mRNA by qPCR in RYGB and SHAM rats

Aliquots of RNA (2ng/μL) was used for qPCR. Y-axis is displayed with averaged expression fold change (RYGB:SHAM). SHAM n=5, RYGB n=8. Error bars are the mean with SEM and * signifies statistically significant as determined by student t test $p<0.05$.

4.3.2 Examination of miR-122 targets in SHAM- and RYGB- operated rats

To examine the targets of hepatic altered miR-122 in RYGB rats, 12 metabolic related enzymes and transcriptional factors, which belong to 10 metabolic processes, were chosen to be measured *ex vivo*. As seen in Table 4.2, both computer predicted putative targets (blue) and experimental validated (red) targets were selected. The metabolic pathways, which are regulated by the selected targets, belong to several aspects of the liver glucose metabolic processes (Figure 4.3). Generally, glucose is absorbed from the intestine into the hepatoportal vein. The hepatocytes are therefore exposed to absorbed glucose, transported through **glucose transporters** (predominantly GLUT2, but also GLUT1 (G W Gould 1993)). Within the hepatocyte, glucose is phosphorylated to glucose 6-phosphate and enters the pathways of **glycogen synthesis** or **glycolysis**. In the carbohydrate excess situation, glucose 6-phosphate can also enter the **pentose phosphate pathway** to generate pentoses, which are required for synthesis of nucleic acids. Glycolysis product, pyruvate, can be oxidised to acetyl-CoA or oxaloacetate and directly metabolised in the **tricarboxylic acid cycle** (TCA). Alternatively, acetyl-CoA could be transported out of mitochondria and enter **fatty acid synthesis** pathway. Besides the aforementioned metabolic pathway enzymes, three energy regulating systems, energy sensor **AMP-activated protein kinase** (AMPK), oxidative phosphorylation related **uncoupling protein** (UCP) and nuclear receptor proteins **peroxisome proliferator-activated receptors** (PPARs), were all included in the following study.

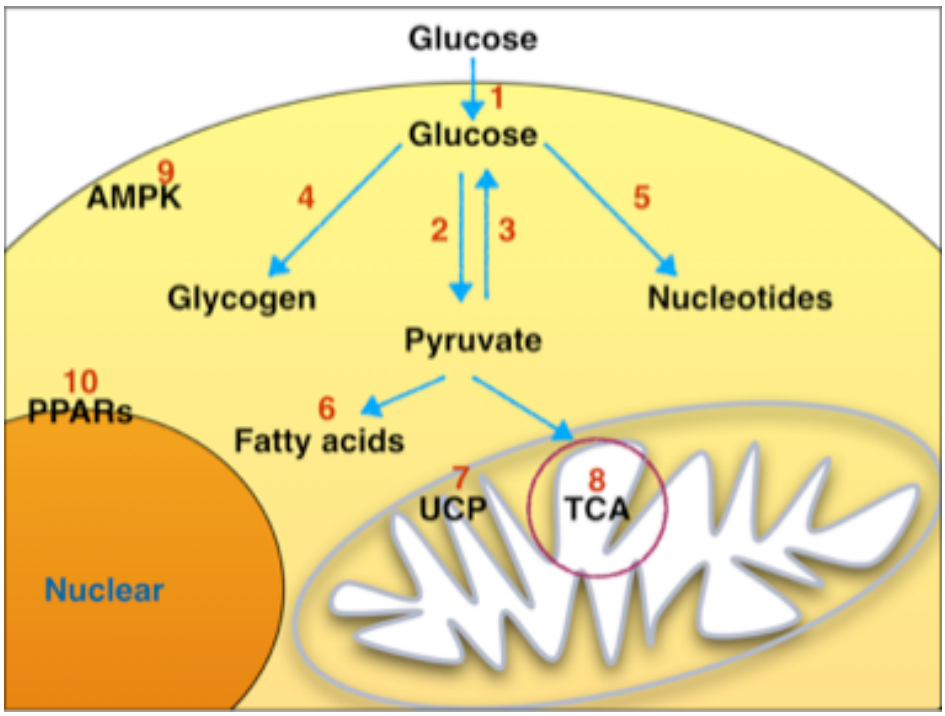

Figure 4-3 metabolic pathways which are targeted by the selected molecules (see also table 4.2)

Table 4-2 miR-122 metabolic targets

No.	Metabolic pathway/ function	Target name	
1	Glucose transportation	Glut1	
2	Glycolysis	ALDOA	
3	Gluconeogenesis	G6PC	
4	Glycogenesis	IDH1	
5	Pentose phosphate pathway	G6PD	
6	Fatty acid metabolism	FASN	
7	Oxidative phosphorylation	UCP2	
8	TCA cycle	CS	
9	AMPKs	AMPKβ1	AMPKβ2
10	PPARs	PPARa	PPARb

Red=experimentally validated by previous study (Boutz *et al*. 2011), blue=computational predicted targets.

The No. in the table corresponds with the pathway number in Figure 4.3

4.3.2.1 Glucose transportation

Glucose plays a central role in cellular homeostasis and metabolism. It is well established that nearly all cell types possess a glucose transportation system, which allows the movement of glucose down its chemical gradient into cells (Olson & Pessin 1996). The class I glucose transporter, GLUT or SLC2A family, is the most common and well-studied glucose transporter protein family in mammalian cells. GLUT1 is widely distributed in fetal tissues and expressed at the highest level in erythrocytes (G W Gould 1993). Albeit highly expressed in fetal tissues, it exists in all cell types and is responsible for the low-level basal glucose uptake required to sustain respiration (Pessin & Bell 1992). Here, *Glut1* is a validated miR-122 target, whose 3' UTR has an exact match to positions 2-8 of the mature miR-122 sequence. Taqman quantitative PCR was used to examine whether reduced miR-122 expression in RYGB could affect *Glut1* mRNA expression in the liver. Ribosome 18S RNA was used to normalize data and results are presented as RYGB to SHAM group fold change (all the following hepatic target experiments used an identical protocol and same normalisation method). As seen in Figure 4.4, although *Glut1* mRNA alteration is not significant (student's t-test, P=0.1477), there is a suggestion that hepatic *Glut1* was up-regulated.

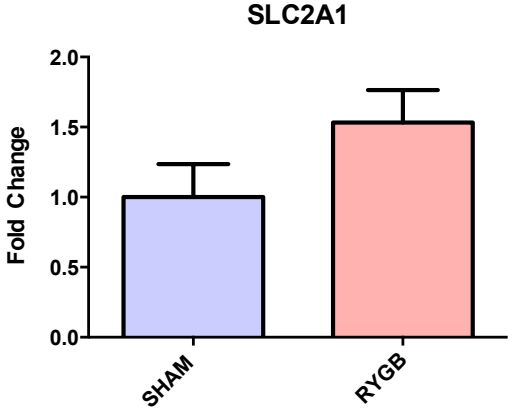

Figure 4-4 Hepatic SLC2A1/GLUT1 mRNA by qPCR in RYGB and SHAM rats

RNA (200 ng/μL) was used for qPCR. Y-axis is displayed with averaged expression fold change (RYGB:SHAM). SHAM n=5, RYGB n=8. Error bars are the mean with SEM.

4.3.2.2 Glycolysis

Glycolysis, occurs in the cytosol of the cell and is a metabolic pathway which converts glucose into pyruvate. Fructose-biphosphate aldolase (aldolase), is an enzyme catalysing a reversible reaction that splits hexose 1,6-biphosphate into two triose sugars, dihydroxyacetone phosphate (a ketone) and glyceraldehyde 2-phosphate, an aldehyde (Figure 4.5). There are three aldolase isozymes (A, B and C), which are encoded by three different genes. Here, I focused on ALDOA since it is an experimentally validated miR-122 target (Elmén *et al*. 2008). Systematically administrating unconjugated locked nucleic acid (LNA) anti-miR-122 led to up-regulation of aldolase A both at the mRNA and protein levels (Elmén *et al*. 2008). As expected and shown in Figure 4.6, RYGB-operated rats exhibited a significant 79.9% up-regulation of *Aldoa* compared to SHAM operated rats (student's t-test, p=0.0051). The result confirmed the hypothesis made in Chapter 3, that the inhibited miR-122 could favour glycolysis by increasing its targ*et aldoa* expression.

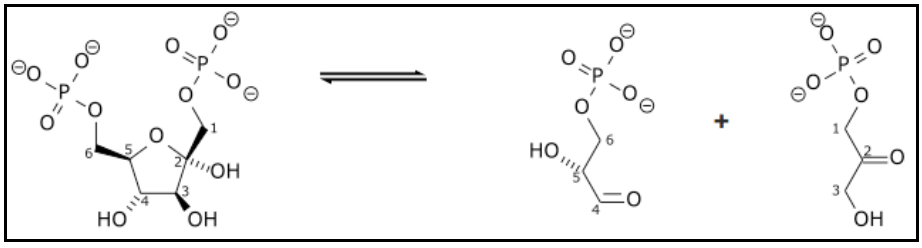

Figure 4-5 Reaction catalysed by aldolase

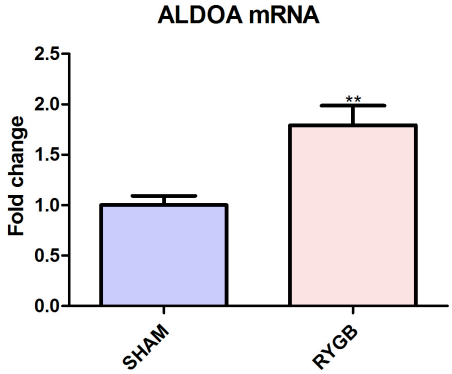

Figure 4-6 Hepatic ALDOA mRNA by qPCR in RYGB and SHAM rats

RNA (200ng/μL) was used for qPCR. Y-axis is displayed with averaged expression fold change (RYGB:SHAM). SHAM n=5, RYGB n=8. Error bars are the mean with SEM and ** signifies statistically significant as determined by student t test p<0.01.

4.3.2.3 Gluconeogenesis

Liver generates glucose by *de novo* synthesis from non-carbohydrate precursors, such as lactate, pyruvate, glycerol and alanine, so called gluconeogenesis process. Compared to glucogenesis, another glucose generating pathway, gluconeogenesis occurs more rapidly and is suggested to be more important with prolonged fasting (GF, 1970). The rate of gluconegenesis is controlled by key metabolic enzymes (phospoenolpyruvate carboxykinase <PEPCK>, fructose-1,6-bisphosphatase and glucose-6-phosphatase <G6PC>) and nuclear transcription factor peroxisome proliferator-activated receptor gamma coactivator 1 alpha (PGC1α). MiR-122 is a predicted regulator of G6PC. Surprisingly, as shown in Figure 4.7, instead of being up-regulated by decreased miR-122 level, *G6pc* mRNA expression was significantly reduced by 82% in the RYGB group (student's t-test, p=0.0039). By decreasing levels of the key enzyme of gluconeogenesis, the conversion rate from non-carbohydrates to glucose in the RYGB-operated rats would be expected to be reduced and indeed it was significantly inhibited in the liver, the result of which was confirmed by NMR based metabonomics study.

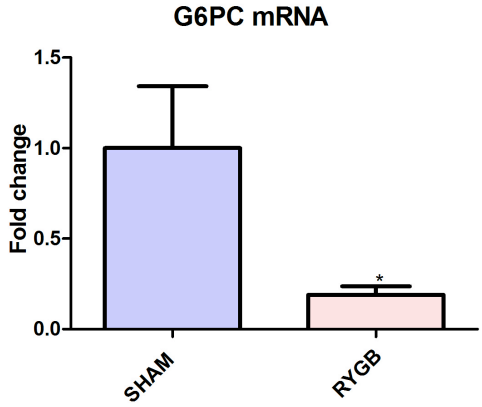

Figure 4-7 Hepatic G6PC mRNA by qPCR in RYGB and SHAM rats

RNA (200ng/μL) was used for qPCR. Y-axis is displayed with averaged expression fold change (RYGB:SHAM). SHAM n=5, RYGB n=8. Error bars are the mean with SEM and * signifies statistically significant as determined by student t test p<0.05.

4.3.2.4 Glycogenesis

The metabolic synthesis of glycogen, in which glucose molecules are added to the chains of glycogen for storage is termed glycogenesis. In liver, this process can be activated by insulin in response to high glucose levels at the post-prandial stage(Miller & Larner 1973). Glycogen synthase (GYS) converts glucose residues one by one into a polymer chain. As the key enzyme of glycogenesis, over-expressing the GYS gene in transgenic mice yielded excess glycogen storage levels (Manchester *et al*. 1996). Hence, the level of GYS expression directly indicates the glycogen synthesis rate. Two isoforms of glycogen synthase exist in mammals. One encoded by *Gys2* appears only to be expressed in the liver, whereas the other one coded by *Gys1*, is expressed in multiple tissues, including skeletal and cardiac muscle, brain and liver with relatively lower amounts (Kaslow & Lesikar 1984; Kaslow *et al*. 1985). Based on computational prediction and previous studies, only *Gys1* is a *bone fide* target of miR-122 (Esau *et al*. 2006). Injection of anti-sense miR-122 systematically leads to a dose-dependently increase in the hepatic *Gys1* expression (Esau *et al*. 2006). As figure 4.8 shows, unexpectedly, there is no significant alteration in *Gys1* mRNA expression between the two biological groups. However, changes in mRNA levels do not necessarily relate directly to activity levels of a particular enzyme as post transcriptional control and cofactor availability will govern protein activity. It is therefore important to confirm activity using enzyme kinetics or metabolite measurement.

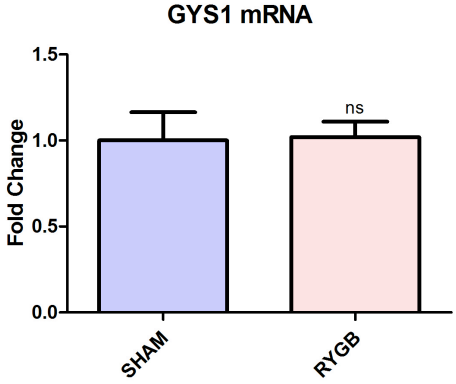

Figure 4-8 Hepatic GYS1 mRNA by qPCR in RYGB and SHAM rats

RNA (200ng/μL) was used for qPCR. Y-axis is displayed with averaged expression fold change (RYGB:SHAM). SHAM n=5, RYGB n=8. Error bars are the mean with SEM.

4.3.2.5 Pentose phosphate pathway

The Pentose phosphate pathway generates NADPH, which is subsequently used in fatty acid biosynthesis, and pentose for nucleic acid synthesis. Glucose-6-phosphate dehydrogenase (G6PD) is the first and rate-limiting enzyme in pentose phosphate pathway. The role of G6PD in diabetes and obesity development process is still controversial. Conflicting results have shown that G6PD and NADPH levels can be inhibited in the liver of ¡diabetes patients (Cedola & Cabarrou 1975) or up-regulated in the liver of of Zucker diabetic *fa/fa* rat (Gupte *et al*. 2009). Genetically, the consensus is that G6PD deficiency is associated with increased risk of diabetes mellitus (Wan *et al*. 2002). G6PD is an experimentally validated target of miR-122 (Boutz *et al*. 2011). Here, in the RYGB-operated rats, the *G6pd* mRNA expression is significantly up-regulated by 91% in the liver of RYGB-operated rats compared to SHAM-operated (Figure 4.9; p=0.0009). G6PD is not only essential for the pentose phosphate pathway, but also plays an important role in defending against oxidative stress by generating NADPH (Pandolfi *et al*. 1995). The up-regulated *G6pd* could indicate a favoured pentose phosphate pathway and an enhanced protection against the accumulated reductive oxygen species generated by intensive oxidative phosphorylation after RYGB surgery.

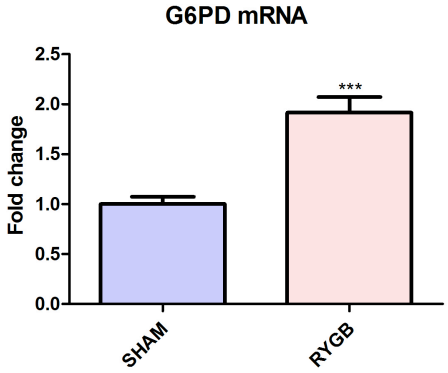

Figure 4-9 Hepatic G6PD mRNA by qPCR in RYGB and SHAM rats

RNA (200ng/µL) was used for qPCR. Y-axis is displayed with averaged expression fold change (RYGB:SHAM). SHAM n=5, RYGB n=8. Error bars are the mean with SEM and *** signifies statistically significant as determined by student t test p<0.0001.

4.3.2.6 Fatty acid metabolism

Fatty acid synthase (FASN), synthesises long-chain fatty acids by using acetyl coenzyme A as a primer, malonyl-CoA as a 2-carbon donor, and NADPH as a cofactor reducing equivalent. It catalyses the last step in the fatty acid biosynthesis pathway and is frequently used as a marker of *de novo* hepatic lipogenesis (Yanxin Wang *et al*. 2004). Numerous studies have focused on the function of FASN in obesity, diabetes and non-alcoholic fatty liver disease (NAFLD) (Menendez *et al*. 2009). Hepatic *Fasn* knock-out mice have previously been used to specifically study FASN function. The mutant mice possess a similar phenotype to the control mice when fed with normal chow diet. However, surprisingly, under a low-fat/high-carbohydrate diet, mice lacking hepatic FASN exhibited accelerated *de novo* lipogenesis with a reduced β-oxidation rate (Chirala *et al*. 2003) (Chakravarthy *et al*. 2005). This mouse model has led to an interesting concept that the fatty acids, in particular palmitate, are synthesised when FASN acts as an agonist to activate a pool of nuclear receptors, such as peroxisome proliferator receptor α (PPARα). These nuclear receptors are in turn responsible for enhancing fatty acid β-oxidation rate (Chakravarthy *et al*. 2005). In the current study, as a validated target of miR-122, *Fasn* was significantly up-regulated by 74% in RYGB rats (p=0.0475). This suggests up-regulation of *de novo* lipogenesis in the liver after RYGB. Whether the increased *Fasn* expression post-RYGB surgery is beneficial for fatty acid oxidation will need to be carefully examined in the future.

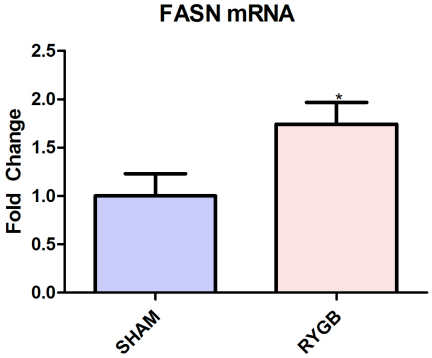

Figure 4-10 Hepatic *Fasn* mRNA by qPCR in RYGB and SHAM rats

RNA (200ng/μL) was used for qPCR. Y-axis is displayed with averaged expression fold change (RYGB:SHAM). SHAM n=5, RYGB n=8. Error bars are the mean with SEM and * signifies statistically significant as determined by student t test $p<0.05$.

4.3.2.7 Oxidative phosphorylation

Oxidative phosphorylation is the ATP-generating process in mitochondria, where ATP synthase makes ATP via chemiosmosis of protons. Uncoupling protein (UCP) creates an alternative way for protons to return to the mitochondrial matrix, by uncoupling the electron transport chain required for ATP synthesis (Brand & Esteves 2005). There are three sub-groups of UCP, namely UCP1, UCP2 and UCP3. Uncoupling protein 2 (UCP2) has been shown to have a crucial role in multiple physiological and pathological processes (Arsenijevic *et al*. 2000; Fleury *et al*. 1997; C.-Y. Zhang *et al*. 2001). Prolonged fasting and exposure to high levels of fatty acids can induce UCP2 expression, which then promotes a metabolic shift from carbohydrate metabolism towards lipid metabolism (Andrews *et al*. 2008). Furthermore, the up-regulation of UCP2 can protect mitochondria from reactive oxygen species generated *via* intensive fatty acid β-oxidation (Patterson, Shah, Matsubara, Krausz & Gonzalez 2012a). In the present study, a significant increase in UCP2 expression was observed in the liver of RYGB-operated rats at both mRNA (71.4%, student's t-test p=0.0039) (Figure 4.11) and protein level (150.7%, student's t-test p=0.0081) (Figure 4.12). The up-regulated UCP2 suggests an accelerated fatty acid oxidation rate and a metabolic shift towards lipid metabolism after RYGB surgery.

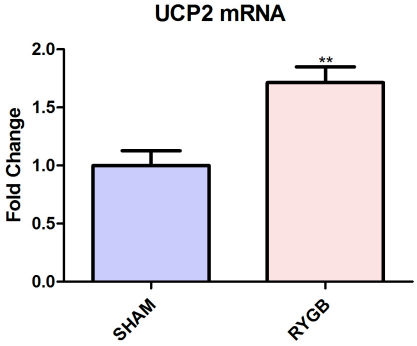

Figure 4-11 Hepatic *Ucp2* mRNA by qPCR in RYGB and SHAM rats

RNA (200ng/μL) was used for qPCR. Y-axis is displayed with averaged expression fold change (RYGB:SHAM). SHAM n=5, RYGB n=8. Error bars are the mean with SEM and ** signifies statistically significant as determined by student t test p<0.01.

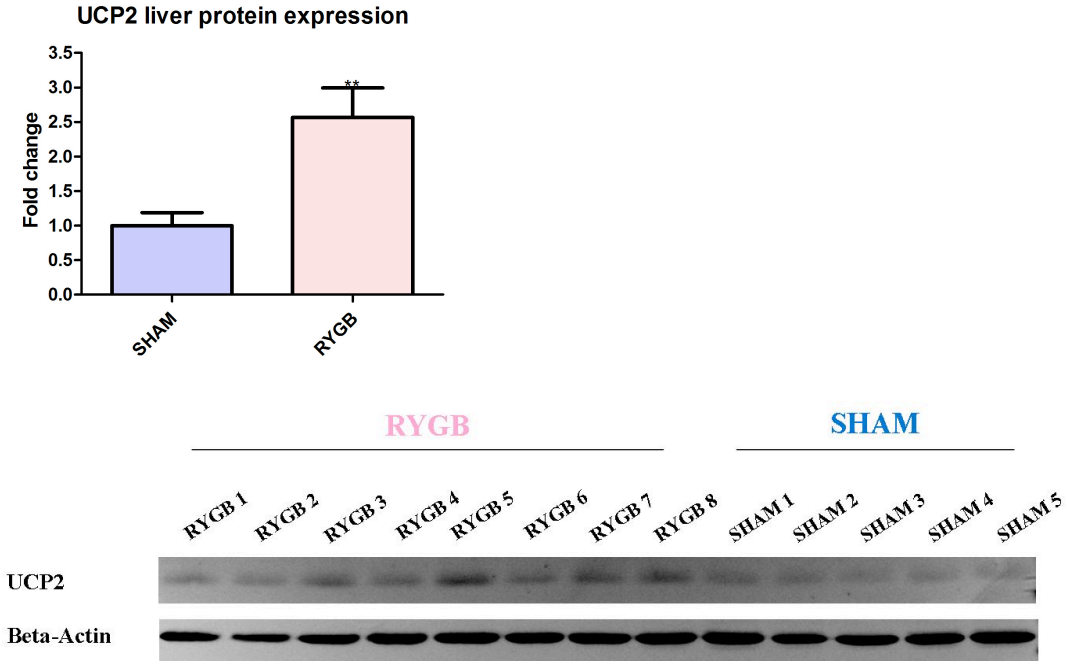

Figure 4-12 Hepatic UCP2 protein expression by immunoblot in RYGB and SHAM rats

Y-axis is displayed with averaged expression fold change (RYGB:SHAM). SHAM n=5, RYGB n=8. Error bars are the mean with SEM and ** signifies statistically significant as determined by student t test $p<0.01$. 20µg of protein was loaded for immunoblot. Protein expression was quantitated using Kodak Imaging Station 4000MM. A total of 20 ng of protein was loaded into each well and β-actin was used as a loading control and normaliser.

4.3.2.8 TCA cycle

Citrate synthase (CS) is an essential enzyme for nearly all living cells and it plays a key role in regulating the tricarboxylic acid (TCA) cycle. It is coded by nuclear genomic DNA, translated in cytoplasm and almost exclusively located in the inner membrane of mitochondria (Wiegand & Remington 1986). CS catalyses the condensation of oxaloacetate and acetyl coenzyme A to form citrate in the TCA cycle. It is the first and rate-limiting step of the TCA cycle and plays a crucial role in regulating energy generation and mitochondrial respiration (Wiegand & Remington 1986). In the present study, post RYGB surgical rats exhibited a 1.8-fold increase in *Cs* expression transcriptionally (student's t-test p=0.0195) (Figure 4.13) and a 2-fold significant increase of CS protein expression in comparison to the SHAM-operated group (student's t-test p=0.0435) (Figure

4.14). This result supports the hypothesis proposed in Chapter 3 that RYGB surgery affects the TCA cycle by regulating its rate-limiting enzyme CS. The favoured TCA cycle would be predicted to sequester acetyl-CoA into TCA instead of generating ketones.

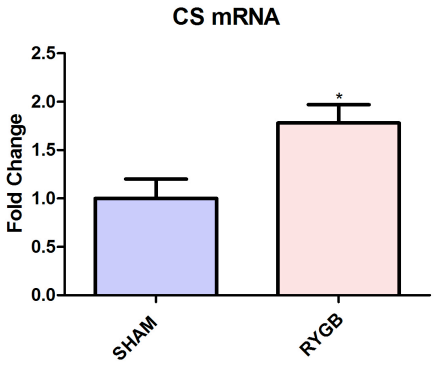

Figure 4-13 Hepatic *CS* mRNA by qPCR in RYGB and SHAM rats

RNA (200ng/μL) was used for qPCR. Y-axis is displayed with averaged expression fold change (RYGB:SHAM). SHAM n=5, RYGB n=8. Error bars are the mean with SEM and * signifies statistically significant as determined by student ttest p<0.05.

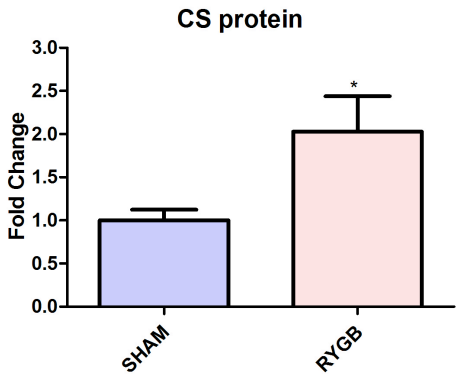

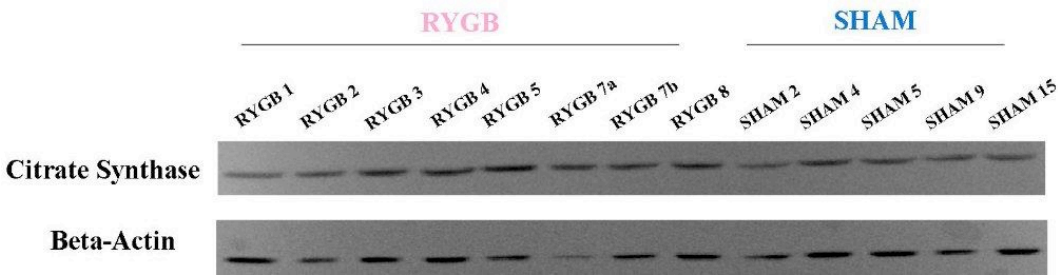

Figure 4-14 Hepatic CS protein expression by immunoblot in RYGB and SHAM rats

Y-axis is displayed with averaged expression fold change (RYGB:SHAM). SHAM n=5, RYGB n=8. Error bars are the mean with SEM and * signifies statistically significant as determined by student t test p<0.05. 20μg of protein was loaded for immunoblot. Protein expression was quantitated using Kodak Imaging Station 4000MM using beta-actin as a loading control.

4.3.2.9 AMPK

AMP-activated protein kinase (AMPK) is a key regulator of energy balance. It is expressed in the central nervous system (brain) and in peripheral tissues, including liver, pancreas, skeletal muscle, heart and adipose cells (B. B. Kahn *et al*. 2005). Generally, AMPK can sense and be modulated by environmental energy status reflected by the AMP:ATP ratio (Hardie *et al*. 2012). Under energy deficient status (high AMP:ATP ratio), for instance glucose deprivation during exercise, AMPK can be activated to switch off ATP-consuming biosynthesis pathways such as fatty acid synthesis, cholesterol synthesis and gluconeogenesis, and switch on ATP-producing catabolic pathways, for example fatty acid oxidation and glycolysis (Hardie *et al*. 2012). AMPK exists as a heterotrimer containing a catalytic α subunit and non-catalytic regulatory β and ɣ subunits (function as scaffold and contain glycogen binding domain) (Hardie *et al*. 2012). Both AMPKβ1 and AMPKβ2 are predicted as miR-122 targets (Mirtarget: www.microRNA.org). The inhibition of AMPKβ1 mRNA (*Prkab1*), but not AMPKβ2 (*Prkab2*), was significantly relieved by decreased miR-122 leads in RYGB- compared to SHAM- operated rats (student's t-test p=0.0067) (Figure 4.15). To confirm the effect of this on *Prkab1* expression, immuno blot was then carried out. Surprisingly, instead of increased expression in line with the mRNA changes, protein expression of AMPKβ1 was significantly down regulated by 61% in the RYGB group (Figure 4.16). The result was consistent in three independent immunoblot experiments. This inconsistency between mRNA and protein expression levels could be explained by the fact that AMPKβ1 unit requires activation *via* phosphorylation. Hence, the decreased non-phosphorylated AMPKβ1 may result from an increased level of active phosphorylated AMPKβ1. Indeed, immunoblot showed that the active phosphorylated-AMPKβ1 protein was significantly up-regulated by 2 fold (Figure 4.16).

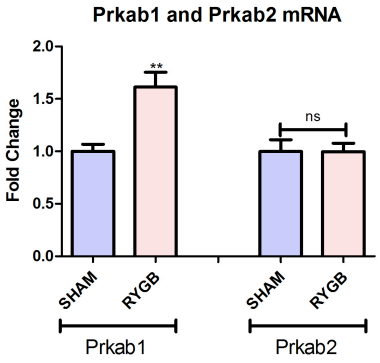

Figure 4-15 Hepatic *Prkab1 and Prkab2* mRNA by qPCR in RYGB and SHAM rats

RNA (200ng/µL) was used for qPCR. Y-axis is displayed with averaged expression fold change (RYGB:SHAM). SHAM n=5, RYGB n=8. Error bars are the mean with SEM and ** signifies statistically significant as determined by student t test p<0.01.

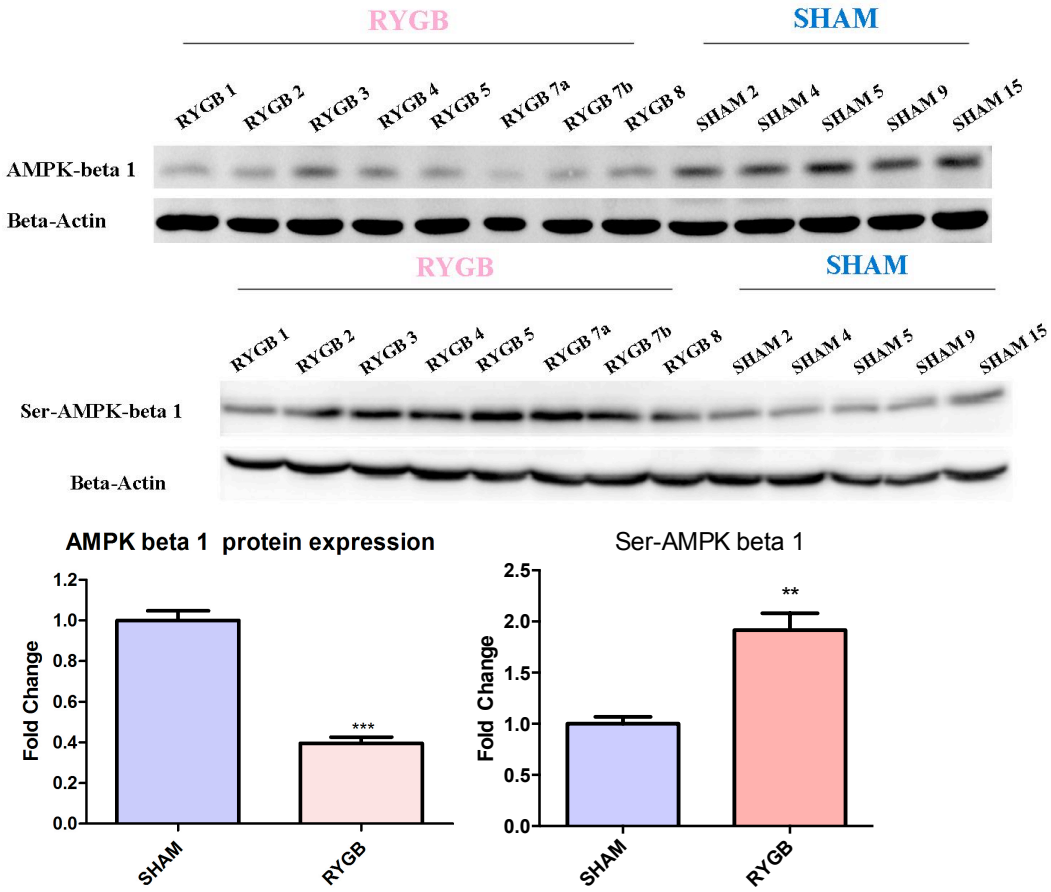

Figure 4-16 Hepatic AMPKβ1 and ser-AMPKβ1 protein expression by immunoblot in RYGB and SHAM rats

Y-axis is displayed with averaged expression fold change (RYGB:SHAM). SHAM n=5, RYGB n=8. Error bars are the mean with SEM and *** signifies statistically significant as determined by student t test p<0.0001. 20µg of protein was loaded for immunoblot. Protein expression was quantitated using Kodak Imaging Station 4000MM.

4.3.2.10 PPARs

Lipid and glucose metabolism are inherently related. The findings of three “lipid-sensing” nuclear receptors, peroxisome proliferator-activated receptors (PPARα, PPARβ/δ and PPARγ) improved our understanding of the links between glucose and lipid metabolism (C.H. Lee *et al*. 2003). These nuclear receptors can be activated by both dietary fatty acids and their metabolic derivatives, and thus serve as lipid sensors which can markedly redirect metabolism (Willson *et al*. 2000). Activating PPARα and PPARβ/δ results in fatty acid oxidation, whereas PPARγ can regulate the whole body insulin sensitivity and maintain a balance between lipogenesis and lipid storage (Evans *et al*. 2004). Both PPARα and PPARβ/δ are predicted to be miR-122 targets (Mirtarget: www.microRNA.org). Hence, their mRNA expression was tested in the RYGB- and SHAM- operated rats. However, no significant alterations of *Pparα* and *Pparβ/δ* expression levels were observed between the two groups of animals (*Pparα* p=0.4146, *Pparβ/δ* p=0.7242) (Figure 4.17). It is worth noting that the unchanged *Ppar* expression does not necessarily indicate unaltered activation of PPARs. Post-operative PPARs activity should be determined by their downstream gene expression and this is certainly worth exploring in the future.

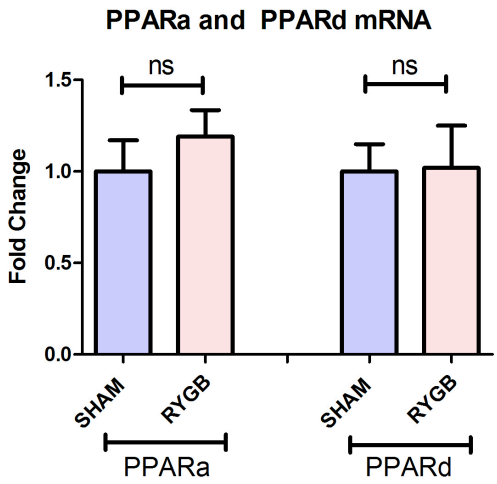

Figure 4-17 Hepatic *Pparα and Pparβ* mRNA by qPCR in RYGB and SHAM rats

RNA (200ng/μL) was used for qPCR. Y-axis is displayed with averaged expression fold change (RYGB:SHAM). SHAM n=5, RYGB n=8. Error bars are the mean with SEM.

4.3.3 Correlation between hepatic miR-122 and its metabolic targets

As expected, non-parametric Pearson correlation exhibited strong negative correlation trends between the expression level of miR-122 and its targeted mRNAs (Figure 4.18). It suggests that miR-122 may play an essential role in regulating its hepatic metabolic targets post RYGB surgery. However, the ultimate determination regarding whether miR-122 possesses the ability to regulate these targets should be examined by a miR-122 manipulating experiment.

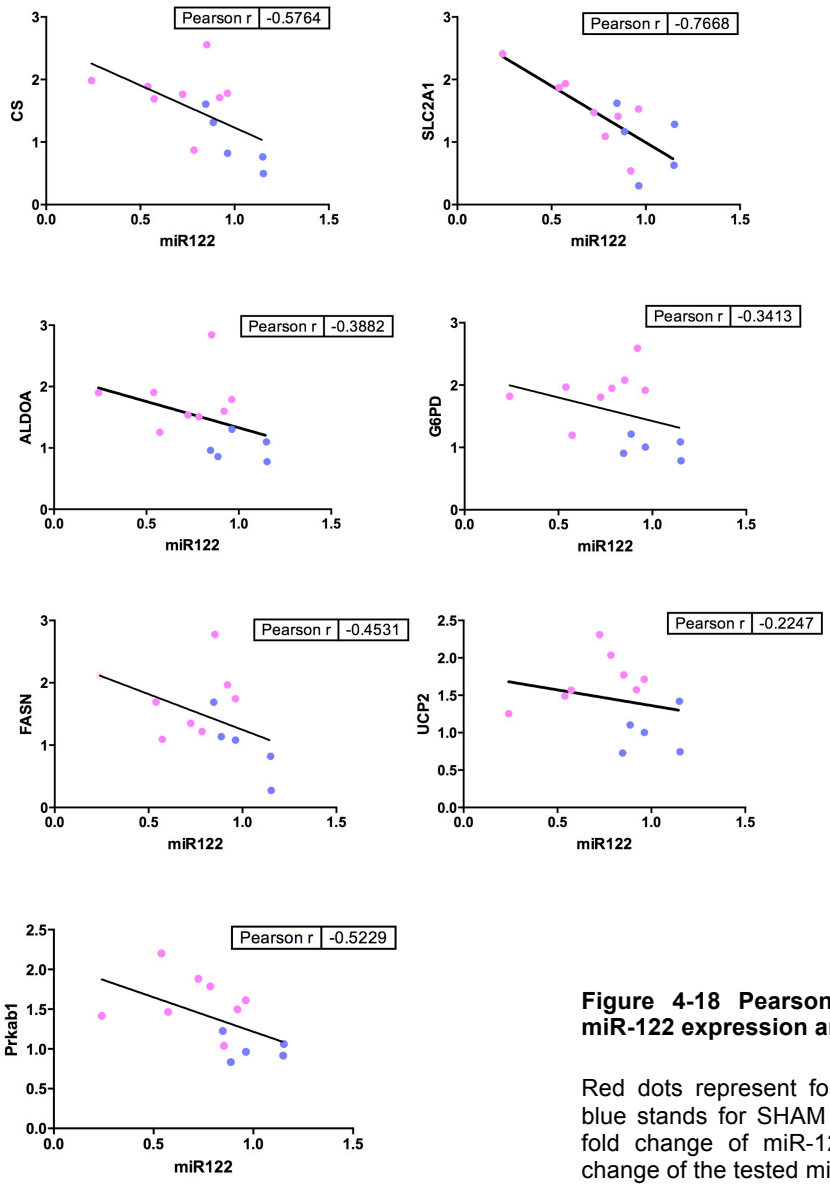

Figure 4-18 Pearson correlation between hepatic miR-122 expression and its altered metabolic targets

Red dots represent for RYGB animals (n=8), whereas blue stands for SHAM (n=5). The horizontal axis is the fold change of miR-122 and vertical axis is the fold change of the tested miR-122 metabolic targets

4.3.4 Observed miR-122 metabolic function in RYGB model could be mimicked by in vitro manipulation

To further confirm that the alterations of the above-mentioned miR-122 targets are induced by a change in the microRNA, expression levels were manipulated in a set of *in vitro* experiments. Firstly, transfection reagent efficiency and dose/ratio optimisation were carried out in rat hepatocarcinoma cell line FAO. Secondly, a miR-122 mimic transfection study was performed in both FAO cells and in a rat pancreatic-derived hepatocyte-like cell line B13H (see section 2.2.6 and 4.3.4.3 for details of this cell line). Finally, the miR-122 targets that were observed to be altered *in vivo* were examined using Taqman qPCR in the successfully transfected B13H cells *in vitro*.

4.3.4.1 Lipofectamine 2000 is the optimal transfection reagent

HiPerFect transfection reagent (Qiagen) and SiPort NeoFX transfection facilitator (Applied Biosystems) were evaluated for transfection efficiency in the rat liver carcinoma cell line FAO using 6-carboxyfluorescein (FAM)-labelled oligonucleotides (25 nucleotide long, random sequence oligo). The ratio of oligonucleotide to transfection reagent was optimised and shown in Figure 4.19. Based on the manufacturer's recommendation, a fixed amount of FAM-labelled oligo (3μL, 1μM) was co-incubated with various volumes of the transfection reagent with the ratios of oligo:transfection reagent (volume:volume) from 2:1 , 3:2, 6:5, 1:1, 6:7 and 3:4, respectively. The background fluorescence reading was measured using a none FAM oligo treated population of cells (negative control). Transfection efficiency was calculated as described below:

$$\text{Transfection efficiency} = \frac{\text{sample fluorescence reading - average negative background control reading}}{\text{average positive control reading - average negative control reading}} \%$$

Unfortunately, none of the following tested samples exhibited a successful transfection outcome (all samples transfection efficiency <8%). Negative transfection efficiency results from fluctuating fluorescence background noise.

Table 4-3 HiPerfect and SiPORT transfection condition with FAM labeled oligos

	Negative control	sample1	sample2	sample3	sample4	sample5	sample6	Positive Control
Transfection reagent	0	1.5	2	2.5	3	3.5	4	0
FAM labelled oligos	0	3	3	3	3	3	3	3
ratio (oligo/trasfection reagent)	/	2:1	3:2	6:5	1:1	6:7	3:4	/

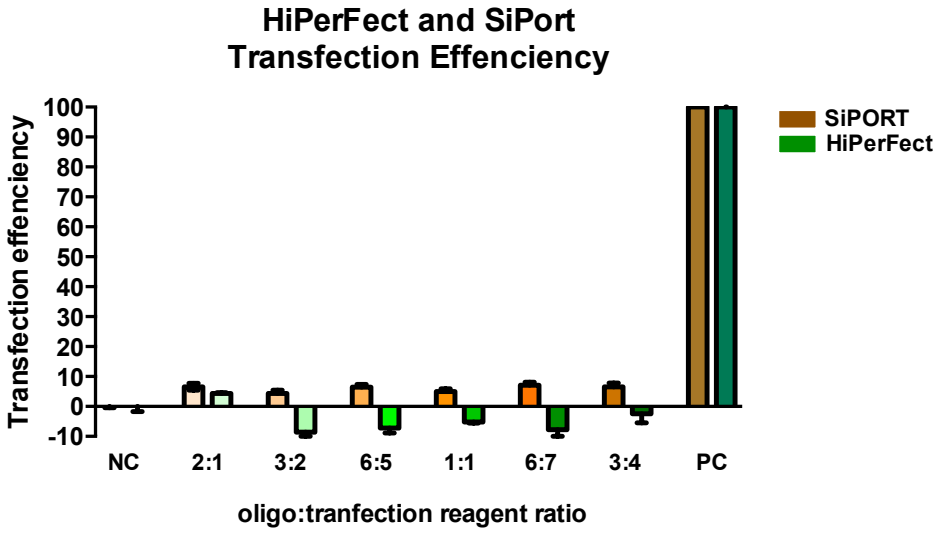

Figure 4-19 Evaluating the transfection efficiency of FAO cells using siPORT and Hiperfect

FAO cells were transfected for 24h with FAM-labelled oligo using either siPORTor or Hiperfect with various oligo:transfection reagent ratios. Y-axis is displayed with calculated transfection efficiency. Data represent mean ± SEM of three independent wells using 24 well plate. Triplicates were used for all tested ratios, NC is negative and PC positive controls.

HiPerFect and SiPort reagents are specifically designed for transfecting small RNAs, such as siRNA and microRNA. However, due to their failure to generate satisfactory transfection efficiency, Lipofectamine 2000 (Invitrogen), a more general transfection reagent for both transfecting of small RNAs and plasmids, was then tested (details about all three transfection regents and transfection procedure can be found in chapter 2). Similarly, six

different dose ratios were evaluated here with 24h transfection incubation time. As figure 4.20 shows, 4μL Lipofectamine 2000 (ratio v:v= 3:4) appeared to be the most efficient transfection ratio (transfection efficiency=28.3%). Therefore, Lipofectamine 2000 was selected as the preferred transfection facilitator and a transfection ratio of 3:4 (V:V) was used for all the following functional studies of miR-122 inhibitor/mimic metabolic targets.

Table 4-4 Lipofectamine 2000 transfection condition with FAM labeled oligos

	Negative control	sample1	sample2	sample3	sample4	sample5	sample6	Positive Control
Transfection reagent	0	3	4	5	6	7	8	0
FAM labelled oligos	0	3	3	3	3	3	3	3
ratio (oligo/trasfection reagent)	/	1:1	3:4	3:5	1:2	3:7	3:8	/

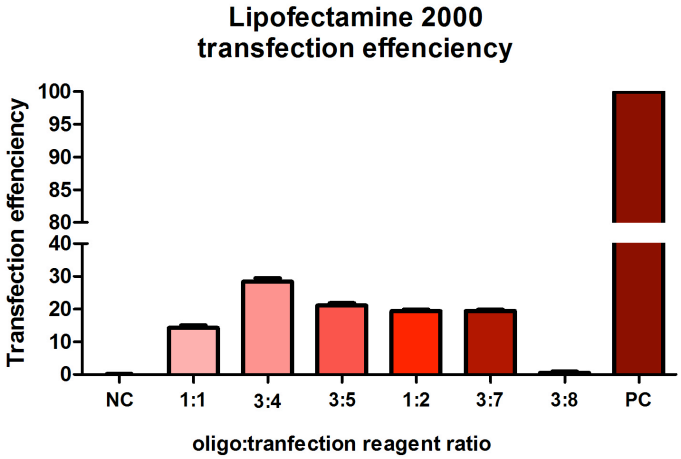

Figure 4-20 Evaluating the transfection efficiency of FAO cells using lipofectamine 2000

FAO cells were transfected for 24h with FAM-labelled oligo using lipofectamine 2000 with various oligo:transfection reagent ratios. Y-axis is displayed with calculated transfection efficiency. Data represent mean ± SEM of three independent wells using 24 well plate. Triplicates were used for all tested ratios, NC is negative controls and PC positive controls.

4.3.4.2 FAO cell is not a good model of rat liver

Following the optimisation of the transfection condition, miR-122 mimic (Thermo Scientific Dharmacon miRIDIAN microRNA Mimics) was transfected into FAO cells in 24 well plates. Cells were incubated with miR-122 mimics (20nM) or the microRNA mimic scramble control (20nM) for 96 hours according to ThermoScientific guidelines (http://www.thermoscientificbio.com/uploadedFiles/Resources/miridian-brochure.pdf).

Treated cells were viable and no significant cell death was observed during the 96 hour treatment time. All cell culture media (Opti-MEM) was removed at the end of the treatment and cells were washed with cold PBS to avoid any microRNA mimic residue contamination. Treatment with miR-122 mimic appeared to result in a significant increase (student's t-test $p<0.0001$, 68 fold up-regulation) in cellular miR-122 level compared to control mimic-transfected cells, which indicated a successful transfection. However, despite the elevated levels of, the treatment failed to reduce the *bona fide* miR-122 target CS expression (Figure 4.21).

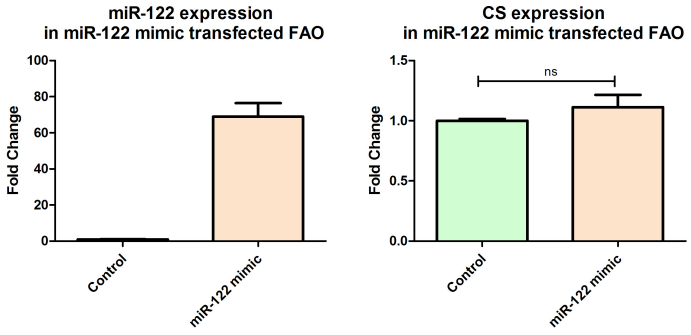

Figure 4-21 MiR-122 transfection in hepatocarcinoma cell line FAO

Quadruplicates were used for both control and miR-122 mimic treated test group. Error bars are the mean with SEM.

A. The cellular expression of miR-122 after 96h transfection. *** signifies statistically significant as determined by student t test $p<0.001$

B. The cellular expression of CS (citrate synthase) after 96h transfection. ns signifies as non significant determined by student t test.

A major hurdle to mimic liver function *in vitro* is the difficulties of generating dividable primary hepatocytes and their inability to retain differentiated phenotypes. Therefore, hepatoma cancer cell lines, which are readily available and easily expanded, are widely used instead. However, these cell lines exhibit limited hepatic phenotype and lack expression of major liver enzymes and crucial nuclear receptors (e.g. CYP450s and C/EBPb) (Rodríguez-Antona *et al*. 2002). Furthermore, the expression of the major hepatocyte-specific microRNA, miR-122, is significantly decreased during hepatocarcinogenesis, hence cancer-derived cell lines exhibit poor miR-122 expression (Kutay *et al*. 2006). Based on these considerations, an alternative *in vitro* rat liver cell model was examined and a rat pancreatic progenitor cell "B13-AR42J" was trans-differentiated to a hepatocyte-like cell line, B13H (Marek *et al*. 2003; Shen *et al*. 2000), and then used in the following study.

4.3.4.3 B13H cell is a hepatocyte-like cell line

B13H cell line, a sub clone derived from a pancreatic AR42J-B13 cell line, was differentiated with glucocorticoid (dexamethasone, 10nM) for two weeks (Marek *et al*. 2003). This allows the transdifferentiation of the pancreatic cell phenotypically into an hepatocyte-like cell line, similar to primary liver cells possessing the liver specific and enriched functional enzymes (Marek *et al*. 2003; Shen *et al*. 2000). Interestingly, as Figure 4.22 shows, miR-122, the most abundant hepatic microRNA, was gradually up-regulated more than 12 fold during the transdifferentiation process. This significant induction indicated 1) pancreatic progenitor cell line, B13H, was gradually transdifferentiated into a hepatocyte-like cell line during the dexamethasone treatment process; 2) consistent with previous study, miR-122 could be behaving as a molecular switch to control the liver differentiation processes (Laudadio *et al*. 2012).

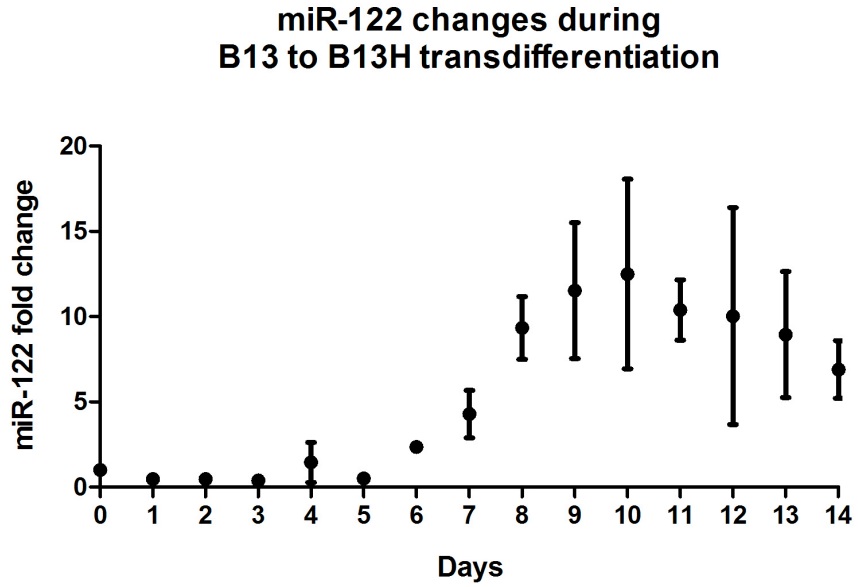

Figure 4-22 MiR-122 expression in B13 cell undergoing transdifferentiation

B13 cells were treated with 10nM dexmethasone for 14 days. Triplicate samples were plated in T25 flask and 3 flasks of cell were harvested at each day during 14 days transdifferentiation. Error bars represents the mean with SEM. Data presented as the miR-122 expression fold change compared to Day 0, the un-treated B13 cells baseline miR-122 expression.

4.3.4.4 Post RYGB hepatic metabolic alteration could be mimicked by altering miR-122 expression *in vitro*

I next investigated whether miR-122 directly modulates mRNA targets by manipulating its expression in the B13H cell line.

Treatment with 10nM dexamethasone was removed at day 14 and cells were left to recover in normal media for 24 hours. MiR-122 mimic (20nM) and microRNA scrambled control (20nM) were transfected into differentiated B13H cells under optimised reduced serum medium (Opti-MEM, Invitrogen) in 6-well plates. Similar to FAO cells, B13H cells were also collected at 96 hours and cells were washed in cold PBS before harvesting. A 72.3 fold clear increase inthe intracellular miR-122 level was confirmed by Taqman qPCR (Figure 4.23 A). Next, by using Taqman mRNA RT-qPCR, I quantified all miR-122 targeted

metabolic enzymes/ regulators, which are significantly altered in the RYGB animal model. As Figure 4.23B shows, *Cs, Slc2a1, Fasn* and *Aldoa* expression exhibited significant inhibition in the B13H cells in contrast to control cells (transfected with scrambled oligo). The inhibition effects on *G6pd, Prkab1* and *Ucp2* were apparent but not statistically significant. Consistent with the aforementioned *in vivo* findings, the *G6pc* expression level was not affected by miR-122.

These results are consistent with the effects of miR-122 noted in the post-RYGB liver.

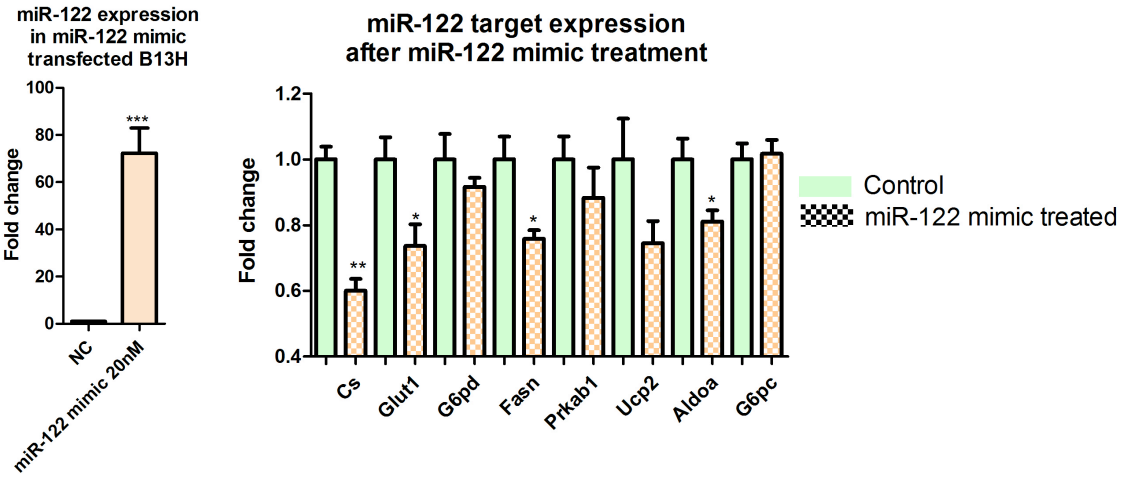

Figure 4-23 MiR-122 transfection in hepatocyte-like cell line B13H

Quadruplicates were used for both control and miR-122 mimic treated test group. Error bars are the mean with SEM.

A. The cellular expression of miR-122 after 96h transfection. *** signifies statistically significant as determined by student t test $p<0.001$

B. The cellular expression of all miR-122 targets after 96h transfection. * and ** signifies statistically significant as determined by student t test $p<0.05$ and $o<0.01$, respectively.

4.3.4.5 *In vivo* treatment with locked-nucleic-acid anti-miR-122 supports the miR-122 induced post-RYGB metabolic targ*et al*teration

Based on the publicly available data from Array Express (http://www.ebi.ac.uk/arrayexpress/), transcriptomics data from diet-induced obese mice treated with LNA (locked-nucleic-acid-modified oligonucleotide) - anti-miR122 was analysed here (Elmen *et al*. 2008). Consistently, a systematic inhibition of miR-122 by anti-miR-122 LNA elicited similar effects on the hepatic protein targets studied in the present thesis (Figure 4.24). All miR-122 targets tested *in vivo* were up-regulated, except for *Prkab1*, which did not show any alteration (Figure 4.24). It is important to note that the changes in these targets are approximately around 1.1 fold, which is much less than expected. This may due to the different mRNA profiling platforms applied. LNA-miR-122 targets presented below were detected using microRNA microarray. Figure 4.24 shows that *Aldoa*, a widely used *bone fide* miR-122 target, only exhibited 1.13 fold up-regulation by microarray. However, qPCR test result generated from the same mouse suggested that the hepatic *Aldoa* expression was up-regulated more than 3 fold in LNA treated animals (data presented in the paper (Elmen *et al*. 2008)). Therefore, the overall relatively smaller induction may result from the difference between profiling platforms.

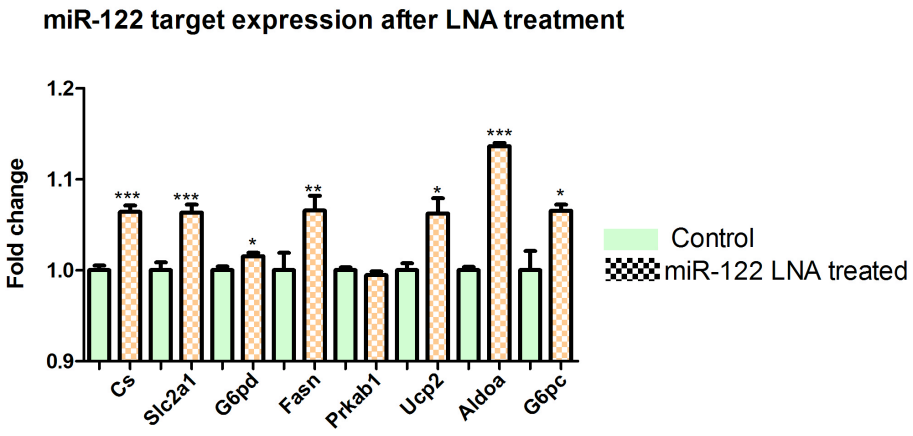

Figure 4-24 Hepatic target expression in LNA miR-122 treated mice

Control n=5, miR-122 LNA treated n=5

* , ** and *** signifies as student t test $p<0.05$, $p<0.01$, and $p<0.001$, respectively.

Data was extracted from ArrayExpress Experiment No.E-MEXP-1406 (give published ref)

Based on the above results, it is concluded that miR-122 directly and significantly modulated *Cs, Glut1, Fasn, Aldoa, G6pd* and *Ucp2*, and to a lesser extent, *Prkab1*. The association between *G6pc* and miR-122 is still peculiar and needs to be further investigated.

4.4 Chapter discussion

Metabolic reactions can be either catabolic (dissimilation of food with the release of energy) or anabolic (absorption and incorporation of food into energy storage). The catabolic and anabolic state are determined mainly by two factors, food intake and energy expenditure. Natural weight loss is associated with compensatory changes in energy expenditure that oppose the maintenance of a body weight, which is different from the usual weight (Leibel *et al*. 1995). The compensatory decreased total energy expenditure may account for the poor long-term efficacy of weight loss treatments for obesity. RYGB surgery, on the other hand, provides sustained long-term weight loss with an increased body energy expenditure rate (Stylopoulos *et al*. 2009). It is possible that under this drastic anatomic alteration, molecules from different levels co-operate to establish a novel metabolic balancing point which is different from the auto-established body homeostasis point. Although many clinical studies and basic research on gut hormones, metabolites and the gut microbiota after bariatric surgery have been reported, there is no clear understanding of the underlying molecular mechanisms for the postoperative increased energy expenditure. Understanding the mechanism of this could not only explain the sustainable weight loss and multiple metabolic benefits post-RYGB surgery, but also provide an opportunity to mimic this effect to control body weight and diabetes using non-invasive methods in the future.

In this chapter, I investigated hepatic miR-122 expression. Although hepatic miR-122 expression in RYGB rats was also decreased, the drop is much less in the liver compared to the plasma. It is possible that the liver produces less miR-122 and releases less into the blood stream. Alternatively, in the RYGB- operated rats, the liver-secreted miR-122 is transported more into other organs as a hormone. In fact, microRNA hormonal effects

have been proposed before. For instance, Vickers *et al.* observed that HDL participates in a mechanism of intercellular communication involving the transport and delivery of microRNAs (Vickers *et al*. 2011). More information about the concept of microRNAs functioning as hormones can be found in a recently published comprehensive review (Cortez *et al*. 2011).

An important point to consider is that even a relatively subtle change in microRNAs can sometime induce a large physiological effect, such as when a positive feedback loop amplifies the change of microRNA and one microRNA simultaneously targets a set of genes that are in a shared pathway or similar function. As shown in Figure 4.25, the anti-fatty acid oxidation function of miR-122 is one example. Activation of AMPK increases fatty acid oxidation either *via* activating PGC1α and PPARα or phosphorylates (inactivate) actyl-CoA carboxylase (ACC) (Cantó & Auwerx 2009; W. J. Lee *et al*. 2006). The ensuing activation of PPARα increased UCP2 which could further inactivate ACC (Kelly *et al*. 2013). PPARα, AMPK, UCP2, PGC1α and phosphorylated ACC typically form a complex network in order to control fatty acid oxidation. The presence of miR-122 may simultaneously shut down all three crucial pathways, which are important for fatty acid oxidation (PGC1α and AMPK are validated miR-122 targets (Burchard *et al*. 2010; Esau *et al*. 2006), UCP2 is a putative target of miR-122 which was also tested in the present study). This effect could be even stronger with other positive feedback loops which reinforce miR-122 expression (An example of the positive feedback loop between miR-122 and PPARs will be further discussed in chapter 5). Hence, even with relatively small alterations of miR-122 in the liver, it is still appropriate to assess all crucial miR-122 metabolic targets in order to generate an overview of RYGB surgery effects.

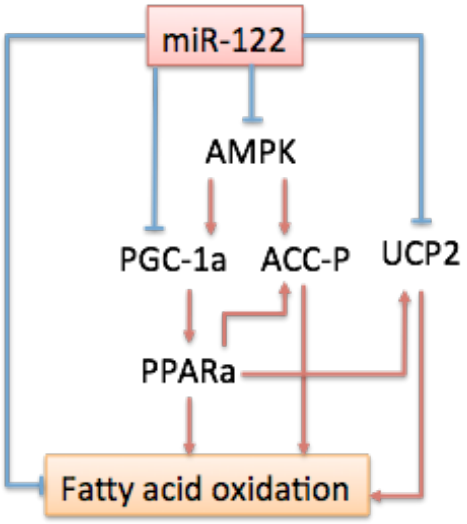

Figure 4-25 An example of one microRNA simultaneously targeting multiple pathways which amplifies small changes and fundamentally influence the homeostasis

Here it was found that, as expected, multiple miR-122 metabolic targets were up-regulated in the liver obtained from the of RYGB-operated rats. As shown in Figure 4.26, these alterations indicated a switch to the anabolism pathways, for instance, glucose transportation, glycolysis, TCA and fatty acid oxidation and a switch from catabolism pathways, such as gluconeogenesis. The extent of the up-regulation of these targets are similar, ranging from 1.53 fold (*Slc2a1*) to 1.91 (*G6pd*) fold. It is worth noting that not all targets were up-regulated as expected, for example, *bone fide* miR-122 target *G6pc* was reduced by 80% while one experimentally validated target *Gys1* and three putative targets *Pparα, Pparβ/δ* and *Prkab2* did not show any changes at all. One possibility that may account for the decreased *G6pc* is that transcriptional inhibitors of *G6pc* are negatively regulated by miR-122 and therefore are up-regulated following miR-122 inhibition. Alternatively, other more potent translation/post-translation regulation mechanisms co-regulate *G6pc* expression and masked the effect of miR-122 up-regulation. The RYGB surgery model we are investigating is a complex multi-input-output system, and not a simple single input - output model. Therefore, any direct causal-consequence link or explanation needs to be carefully evaluated.

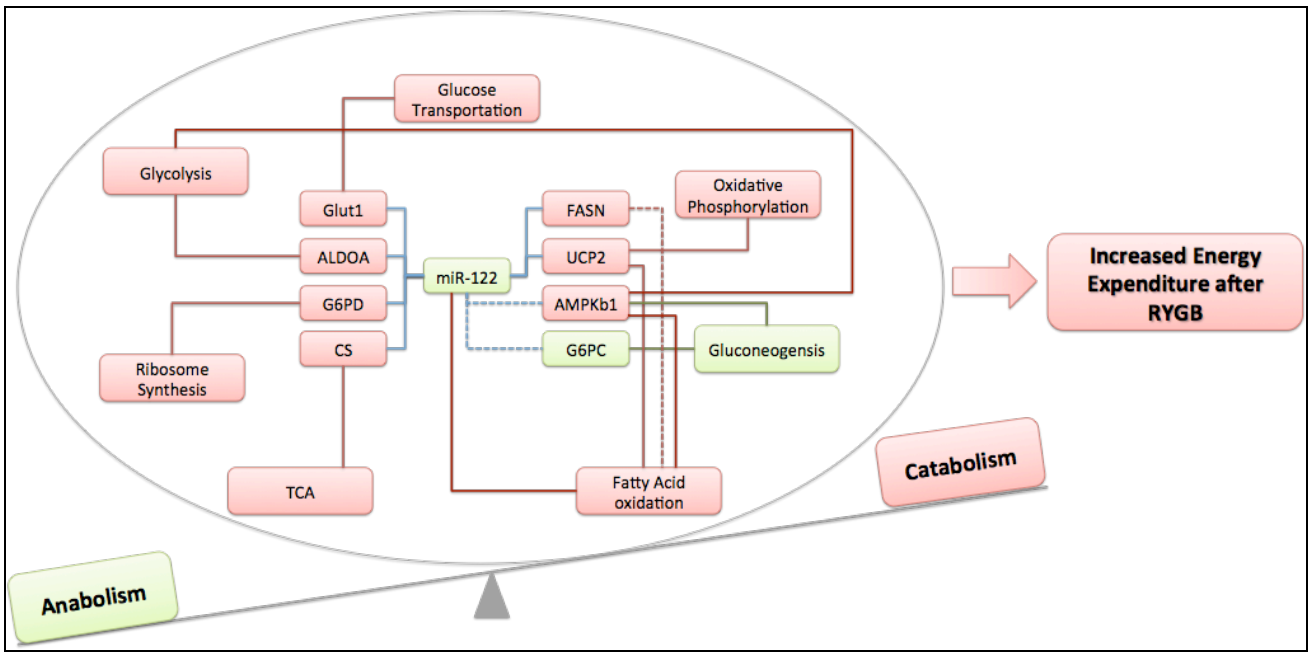

Figure 4-26 Summary of the potential metabolic shift towards catabolism mediated via miR-122 regulated metabolic targets

Red= up-regulated/activated/favoured Green= down-regulated/ inactivated/ inhibited

In mechanistic studies I examined miR-122 and its target relationships *in vitro* using pancreatic progenitor cell derived hepatocyte B13H. Here it was found that expression of all miR-122 targets were reduced to different extents except for *G6pc* (not affected), which is consistent with the *in vivo* finding. Additionally, i*n vivo* data from public available data of LNA miR-122 treatment experiments further confirmed this conclusion. Whether miR-122 is the only (crucial) molecule that causes the post RYGB benefits needs to be carefully explored. To unequivocally conclude that inhibition of miR-122 contributes to post-RYGB benefits, operated rats should be administrated miR-122 mimics after surgery to examine whether post surgery metabolic benefits are diminished. Alternatively, the surgery could be carried out in miR-122 knockout animals with the prediction that less surgical benefits are to be expected.

The current findings are consistent with previous studies related to post surgery effects. Mencarelli *et al*. have recently investigated the effects of ileal interposition (IT), where the

distal ileum is relocated into the proximal jejunum, which mimics a partial procedure of RYGB surgery (Mencarelli *et al*. 2013). Consistent with my RYGB results, the hepatic expression of *G6pc* was also suppressed in this IT model (Mencarelli *et al*. 2013). Furthermore, Peng *et al.* observed that RYGB increases hepatic levels of SIRT1, AMPK, and p-AMPK (Peng *et al*. 2010). In the RYGB model, I also observed *Prkab1* up-regulation in mRNA level and ser-AMPKβ1 in protein. In terms of accelerated TCA cycle, Li *et al.* have shown that urinary TCA cycle intermediates, including succinate, 2-oxoglutarate, citrate and fumarate, are all decreased in RYGB-operated rats (2, 4, 6 and 8 weeks post surgery) (J. V. Li *et al*. 2011a). Consistent with the up-regulation of CS, the TCA cycle key enzyme I observed, these decreased urinary metabolites indicate an increased utilisation of TCA cycle intermediates and an accelerated TCA cycle.

In conclusion, it is likely that the individual metabolic effects I and other researchers observed are tightly linked by the alterations of this small non-coding hepatic microRNA, miR-122. The potential reasons, which caused miR-122 changes, will be discussed in Chapter 5.

5. Causes of Hepatic miR-122 Alteration after RYGB surgery

5.1 Introduction

In chapter 3, a set of microRNAs which were significantly altered by RYGB surgery was described. In chapter 4, a paradigm microRNA, namely miR-122, was focused upon to reveal its crucial role in mediating post-RYGB metabolic related alterations. The study thus far examined the microRNA profiles following bariatric surgery and what the metabolic consequences were. Another important question is what are the fundamental causes of these observed microRNA changes? Therefore, in this chapter, I will investigate the potential causes of the altered hepatic miR-122 with focus on 1) changed metabolic environment and 2) activated transcriptional factors.

5.1.1 Metabolic environment and microRNA expression are tightly linked

Physiologically and pathologically altered metabolic environments are frequently associated with dysregulated microRNA expression. Here, I will introduce this microRNA-metabolism link with three aspects, glucose, fatty acids and hormones.

5.1.1.1 Impaired glucose metabolism is associated with alteration of microRNA expression.

A well-studied example is microRNA-375. In 2004, the pancreatic islet specific miR-375 was found to maintain glucose homeostasis and regulate insulin secretion via targeting exocytosis protein mytorphin (Mtpn) (Poy *et al*. 2004). By over-expressing miR-375, glucose-induced insulin secretion could be suppressed, and conversely, inhibition of endogenous miR-375 improved insulin secretion function. Ouaamari *et al.* reported that

diabetic Goto-Kakizaki rats exhibited an elevated pancreatic miR-375 expression level (Ouaamari *et al*. 2008). Interestingly, increasing environmental glucose concentration to 11 mM and 22 mM could decrease miR-375 expression both in INS-1E pancreatic cell line and in freshly isolated rat pancreatic islets, respectively (Ouaamari *et al*. 2008). These findings highlighted the possibility that microRNAs can operate as mediators to sense environmental glucose concentration and adjust its own expression to maintain the normal glucose level. Besides miR-375, miR-296 and miR-9 were also found to be up-regulated by increased glucose concentration (Ouaamari *et al*. 2008).

5.1.1.2 Elevated fatty acid concentration is a predisposing factor for diabetes and non-alcoholic fatty liver disease (NAFLD), the mechanism of which is believed to involve microRNAs.

For instance, prolonged exposure of the pancreatic beta-cell line MIN6B1 and primary pancreatic islets to palmitate caused a time- and dose-dependent increase of miR-34a and miR-146 (Lovis, Roggli, *et al*. 2008b). Elevated levels of miR-34a and miR-146 were also observed in islets of diabetic db/db mice (Lovis, Roggli, *et al*. 2008b). It is believed that at least part of the detrimental effect of palmitate on beta-cells (such as reduced insulin production, defective insulin secretion, and apoptosis) is caused by alterations of specific microRNAs. Additionally, microRNAs (including miR-122, miR-34a, miR-132 and miR-150) were all dysregulated in the visceral adipose tissue and plasma of NAFLD patients (Estep *et al*. 2010). Like glucose-responsive microRNAs (e.g. miR-375), it is possible that miR-122, miR-34a, miR-132 and miR-150 are responsive to the altered environmental fatty acids level. Indeed, by feeding mice with high-fat diet, multiple microRNAs (including miR-122, miR-192, miR-30c* etc.) were down-regulated (J. Zhang *et al*. 2009b). It has been suggested that these microRNAs together with PPAR and cpt-1α were working together to

adapt to the increased FFA by increasing fatty acid oxidation rate (Gatfield *et al*. 2009). Previous studies also showed that

5.1.1.3 Exposure to hormones, such as insulin and glucocorticoids, significantly affected microRNA profiles.

For example, insulin treatment down-regulates the expression of 39 microRNAs in human skeletal muscle including miR-1, miR-133a and miR-30a/miR-30e family (Granjon *et al*. 2009). Additionally, two independent studies showed that treatment with glucocorticoid (dexamethasone) represses expression of miR-17-92 family in rat (Molitoris *et al*. 2011) (Smith *et al*. 2010). In summary, these previous studies highlight both the capability of metabolites and hormones to behave as microRNA regulators, and microRNAs' ability to adapt to these environmental metabolic changes which in turn help the biological system to maintain metabolism homeostasis.

5.1.2 Bariatric surgery influences metabolic processes, which could trigger decreased hepatic miR-122 expression

Not surprisingly, dramatic anatomical alteration such as bariatric surgery fundamentally influences metabolic processes, such as glucose, fatty acid and glucocorticoid metabolism. 1) Bariatric surgery is reported to be the most effective treatment for type 2 diabetes and significantly influences glucose homeostasis, since I) diabetes often resolves within days after surgery, long before weight-loss has occurred (Rubino & Marescaux 2004); and II) homeostatic model assessment of insulin resistance (HOMA-IR) and basal glucose production is reduced within 1 week (Bojsen-Møller *et al*. 2013). To investigate bariatric surgery related glucose controlling mechanisms, the majority of previous studies focused on the fasting stage. However, it was shown that the metabolic changes are more

pronounced in the postprandial stage rather than in the fasted period after RYGB surgery (Camastra *et al*. 2013) (Jacobsen *et al*. 2013). Peripheral postprandial glucose, for example, exhibits a biphasic profile with a rapid increase followed by a sharp drop, a pattern that was mirrored by glucagon and insulin secretion (Camastra *et al*. 2013). Circulating glucose concentration represents the net effect of multiple metabolic processes, including dietary intake and absorption, endogenous glucose production (via gluconeogenesis and glycogenolysis), and glucose utilisation. Jacobson *et al.* proposed that the driving force for the altered postprandial circulating glucose levels after RYGB is the rapid entry of glucose into the systemic circulation brought about by modified gastrointestinal anatomy, causing hypersecretion of insulin and other hormones, which in turn influence glucose disappearance and endogenous glucose production (Jacobsen *et al*. 2013). In fact, in our study, metabonomics data also showed that hepatic glucose and glycogen levels were significantly higher in RYGB operated rats compared to SHAM animals, which suggested altered glucose metabolism after RYGB surgery. Hence, glucose concentration is potentially important to the regulation of hepatic miR-122 expression. 2) Fatty acid metabolism is significantly influenced after RYGB. The most symbolic effect of bariatric surgery is sustainable drastic weight loss. Multiple obesity related lipid dysfunction effects could be normalised after RYGB surgery. Specifically, post-RYGB surgery patients consistently showed a reduction in circulating cholesterol, triglycerides and an increase in high density lipoprotein levels (Williams *et al*. 2007). However, very few studies suggest mechanisms related to the observed altered lipid metabolism after RYGB. Thus, in this study, fatty acids will also be tested to examine whether they promote reduction of miR-122, in turn accelerating fatty acid metabolism. 3) Glucocorticoid levels could be altered by the reduced body weight associated with bariatric surgery. It is well-known that increased local glucocorticoid (such as cortisol) levels in

adipose tissue and liver is an important factor in the insulin resistance syndrome (RIZZA *et al*. 1982). Previous studies have suggested that in obese subjects, cortisol secretion is elevated but circulatory concentrations of cortisol are normal or low, suggesting that peripheral disappearance rate is elevated (Andrew *et al*. 1998). Surprisingly, weight loss could further stimulate tissue cortisol rate by activating key cortisone-contisol metabolic enzyme, 11β-Hydroxysteroid Dehydrogenase Type 1 (Tomlinson *et al*. 2004). Notably, 6 month after laparoscopic adjustable gastric banding (LAGB), patients showed a significant inhibition of plasma cortisol levels (Ram *et al*. 2005). These observations lead me to propose that glucocorticoids could also play a role in miR-122 regulation.

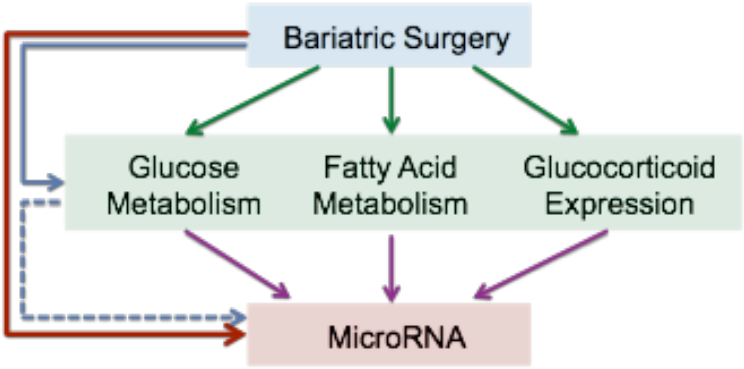

Figure 5-1 The relationship between bariatric surgery, metabolism and microRNA proposed in this thesis

As mentioned above, bariatric surgery dramatically changed multiple metabolic processes (such as glucose, fatty acid and glucocorticoid metabolism, Figure 5.1 blue arrow), and could also drastically influence microRNA expression profile (Figure 5.1, red arrow). Moreover, it has been shown that these metabolic processes, which were greatly influenced by surgery, are tightly linked with microRNA function (Figure 5.1 purple arrow).

5.1.3 MicroRNA maintaining system homeostasis *via* transcriptional factors

The activity of microRNAs is believed to offer robustness to biological processes by aiding transcriptional regulation and attenuating aberrant transcripts (Ebert & Sharp 2012). Networks and feedback mechanisms are likely to help suppress random fluctuation in transcript copy number (Hobert 2004). MicroRNAs are of course not the only class of cellular transcriptional regulatory factors that contribute to system robustness. Interestingly, transcriptional factors (TFs), share a lot of similarities with microRNAs. Recently, it was found that microRNAs and TFs are often linked in gene regulatory pathways, specifically, microRNA expression is determined by complex transcriptional regulatory inputs and microRNAs themselves show a propensity to regulate TFs (Shalgi *et al*. 2007). Additionally, microRNAs and TFs could also co-ordinate to regulate common targets (Shalgi *et al*. 2007). Furthermore, microRNA and their targets are often involved in feedback loops with switch-like behavior to amplify changes (such as carcinogenesis and development process). Negative feedback loops function to “fine tune” in order to maintain system homeostasis (such as metabolism control). In view of the common crosstalk between TFs and microRNAs and the mechanistic studies reported in chapter 4, we focused on one class of transcriptional factor, peroxsiome proliferation associated receptors (PPAR) in this chapter, to investigate whether the activation of PPAR could be responsible for decreased hepatic miR-122.

Thus, in this chapter, I will examine potential mechanisms involved in the control of hepatic miR-122, with focus on metabolites (glucose, and fatty acids), hormones (glucocorticoid) and TFs (PPARs).

5.2 Methods and experiment outline

1. FAO and B13/B13H cell line culture condition is described in 2.2.5 and 2.2.6, respectively.
2. Design and detail of glucose treatment is described in 2.2.7
3. Design and detail of dexamethasone treatment is described in 2.2.8
4. Design and detail of PPARα/γ (fenofibrate/rosiglitazone) treatment is described in 2.2.9
5. Design and detail of fatty acid (arachidonic acid) treatment is described in 2.2.10
6. Cell total RNA extraction is described in 2.3.2
7. Taqman single microRNA assay is described in 2.4.2
8. Semi-quantitative PCR and primer sequences is described in 2.4.3

5.3 Results with discussion

5.3.1 The acute post-prandial high hepatic glucose concentration may not be the reason of inhibited miR-122 after RYGB

Most published gastric bypass related glucose/insulin resistance research has utilized methods based on fasting measurements, such as Homeostatic Model Assessment (HOMAs) and giving glucose challenge, such as Oral Glucose Tolerance Test (OGTT). However, these approaches lack the capacity to investigate the impact of digestion and absorption processes. The most prominent effect of RYGB surgery is on the subject's physiology, due to its drastic anatomical change of digestive organ organization. Clearly, investigating the impact of RYGB on the disposition of a mixed meal is a more physiological relevant approach to understand the consequence of surgery. Additionally, besides fasting, the postprandial period could also be a crucial stage, alteration of which may tightly relate to post-surgical benefits. In 2013, several studies reported the effect of gastric bypass on altered postprandial metabolism (such as glucose and branch chain amino acid metabolism) by using Mixed Meal Test (MTT) (Camastra *et al*. 2013). Consistently, these studies have reported that although the overall glucose response (measured as area under the curve during meal challenge) is unchanged after RYGB surgery, the postprandial plasma glucose peak shifts to the left, which indicates a more rapid absorption and clearance of glucose (Camastra *et al*. 2013) (Figure 5.2).

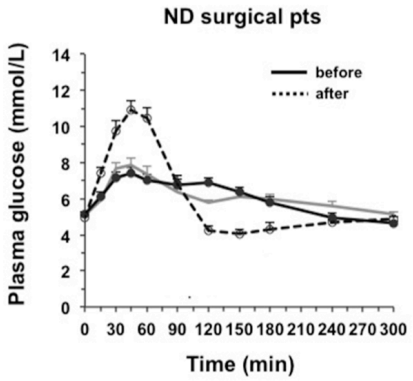

Figure 5-2 Postprandial plasma glucose concentration shift before and after RYGB surgery

Here in our study, we observed an increased hepatic glucose and glycogen concentration in RYGB compared to SHAM operated rats (by Dr. Jia Li, shown in Table 3.4). I therefore investigated whether the increased glucose concentration alone could inhibit endogenous miR-122 expression using a cell culture model with rat FAO cells. Short treatment time points (2h and 8h) were used because the relatively high-glucose exposure post-RYGB is limited within the postprandial stage, normally only lasting around 2 hours (Camastra *et al*. 2013). In my FAO cell culture experiments, glucose concentrations of 5mM, 15mM and 25mM were chosen since 1) normal rat plasma glucose concentration is similar to human (around 5.5mM ≡ 100mg/dL) 2) the plasma and portal vein glucose concentration (which indicate liver glucose concentration) could be increased to as high as 13.75mM (≡ 250mg/dL) after a meal (the postprandial glucose concentration varies and depends on the meal size)(Strubbesteffens AB, 1977). As Figure 5.3 shows, treating hepatic cell line FAO with different doses (5mM and 15mM) of α-D-glucose did not result in any inhibition of miR-122 compared to non-glucose treated FAO.

Surprisingly, treating FAO cells with the highest dose of glucose (25mM) resulted in a significant ($p=0.0216$) increase in miR-122, up to 1.84 fold compared to control at 2 hours and a significant 1.6 fold up-regulation at 8 hours ($p=0.0364$) (Figure 5.3). This result suggested that FAO cells were under stress with high concentration glucose treatment. In support of this, using another human hepatocarcinoma cell line HepG2, two independent studies reported that 25mM and 50mM glucose were enough to induce glucotoxicity (Gautier-Stein *et al*. 2012). It has been reported before that cellular responses to high glucose are numerous and varied, but the ultimate result is functional change often leading to cell death (Baumgartnerparzer *et al*. 1995). The mechanism of glucose induced apoptosis has been reported to include induced expression of oxidative and nitrosative

stress caused by generation of species such as superoxide, nitric oxide and peroxynitrite (Allen *et al*. 2005). Furthermore, high glucose concentration can also cause activation of apoptotic related proteins, such as Bcl-2 families (H. K. Li *et al*. 2005). Interestingly, the anti-apoptotic Bcl-2 is an experimentally verified miR-122 targets (C. J.-F. Lin *et al*. 2008). Therefore, it is possible that in my experiment the increased expression of miR-122 decreases the anti-apoptotic Bcl-2 which subsequently led to the reduction of cell viability under high concentration of glucose treatment.

In all, these data suggest that increased postprandial hepatic glucose concentration is unlikely to lead to inhibition of miR-122 expression post-RYGB.

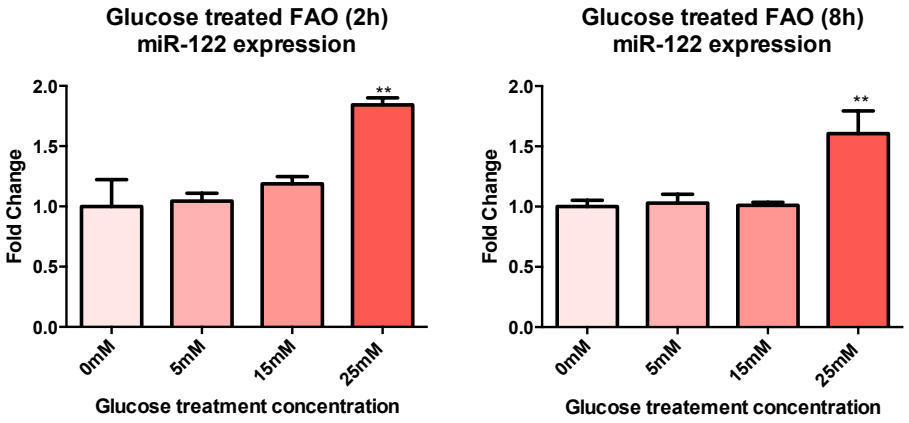

Figure 5-3 MiR-122 expression in rat liver FaO cells with glucose treatment

RNA (2ng/μL) was used for qPCR. Y-axis indicates averaged expression fold change (treatment:control<0mM>). U6 was used for qPCR normalization. N=3 across all groups. Values are the mean with SEM and ** signifies statistically significant ($p<0.01$) as determined by one-way ANOVA with Dunnett's multiple comparisons test.

5.3.2 Glucocorticoid involvement in altered miR-122 expression

Previous studies link obesity and metabolic syndrome with increased plasma glucocorticoid level (such as cortisol). Human obesity shares similar clinical features with hypercortisolism, for example, increased insulin resistance, impaired glucose tolerance, elevated blood pressure, and dyslipidemia (Bjorntorp & Rosmond 2000). Several animal models of obesity have also characterised an increased secretion of glucocorticoids (Bjorntorp & Rosmond 2000). Additionally, clinically administrating glucocorticoids to treat inflammatory disease has also been associated with metabolic adverse effects such as hypertension, obesity, hyperlipidemia and insulin resistance as seen in metabolic syndrome (Minghan Wang 2005).

Cortisol is the natural glucocorticoid (GC) hormone which can be converted to/from cortisone *via* 11β-hydroxysteroid dehydrogenase (11β-HSD). Two forms of 11β-HSD exist, 11β-HSD1 converts inactive cortisone to cortisol in human or inactive 11-dehydrocorticosterone (11-DHC) to corticosterone in rodents, while 11β-HSD2 catalyses the opposite reaction (van Uum & Hermus 1998). GC's action is mediated by glucocorticoid receptors (GR), a nuclear receptor that regulates physiological events through activation or repression of target genes involved in inflammation, gluconeogenesis and adipocyte differentiation (Bamberger *et al*. 1996). In the active state, a GR dimer binds to GC response elements (GRE), which interact with components of the transcription machinery to activate/repress the transcription of downstream genes (Schoneveld *et al*. 2004). Over-expression of 11β-HSD1 in liver could subsequently elevate GC levels, which is sufficient to trigger insulin resistance and increased hepatic lipid synthesis and flux (Paterson *et al*. 2004). On the contrary, 11β-HSD1 knockout mice are protected from high-fat diet-induced pre-adipocyte differentiation and obesity (Kotelevtsev *et al*. 1997). Obesity

is highly correlated with increased 11β-HSD1, which could favour cortisone-cortisol transition and activate GRs (Figure 5.4). GR activation mediated hyperglycaemia and dyslipidemia could be explained by increased hepato-gluconeogenesis (*via* phosphoenolpyruvate carboxykinase, PEPCK; and glucose-6-phosphatase, G6Pase), reduced fatty acid oxidation (*via* acetyl-Coenzyme A carboxylase 2, ACACB; acetyl-Coenzyme A acyltransferase 2, ACAA2; and carnitine palmitoyl transferase 1, CPT1) and decreased triacylglycerol hydrolysis (via pancreatic lipase, PNL; and PNL-related protein 2, PNLRP2)1 (Jen-Chywan Wang *et al*. 2012).

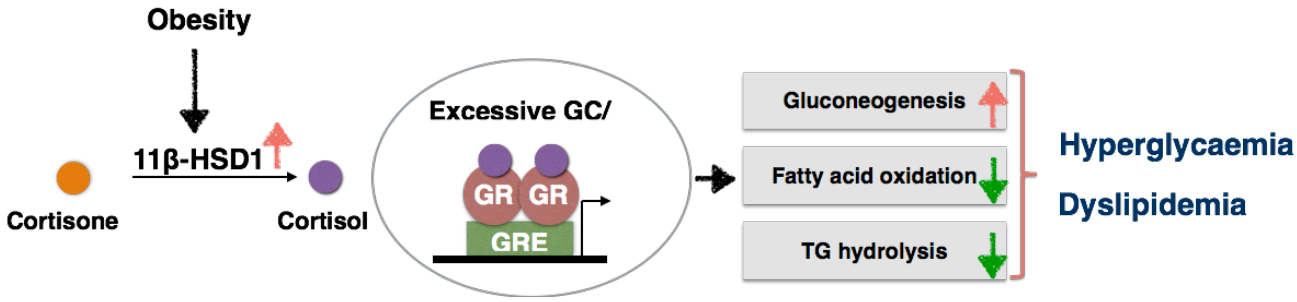

Figure 5-4 The relationship between obesity, cortisol and altered metabolic process

As described in chapter 4, RYGB in the rat favored fatty acid oxidation and inhibited gluconeogenesis compared to SHAM operated rats. This mirrors reduced GC-GR activation. In fact, previous studies in humans have shown a significant decrease in 11b-HSD1 expression in subcutaneous adipose tissue and a decreased cortisol/cortisone ratio after gastric bypass surgery (Simonyte *et al*. 2010). Hence, I hypothesized that reduced expression of endogenous glucocorticoid after RYGB surgery may contribute to the inhibited hepatic miR-122 expression, and thus the activation of glucocorticoid receptor could potentially increase hepatic miR-122 expression. To test this hypothesis, I have used an *in vitro* cell culture model and glucocorticoid treatment.

5.3.2.1 Treatment with glucocorticoid significantly induced miR-122 expression

Treating with glucocorticoid allows the transdifferentiation of the pancreatic cell B13 into a hepatocyte-like cell line B13H, similar to primary liver cells possessing the liver specific and enriched functional enzymes, such as albumin and Cyps (Shen *et al*. 2000; Marek *et al*. 2003). By treating the pancreatic progenitor cell derived B13 cell with 10nM dexamethasone (synthesized glucocorticoid), cells exhibited a more than 300 fold up-regulation of miR-122 at week 2, 3 and 4 compared to un-treated cells (Figure 5.5). This finding is compatible with my hypothesis, which suggests that activating glucocorticoid receptor might up-regulate miR-122 expression in the hepatocyte. However, it is important to note that 1) B13 is not originally a liver cell line. 2) In view of its dramatic up-regulation, miR-122 might be behaving as a molecular "switch", mediating the differentiation process, instead of a cellular "fine tuner", which maintains metabolic homeostasis. Therefore, additional dexamethasone treatment experiments were performed in the rat liver cell line, FaO.

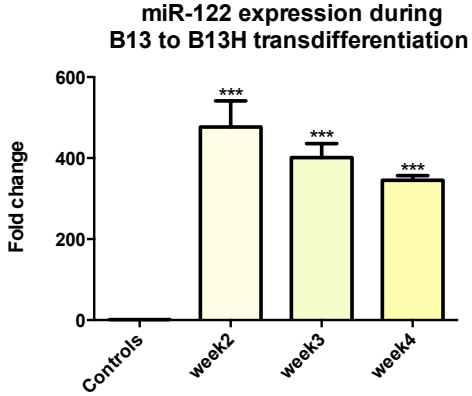

Figure 5-5 MiR-122 mRNA expression during pancreatic to hepatic transdifferentiation process in B13/B13H cells

Transdifferentiation was induced by continuous dexamethasone treatment (10nM). RNA (2ng/μL) was used for qPCR. Y-axis shows averaged expression fold change compared to untreated cells. U6 was used for qPCR normalization. N=3 across all groups. Values are the mean with SEM and *** signifies statistically significant ($p<0.001$) as determined by one-way ANOVA with Dunnett's multiple comparisons test.

5.3.2.2 Treatment of rat liver cell line FaO with glucocorticoid

FaO cell line is a well differentiated rat hepatoma cell line which possesses an active gluconeogenic pathway . Dexamethasone treatment (10nM) was used since 1) B13 cell line responded successfully to treatment with dexamethasone (10nM) and 2) physiological cortisol expression level various during the day and night time average around 300 nM (Selmaoui & Touitou 2003) and the glucocorticoid effect of dexamethasone is 25 times more potent than cortisol, hence 10nM treatment should fall in the meaningful physiological range of endogenous glucocorticoid level. Dexamethasone was dissolved in ethanol, so ethanol was used as a vehicle control. As Figure 5.6 shows, treating FAO cells with 10nM dexamethasone for 24 and 96 hours did not cause any up-regulation of intracellular miR-122 expression. This suggested that short-term activation of GC-GR may not influence the expression of miR-122. However, expanded time and dose dependent experiments need to be carried out in future before drawing any final conclusion.

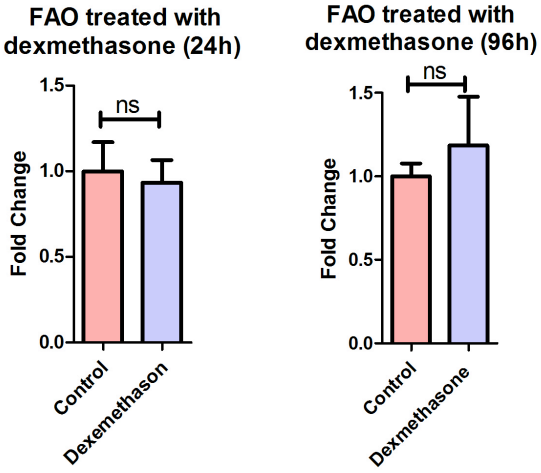

Figure 5-6 MiR-122 expression in FAO cells after glucocorticoid dexamethasone (10nM) treatment in 24 and 96 hours

RNA (2ng/μL) was used for qPCR. Y-axis shows averaged expression fold change compared to untreated control cells. U6 was used for qPCR normalization. N=3 in 24 hours treatment groups and n=6 in 96 hours treatment groups. Error bars are the mean with SEM. One-way ANOVA was used for statistical analysis.

5.3.3 Do fatty acids influence miR-122 expression?

Nuclear receptors are a class of ligand-activated transcription factors, which can regulate gene expression in response to small lipophilic compounds. For example, the oxidised derivatives of cholesterol, oxysterols, can regulate liver X factor (LXR), bile acids are able to activate farnesoid X receptor (FXR) and retinoid acid can bind to retinoid acid receptor (RXR) (Repa & Mangelsdorf 1999). The finding of peroxisome proliferation-activated receptors (PPARs) greatly aided our understanding of lipid metabolism. Followed the discovery of the first PPAR (PPARα) in the early 1990's, a galaxy of studies examined PPAR's powerful regulation in metabolic related gene transcription. There are three PPAR subtypes (namely α, β/δ and γ), which can be activated by both dietary fatty acids and their metabolic derivatives in the body, and serve as lipid sensors possessing the capacity to markedly redirect metabolism (Evans *et al*. 2004). These three PPARs exhibit distinct tissue expression patterns; PPARα is highly expressed in liver, brown adipose tissue, kidney, heart and skeletal muscle; PPARγ is most highly expressed in adipose tissue, but is also in muscle, colon and liver; PPARβ/δ shows pan-expression pattern with relatively low levels in liver (Evans *et al*. 2004). The activation of PPARs require heterodimerization with the retinoid X receptor (RXR) and binding to specific sequences (namely, PPAR-response elements <PPRE>, DNA sequence <aggtca>) in the promoter regions of target genes (Figure 5.7) resulting in either activation or inhibition of target genes.

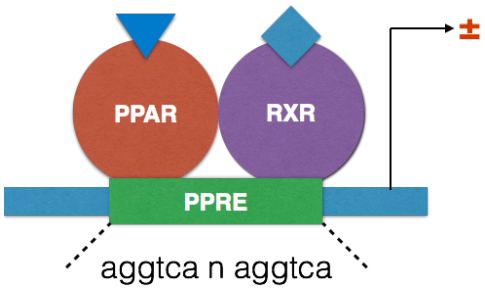

Figure 5-7 The heterodimer PPAR and RXR system and their binding with the PPRE region

All three PPARs are involved in regulation of glucose and fatty acid metabolism with different targets and pathways.

PPARα directly regulates genes related to fatty acid β oxidation (acyl-CoA oxidase) and fatty acid uptake associated fatty acid binding protein (FATP). PPARα knock out mice do not show any obvious phenotype alteration under normal diet. However, when fasted or fed with a high-fat diet, these mice accumulate massive amounts of lipid in their livers and also exhibit hypoglycaemia and increased circulating non-esterified fatty acids which indicate a deficiency in fatty acid uptake and oxidation (Guerre-Millo *et al*. 2001).

PPAR β/δ has been less investigated due to its pan-expression pattern and the lack of specific agonists. PPAR β/δ has been shown to regulate fatty acid oxidation and energy metabolism as well (Y X Wang *et al*. 2003). The transgenetic expression of activated PPAR β/δ produces lean animals, which are resistant to obesity and hyperlipidemia induced by high fat diets(Y X Wang *et al*. 2003). On the contrary, by knocking down PPAR β/δ, mice exhibited a reduction in energy expenditure *via* uncoupling proteins (UCP) and are prone to obesity (Y X Wang *et al*. 2003).

Both PPARa and β/δ have been linked with fatty acid oxidation, whereas the most extensively studied family member **PPARγ** has been linked with 1) regulating glucose homeostasis *via* reducing insulin resistance, increasing glucose uptake (glucose transporter 4, GLUT4), inhibiting liver gluconeogenesis (pyruvate dehydrogenase 4, PDK4 and phosphoenolpyruvate carboxykinase, PEPCK); 2) controlling adipogenesis; 3) maintaining lipogenesis and lipid storage (FATP, and acyl-CoA synthetase) and 4) increasing energy expenditure (UCP2, UCP3 and glycerol kinase, GyK) (Rogue *et al*. 2010).

As Figure 5.8 shows, the PPAR system and miR-122 share metabolic functions, such as fatty acid oxidation, energy expenditure and glucose uptake/metabolism. More interestingly, PPARα, PPARβ, PPARα co-activator (SMARCD1/BAF60a) and PPARγ co-activator (PGC1α) are all *bone fide* miR-122 targets (Gatfield *et al*. 2009), thus miR-122 is capable of regulating PPAR member expression through direct targeting (as Figure 5.8 blue line shows). Since miR-122 and PPARs share so many function similarities, I hypothesised that PPARs may also posses the ability to control miR-122 expression (as Figure 5.8 red dash line indicates).

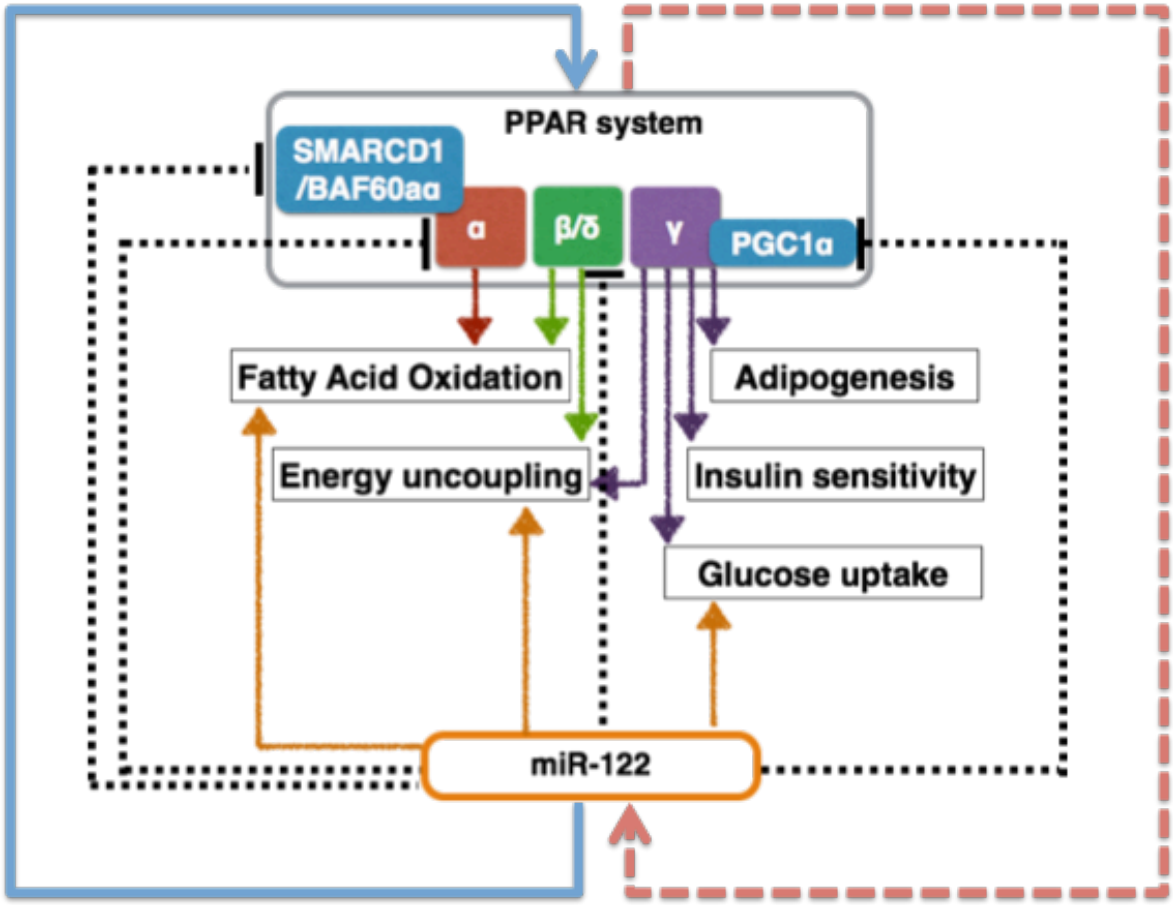

Figure 5-8 The crosstalk between PPAR system and miR-122

Blue line shows miR-122 is able to regulate PPAR system. Red dotted line indicates relationship postulated in this study. Coloured line with arrow shows known mechanisms of PPARs and miR-122 in regulating metabolism. Black dotted line shows the *bone fide* target of miR-122

5.3.3.1 PPAR binding site (PPRE) in the promoter region of miR-122

To test whether PPARs could potentially directly regulate miR-122 expression, I attempted to identify if there are any PPAR responsive elements (PPRE) in the promoter region of miR-122. PPRE (also called peroxisome proliferator hormone response element) is the DNA region where PPAR and RXR heterodimer binds. PPRE consists of direct repeats of AGGTCA (or TGACCT) motifs with a variable number of intervening or spacer nucleotides and a tolerance of mismatches. First, by using UCSC genome browser (http://genome-euro.ucsc.edu/index.html), I identified that miR-122 genome expression region is located in chromosome18,59,956,811-59,956,895 (*Rattus norvegicus)* and conservatively exists across human, rhesus, mouse, rat and dog. By screening 5 kilobase upstream of miR-122, potential PPREs were found by Dragon PPAR Response Element (PPRE) Spotter v.2.0 (http://www.cbrc.kaust.edu.sa/ppre/index.php) and shown below (Figure 5.9). Thus PPARs are indeed possibly involved in the regulation of miR-122 expression.

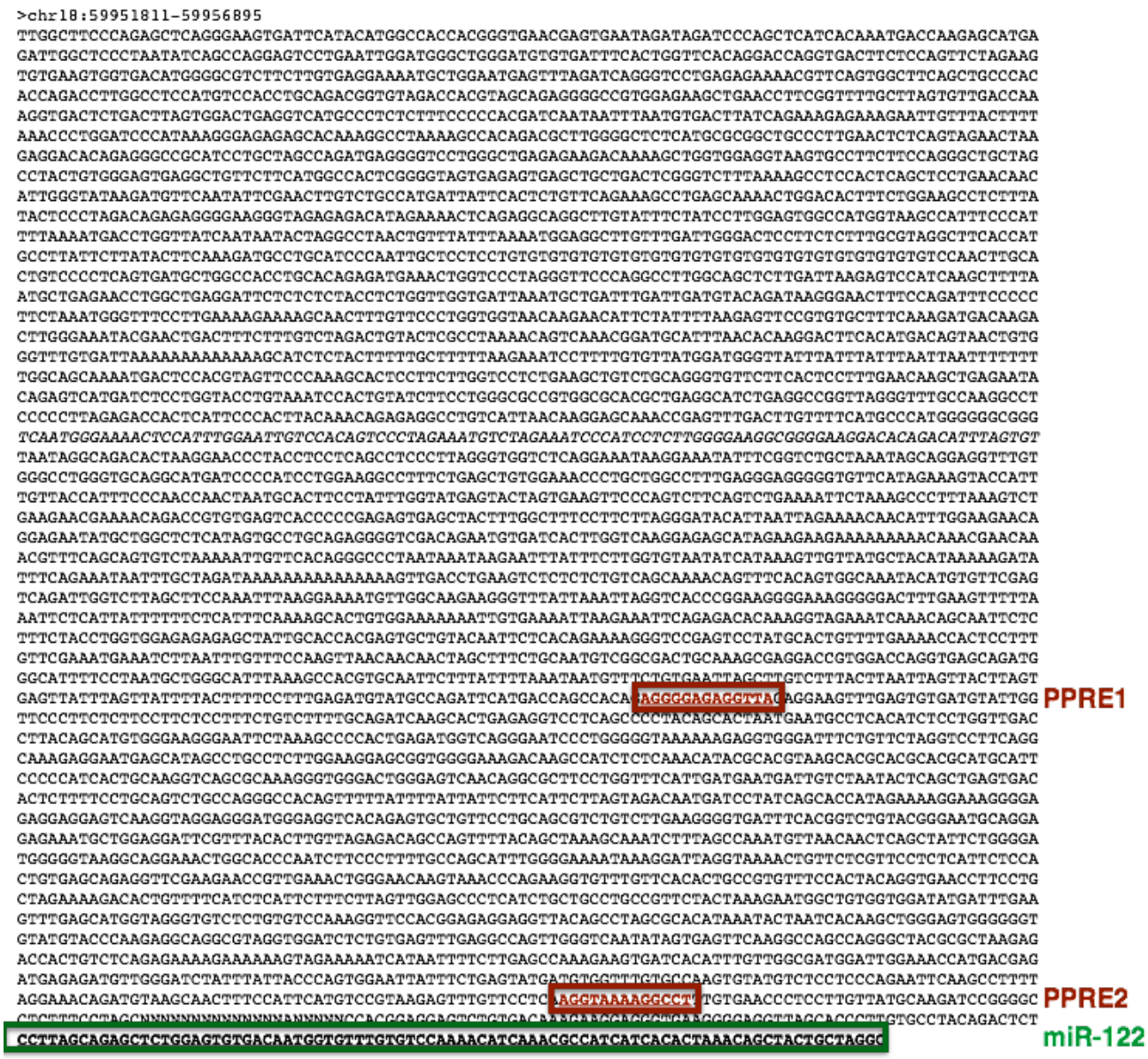

Figure 5-9 Potential PPREs exist in the promoter region of miR-122

5.3.3.2 PPAR agonists are able to regulate hepatic miR-122 expression in vivo

To prove that PPAR agonists could regulate miR-122 expression, I examined the liver of rats treated with PPAR agonists. Diethylhexylphthalate (DEHP) is a compound widely used as a plasticizer, which possess the ability to activate PPARα and induce the expression of PPARγ (Hao *et al*. 2013). Cinnamyl Anthranilate (CA) is a synthetic food

flavouring and fragrance agent which is also a PPARα agonist (Klaunig *et al*. 2003). Dehydroepiandrosterone (DEHA), is a pan-PPAR agonist which can activate all three PPARs (Mastrocola *et al*. 2003). Rat (Sprague Dawley) were treated with DEHP (12000ppm), DEHA (25000 ppm) and CA(1250 ppm) in the diet for 7 consecutive days and killed on day 8. Livers were harvested and used for transcriptomics analysis. In the first instance, to prove that all three compounds did activate PPARs during the 7 days i*n vivo* treatment, transcriptomic data of PPAR downstream genes Cyp4a1, Pex11a and PDK4 was analysed in GeneSpring® software. As Figure 5.10 shows, all compounds significantly induced PPAR downstream gene expression compared to the control. The results indicated that PPARs were indeed activated in these chemical treated rat livers. All transcriptomics data mentioned-above was acquired by Syngenta.

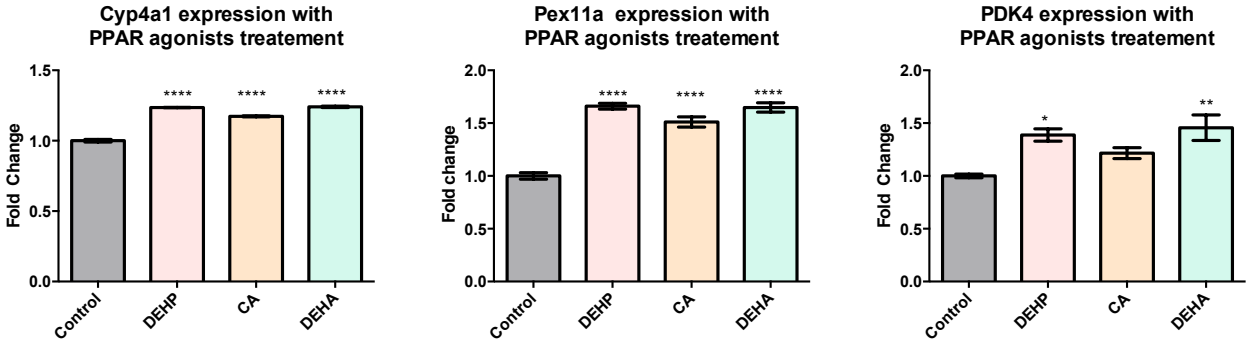

Figure 5-10 Rat hepatic PPAR downstream gene mRNA expression with DEHP, CA and DEHA treatment examined by Agilent microarray

Data was acquired by Syngenta. Y-axis shows average expression fold change compared to control group. N=5 across all control groups and n=3 in all treatment groups. Error bars are the mean with SEM. *, ** and **** signifies statistically significant as determined by one-way ANOVA with Dunnett's multiple comparisons test $p<0.05$, $p<0.01$ and $p<0.0001$, respectively.

In vivo hepatic miR-122 expression was then examined in the liver of the rats treated with the three PPAR agonists (sacrificed after 7 days of treatment). To examine the hepatic miR-122 expression, Taqman single microRNA test was used with snoRNA as a normalization control. As Figure 5.11 shows, the livers of rats treated with all three

chemicals exhibit significant reduction of hepatic miR-122 expression, 26% by DEHP, 41% by CA and 63% by DEHA. These results suggested that PPARs could be involved in miR-122 regulation. However, it is important to note that 1) all three compounds were used at a toxic dose which is likely to have affected many other biological activities besides of PPAR activity and 2) none of these compounds are PPAR subtype specific. Therefore, it is necessary to carefully examine whether pure natural/synthetic PPAR subtype specific agonists could elicit similar regulating effects on miR-122.

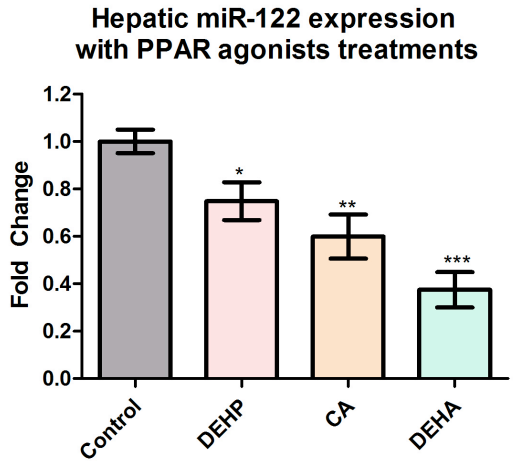

Figure 5-11 Rat hepatic miR-122 expression after DEHP, CA and DEHA treatment, examined by qPCR

Y-axis shows averaged expression fold change compared to control group. U6 was used for normalization. N=5 across all control groups and n=3 in all treatment groups. Values are mean with SEM. *, ** and *** signifies statistically significant as determined by one-way ANOVA with Dunnett's multiple comparisons test $p<0.05$, $p<0.01$ and $p<0.001$, respectively.

5.3.3.3 B13H cell line possess functional PPAR system

One of the biggest challenges in toxicology is to model liver function *in vitro.* Primary hepatocytes are able to express drug metabolism enzymes and various types of nuclear receptors. However, such activity rapidly declines within 2 hours of isolation (Boess *et al*. 2003). The viability and differentiated functions, such as the presence of liver-specific markers like albumin and the maintenance of a response to peroxisome proliferators, are maintained for only 2-3 days (UI *et al*. 1969). Hence, most published studies of *in vitro* PPAR activation use recombinant adenovirus vector to induce PPAR expression. I therefore choose to verify whether the pancreatic cell derived hepatocyte-like B13H cells (See section 5.3.2.1) possess functional PPAR systems. In the first instance, I treated B13H cells with the PPARα agonist fenofibrate with 3 different concentrations, 10μM, 30μM and 50μM. Treated cells were collected at 24 hours and total RNA extracted following standard TRIZOL protocol. By using semi-quantitative qPCR, I examined three PPAR down stream genes Cyp4a1, fatty acid binding protein (FABP) and acyl-CoA oxidise (ACO) expression using beta-actin as loading control and for normalization. As a positive control, the same amount of normal rat liver homogenate was used with identical extraction and measurement protocol. Details about semi-qPCR primer sequence, denature temperature, protein quantification method and standard curve were presented in section 2.4.3. By quantifying the bands using Kodak Imaging Station 4000MM, we found that the PPARα agonist fenofibrate indeed induced a clear up-regulation of all three PPARα down-stream genes, whereas the control beta-actin expression remained stable across all treatments (Figure 5.12). This result indicated that B13H cell possess a functional PPAR system.

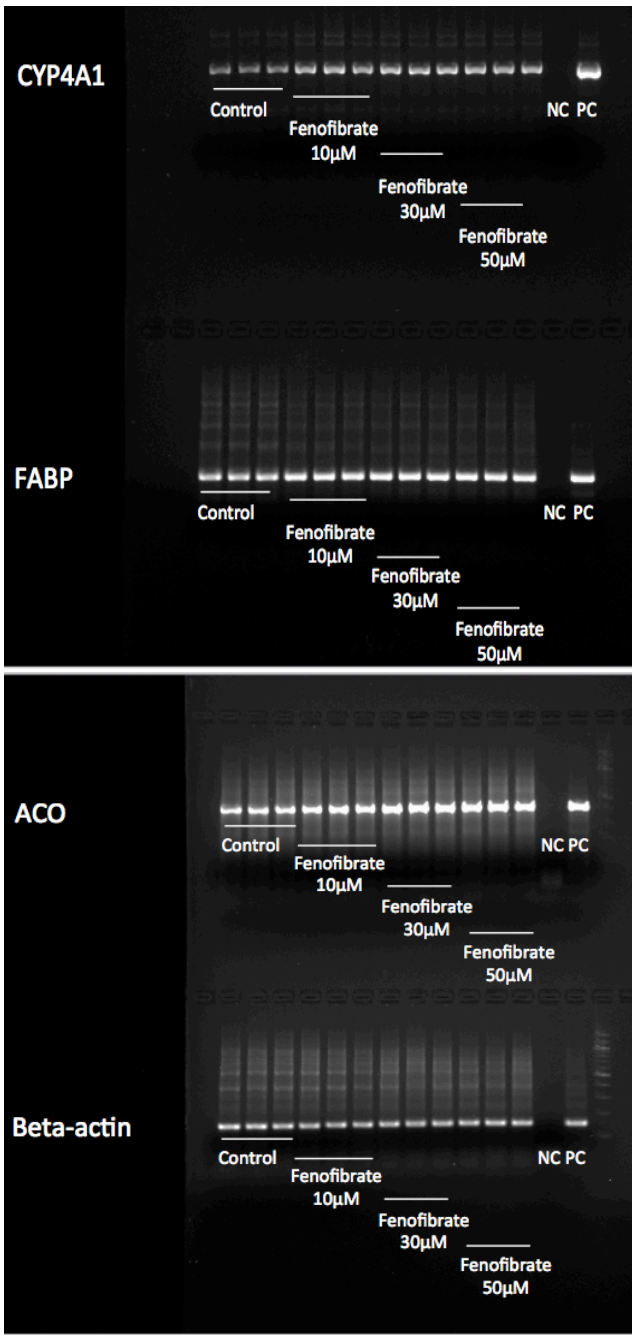

Figure 5-12 PPAR downstream gene expression following fenofibrate treatment

A. PPAR downstream gene expression in B13 cells with fenofibrate treatment examined by semi-qPCR

B. The quantitation of PPAR downstream gene expression in B13 cells with fenofibrate treatment

Y-axis shows average expression fold change compared to control group. β-actin was used for normalization. N=3 across all groups. Error bars are the mean with SEM. **, *** and **** signifies statistically significant as determined by ANOVA with Dunnett's multiple comparisons test $p<0.01$, $p<0.001$ and $p<0.0001$, respectively.

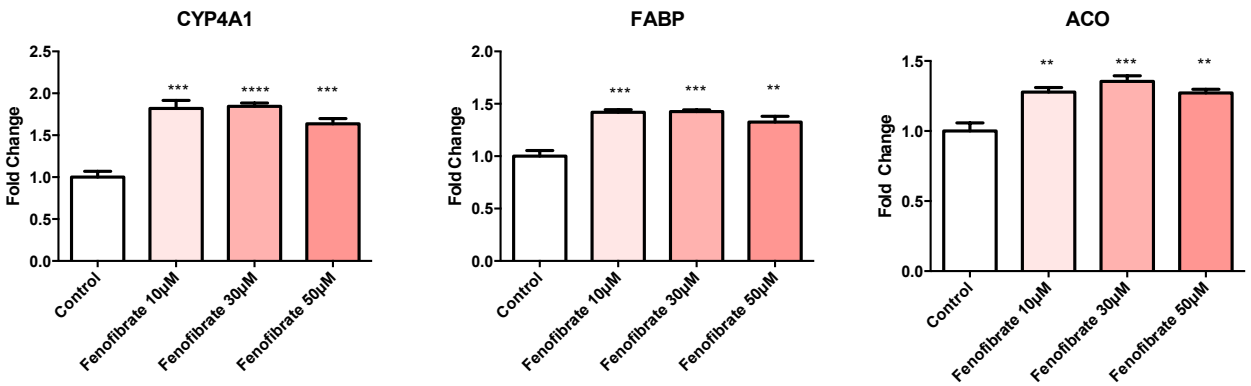

5.3.3.4 Activation of PPARα does not alter the expression of miR-122

PPARα can bind to various ligands, such as arachidonic acid metabolites (prostaglandins and leukotrienes), plasticizers (DEHP) and synthetic fibrate drugs, including clofibrate, bezafibrate and fenofibrate (Staels *et al*. 1998). The fibrate class of drugs have been used since 1960s' to treat a wide range of metabolic disorders, particularly hypercholesterolemia. To examine whether PPAR subtype α could regulate endogenous miR-122 expression, we first treated B13H cell for 24 hours with the selective PPARα agonist fenofibrate (Abcam, ab120832) with concentrations of 10μM, 30μM and 50μM. Fenofibrate was dissolved in DMSO and the same amount of DMSO was used as a negative vehicle control. Using Taqman single microRNA qPCR, we found that cellular miR-122 levels were only marginally reduced at all three concentrations. However, none of these treatments significantly different from control, based on one-way ANOVA test (Figure 5.13). Since fenofibrate is a potent and selective PPARα agonist, I conclude that PPARα is probably not responsible for regulating miR-122 expression.

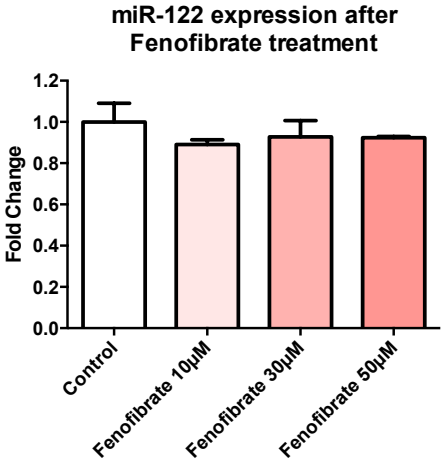

Figure 5-13 MiR-122 expression with 24h fenofibrate treatments in B13H cells

Y-axis shows average expression fold change compared to control group. U6 was used for normalization. N=3 across all groups. Values are the mean with SEM.

5.3.5 Activation of PPARγ can inhibit miR-122 expression

To investigate the potential of PPAR subtype γ to regulate miR-122 expression, the *in vitro* PPARγ agonist rosiglitazone was used to treat B13H cells. Rosiglitazone was a commercialised anti-diabetic drug that belongs to the thiazolidinedione class of drug. By selectively activating PPARγ, rosiglitazone is capable of inducing regression of fasting and postprandial glycemia in human (Raskin *et al*. 2000). The mechanism is believed to involve regulating adipocyte differentiation, stimulating muscle glucose disposal and inhibiting hepatic glucose output (C. R. Kahn *et al*. 2000). Using the B13H cell culture model and 3 concentrations of rosiglitazone (10μM, 20μM and 30μM) for 24 hours, I observed a dose-dependent reduction of endogenously expressed miR-122, with 6% reduction in 10μM, 47% in 20μM and a significant 63% decrease with 30μM treatment (Figure 5.14). This result suggested that PPARγ may possess the capability to regulate hepatic miR-122 expression.

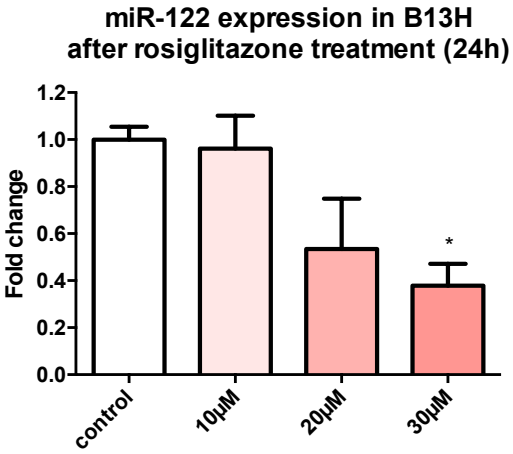

Figure 5-14 MiR-122 expression with 24h rosiglitazone treatment in B13H cells

Y-axis shows average expression fold change compared to control group. U6 was used for normalization. N=3 across all groups. Values are the mean with SEM.* signifies statistically significant as determined by ANOVA with Dunnett's multiple comparisons $p<0.05$.

5.3 Can miR-122 expression be altered by unsaturated fatty acid?

It has been shown that PPAR is an important fatty acid sensor and all three types of PPARs can be activated by fatty acids, with preference for unsaturated fatty acids, such as docosahexaenoic acid, linolenic acid, linoleum acid and arachidonic acid (Keller, *et al*. 1993). Hence, the existence of fatty acid can control its own intracellular concentration *via* nuclear receptor PPARs (Figure 5.15). Thus, a simple negative feedback loop exists between PPARs (B in Figure 5.15) and environmental fatty acids (A in Figure 5.15).

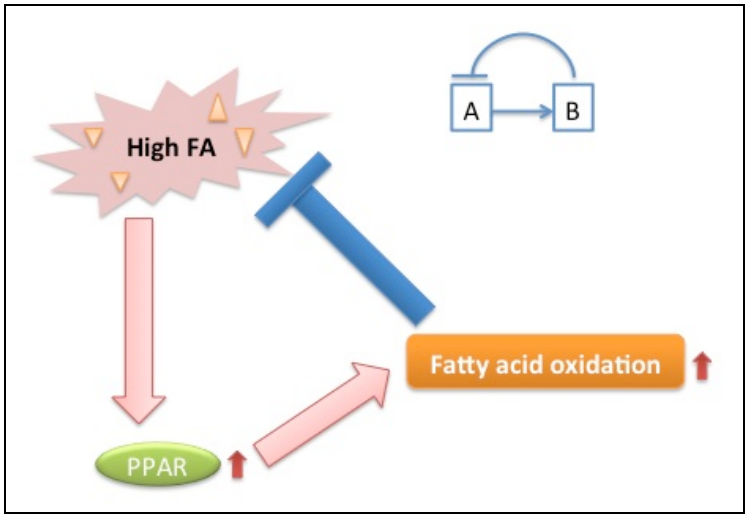

Figure 5-15 The two component negative feedback system of environmental fatty acids and PPAR

Previous study showed that by feeding animals a high fat diet, PPAR activation and miR-122 reduction could be induced simultaneously (J. Zhang *et al*. 2009b). Additionally, the activation of PPAR and reduced expression of miR-122 could both lead to increased energy expenditure, in favor of fatty acid oxidation and reduced circulating cholesterol levels (Esau *et al*. 2006; Evans *et al*. 2004). Therefore, I hypothesized that, fatty acids, as a class of natural PPAR ligand, could active PPARs which then directly targets and decreases cellular miR-122 expression (Figure 5.16). The decreased miR-122 could in turn release the inhibition effect on PPARα, PPARβ, PPARα coactivators and PPARγ

coactivators. Thus, the activity of miR-122 adds another layer to PPAR mediated fatty acid metabolism regulation. A positive feedback loop may be formed between PPARs (B in Figure 5.16) and miR-122 (C in Figure 5.16), which could amplify the response of the input signal (increased environmental FFAs, A in Figure 5.16). Furthermore, both PPAR activation (B) and decreased miR-122 expression (C) could generate double negative feedback loops, which simultaneously decrease FA generation and increase FA oxidation resulting in the maintenance of overall fatty acid homeostasis.

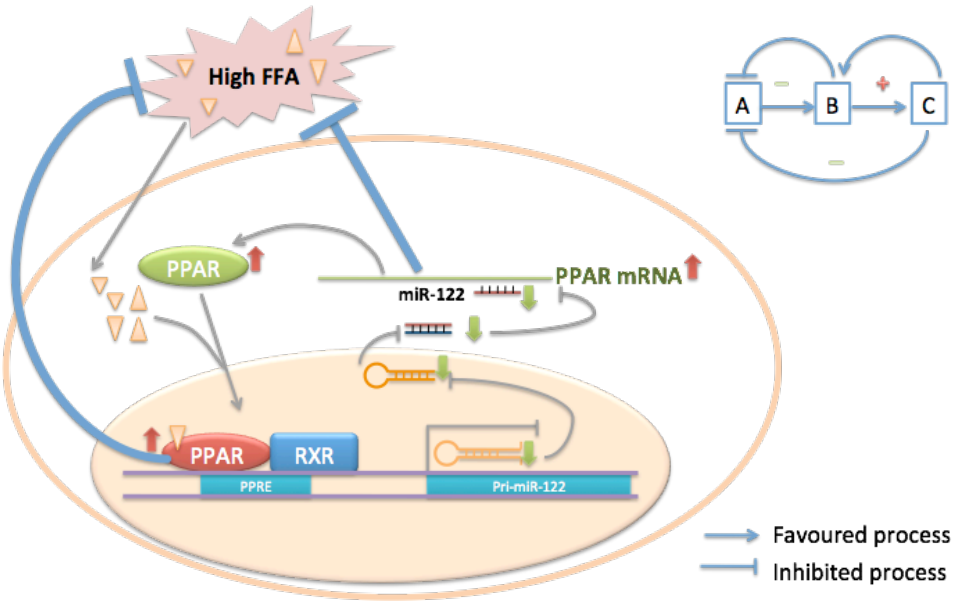

Figure 5-16 The potential of miR-122 to regulate fatty acid homeostasis

To test this hypothesis, a polyunsaturated omega-6 fatty acid, arachidonic acid, was used. Arachidonic acid was selected since 1) it is capable of activating PPARs (α, β and γ) (Gottlicher *et al*. 1992; Krey *et al*. 1997) and 2) bariatric surgery patients exhibited increased circulating arachidonic acid concentrations (Jia Li, metabonomics data). The majority of previous studies with arachidonic acid used short exposure times, such as 5 minutes to 1h (Keller *et al*. 1993; Forman *et al*. 1997). Therefore, in the first instance, three concentrations (30μM, 100μM and 300μM) and 1 hour treatment with arachidonic acid was employed to investigate whether natural fatty acids could directly regulate miR-122

expression (Keller *et al*. 1993; Forman *et al*. 1997). Figure 5.17 shows that at the concentrations of arachidonic acid used, there was a marginal reduction of miR-122, with the maximum effect at 100μM, however, none of these effects was statistically significant by one-way ANOVA.

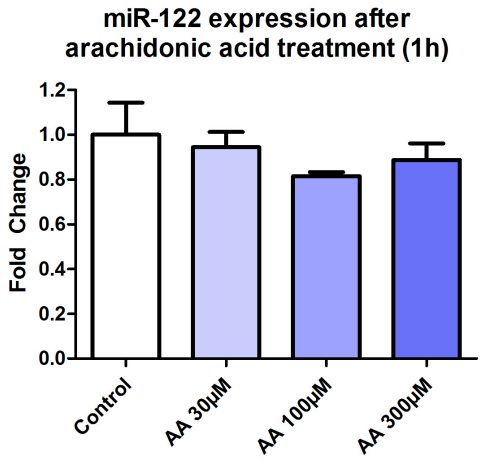

Figure 5-17 MiR-122 expression with 1h arachidonic treatments in B13H cells

Y-axis shows averaged expression fold change compared to control group. U6 was used for normalization. N=3 across all groups. Values are the mean with SEM.

To further examine this result, a more comprehensive experiment was then employed with an increased time of exposure and concentrations around 100μM. Three concentrations (50μM, 100μM and 150μM) and 4 time points (10 min, 1hour, 4hour and 10hours) were subsequently used. Unfortunately, none of the tested concentrations successfully induced a statistically significant decrease of mature miR-122 expression at any time point (Figure 5.18). There are several possible explanations for this negative result, 1) compared to rosiglitazone, arachidonic acid is a much less potent PPARγ agonist; 2) mature microRNA's half life is surprisingly long; previous studies have suggested it could be 5-12 days (Gantier *et al*. 2011). Perhaps the relatively small inhibition effects were difficult to detect in the large pool of endogenous mature miR-122. Since the metabolic homeostasis regulation function of microRNA is thought to "fine tune" gene expression, relatively small fold changes are likely to be important in preserving homeostasis. Therefore, to understand this delicate "fine tune" mechanism, it may be more appropriate to evaluate

endogenous pri- or pre-microRNA to study in greater depth the relationship between miR-122 and fatty acids. It should also be borne in mind that arachidonic acid is only one of a large number of fatty acids and its use in experiments such as those described here may not be optimal.

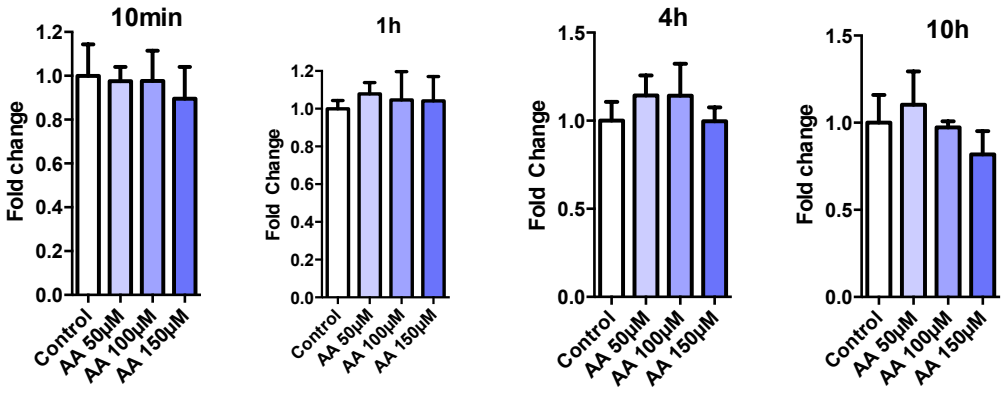

Figure 5-18 MiR-122 expression with arachidonic treatments in B13H cells

Y-axis shows average expression fold change compared to control group. U6 was used for normalization. N=3 across all groups. Values are the mean with SEM

5.4 Chapter discussion

In this chapter, I have attempted to investigate the mechanism of reduction of hepatic miR-122 expression post-bariatric surgery with focus on three aspects, glucose, glucocorticoid and fatty acids. Given the fact that RYGB surgery is a complex anatomical alteration, it is highly likely that not one, but a combination of factors would contribute to the post surgery decrease in hepatic miR-122. Moreover, the overall complexity of *in vivo* digestion, absorption process and changed metabolism is difficult to mimic in an *in vitro* model.

- **What factors could influence microRNA expression?**

To understand the causes of the decreased hepatic miR-122, we should try to understand the possible factors that contribute to microRNA expression regulation. Although a huge amount of research has been completed with microRNA expression profiling under various conditions and what targets microRNAs may regulate, surprisingly there are very few studies that identify what the crucial factors are and the fundamental mechanisms controlling microRNA expression. To address this question, one must consider microRNA expression as a dynamic process, where the microRNA expression level balances biosynthesis and degradation.

For microRNA biosynthesis, transcriptional factors and epigenetic regulation (e.g. methylation) directly regulate microRNA generation. For instance, the oncogenic transcription factor c-Myc directly binds to the DNA sequence (CATGTG) located 1.5kb upstream of miR-17 family, which was shown to promote tumourgenesis (Thomas *et al*. 2013). Furthermore, a liver enriched transcriptional factor, namely hepatocyte nuclear factor 4α (HNF-4α), was demonstrated to directly bind to the miR-122 promoter region to activate miR-122 expression (Z.-Y. Li *et al*. 2011b). Interestingly, this activation could be

further augmented by addition of PGC1α (Z.-Y. Li *et al*. 2011b). Furthermore, it has been suggested that microRNAs are epigenetically regulated (Baer *et al*. 2013). For example, the transcription of microRNAs such as miR-148a, miR-9 and miR-34 family has been shown to be dependent on their methylation status and the activity of DNA methyltransferases (DNMT1 and DNMT3b) (Toyota *et al*. 2008; Lehmann *et al*. 2008).

For the microRNA degradation process, multiple modifications could significantly affect microRNA stability. For instance, uridylation of the 3' end by TUT4/Zcch11 and PUP2 destabilises microRNA (Kai & Pasquinelli 2010), whereas 3′-terminal adenylation by GLD-2 is required for the selective stabilization of microRNA in the liver (Katoh *et al*. 2009). Perhaps both the biosynthesis and degradation control exist to regulate a single microRNA's expression. In this study, I only focused on the final outcome, the amount of mature microRNA expressed. Clearly, it is also interesting to explore if the decreased expression of mature hepatic miR-122 in RYGB rats resulted from inhibited synthesis or increased destabilisation. This could be examined by cutting-edge nascent RNA sequencing with RNA polymerase II pull down in future work.

- **Are the altered metabolite/ hormone levels noted after RYGB the reason for or caused by changes in the expression of microRNAs?**

RYGB surgery fundamentally influences systematic metabolism homeostasis. Data in chapter 4 have already showed that post RYGB animals liver exhibited a shifted metabolic preference towards catabolism instead of anabolism. It is reasonable to speculate that the body would be exposed to altered amounts of both consumed and endogenous generated nutrients and metabolites. Hence, I hypothesized that these altered levels of environmental metabolites and hormones significantly influenced the microRNAome,

which is believed to be crucial to maintain metabolic homeostasis. The obvious assumption of this hypothesis is that metabolites and hormones were altered first by the surgery, and the microRNA changes subsequently. I hypothesis that in reality, RYGB induced drastic alteration of metabolite levels may also happen before any underlining metabolic beneficial mechanism begins. A similar example of this cause-effect conundrum is the relationship between reduced energy intake and reduced appetite after RYGB surgery. One may think that the reduced appetite happens immediately after surgery and is the direct cause of reduced energy intake. However in reality, a Yoyo effect was observed for the energy intake (Zheng *et al*. 2009). By giving the rats three-choices of diet 10 days after surgery, the rats did not immediately reduce their food intake, instead, they consumed a large amount of food on the first day, but only eat very little the next day (Zheng *et al*. 2009). The later reported overall reduced appetite and shifted food choice towards low fat diets, suggests the consequence of longer-term adaption. Similar with the relationship between microRNAs and metabolites, I believe it is unlikely that microRNA, the most highly and stably expressed of the nucleotides, which are believed to buffer biological system noise and maintain robustness, would be changed immediately after surgery. Instead, it seems likely that these altered microRNAs are an adaptation process to accommodate the shifted metabolism. It is probable that after the initial response, microRNA alteration could in turn regulate metabolites and therefore form feedback/feed forward control loops to establish the new metabolic balancing point.

- Are glucose, glucocorticoids and fatty acid the causes of decreased miR-122 expression?

Three metabolites/hormones were tested in this chapter in order to probe the causes of reduced miR-122 expression. I found that 1) short time exposure to a large amount of

glucose is not a factor contributing to reduced miR-122 expression. The different glucose treatments (time and dose) were selected in order to mimic the postprandial shifted glucose peak after RYGB surgery. Surprisingly, instead of decreasing miR-122 expression, the highest concentration of glucose (25mM) significantly induced miR-122 in the *in vitro* model. This unexpected result highlighted miR-122 as a potential mediator of glucotoxicity, the mechanism of which was not fully tested in my study, but is worth exploring in the future. 2) The altered glucocorticoid level noted after RYGB may not change miR-122 expression. As a crucial metabolically regulated hormone, glucocorticoid was examined to determine its ability to regulate hepatic miR-122. Again, the synthetic glucocorticoid, dexamethasone, failed to elicit miR-122 alteration in 24 and 96 hours. 3) Finally, exposing cells to unsaturated fatty acid (arachidonic acid) did not significantly alter mature miR-122 expression. As mentioned before, these three negative results were based on Taqman RT-qPCR testing of mature microRNA. However, to observe the subtle physiological changes induced in microRNA alteration, it might be reasonable to examine freshly synthesised pri- and pre- microRNA expression in future studies. It is a challenge to mimic the *in vivo* spatial and temporal microRNA expression in *in vitro* models. It is important to note that in our *in vivo* surgical rat model, the rats were exposed to significantly shifted metabolic environments for 4 weeks post surgery. Hence, there is a need to further assess the post-surgery time in order to better understand these effects.

- **Is the crosstalk between transcriptional factors and microRNAs universal?**

All cells carry a full set of genes, but only about 20% of them express at a particular time. Hence, gene expression must be tightly controlled in biological systems. As seen in Figure 5.19, among the various gene regulatory steps from DNA to protein, transcriptional and post-transcriptional control *via* microRNAs are very important steps.

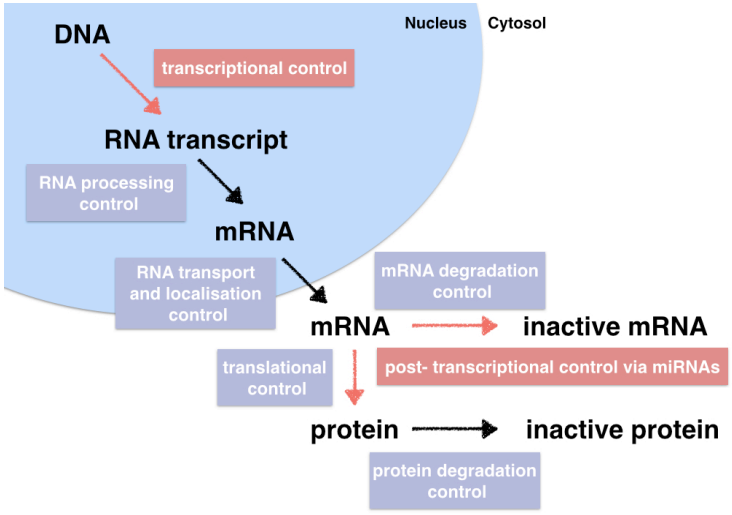

Figure 5-19 Gene expression regulation mechanisms

Both gene regulators, transcriptional factors (TF) and microRNAs, share a significant amount of similarity (K. Chen & Rajewsky 2007; Hobert 2008). For example, both TF and microRNA regulation are combinatorial processes, meaning that each microRNA/TF is expected to regulate hundreds of targets, while a given target could be regulated by multiple microRNAs/TFs. Furthermore, with such combinatorial effects, both TF and microRNA have been suggested to work as key components of complex regulatory networks. It is reasonable to propose the existence of connectivity between these gene regulation factors. Indeed, a recent theoretical model has shown that multiple feedback/feedforward controls may exist between transcriptional factors and microRNAs (Re *et al*. 2009). Like man-made control systems, the microRNA mediated control mechanism can be classified as type I (incoherent) feedforward loop (FFL) and type2 (coherent) FFL (Figure 5.20). Type I circuit allows a fine tuning of gene expression, whereas type II circuit leads to a reinforcement of transcriptional regulation at the post-transcriptional level, which might behave as a switch to mediate development and disease progression.

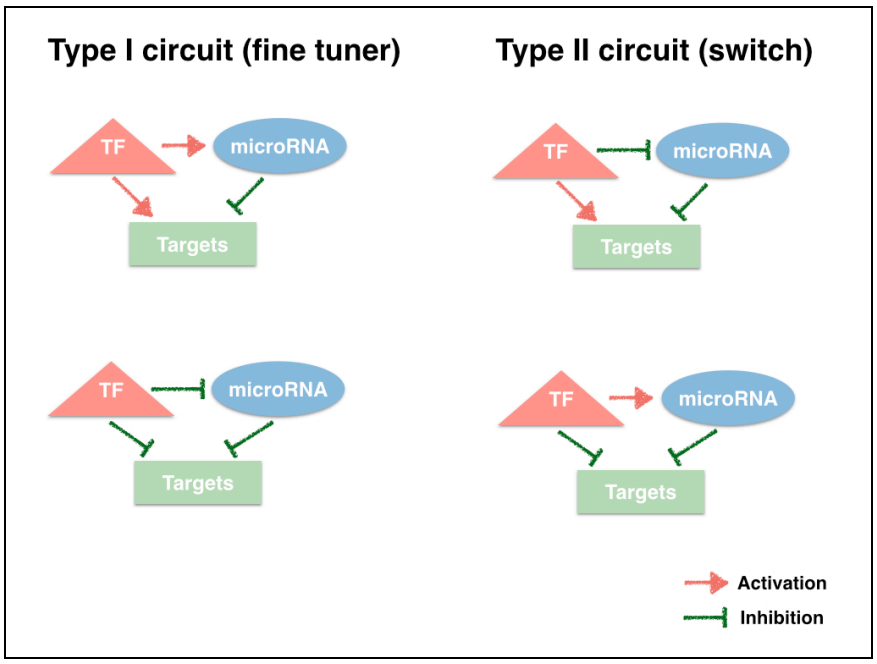

Figure 5-20 Type I and type II microRNA mediated gene expression circuits

Although the theoretical model has indicated the connection between TFs and microRNAs, there is no *bone fide* universal biological link established between these two classes of regulators. An interesting finding in this chapter was the capacity of PPAR's ability to decrease miR-122 expression both *in vivo* and *in vitro* and the potential type II feedback/feedforward loops between miR-122 and PPAR (Figure 5.21). It will be interesting to further explore whether this coordinated regulation between transcriptional factors and microRNA is universal and if so, which biological link mediates this crosstalk.

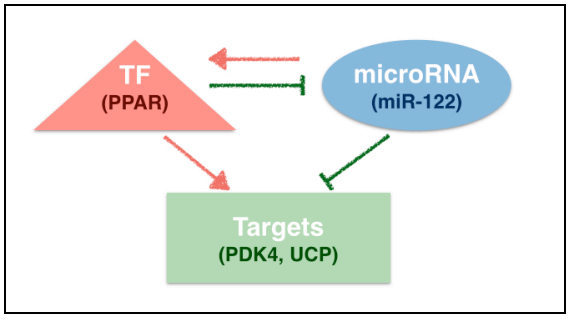

Figure 5-21 MiR-122 mediated type II gene expression circuit

6. Chapter 6 General Discussion

6.1 General conclusion of the project

Bariatric surgery is the most effective treatment for morbid obesity. Surprisingly, improvements in glucose homeostasis after RYGB are observed well before the well-described significant weight loss has happened. This intriguing effect has stimulated mechanistic studies to interpret the underlying metabolic alterations after bariatric surgery, in the hopes of finding direct non-invasive treatments, which will eventually replace invasive surgery. During the past five years, mechanistic studies offering several possible explanations for post-surgery metabolic benefits, such as the shifted gut microbiota, the altered levels of gastrointestinal hormones and the influences on central neuron system have been suggested (J. V. Li *et al*. 2011a; Miras & le Roux 2013). However, it is important to note that 1) it is not clear whether these observed effects are the cause or the result of bariatric surgery benefits and 2) all of these previous studies have focused on a specific part of the surgical induced effect, but there is still lack of information on how these multi-layer effects coordinate each other and which is/are the key molecule(s) mediating these effects.

Given the fact that microRNA is an important class of gene expression regulator, we have addressed microRNA's potential metabolic regulation effect in bariatric surgery model (Roux-en-Y, RYGB). Briefly, among the key findings were:

A) RYGB surgery fundamentally changed circulating and colorectal miRNome.

B) There is a possible link between altered circulating and colorectal microRNAs and the neurodegenerative disease/ neurotransmitter related pathways- as indicated by microRNA pathway analysis.

C) One novel rat microRNA (rno-miR-676) and another small nuclear RNA (rno-snord95) were identified.

D) The alteration of miR-122 could contribute to post-RYGB benefits *via* regulating various key metabolic enzymes/ receptors in liver.

E) PPARγ could be involved in regulating miR-122 expression with a positive feedforward mechanism.

6.2 Everything is linked: microRNA, metabolites and metabolic enzymes

The mechanisms of RYGB surgery are complex. Here in this study, I profiled the whole circulating miRNOME, and focused on the most dramatically altered circulating microRNA (miR-122) to investigate its metabolic function in RYGB model. MiR-122 is a liver-produced microRNA. The effect of RYGB was to induce a lowered level of expression of miR-122 in the liver and a very pronounced lowing of serum miR-122. This model lowing expression of miR-122 in the liver compared with plasma suggested a restrained miR-122 release into the blood stream. By antagonizing miR-122 in diet-induced obese mice for six weeks, total cholesterol level decreased by 30% without lipid accumulation in the liver (Elmen *et al*. 2008). Esau *et al.* demonstrated that injecting miR-122 antisense oligonucleotide into mice for 5 weeks results in reduced plasma cholesterol levels, increased hepatic fatty acid oxidation, decreased hepatic fatty acid and cholesterol synthesis rate (Esau *et al*. 2006), effects that are also seen in primates (Elmen *et al*. 2008). The first microRNA target drug (Miravirsen) which entered human clinical trials was designed to recognize and sequester miR-122 in order to treat hepatitis C. Interestingly, besides the intriguing anti-virus effect, Miravisen also decreased circulating cholesterol level in human, which is consistent with the animal studies (Janssen *et al*. 2013). These facts have led us to hypothesis that miR-122 could potentially behave as a key regulator mediating post RYGB metabolic benefits.

As seen in figure 6.1, miR-122, metabolites and key metabolic enzymes are linked as a network, which coordinately alter the metabolic homeostasis point post RYGB.

Following RYGB surgery, we observed increased glucose transportation, accelerated glycolysis and inhibited gluconeogenesis in the RYGB rats. *Glut1*, a glucose transporter, was up-regulated consistent with the decreased miR-122 expression in the liver and

increased levels of hepatic glucose and glycogen were observed, indicating that RYGB promoted glucose transportation and glycogen synthesis. The metabolic and miR-122 target expression data showed that RYGB surgery suppressed gluconeogenesis and stimulated glycolysis, evidenced by the down-regulation of *G6pc* and up-regulation of *Aldoa*. Furthermore, the result was further proved by elevated concentrations of glycolysis end products including pyruvate, alanine and lactate in the liver and plasma. Mencarelli *et al*. have recently investigated the effects of ileal interposition (IT), where the distal ileum is relocated into the proximal jejunum, which mimics a partial procedure of RYGB surgery (Mencarelli *et al*. 2013). Consistent with our results, the hepatic expression of *G6pc* was also suppressed in this IT model. Furthermore, *G6pd* was found to be up-regulated and this is an indicator for the oxidative activity of the pentose phosphate pathway. *G6pd* is probably stimulated by the unbalanced ratio of NADPH/NADP+ (normally 100:1 in the hepatic cytosol) to produce NADPH. This unbalanced ratio could be due to the utilization of NADPH in the liver by reductive biosynthesis, such as lipid biosynthesis. G6PD expression and enzyme activity have been reported to be up-regulated in the Roux limb of RYGB-operated rats, as well as *Glut1*, and the authors concluded that the reprogramming of intestinal glucose, including enhanced basolateral glucose uptake, augmented glycolysis and stimulated pentose phosphate pathway, could contribute to the glycemic control after RYGB (Saeidi *et al*. 2013).

Decreased miR-122 levels induced the up-regulation of *Cs* (CS) and *Ucp2* (UCP2). CS is a well-studied rate-limiting enzyme in TCA cycle, whereas the metabolic function of UCP2 is still controversial and varies between various types of tissues (Brand & Esteves 2005). Hepatic UCP2 expression, which uncouples oxidative phosphorylation with ATP production, is highly associated with oxidative phosphorylation and fatty acid oxidation.

The up-regulation of UCP2 and CS indicates that the RYGB-operated animals exhibit higher cellular metabolic activity such as in favoured fatty acid oxidation and increased TCA cycle metabolism, which is further supported by the decreased levels of urinary TCA cycle intermediates. Furthermore, UCP2 is a downstream effector of AMPK. In my study, I also observed increased *Prkab1* expression followed by up-regulated UCP2. After RYGB, fat stored in adipose tissue could be mobilized and metabolized in the liver (Johansson *et al*. 2008), generating increased levels of free fatty acids, which could result in up-regulated UCP2 (Samec *et al*. 1998). It has been shown that increased UCP2 could not only promote the energy expenditure towards lipid utilization (Mattiasson & Sullivan 2006) and compensate reduction of reactive oxygen species (ROS) (Castro *et al*. 2011), but also reduce oxidative stress (Collins *et al*. 2005) and protect mitochondria during fatty acid β-oxidation (Patterson, Shah, Matsubara, Krausz & Gonzalez 2012b). This is consistent with decreased ROS reported in patients after bariatric surgery (Ueda *et al*. 2011; Huang *et al*. 2011). We noticed that fatty acid synthase (*fasn*) also increased following RYGB. The underlying reason is unclear, but one possibility is that RYGB extensively affects lipid metabolism and leads to a restoration of adipose redox balance. Therefore, further studies should address lipid metabolism during the re-adjustment period after bariatric surgery.

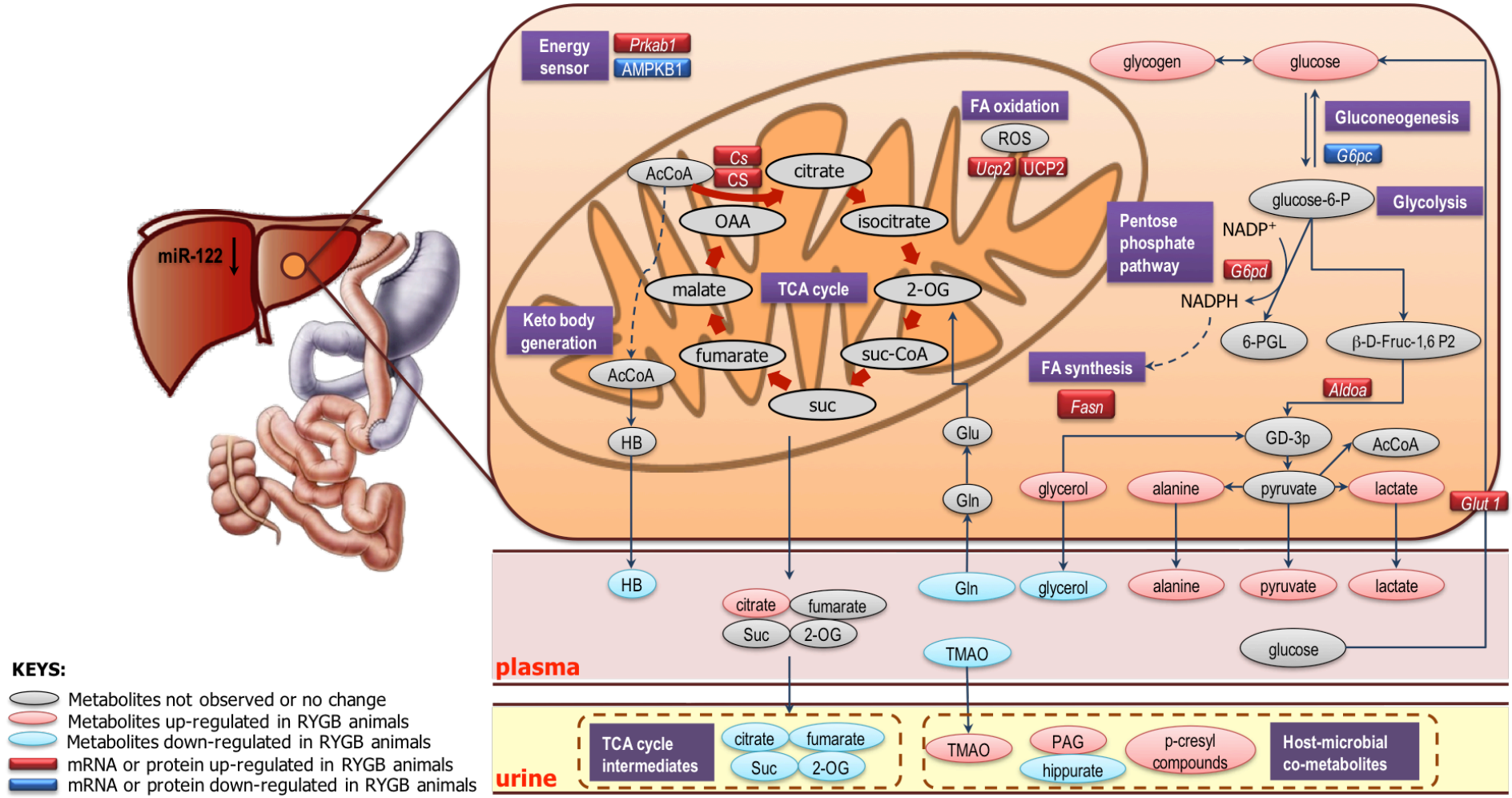

Figure 6-1 Modulation of metabolic activity by the down-regulation of miR-122 following Roux-en-Y gastric bypass surgery.

RYGB-induced metabolic changes in liver, plasma and urine (red and blue oval), metabolic enzymes (red and blue 3D boxes), and metabolic pathways (red and green flat boxes) are summarized.

6.3 Future work

Based on the main findings of this project, there are several further lines of research that can be pursued in future.

6.3.1 Validation of the altered microRNAs in other models

A first obvious experiment is to validate these altered circulating microRNAs 1) in a obese and diabetic rat model (such as ob/ob), to explore whether the microRNA profiles would be similar in a disease situation, 2) in a body weight matched experiment, in which weight-loss dependent mechanisms could be eliminated and 3) in the human blood samples, to investigate the conservatism of these observed effects.

6.3.2 Determine the *bone fide* microRNA targets

In this study, in order to examine whether the miR-122 could directly regulate metabolic enzymes/ receptors, we used microRNA mimic assay. However, it should be noted that microRNA mimic assay is highly artificial and up-regulated cellular miR-122 expression more than 70 fold, the level of which does not correspond to the normal physiological microRNA fluctuation range. Hence, further experiments should be carefully carried out to examine the two novel miR-122 targets (*Prkab1* and *Ucp2*).

To date, there are three primary methods to determine microRNA targets (Hausser & Zavolan 2014): 1) microRNA manipulation experiments (such as microRNA mimic, anti-miR, microRNA target protector and microRNA sponge) (Krutzfeldt *et al*. 2005; Ebert *et al*. 2007); 2) Ago cross-linking immunoprecipitation (Ago-CLIP) experiments, such as high throughput – CLIP (HITS-CLIP), photo activatable ribonucleotide analogue – CLIP (PAR-CLIP), the individual nucleotitide resolution CLIP (iCLIP) and the most recent CLASH

method (cross linking ligation and sequencing of hybrids) (Darnell 2010; Chi *et al*. 2009; Helwak & Tollervey 2014); 3) the gold standard 3'UTR assay, which validate microRNA targets by including 3' untranslated region of a microRNA target coupled to a reporter gene (Lytle *et al*. 2007). However, these systems are highly artificial and there is no indication of the *in vivo* stoichiometry between the microRNA and targets. Recent study has used the newly developed CRISPR-Cas genome engineering technology to determine *bone fide* microRNA targets. The mechanism involves using CRISPR-mediated homology-directed repair with short oligonucleotide donors to delete the endogenous MRE sequence and subsequently assess the MRE activity (Bassett *et al*. 2014). Clearly, these above mentioned cutting-edge methods should be considered in microRNA target validation experiments in future.

6.3.3 Study the miR-122 and PPARγ coherent feedforward loop

In chapter 5, I showed that the activation of PPARγ could dose-dependently inhibit cellular miR-122 expression. It has been shown before that both PPARγ and PGC-1α are *bone fide* miR-122 targets. This raised an interesting question of whether miR-122 and PPARγ could form a coherent feedforward loop, which accelerated the efficiency of fatty acid metabolism. In order to quantitively investigate this effect and determine whether fatty acid oxidation rate could indeed be accelerated or not, four hepatic cell models should be established (See Figure 6.2). 1) Wild type model can be applied to calculate the intrinsic miR-122 and PPARγ mediated fatty acid oxidation rate (FAOR); 2) MiR-122 knock out (KO) model used to determine PPARγ mediated FAOR; 3) the PPARγ KO model can be applied to test miR-122 mediated FAOR; 4) MiR-122 and PPARγ dual KO model to decide the background FAOR, the rate of which could be controlled *via* other cellular mechanisms. Recently, with the rapid development of genome engineering technology,

these cell knock out models are feasible and could be readily generated (Sander & Joung 2014). Multiple *in vitro* fatty acid oxidation assays are also available and can be applied quantitively (Hirschey & Verdin 2010).

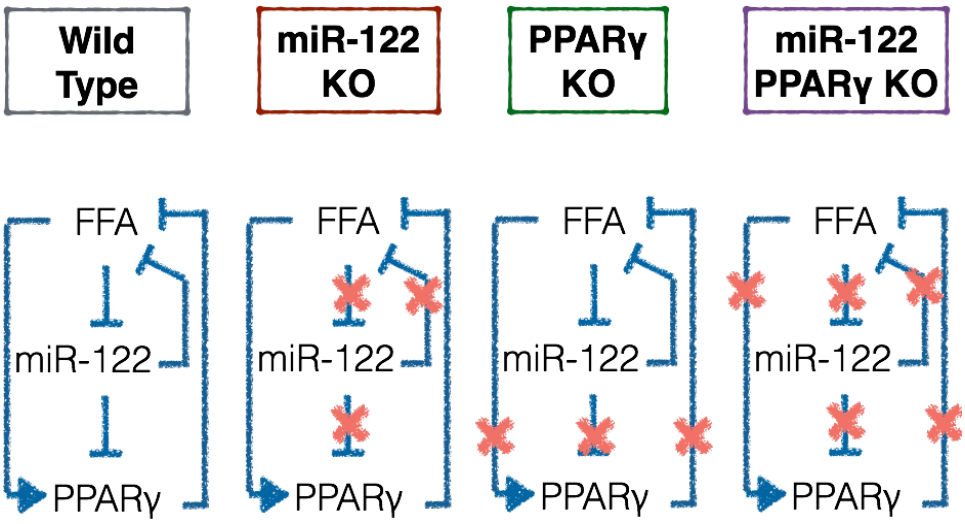

Figure 6-2 Models to investigate the coherent feedforward loop of miR-122 and PPARγ

6.3.4 Examine the potential microRNA mediated gut-brain effect

In chapter 3, I showed that both RYGB altered circulating microRNAs and colorectal microRNAs are predicted to regulate neurotransmitter and neurodegenerative disease related pathways. This sheds some light on the potential mechanism of 1) colorectal microRNA regulate neurological receptors in gut and 2) microRNAs are transported between gut cell and neurons and behave as neurotransmitters. The first point has been extensively discussed in chapter 3 discussion section. Here I will suggest two experiments to test the potential of microRNA as neurotransmitters.

1) The first step is to determine whether microRNA can be enclosed in synapsis vesicles or not. Synapsis vesicle isolation has been developed and it has been shown that antibody specific for vesicular neurotransmitter transporters can be used to quantitatively immune isolate synaptic vesicles which are specific for the

transmitter (such as GABA), with no contamination by vesicles specific for other neurotransmitters (Takamori *et al*. 2000). Subsequently, microRNA profiling (such as deep sequencing) could be carried out to determine whether synapsis vesicle contains microRNA or not. Alternately, qPCR could be used to target neuron enriched microRNAs in synapsis vesicles.

2) The second possibility to test microRNA as neurotransmitters is to investigate mRNA and microRNA localization in a spatial specific fashion by establishing a primary culture system for intestinal cells (such as L-cells) and neurons. MicroRNA expression and localization can then be visualised *via* single cell fluorescence *in situ* hybridization (FISH) (Figure 6.3). A similar co-culture cell model was established before in *C elegans*, in which neuron cell-specific GFP reporters are expressed in culture to enrich the primary neuron cells by fluorescence-activated cell sorting (Christensen *et al*. 2002). Furthermore, it is known that the mRNA and protein expression are highly variant in dendritic tree, cell body and axons (Quattrone *et al*. 2012). Generally, two types of protein exist in neuron cells, distal-site synthesis (DSS) proteins and the transport after synthesis (TAS) proteins (Weatheritt *et al*. 2014). The DSS mRNA is transported into the distal site and then translated. DSS protein is enriched for post transcription regulating site (Weatheritt *et al*. 2014), the mechanism of which is possibly involved in microRNAs. It is possible that intestinal enriched microRNAs could be transported *via* synapsis and regulates the neuron DSS proteins in axon. Hence, the expression of these microRNAs and their target mRNA may be highly spatial specific in the axon and can be visualized *via* FISH *in vitro*.

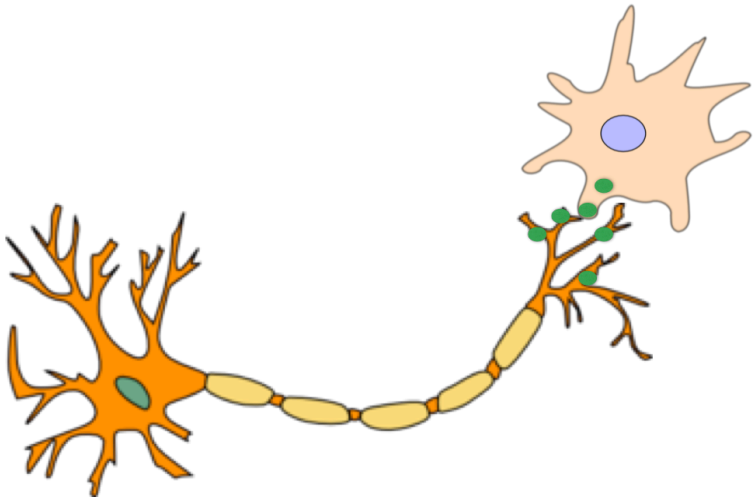

Figure 6-3 Co-culture model of neurons and intestinal cells

7. Reference

Alberti, K., Zimmet, P. & Shaw, J., 2006. Metabolic syndrome - a new world-wide definition. A consensus statement from the international diabetes federation. *Diabetic medicine*, 23(5), pp.469–480.

Alberti, K.G.M.M. & Zimmet, P.Z., 1998. Definition, diagnosis and classification of diabetes mellitus and its complications. Part 1: diagnosis and classification of diabetes mellitus. Provisional report of a WHO Consultation. *Diabetic medicine*, 15(7), pp.539–553.

Allen, D.A., Yaqoob, M.M. & Harwood, S.M., 2005. Mechanisms of high glucose-induced apoptosis and its relationship to diabetic complications. *Journal of Nutritional Biochemistry*, 16(12), pp.705–713.

Anders, S. & Huber, W., 2010. Differential expression analysis for sequence count data. *Genome biology*, 11(10), p.R106.

Andrew, R., Phillips, D. & Walker, B.R., 1998. Obesity and gender influence cortisol secretion and metabolism in man. *The Journal of clinical endocrinology and metabolism*, 83(5), pp.1806–1809.

Andrews, Z.B. *et al*., 2008. UCP2 mediates ghrelin's action on NPY/AgRP neurons by lowering free radicals. *Nature*, 454(7206), pp.846–851.

Aravin, A. *et al*., 2006. A novel class of small RNAs bind to MILI protein in mouse testes. *Nature*.

Aronne, L.J., 2002. Obesity as a Disease: Etiology, Treatment, and Management Considerations for the Obese Patient. *Obesity research*, 10(S12), pp.95S–96S.

Arsenijevic, D. *et al*., 2000. Disruption of the uncoupling protein-2 gene in mice reveals a role in immunity and reactive oxygen species production. *Nature genetics*, 26(4), pp.435–439.

Ashrafian, H. *et al*., 2011. Metabolic surgery and cancer - Ashrafian - 2010 - Cancer - Wiley Online Library. *Cancer*.

Ayyad, C. & Andersen, T., 2000. Long-term efficacy of dietary treatment of obesity: a systematic review of studies published between 1931 and 1999. *Obesity reviews*, 1(2), pp.113–119.

Baer, C., Claus, R. & Plass, C., 2013. Genome-Wide Epigenetic Regulation of microRNAs in Cancer. *Cancer Research*, 73(2), pp.473–477.

Baggio, L.L. & Drucker, D.J., 2007. Biology of incretins: GLP-1 and GIP. *Gastroenterology*, 132(6), pp.2131–2157.

Balasubramanyam, M. *et al*., 2011. Impaired miR-146a expression links subclinical inflammation and insulin resistance in Type 2 diabetes. *Molecular and Cellular Biochemistry*, 351(1-2), pp.197–205.

Bamberger, C.M., Schulte, H.M. & Chrousos, G.P., 1996. Molecular determinants of glucocorticoid receptor function and tissue sensitivity to glucocorticoids. *Endocrine Reviews*, 17(3), pp.245–261.

Barazzoni, R. *et al*., 2013. Gastric bypass does not normalize obesity-related changes in ghrelin profile and leads to higher acylated ghrelin fraction. *Obesity*, 21(4), pp.718–722.

Baroukh, N. *et al*., 2007. MicroRNA-124a regulates Foxa2 expression and intracellular signaling in pancreatic beta-cell lines. *Journal of Biological Chemistry*, 282(27), pp.19575–19588.

Barrès, R. *et al*., 2009. Non-CpG methylation of the PGC-1alpha promoter through DNMT3B controls mitochondrial density. *Cell metabolism*, 10(3), pp.189–198.

Barrès, R. *et al*., 2013. Weight Loss after Gastric Bypass Surgery in Human Obesity Remodels Promoter Methylation. *Cell reports*, 3(4), pp.1020–1027.

Bartel, D.P. & Chen, C.-Z., 2004. Micromanagers of gene expression: the potentially widespread influence of metazoan microRNAs. *Nature Reviews Genetics*, 5(5), pp.396–400.

Bassett, A.R. *et al*., 2014. Understanding functional microRNA-target interactions in vivo by site-specific genome engineering. *Nature communications*, 5, p.4640.

BAUMGARTNERPARZER, S.M. *et al*., 1995. High-Glucose-Triggered Apoptosis in Cultured Endothelial-Cells. *Diabetes*, 44(11), pp.1323–1327.

Bindels, L.B., Dewulf, E.M. & Delzenne, N.M., 2013a. GPR43/FFA2: physiopathological relevance and therapeutic prospects. *Trends in Pharmacological Sciences*, 34(4), pp.226–232.

Bindels, L.B., Dewulf, E.M. & Delzenne, N.M., 2013b. GPR43/FFA2: physiopathological relevance and therapeutic prospects. *Trends in pharmacological ….*

Bjorntorp, P. & Rosmond, P., 2000. Obesity and cortisol. *Nutrition*, 16(10), pp.924–936.

Boess, F. *et al*., 2003. Gene expression in two hepatic cell lines, cultured primary hepatocytes, and liver slices compared to the in vivo liver gene expression in rats: possible implications for toxicogenomics use of in vitro systems. *Toxicological sciences : an official journal of the Society of Toxicology*, 73(2), pp.386–402.

Bohnsack, M.T., Czaplinski, K. & Gorlich, D., 2004. Exportin 5 is a RanGTP-dependent dsRNA-binding protein that mediates nuclear export of pre-microRNAs. *RNA (New York, N.Y.)*, 10(2), pp.185–191.

Bojsen-Møller, K.N. *et al*., 2013. Early enhancements of hepatic and later of peripheral insulin sensitivity combined with increased postprandial insulin secretion contribute to improved glycemic control after Roux-en-Y gastric bypass. *Diabetes*, p.DB_131307.

Bolmeson, C. *et al*., 2011. Differences in islet-enriched microRNAs in healthy and glucose intolerant human subjects. *Biochemical and Biophysical Research Communications*, 404(1), pp.16–22.

Borg, C.M. *et al*., 2006. Progressive rise in gut hormone levels after Roux-en-Y gastric bypass suggests gut adaptation and explains altered satiety. *British Journal of Surgery*, 93(2), pp.210–215.

Boutz, D.R. *et al*., 2011. Two-tiered approach identifies a network of cancer and liver disease-related genes regulated by miR-122. *The Journal of biological chemistry*, 286(20), pp.18066–18078.

Brand, M.D. & Esteves, T.C., 2005. Physiological functions of the mitochondrial uncoupling proteins UCP2 and UCP3. *Cell metabolism*, 2(2), pp.85–93.

Buchwald, H. & Oien, D.M., 2009. Metabolic/Bariatric Surgery Worldwide 2008. *Obesity surgery*, 19(12), pp.1605–1611.

Buchwald, H., Avidor, Y., Braunwald, E. & Jensen, M.D., 2004a. Bariatric surgery: a systematic review and meta-analysis. *JAMA : the journal of the American Medical Association*.

Buchwald, H., Avidor, Y., Braunwald, E., Jensen, M.D., *et al*., 2004b. Bariatric Surgery: A Systematic Review and Meta-analysis. *JAMA : the journal of the American Medical Association*, 292(14), pp.1724–1737.

Burchard, J. *et al*., 2010. microRNA-122 as a regulator of mitochondrial metabolic gene network in hepatocellular carcinoma. *Molecular Systems Biology*, 6, p.402.

Camastra, S. *et al*., 2013. Long-term effects of bariatric surgery on meal disposal and ss-cell function in diabetic and nondiabetic patients. *Diabetes*, 62(11), pp.3709–3717.

Cantó, C. & Auwerx, J., 2009. PGC-1α, SIRT1 and AMPK, an energy sensing network that controls energy expenditure. *Current Opinion in Lipidology*, 20(2), pp.98–105.

Castro, M.C. *et al*., 2011. Rat liver uncoupling protein 2: Changes induced by a fructose-rich diet. *Life Sciences*, 89(17-18), pp.609–614.

Cedola, N. & Cabarrou, A., 1975. The liver in human diabetes: concentration of some induced enzymes. *Acta diabetologia latina*, pp.1–9.

Chakravarthy, M.V. *et al*., 2005. “New” hepatic fat activates PPARalpha to maintain glucose, lipid, and cholesterol homeostasis. *Cell metabolism*, 1(5), pp.309–322.

Chang, J. *et al*., 2004. miR-122, a Mammalian Liver-Specific microRNA, is Processed from hcr mRNA and MayDownregulate the High Affinity Cationic Amino Acid Transporter CAT-1. *RNA Biology*, 1(2), pp.106–113.

Chartoumpekis, D.V. *et al*., 2012. Differential expression of microRNAs in adipose tissue after long-term high-fat diet-induced obesity in mice. *PLOS ONE*, 7(4), p.e34872.

Chen, H. *et al*., 2003. Weight loss in Parkinson's disease. *Annals of Neurology*, 53(5), pp.676–679.

Chen, K. & Rajewsky, N., 2007. The evolution of gene regulation by transcription factors and microRNAs. *Nature Reviews Genetics*, 8(2), pp.93–103.

Chen, X. *et al*., 2008. Characterization of microRNAs in serum: a novel class of biomarkers for diagnosis of cancer and other diseases. *Cell Research*, 18(10), pp.997–1006.

Chi, S.W. *et al*., 2009. Argonaute HITS-CLIP decodes microRNA-mRNA interaction maps. *Nature*, 460(7254), pp.479–486.

Chirala, S.S. *et al*., 2003. Fatty acid synthesis is essential in embryonic development: fatty acid synthase null mutants and most of the heterozygotes die in utero. *Proceedings of the National Academy of Sciences of the United States of America*, 100(11), pp.6358–6363.

Christensen, M. *et al*., 2002. A primary culture system for functional analysis of C-elegans neurons and muscle cells. *Neuron*, 33(4), pp.503–514.

Christodoulides, C. *et al*., 2009. Adipogenesis and WNT signalling. *Trends in Endocrinology & Metabolism*, 20(1), pp.16–24.

Christodoulides, C. *et al*., 2006. WNT10B mutations in human obesity., 49(4), pp.678–684.

Collins, P. *et al*., 2005. Increased expression of uncoupling protein 2 in HepG2 cells attenuates oxidative damage and apoptosis. *Liver International*, 25(4), pp.880–887.

Cone, R.D., 2005. Anatomy and regulation of the central melanocortin system. *Nature Neuroscience*, 8(5), pp.571–578.

Cortez, M.A. *et al*., 2011. MicroRNAs in body fluids—the mix of hormones and biomarkers. *Nature Reviews Clinical Oncology*, 8(8), pp.467–477.

Cummings, D.E. *et al*., 2002. Plasma Ghrelin Levels after Diet-Induced Weight Loss or Gastric Bypass Surgery. *The New England journal of medicine*, 346(21), pp.1623–1630.

Cummings, D.E., Overduin, J. & Foster-Schubert, K.E., 2013. Gastric Bypass for Obesity: Mechanisms of Weight Loss and Diabetes Resolution. *dx.doi.org*.

Darnell, R.B., 2010. HITS-CLIP: panoramic views of protein–RNA regulation in living cells. *Wiley Interdisciplinary Reviews: RNA*, 1(2), pp.266–286.

Date, Y. *et al*., 2000. Ghrelin, a novel growth hormone-releasing acylated peptide, is synthesized in a distinct endocrine cell type in the gastrointestinal tracts of rats and humans. *Endocrinology*, 141(11), pp.4255–4261.

Dixon, A.F.R., Dixon, J.B. & O'Brien, P.E., 2005. Laparoscopic adjustable gastric banding induces prolonged satiety: a randomized blind crossover study. *The Journal of clinical endocrinology and metabolism*, 90(2), pp.813–819.

Dumortier, O., Hinault, C. & Van Obberghen, E., 2013. MicroRNAs and Metabolism Crosstalk in Energy Homeostasis. *Cell metabolism*.

Duvoisin, R.M. *et al*., 2005. Increased measures of anxiety and weight gain in mice lacking the group III metabotropic glutamate receptor mGluR8. *European Journal of Neuroscience*, 22(2), pp.425–436.

Ebert, M.S. & Sharp, P.A., 2012. Roles for microRNAs in conferring robustness to biological processes. *Cell*, 149(3), pp.515–524.

Ebert, M.S., Neilson, J.R. & Sharp, P.A., 2007. MicroRNA sponges: competitive inhibitors of small RNAs in mammalian cells. *Nature Methods*, 4(9), pp.721–726.

El-Hefnawy, T. *et al*., 2004. Characterization of amplifiable, circulating RNA in plasma and its potential as a tool for cancer diagnostics. *Clinical chemistry*, 50(3), pp.564–573.

Elmen, J. *et al*., 2008. LNA-mediated microRNA silencing in non-human primates. *Nature*, 452(7189), pp.896–U10.

Elmén, J. *et al*., 2008. Antagonism of microRNA-122 in mice by systemically administered LNA-antimiR leads to up-regulation of a large set of predicted target mRNAs in the liver. *Nucleic Acids Research*, 36(4), pp.1153–1162.

Esau, C. *et al*., 2004. MicroRNA-143 regulates adipocyte differentiation. *Journal of Biological Chemistry*, 279(50), pp.52361–52365.

Esau, C. *et al*., 2006. miR-122 regulation of lipid metabolism revealed by in vivo antisense targeting. *Cell metabolism*, 3(2), pp.87–98.

Estep, M. *et al*., 2010. Differential expression of microRNAs in the visceral adipose tissue of patients with non-alcoholic fatty liver disease. *Alimentary pharmacology & therapeutics*, 32(3), pp.487–497.

Evans, R.M., Barish, G.D. & Wang, Y.X., 2004. PPARs and the complex journey to obesity. *Nature Medicine*, 10(4), pp.355–361.

Fiorucci, S. *et al*., 2010. Bile acid-activated receptors in the treatment of dyslipidemia and related disorders. *Progress in lipid research*, 49(2), pp.171–185.

Fleischhacker, S.N., Bauersachs, S., Wehner, A., Hartmann, K. & Weber, K., 2013a. Differential expression of circulating microRNAs in diabetic and healthy lean cats. *Veterinary journal (London, England : 1997)*, 197(3), pp.688–693.

Fleischhacker, S.N., Bauersachs, S., Wehner, A., Hartmann, K. & Weber, K., 2013b. Differential expression of circulating microRNAs in diabetic and healthy lean cats. *The Veterinary Journal*, 197(3), pp.688–693.

Fleury, C. *et al*., 1997. Uncoupling protein-2: a novel gene linked to obesity and hyperinsulinemia. *Nature genetics*, 15(3), pp.269–272.

Forman, B.M., Chen, J. & Evans, R.M., 1997. Hypolipidemic drugs, polyunsaturated fatty acids, and eicosanoids are ligands for peroxisome proliferator-activated receptors alpha and delta. *Proceedings of the National Academy of Sciences of the United States of America*, 94(9), pp.4312–4317.

Fred, R.G. *et al*., 2010. High Glucose Suppresses Human Islet Insulin Biosynthesis by Inducing miR-133a Leading to Decreased Polypyrimidine Tract Binding Protein-Expression. *PLOS ONE*, 5(5).

Friedman, R.C. *et al*., 2009. Most mammalian mRNAs are conserved targets of microRNAs. *Genome Research*, 19(1), pp.92–105.

G W Gould, G.D.H., 1993. The glucose transporter family: structure, function and tissue-specific expression. *Biochemical Journal*, 295(Pt 2), p.329.

Gallagher, I.J. *et al*., 2010. Integration of microRNA changes in vivo identifies novel molecular features of muscle insulin resistance in type 2 diabetes. *Genome medicine*, 2(2), p.9.

Gantier, M.P. *et al*., 2011. Analysis of microRNA turnover in mammalian cells following Dicer1 ablation. *Nucleic Acids Research*, 39(13), pp.5692–5703.

Gatfield, D. *et al*., 2009. Integration of microRNA miR-122 in hepatic circadian gene expression. *Genes & …*.

Gautier-Stein, A. *et al*., 2012. Glucotoxicity Induces Glucose-6-Phosphatase Catalytic Unit Expression by Acting on the Interaction of HIF-1 alpha With CREB-Binding Protein. *Diabetes*, 61(10), pp.2451–2460.

GF, C., Jr, 1970. Starvation in man. *The New England journal of medicine*, 282(12), pp.668–675.

Girard, A. *et al*., 2006. A germline-specific class of small RNAs binds mammalian Piwi proteins. *Nature*.

Glass, M.J., Billington, C.J. & Levine, A.S., 1999. Opioids and food intake: distributed functional neural pathways? *Neuropeptides*, 33(5), pp.360–368.

GOTTLICHER, M. *et al*., 1992. Fatty-Acids Activate a Chimera of the Clofibric Acid-Activated Receptor and the Glucocorticoid Receptor. *Proceedings of the National Academy of Sciences of the United States of America*, 89(10), pp.4653–4657.

Granjon, A. *et al*., 2009. The microRNA Signature in Response to Insulin Reveals Its Implication in the Transcriptional Action of Insulin in Human Skeletal Muscle and the Role of a Sterol Regulatory Element–Binding Protein-1c/Myocyte Enhancer Factor 2C Pathway. *Diabetes*, 58(11), pp.2555–2564.

Grundy, S.M. *et al*., 2004. Definition of metabolic syndrome: Report of the National Heart, Lung, and Blood Institute/American Heart Association conference on scientific issues related to definition. In Circulation. Lippincott Williams & Wilkins, pp. 433–438.

Guerre-Millo, M. *et al*., 2001. PPAR-alpha-null mice are protected from high-fat diet-induced insulin resistance. *Diabetes*, 50(12), pp.2809–2814.

Guo, H. *et al*., 2010. Mammalian microRNAs predominantly act to decrease target mRNA levels. *Nature*, 466(7308), pp.835–840.

Guo, X. *et al*., 2009. Rapid evolution of mammalian X-linked testis microRNAs. *BMC genomics*, 10, p.97.

Gupte, R.S. *et al*., 2009. Synergistic activation of glucose-6-phosphate dehydrogenase and NAD(P)H oxidase by Src kinase elevates superoxide in type 2 diabetic, Zucker fa/fa, rat liver. *Free radical biology & medicine*, 47(3), pp.219–228.

Gutzwiller, J.P. *et al*., 1999. Glucagon-like peptide-1: a potent regulator of food intake in humans. *Gut*, 44(1), pp.81–86.

Hackenberg, M. *et al*., 2009. miRanalyzer: a microRNA detection and analysis tool for next-generation sequencing experiments. *Nucleic Acids Research*, 37(Web Server issue), pp.W68–76.

Hahn, T.M. *et al*., 1998. Coexpression of Agrp and NPY in fasting-activated hypothalamic neurons. *Nature Neuroscience*, 1(4), pp.271–272.

Han, J. *et al*., 2004. The Drosha-DGCR8 complex in primary microRNA processing. *Genes & Development*, 18(24), pp.3016–3027.

Hao, C. *et al*., 2013. Perinatal exposure to diethyl-hexyl-phthalate induces obesity in mice. *Frontiers in bioscience (Elite edition)*, 5, pp.725–733.

Hardie, D.G., 2008. AMPK: a key regulator of energy balance in the single cell and the whole organism. *International Journal of Obesity*, 32, pp.S7–S12.

Hardie, D.G., Ross, F.A. & Hawley, S.A., 2012. AMPK: a nutrient and energy sensor that maintains energy homeostasis. *Nature Reviews Molecular Cell Biology*, 13(4), pp.251–262.

Hashimoto, N. *et al*., 2006. Ablation of PDK1 in pancreatic β cells induces diabetes as a result of loss of β cell mass. *Nature genetics*, 38(5), pp.589–593.

Hausser, J. & Zavolan, M., 2014. Identification and consequences of microRNA–target interactions — beyond repression of gene expression. *Nature Reviews Genetics*, pp.1–14.

Hayes, M.T. *et al*., 2011. Is intestinal gluconeogenesis a key factor in the early changes in glucose homeostasis following gastric bypass? *Obesity surgery*, 21(6), pp.759–762.

He, L. & Hannon, G.J., 2004. MicroRNAs: small RNAs with a big role in gene regulation. *Nature Reviews Genetics*, 5(7), pp.522–531.

He, X. *et al*., 2004. LDL receptor-related proteins 5 and 6 in Wnt/beta-catenin signaling: Arrows point the way. *Development*, 131(8), pp.1663–1677.

Heijboer, A.C. *et al*., 2006. Gut-brain axis: regulation of glucose metabolism. *Journal of neuroendocrinology*, 18(12), pp.883–894.

Helwak, A. & Tollervey, D., 2014. Mapping the microRNA interactome by cross-linking ligation and sequencing of hybrids (CLASH). *Nature Protocols*, 9(3), pp.711–728.

Heneghan, H.M., Miller, N. & Kerin, M.J., 2010. Role of microRNAs in obesity and the metabolic syndrome. *Obesity reviews*, 11(5), pp.354–361.

Herrera, B.M. *et al*., 2009. MicroRNA-125a is over-expressed in insulin target tissues in a spontaneous rat model of Type 2 Diabetes. *Bmc Medical Genomics*, 2(1).

Hirschey, M.D. & Verdin, E., 2010. Measuring fatty acid oxidation in tissue homogenates.

Hobert, O., 2004. Common logic of transcription factor and microRNA action. *Trends in Biochemical Sciences*, 29(9), pp.462–468.

Hobert, O., 2008. Gene regulation by transcription factors and microRNAs. *Science (New York, N.Y.)*, 319(5871), pp.1785–1786.

Hoekstra, M. *et al*., 2012. Nonalcoholic fatty liver disease is associated with an altered hepatocyte microRNA profile in LDL receptor knockout mice. *The Journal of nutritional biochemistry*, 23(6), pp.622–628.

Hornby, P.J., 2001. II. Excitatory amino acid receptors in the brain-gut axis | Gastrointestinal and Liver Physiology. *… Journal of Physiology-Gastrointestinal and Liver ….*

Horton, J.D., Goldstein, J.L. & Brown, M.S., 2002. SREBPs: activators of the complete program of cholesterol and fatty acid synthesis in the liver. *Journal of Clinical Investigation*, 109(9), pp.1125–1131.

Huang, H. *et al*., 2011. Gastric bypass surgery reduces plasma ceramide subspecies and improves insulin sensitivity in severely obese patients. *Obesity*, 19(11), pp.2235–2240.

Jacobsen, S.H. *et al*., 2013. Effects of gastric bypass surgery on glucose absorption and metabolism during a mixed meal in glucose-tolerant individuals. *Diabetologia*, 56(10), pp.2250–2254.

Janssen, H.L.A. *et al*., 2013. Treatment of HCV Infection by Targeting MicroRNA. *The New England journal of medicine*, 368(18), pp.1685–1694.

Johansson, L. *et al*., 2008. Lipid mobilization following Roux-en-Y gastric bypass examined by magnetic resonance imaging and spectroscopy. *Obesity surgery*, 18(10), pp.1297–1304.

Jopling, C.L. *et al*., 2005. Modulation of hepatitis C virus RNA abundance by a liver-specific MicroRNA. *Science (New York, N.Y.)*, 309(5740), pp.1577–1581.

Jordan, S.D. *et al*., 2011. Obesity-induced overexpression of microRNA-143 inhibits insulin-stimulated AKT activation and impairs glucose metabolism. *Nature cell biology*, 13(4), pp.434–446.

Kahn, B.B. *et al*., 2005. AMP-activated protein kinase: Ancient energy gauge provides clues to modern understanding of metabolism. *Cell metabolism*, 1(1), pp.15–25.

Kahn, C.R., Chen, L. & Cohen, S.E., 2000. Unraveling the mechanism of action of thiazolidinediones. *Journal of Clinical Investigation*, 106(11), pp.1305–1307.

Kai, Z.S. & Pasquinelli, A.E., 2010. MicroRNA assassins: factors that regulate the disappearance of microRNAs. *Nature Structural & Molecular Biology*, 17(1), pp.5–10.

Karaki, S.-I. *et al*., 2006. Short-chain fatty acid receptor, GPR43, is expressed by enteroendocrine cells and mucosal mast cells in rat intestine. *Cell and tissue research*, 324(3), pp.353–360.

Kashyap, S.R. *et al*., 2010. Acute effects of gastric bypass versus gastric restrictive surgery on beta-cell function and insulinotropic hormones in severely obese patients with type 2 diabetes. *International Journal of Obesity*, 34(3), pp.462–471.

Kaslow, H.R. & Lesikar, D.D., 1984. Isozymes of glycogen synthase. *FEBS letters*, 172(2), pp.294–298.

Kaslow, H.R. *et al*., 1985. L-type glycogen synthase. Tissue distribution and electrophoretic mobility. *Journal of Biological Chemistry*.

Katoh, T. *et al*., 2009. Selective stabilization of mammalian microRNAs by 3' adenylation mediated by the cytoplasmic poly(A) polymerase GLD-2. *Genes & Development*, 23(4), pp.433–438.

Katsuma, S., Hirasawa, A. & Tsujimoto, G., 2005. Bile acids promote glucagon-like peptide-1 secretion through TGR5 in a murine enteroendocrine cell line STC-1. *Biochemical and Biophysical Research Communications*, 329(1), pp.386–390.

Kaur, K. *et al*., 2011. Comprehensive miRNome and in silico analyses identify the Wnt signaling pathway to be altered in the diabetic liver. *Molecular bioSystems*, 7(12), pp.3234–3244.

KELLER, H., DREYER, C., MEDIN, J., MAHFOUDI, A., OZATO, K. & WAHLI, W., 1993a. Fatty-Acids and Retinoids Control Lipid-Metabolism Through Activation of Peroxisome Proliferator-Activated Receptor Retinoid-X Receptor Heterodimers. *Proceedings of the National Academy of Sciences of the United States of America*, 90(6), pp.2160–2164.

KELLER, H., DREYER, C., MEDIN, J., MAHFOUDI, A., OZATO, K. & WAHLI, W., 1993b. Fatty-Acids and Retinoids Control Lipid-Metabolism Through Activation of Peroxisome Proliferator-Activated Receptor Retinoid-X Receptor Heterodimers. *Proceedings of the National Academy of Sciences of the United States of America*, 90(6), pp.2160–2164.

Kelly, L.J. *et al*., 2013. Peroxisome Proliferator-Activated Receptors γ and α Mediate in Vivo Regulation of Uncoupling Protein (UCP-1, UCP-2, UCP-3) Gene Expression. *dx.doi.org*.

Kenler, H.A., Brolin, R.E. & Cody, R.P., 1990. Changes in eating behavior after horizontal gastroplasty and Roux-en-Y gastric bypass. *The American journal of clinical nutrition*, 52(1), pp.87–92.

Kere, J. *et al*., 1996. X-linked anhidrotic (hypohidrotic) ectodermal dysplasia is caused by mutation in a novel transmembrane protein. *Nature genetics*, 13(4), pp.409–416.

Kim, V.N., 2006. Small RNAs just got bigger: Piwi-interacting RNAs (piRNAs) in mammalian testes. *Genes & Development*, 20(15), pp.1993–1997.

Kindel, T.L. *et al*., 2009. Duodenal-jejunal exclusion improves glucose tolerance in the diabetic, Goto-Kakizaki rat by a GLP-1 receptor-mediated mechanism. *Journal of gastrointestinal surgery : official journal of the Society for Surgery of the Alimentary Tract*, 13(10), pp.1762–1772.

Kiss, T., 2001. Small nucleolar RNA-guided post-transcriptional modification of cellular RNAs. *The EMBO journal*, 20(14), pp.3617–3622.

Klaunig, J.E. *et al*., 2003. PPARalpha agonist-induced rodent tumors: modes of action and human relevance. *Critical reviews in toxicology*, 33(6), pp.655–780.

Klok, M.D., Jakobsdottir, S. & Drent, M.L., 2007. The role of leptin and ghrelin in the regulation of food intake and body weight in humans: A review. *Obesity reviews*, 8(1), pp.21–34.

Kohli, R. *et al*., 2013. Weight loss induced by Roux-en-Y gastric bypass but not laparoscopic adjustable gastric banding increases circulating bile acids. *The Journal of clinical endocrinology and metabolism*, 98(4), pp.E708–12.

Kong, L. *et al*., 2011. Significance of serum microRNAs in pre-diabetes and newly diagnosed type 2 diabetes: a clinical study. *Acta Diabetologica*, 48(1), pp.61–69.

Kornfeld, J.-W. *et al*., 2013. Obesity-induced overexpression of miR-802 impairs glucose metabolism through silencing of Hnf1b. *Nature*, 494(7435), pp.111–115.

Kotelevtsev, Y. *et al*., 1997. 11beta-hydroxysteroid dehydrogenase type 1 knockout mice show attenuated glucocorticoid-inducible responses and resist hyperglycemia on obesity or stress. *Proceedings of the National Academy of Sciences of the United States of America*, 94(26), pp.14924–14929.

Krey, G. *et al*., 1997. Fatty acids, eicosanoids, and hypolipidemic agents identified as ligands of peroxisome proliferator-activated receptors by coactivator-dependent receptor ligand assay. *Molecular Endocrinology*, 11(6), pp.779–791.

Krutzfeldt, J. *et al*., 2005. Silencing of microRNAs in vivo with “antagomirs.” *Nature*, 438(7068), pp.685–689.

Kuchenbauer, F. *et al*., 2011. Comprehensive analysis of mammalian microRNA* species and their role in myeloid cells. *Blood*, 118(12), pp.3350–3358.

Kutay, H. *et al*., 2006. Downregulation of miR-122 in the rodent and human hepatocellular carcinomas. *Journal of cellular biochemistry*, 99(3), pp.671–678.

Laferrère, B. *et al*., 2008. Effect of weight loss by gastric bypass surgery versus hypocaloric diet on glucose and incretin levels in patients with type 2 diabetes. *The Journal of clinical endocrinology and metabolism*, 93(7), pp.2479–2485.

Laffel, L., 1999. Ketone bodies: a review of physiology, pathophysiology and application of monitoring to diabetes. *Diabetes/metabolism research and reviews*, 15(6), pp.412–426.

Lagos-Quintana, M. *et al*., 2002. Identification of tissue-specific microRNAs from mouse. *Current biology : CB*, 12(9), pp.735–739.

Lagos-Quintana, M. *et al*., 2003. New microRNAs from mouse and human. *RNA (New York, N.Y.)*, 9(2), pp.175–179.

Lau, N.C. *et al*., 2006. Characterization of the piRNA complex from rat testes. *Science (New York, N.Y.)*, 313(5785), pp.363–367.

Laudadio, I. *et al*., 2012. A feedback loop between the liver-enriched transcription factor network and miR-122 controls hepatocyte differentiation. *Gastroenterology*, 142(1), pp.119–129.

Le Roux, C.W. *et al*., 2006. Gut hormone profiles following bariatric surgery favor an anorectic state, facilitate weight loss, and improve metabolic parameters. *Annals of …*, 243(1), pp.108–114.

Lee, C.-H., Olson, P. & Evans, R.M., 2003. Minireview: Lipid Metabolism, Metabolic Diseases, and Peroxisome Proliferator-Activated Receptors. *Endocrinology*, 144(6), pp.2201–2207.

Lee, R.C., Feinbaum, R.L. & Ambros, V., 1993. The C. elegans heterochronic gene lin-4 encodes small RNAs with antisense complementarity to lin-14. *Cell*, 75(5), pp.843–854.

Lee, W.J. *et al*., 2006. AMPK activation increases fatty acid oxidation in skeletal muscle by activating PPARalpha and PGC-1. *Biochemical and Biophysical Research Communications*, 340(1), pp.291–295.

Lehmann, U. *et al*., 2008. Epigenetic inactivation of microRNA gene hsa-mir-9-1in human breast cancer. *The Journal of Pathology*, 214(1), pp.17–24.

Leibel, R.L., Rosenbaum, M. & Hirsch, J., 1995. Changes in energy expenditure resulting from altered body weight. *The New England journal of medicine*, 332(10), pp.621–628.

Ley, R.E. *et al*., 2005. Obesity alters gut microbial ecology. *Proceedings of the National Academy of Sciences of the United States of America*, 102(31), pp.11070–11075.

Li, H.K. *et al*., 2005. High glucose inhibits apoptosis induced by serum deprivation in vascular smooth muscle cells via upregulation of Bcl-2 and Bcl-xl. *Diabetes*, 54(2), pp.540–545.

Li, J.V. *et al*., 2011a. Metabolic surgery profoundly influences gut microbial-host metabolic cross-talk. *Gut*, 60(9), pp.1214–1223.

Li, Z.-Y. *et al*., 2011b. Positive regulation of hepatic miR-122 expression by HNF4α. *Journal of hepatology*, 55(3), pp.602–611.

Lin, C.J.-F. *et al*., 2008. miR-122 targets an anti-apoptotic gene, Bcl-w, in human hepatocellular carcinoma cell lines. *Biochemical and Biophysical Research Communications*, 375(3), pp.315–320.

Ling, H.-Y. *et al*., 2009. CHANGES IN microRNA (miR) PROFILE AND EFFECTS OF miR-320 IN INSULIN-RESISTANT 3T3-L1 ADIPOCYTES. *Clinical and Experimental Pharmacology and Physiology*, 36(9), pp.e32–e39.

Liou, A.P., Paziuk, M., Jesus-Mario Luevano, J., Machineni, S., Turnbaugh, P.J. & Kaplan, L.M., 2013a. Conserved Shifts in the Gut Microbiota Due to Gastric Bypass Reduce Host Weight and Adiposity. *Science translational medicine*, 5(178), pp.178ra41–178ra41.

Liou, A.P., Paziuk, M., Jesus-Mario Luevano, J., Machineni, S., Turnbaugh, P.J. & Kaplan, L.M., 2013b. Conserved Shifts in the Gut Microbiota Due to Gastric Bypass Reduce Host Weight and Adiposity. *Science translational medicine*, 5(178), pp.178ra41–178ra41.

Livak, K.J. & Schmittgen, T.D., 2001. Analysis of Relative Gene Expression Data Using Real-Time Quantitative PCR and the 2−ΔΔCT Method. *Methods (San Diego, Calif.)*, 25(4), pp.402–408.

Lovis, P., Gattesco, S. & Regazzi, R., 2008a. Regulation of the expression of components of the exocytotic machinery of insulin-secreting cells by microRNAs. *Biological Chemistry*, 389(3), pp.305–312.

Lovis, P., Roggli, E., *et al*., 2008b. Alterations in microRNA expression contribute to fatty acid-induced pancreatic beta-cell dysfunction. *Diabetes*, 57(10), pp.2728–2736.

Lytle, J.R., Yario, T.A. & Steitz, J.A., 2007. Target mRNAs are repressed as efficiently by microRNA-binding sites in the 5 “ UTR as in the 3 ” UTR. *Proceedings of the National Academy of Sciences of the United States of America*, 104(23), pp.9667–9672.

MacDonald, B.T., Tamai, K. & He, X., 2009a. Wnt/beta-Catenin Signaling: Components, Mechanisms, and Diseases. *Developmental Cell*, 17(1), pp.9–26.

MacDonald, B.T., Tamai, K. & He, X., 2009b. Wnt/β-Catenin Signaling: Components, Mechanisms, and Diseases. *Developmental Cell*, 17(1), pp.9–26.

MacRae, I.J. *et al*., 2008. In vitro reconstitution of the human RISC-loading complex. *Proceedings of the National Academy of Sciences of the United States of America*, 105(2), pp.512–517.

Maggard, M.A. *et al*., 2005. Meta-analysis: Surgical treatment of obesity. *Annals of Internal Medicine*, 142(7), pp.547–559.

Malone, C.D. *et al*., 2009. Specialized piRNA Pathways Act in Germline and Somatic Tissues of the Drosophila Ovary. *Cell*, 137(3), pp.522–535.

Manchester, J. *et al*., 1996. Increased glycogen accumulation in transgenic mice overexpressing glycogen synthase in skeletal muscle. *Proceedings of the National Academy of Sciences of the United States of America*, 93(20), pp.10707–10711.

Marek, C.J. *et al*., 2003. Generation of hepatocytes expressing functional cytochromes P450 from a pancreatic progenitor cell line in vitro. *Biochemical Journal*, 370(Pt 3), pp.763–769.

Martin, G. *et al*., 2007. Prediction and validation of microRNA targets in animal genomes. *Journal of biosciences*, 32(6), pp.1049–1052.

Maslowski, K.M. *et al*., 2009. Regulation of inflammatory responses by gut microbiota and chemoattractant receptor GPR43. *Nature*, 461(7268), pp.1282–1286.

Mastrocola, R. *et al*., 2003. Pro-oxidant effect of dehydroepiandrosterone in rats is mediated by PPAR activation. *Life Sciences*, 73(3), pp.289–299.

Mattiasson, G. & Sullivan, P.G., 2006. The Emerging Functions of UCP2 in Health, Disease, and Therapeutics. *dx.doi.org*.

Mencarelli, A. *et al*., 2013. Dissociation of intestinal and hepatic activities of FXR and LXRα supports metabolic effects of terminal ileum interposition in rodents. *Diabetes*, 62(10), pp.3384–3393.

Menendez, J.A. *et al*., 2009. Fatty acid synthase: association with insulin resistance, type 2 diabetes, and cancer. *Clinical chemistry*, 55(3), pp.425–438.

Mestdagh, P. *et al*., 2009. A novel and universal method for microRNA RT-qPCR data normalization. *Genome biology*, 10(6), p.R64.

Mi, H. *et al*., 2013. Large-scale gene function analysis with the PANTHER classification system. *Nature Protocols*, 8(8), pp.1551–1566.

Miller, T.B. & Larner, J., 1973. Mechanism of control of hepatic glycogenesis by insulin. *Journal of Biological Chemistry*, 248(10), pp.3483–3488.

Miras, A.D. & le Roux, C.W., 2013. Mechanisms underlying weight loss after bariatric surgery. *Nature reviews. Gastroenterology & hepatology*, 10(10), pp.575–584.

Mitchell, P.S. *et al*., 2008. Circulating microRNAs as stable blood-based markers for cancer detection. *Proceedings of the National Academy of Sciences of the United States of America*, 105(30), pp.10513–10518.

Molitoris, J.K., McColl, K.S. & Distelhorst, C.W., 2011. Glucocorticoid-Mediated Repression of the Oncogenic microRNA Cluster miR-17~92 Contributes to the Induction of Bim and Initiation of Apoptosis. *Molecular Endocrinology*, 25(3), pp.409–420.

Najafi-Shoushtari, S.H. *et al*., 2010. MicroRNA-33 and the SREBP Host Genes Cooperate to Control Cholesterol Homeostasis. *Science (New York, N.Y.)*, 328(5985), pp.1566–1569.

Näslund, E. & Hellström, P.M., 2007. Appetite signaling: From gut peptides and enteric nerves to brain. *Physiology & behavior*, 92(1-2), pp.256–262.

Olson, A.L. & Pessin, J.E., 1996. Structure, function, and regulation of the mammalian facilitative glucose transporter gene family. *Annual review of nutrition*.

Ortega, F.J. *et al*., 2013. Targeting the circulating microRNA signature of obesity. *Clinical chemistry*, 59(5), pp.781–792.

Osundiji, M.A. *et al*., 2012. Brain glucose sensors play a significant role in the regulation of pancreatic glucose-stimulated insulin secretion. *Diabetes*, 61(2), pp.321–328.

Ouaamari, El, A. *et al*., 2008. miR-375 targets 3'-phosphoinositide-dependent protein kinase-1 and regulates glucose-induced biological responses in pancreatic beta-cells. *Diabetes*, 57(10), pp.2708–2717.

Pandolfi, P.P. *et al*., 1995. Targeted disruption of the housekeeping gene encoding glucose 6-phosphate dehydrogenase (G6PD): G6PD is dispensable for pentose synthesis but essential for defense against oxidative stress. *The EMBO journal*, 14(21), pp.5209–5215.

Parton, L.E. *et al*., 2007. Glucose sensing by POMC neurons regulates glucose homeostasis and is impaired in obesity. *Nature*, 449(7159), pp.228–232.

Paterson, J.M., Morton, N.M. & Fievet, C., 2004. Metabolic syndrome without obesity: hepatic overexpression of 11β-hydroxysteroid dehydrogenase type 1 in transgenic mice. In Proceedings of the ….

Patterson, A.D., Shah, Y.M., Matsubara, T., Krausz, K.W. & Gonzalez, F.J., 2012a. Peroxisome proliferator-activated receptor alpha induction of uncoupling protein 2 protects against acetaminophen-induced liver toxicity. *Hepatology*, 56(1), pp.281–290.

Patterson, A.D., Shah, Y.M., Matsubara, T., Krausz, K.W. & Gonzalez, F.J., 2012b. Peroxisome proliferator-activated receptor alpha induction of uncoupling protein 2 protects against acetaminophen-induced liver toxicity. *Hepatology*, 56(1), pp.281–290.

Peng, Y. *et al*., 2010. Does LKB1 mediate activation of hepatic AMP-protein kinase (AMPK) and sirtuin1 (SIRT1) after Roux-en-Y gastric bypass in obese rats? *Journal of gastrointestinal surgery : official journal of the Society for Surgery of the Alimentary Tract*, 14(2), pp.221–228.

Pessin, J.E. & Bell, G.I., 1992. Mammalian facilitative glucose transporter family: structure and molecular regulation. *Annual review of physiology*, 54, pp.911–930.

Petri, S. *et al*., 2011. Increased siRNA duplex stability correlates with reduced off-target and elevated on-target effects. *RNA (New York, N.Y.)*, 17(4), pp.737–749.

Pfeiffer, R.F., 2003. Gastrointestinal dysfunction in Parkinson's disease. *The Lancet Neurology*, 2(2), pp.107–116.

Plaisance, V. *et al*., 2006. MicroRNA-9 controls the expression of Granuphilin/Slp4 and the secretory response of insulin-producing cells. *Journal of Biological Chemistry*, 281(37), pp.26932–26942.

Pories, W.J. *et al*., 1995. Who would have thought it? An operation proves to be the most effective therapy for adult-onset diabetes mellitus. *Annals of surgery*, 222(3), p.339.

Porreca, F., Galligan, J.J. & Burks, T.F., 1986. Central opioid receptor involvement in gastrointestinal motility. *Trends in Pharmacological Sciences*, 7, pp.104–107.

Poy, M.N. *et al*., 2004. A pancreatic islet-specific microRNA regulates insulin secretion. *Nature*, 432(7014), pp.226–230.

Poy, M.N. *et al*., 2009. miR-375 maintains normal pancreatic alpha- and beta-cell mass. *Proceedings of the National Academy of Sciences of the United States of America*, 106(14), pp.5813–5818.

Preston, S.H. *et al*., 2014. Projecting the effect of changes in smoking and obesity on future life expectancy in the United States. *Demography*, 51(1), pp.27–49.

Quattrone, A., Dahm, R. & Macchi, P., 2012. Subcellular RNA Localizationand Translational Control:. pp.1–18.

Ram, E. *et al*., 2005. Impact of gastric banding on plasma ghrelin, growth hormone, cortisol, DHEA and DHEA-S levels. *Obesity surgery*, 15(8), pp.1118–1123.

Raskin, P. *et al*., 2000. Rosiglitazone short-term monotherapy lowers fasting and post-prandial glucose in patients with Type II diabetes. *Diabetologia*, 43(3), pp.278–284.

Rayner, K.J. *et al*., 2010. MiR-33 Contributes to the Regulation of Cholesterol Homeostasis. *Science (New York, N.Y.)*, 328(5985), pp.1570–1573.

Re, A. *et al*., 2009. Genome-wide survey of microRNA-transcription factor feed-forward regulatory circuits in human. *Molecular bioSystems*, 5(8), pp.854–867.

Reinhart, B.J. *et al*., 2000. The 21-nucleotide let-7 RNA regulates developmental timing in Caenorhabditis elegans. *Nature*, 403(6772), pp.901–906.

Repa, J.J. & Mangelsdorf, D.J., 1999. Nuclear receptor regulation of cholesterol and bile acid metabolism. *Current opinion in biotechnology*, 10(6), pp.557–563.

Resnick, K.E. *et al*., 2009. The detection of differentially expressed microRNAs from the serum of ovarian cancer patients using a novel real-time PCR platform. *Gynecologic Oncology*, 112(1), pp.55–59.

Rintelen, F. *et al*., 2001. PDK1 regulates growth through at and S6K in Drosophila. *Proceedings of the National Academy of Sciences of the United States of America*, 98(26), pp.15020–15025.

RIZZA, R.A., MANDARINO, L.J. & GERICH, J.E., 1982. Cortisol-Induced Insulin Resistance in Man - Impaired Suppression of Glucose-Production and Stimulation of Glucose-Utilization Due to a Postreceptor Defect of Insulin Action. *The Journal of clinical endocrinology and metabolism*, 54(1), pp.131–138.

Rocca, A.S. & Brubaker, P.L., 1999. Role of the vagus nerve in mediating proximal nutrient-induced glucagon-like peptide-1 secretion. *Endocrinology*, 140(4), pp.1687–1694.

Rodríguez-Antona, C. *et al*., 2002. Cytochrome P450 expression in human hepatocytes and hepatoma cell lines: molecular mechanisms that determine lower expression in cultured cells. *Xenobiotica; the fate of foreign compounds in biological systems*, 32(6), pp.505–520.

Roggli, E. *et al*., 2010. Involvement of MicroRNAs in the Cytotoxic Effects Exerted by Proinflammatory Cytokines on Pancreatic beta-Cells. *Diabetes*, 59(4), pp.978–986.

Rogue, A. *et al*., 2010. Gene Expression Changes Induced by PPAR Gamma Agonists in Animal and Human Liver. *PPAR research*, 2010, p.325183.

Ross, S.E. *et al*., 2000. Inhibition of adipogenesis by Wnt signaling. *Science (New York, N.Y.)*, 289(5481), pp.950–953.

Roux, C.W.L. *et al*., 2006. Gut Hormone Profiles Following Bariatric Surgery Favor an Anorectic State, Facilitate Weight Loss, and Improve Metabolic Parameters. *Annals of surgery*, 243(1), pp.108–114.

Rubino, F. *et al*., 2010. Metabolic surgery to treat type 2 diabetes: clinical outcomes and mechanisms of action. *Annual review of medicine*, 61, pp.393–411.

Rubino, F.A. & Marescaux, J., 2004. Effect of duodenal-jejunal exclusion in a non-obese animal model of type 2 diabetes - A new perspective for an old disease. *Annals of surgery*, 239(1), pp.1–11.

Rulifson, I.C. *et al*., 2007. Wnt signaling regulates pancreatic beta cell proliferation. *Proceedings of the National Academy of Sciences of the United States of America*, 104(15), pp.6247–6252.

RYKOVA, E.Y. *et al*., 2006. Concentrations of Circulating RNA from Healthy Donors and Cancer Patients Estimated by Different Methods. *Annals of the New York Academy of Sciences*, 1075(1), pp.328–333.

Saba, R. *et al*., 2008. A microRNA Signature of Prion Induced Neurodegeneration. *PLOS ONE*, 3(11).

Saeidi, N. *et al*., 2013. Reprogramming of intestinal glucose metabolism and glycemic control in rats after gastric bypass. *Science (New York, N.Y.)*, 341(6144), pp.406–410.

Samec, S., Seydoux, J. & Dulloo, A.G., 1998. Role of UCP homologues in skeletal muscles and brown adipose tissue: mediators of thermogenesis or regulators of lipids as fuel substrate? *Faseb Journal*, 12(9), pp.715–724.

Samuel, B.S. *et al*., 2008. Effects of the gut microbiota on host adiposity are modulated by the short-chain fatty-acid binding G protein-coupled receptor, Gpr41. *Proceedings of the National Academy of Sciences of the United States of America*, 105(43), pp.16767–16772.

Sander, J.D. & Joung, J.K., 2014. CRISPR-Cas systems for editing, regulating and targeting genomes. *Nature biotechnology*.

SANGER, G., 2008. 5-Hydroxytryptamine and the gastrointestinal tract: where next? *Trends in Pharmacological Sciences*, 29(9), pp.465–471.

Schauer, P.R. *et al*., 2004. Effect of Laparoscopic Roux-en-Y Gastric Bypass on Type 2 Diabetes Mellitus. *Nutrition in Clinical Practice*, 19(1), pp.60–61.

Schee, K. *et al*., 2013. Deep Sequencing the MicroRNA Transcriptome in Colorectal Cancer. *PLOS ONE*, 8(6), p.e66165.

Schoneveld, O.J.L.M., Gaemers, I.C. & Lamers, W.H., 2004. Mechanisms of glucocorticoid signalling. *Biochimica et Biophysica Acta (BBA) - Gene Structure and Expression*, 1680(2), pp.114–128.

Schulte, J.H. *et al*., 2010. Deep sequencing reveals differential expression of microRNAs in favorable versus unfavorable neuroblastoma. *Nucleic Acids Research*, 38(17), pp.5919–5928.

Schwartz, M.W., 2006. Central nervous system regulation of food intake. *Obesity*, 14(2S), pp.1S–8S.

Selmaoui, B. & Touitou, Y., 2003. Reproducibility of the circadian rhythms of serum cortisol and melatonin in healthy subjects: a study of three different 24-h cycles over six weeks. *Life Sciences*.

Seyfried, F., le Roux, C.W. & Bueter, M., 2011. Lessons learned from gastric bypass operations in rats. *Obesity facts*, 4 Suppl 1(Suppl. 1), pp.3–12.

Shalgi, R. *et al*., 2007. Global and Local Architecture of the Mammalian microRNA–Transcription Factor Regulatory Network. *PLoS computational biology*, 3(7), p.e131.

Shen, C.N., Slack, J.M. & Tosh, D., 2000. Molecular basis of transdifferentiation of pancreas to liver. *Nature cell biology*, 2(12), pp.879–887.

Simonen, M. *et al*., 2012. Conjugated bile acids associate with altered rates of glucose and lipid oxidation after Roux-en-Y gastric bypass. *Obesity surgery*, 22(9), pp.1473–1480.

Simonyte, K. *et al*., 2010. Weight Loss after Gastric Bypass Surgery in Women Is Followed by a Metabolically Favorable Decrease in 11 beta-Hydroxysteroid Dehydrogenase 1 Expression in Subcutaneous Adipose Tissue. *The Journal of clinical endocrinology and metabolism*, 95(7), pp.3527–3531.

Singh, P.K., Brand, R.E. & Mehla, K., 2012. MicroRNAs in pancreatic cancer metabolism. *Nature reviews. Gastroenterology & hepatology*, 9(6), pp.334–344.

Siomi, M.C. *et al*., 2011. PIWI-interacting small RNAs: the vanguard of genome defence. *Nature Reviews Molecular Cell Biology*, 12(4), pp.246–258.

Sjostrom, L. *et al*., 2004. Lifestyle, diabetes, and cardiovascular risk factors 10 years after bariatric surgery. *The New England journal of medicine*, 351(26), pp.2683–2693.

Smith, L.K., Shah, R.R. & Cidlowski, J.A., 2010. Glucocorticoids modulate microRNA expression and processing during lymphocyte apoptosis. *The Journal of biological chemistry*, 285(47), pp.36698–36708.

Staels, B. *et al*., 1998. Mechanism of action of fibrates on lipid and lipoprotein metabolism. *Circulation …*.

Starkey Lewis, P.J. *et al*., 2011. Circulating microRNAs as potential markers of human drug-induced liver injury. *Hepatology*, 54(5), pp.1767–1776.

STRUBBE, J.H.STEFFENS, AB, 1977. Blood-Glucose Levels in Portal and Peripheral-Circulation and Their Relation to Food-Intake in Rat. *Physiology & behavior*, 19(2), pp.303–307.

Stylopoulos, N., Hoppin, A.G. & Kaplan, L.M., 2009. Roux-en-Y Gastric Bypass Enhances Energy Expenditure and Extends Lifespan in Diet-induced Obese Rats. *Obesity*, 17(10), pp.1839–1847.

Suzuki, S. *et al*., 2005. Changes in GI hormones and their effect on gastric emptying and transit times after Roux-en-Y gastric bypass in rat model. *Surgery*, 138(2), pp.283–290.

Tadross, J.A. & Le Roux, C.W., 2009. The mechanisms of weight loss after bariatric surgery. *International Journal of Obesity*, 33, pp.S28–S32.

Takamori, S., Riedel, D. & Jahn, R., 2000. Immunoisolation of GABA-specific synaptic vesicles defines a functionally distinct subset of synaptic vesicles. *Journal of Neuroscience*, 20(13), pp.4904–4911.

Talley, N.J., 1992. Review article: 5-hydroxytryptamine agonists and antagonists in the modulation of gastrointestinal motility and sensation: clinical implications. *Alimentary pharmacology & therapeutics*, 6(3), pp.273–289.

Tang, F. *et al*., 2006. 220-plex microRNA expression profile of a single cell. *Nature Protocols*, 1(3), pp.1154–1159.

Tang, X. *et al*., 2009. Identification of glucose-regulated microRNAs from pancreatic beta cells reveals a role for miR-30d in insulin transcription. *RNA (New York, N.Y.)*, 15(2), pp.287–293.

Telernan, A.A. & Cohen, S.M., 2006. Drosophila lacking microRNA miR-278 are defective in energy homeostasis. *Genes & Development*, 20(4), pp.417–422.

THIRLBY, R. *et al*., 2006. Effect of Roux-en-Y Gastric Bypass on Satiety and Food Likes: The Role of Genetics. *Journal of Gastrointestinal Surgery*, 10(2), pp.270–277.

Thomas, M. *et al*., 2013. Analysis of Transcriptional Regulation of the Human miR-17-92 Cluster; Evidence for Involvement of Pim-1. *International Journal of Molecular Sciences*, 14(6), pp.12273–12296.

Thomson, T. & Lin, H., 2009. The Biogenesis and Function of PIWI Proteins and piRNAs: Progress and Prospect. *Annual Review of Cell and Developmental Biology*, 25(1), pp.355–376.

Tomari, Y. *et al*., 2004. A protein sensor for siRNA asymmetry. *Science (New York, N.Y.)*, 306(5700), pp.1377–1380.

Tomlinson, J.W. *et al*., 2004. Weight loss increases 11 beta-hydroxysteroid dehydrogenase type 1 expression in human adipose tissue. *The Journal of clinical endocrinology and metabolism*, 89(6), pp.2711–2716.

Toyomasu, Y. *et al*., 2010. Intragastric monosodium L-glutamate stimulates motility of upper gut via vagus nerve in conscious dogs. *American journal of physiology. Regulatory, integrative and comparative physiology*, 298(4), pp.R1125–35.

Toyota, M. *et al*., 2008. Epigenetic Silencing of MicroRNA-34b/c and B-Cell Translocation Gene 4 Is Associated with CpG Island Methylation in Colorectal Cancer. *Cancer Research*, 68(11), pp.4123–4132.

Troy, S. *et al*., 2008. Intestinal gluconeogenesis is a key factor for early metabolic changes after gastric bypass but not after gastric lap-band in mice. *Cell metabolism*, 8(3), pp.201–211.

Turek, F.W., 2005. Obesity and Metabolic Syndrome in Circadian Clock Mutant Mice. *Science (New York, N.Y.)*, 308(5724), pp.1043–1045.

Turnbaugh, P.J. *et al*., 2008. A core gut microbiome in obese and lean twins. *Nature*, 457(7228), pp.480–484.

Turnbaugh, P.J. *et al*., 2006. An obesity-associated gut microbiome with increased capacity for energy harvest. *Nature*, 444(7122), pp.1027–131.

Ueda, Y. *et al*., 2011. Reduction of 8-iso-prostaglandin F2α in the first week after Roux-en-Y gastric bypass surgery. *Obesity*, 19(8), pp.1663–1668.

UI, R., TASHJIAN, A.H. & LEVINE, L., 1969. Establishment of a Clonal Strain of Hepatoma Cells Which Secrete Albumin. *Journal of Cell Biology*, 40(1), pp.236–&.

van Uum, S. & Hermus, A., 1998. The role of 11β-hydroxysteroid dehydrogenase in the pathogenesis of hypertension. *Cardiovascular ….*

Vickers, K.C. *et al*., 2011. MicroRNAs are transported in plasma and delivered to recipient cells by high-density lipoproteins. *Nature cell biology*, 13(4), pp.423–433.

Vincent, R.P. & Le Roux, C.W., 2008. Changes in gut hormones after bariatric surgery. *Clinical Endocrinology*, 69(2), pp.173–179.

Wan, G.H., Tsai, S.C. & Chiu, D., 2002. Decreased blood activity of glucose-6-phosphate dehydrogenase associates with increased risk for diabetes mellitus. *Endocrine*.

Wang, Jen-Chywan *et al*., 2012. Regulation of triglyceride metabolism by glucocorticoid receptor. *Cell and Bioscience*, 2(1).

Wang, Minghan, 2005. The role of glucocorticoid action in the pathophysiology of the Metabolic Syndrome. *Nutrition & Metabolism*, 2(1), p.3.

Wang, Qiang *et al*., 2008. miR-17-92 cluster accelerates adipocyte differentiation by negatively regulating tumor-suppressor Rb2/p130. *Proceedings of the National Academy of Sciences*, 105(8), pp.2889–2894.

Wang, Y X *et al*., 2003. Peroxisome-proliferator-activated receptor delta activates fat metabolism to prevent obesity. *Cell*, 113(2), pp.159–170.

Wang, Yanxin *et al*., 2004. The human fatty acid synthase gene and de novo lipogenesis are coordinately regulated in human adipose tissue. *The Journal of nutrition*, 134(5), pp.1032–1038.

Wang, Yong & Liu, J., 2009. Combination of Bypassing Stomach and Vagus Dissection in High-Fat Diet-Induced Obese Rats—A Long-Term Investigation. *Obesity surgery*, 20(3), pp.375–379.

Weatheritt, R.J., Gibson, T.J. & Babu, M.M., 2014. Asymmetric mRNA localization contributes to fidelity and sensitivity of spatially localized systems. *Nature Structural & Molecular Biology*, 21(9), pp.833–839.

Wiegand, G. & Remington, S.J., 1986. Citrate synthase: structure, control, and mechanism. *Annual review of biophysics and biophysical chemistry*, 15(1), pp.97–117.

Wilfred, B.R., Wang, W.-X. & Nelson, P.T., 2007. Energizing microRNA research: A review of the role of microRNAs in lipid metabolism, with a prediction that miR-103/107 regulates human metabolic pathways. *Molecular Genetics and Metabolism*, 91(3), pp.209–217.

Williams, D.B. *et al*., 2007. Gastric bypass reduces biochemical cardiac risk factors. *Surgery for Obesity and Related Diseases*, 3(1), pp.8–13.

Willson, T.M. *et al*., 2000. The PPARs: From Orphan Receptors to Drug Discovery †. *Journal of Medicinal Chemistry*, 43(4), pp.527–550.

Witkos, T.M., Koscianska, E. & Krzyzosiak, W.J., 2011. Practical Aspects of microRNA Target Prediction. *Current Molecular Medicine*, 11(2), pp.93–109.

Wolff, B.S. *et al*., 2009. Roux-en-Y gastric bypass alters small intestine glutamine transport in the obese Zucker rat. *American Journal of Physiology - Gastrointestinal and Liver Physiology*, 297(3), pp.G594–601.

Xu, P. *et al*., 2003. The Drosophila MicroRNA Mir-14 Suppresses Cell Death and Is Required for Normal Fat Metabolism. *Current Biology*, 13(9), pp.790–795.

Xu, Y. *et al*., 2008. 5-HT2CRs Expressed by Pro-Opiomelanocortin Neurons Regulate Energy Homeostasis. *Neuron*, 60(4), pp.582–589.

Yach, D., Stuckler, D. & Brownell, K.D., 2006. Epidemiologic and economic consequences of the global epidemics of obesity and diabetes (vol 12, pg 62, 2006). *Nature Medicine*, 12(3), pp.367–367.

Ye, J. & DeBose-Boyd, R.A., 2011. Regulation of Cholesterol and Fatty Acid Synthesis. *Cold Spring Harbor Perspectives in Biology*, 3(7).

Yeung, K.Y. & Ruzzo, W.L., 2001. Principal component analysis for clustering gene expression data. *Bioinformatics (Oxford, England)*, 17(9), pp.763–774.

Yin, H. *et al*., 2012. MicroRNA-217 promotes ethanol-induced fat accumulation in hepatocytes by down-regulating SIRT1. *The Journal of biological chemistry*, 287(13), pp.9817–9826.

Yue, D., Liu, H. & Huang, Y., 2009. Survey of Computational Algorithms for MicroRNA Target Prediction. *Current Genomics*, 10(7), pp.478–492.

Zampetaki, A. *et al*., 2010. Plasma microRNA profiling reveals loss of endothelial miR-126 and other microRNAs in type 2 diabetes. *Circulation research*, 107(6), pp.810–817.

Zhang, C.-Y. *et al*., 2001. Uncoupling Protein-2 Negatively Regulates Insulin Secretion and Is a Major Link between Obesity, β Cell Dysfunction, and Type 2 Diabetes. *Cell*, 105(6), pp.745–755.

Zhang, H. *et al*., 2009a. Human gut microbiota in obesity and after gastric bypass. *Proceedings of the National Academy of Sciences*, 106(7), pp.2365–2370.

Zhang, J. *et al*., 2009b. Maternal high fat diet during pregnancy and lactation alters hepatic expression of insulin like growth factor-2 and key microRNAs in the adult offspring. *BMC genomics*, 10(1), p.478.

Zhang, Y. *et al*., 2010. Secreted Monocytic miR-150 Enhances Targeted Endothelial Cell Migration. *Molecular cell*.

Zhao, H. *et al*., 2010. Up-Regulated Pancreatic Tissue MicroRNA-375 Associates With Human Type 2 Diabetes Through β-Cell Deficit and Islet Amyloid Deposition. *Pancreas*, 39(6), pp.843–846.

Zheng, H. *et al*., 2009. Meal patterns, satiety, and food choice in a rat model of Roux-en-Y gastric bypass surgery. *American journal of physiology. Regulatory, integrative and comparative physiology*, 297(5), pp.R1273–82.

8. Appendices

Table 8-1 All detectable rat colon mature microRNA list

ID	log2FoldChange	padj	ID		padj
rno-miR-217-5p	Inf	4.35E-44	rno-miR-6315	-Inf	0.9679
rno-miR-150-5p	-2.95E+00	2.89E-29	rno-miR-29c-5p	-5.92E-01	0.9679
rno-miR-216a-5p	Inf	3.76E-24	rno-miR-199a-5p	-2.39E-01	0.9679
rno-miR-142-5p	-2.17E+00	3.15E-12	rno-miR-411-5p	0.4534	0.9679
rno-miR-6215	-2.77E+00	3.97E-10	rno-miR-664-3p	0.0026	0.9679
rno-miR-19b-3p	1.24	2.19E-06	rno-miR-101b-3p	0.0149	0.9679
rno-miR-216b-5p	Inf	1.09E-05	rno-miR-203a-3p	0.0293	0.9679
rno-miR-19a-3p	1.44	3.25E-05	rno-mir-145*	-2.43E+00	0.9679
rno-miR-142-3p	-1.90E+00	6.34E-05	rno-miR-137-3p	Inf	0.9679
rno-miR-181a-5p	-9.99E-01	0.0002	rno-miR-183-3p	-2.97E-01	0.9679
rno-miR-342-3p	-2.11E+00	0.0002	rno-miR-542-5p	-Inf	0.9679
rno-miR-196c-5p	1.16	0.0143	rno-miR-133b-3p	Inf	0.9679
rno-miR-541-5p	1.42	0.0344	rno-miR-181d-5p	-1.40E-01	0.9679
rno-miR-345-5p	1.28	0.0537	rno-miR-331-5p	Inf	0.9679
rno-miR-672-5p	Inf	0.0701	rno-miR-542-3p	-1.37E+00	0.9679
rno-miR-598-3p	1.63	0.0701	rno-let-7f-1-3p	0.2098	0.9679
rno-miR-338-5p	2.05	0.0701	rno-miR-138-5p	0.0726	0.9679
rno-miR-92b-3p	-1.19E+00	0.0703	rno-miR-29a-3p	-2.34E-01	0.9679
rno-miR-802-5p	Inf	0.0703	rno-miR-322-3p	-3.45E-01	0.9679
rno-miR-145-5p	0.6567	0.0703	rno-miR-152-5p	-2.30E-01	0.9679
rno-miR-455-3p	-1.31E+00	0.0703	rno-miR-6321	-2.74E+00	0.9679
rno-miR-451-5p	1.47	0.0775	rno-miR-217-3p	Inf	0.9679
rno-miR-374-5p	0.8452	0.0997	rno-miR-126a-5p	0.0257	0.9679
rno-miR-22-5p	0.9223	0.1033	rno-miR-219-5p	Inf	0.9679
rno-miR-98-5p	0.5495	0.1033	rno-miR-410-3p	0.1783	0.9679
rno-miR-363-3p	-2.58E+00	0.1033	rno-miR-143-3p	0.0768	0.9679
rno-miR-181a-2-...	-1.83E+00	0.1033	rno-miR-196b-3p	-1.60E+00	0.9679
rno-miR-204-5p	0.2648	0.1033	rno-miR-324-3p	0.3294	0.9679
rno-miR-351-5p	-8.29E-01	0.1033	rno-miR-30b-5p	0.1645	0.9679

rno-miR-423-5p	-6.75E-01	0.1426	rno-miR-504	-7.45E-01	0.9679
rno-miR-200b-5p	0.8549	0.1802	rno-miR-330-3p	-1.11E-01	0.9679
rno-miR-92a-3p	-5.70E-01	0.1802	rno-miR-17-5p	0.276	0.9679
rno-miR-872-5p	-7.21E-01	0.182	rno-miR-425-3p	-1.91E+00	0.9679
rno-miR-376b-5p	0.1531	0.2177	rno-miR-125b-1-...	-1.73E-01	0.9679
rno-miR-214-3p	-6.67E-01	0.2712	rno-miR-505-3p	-2.75E-01	0.9679
rno-miR-154-5p	3.64	0.2818	rno-miR-185-5p	-4.35E-01	0.9679
rno-miR-194-3p	0.847	0.3165	rno-miR-376b-3p	Inf	0.9679
rno-miR-125a-5p	-5.36E-01	0.3165	rno-miR-30e-3p	-2.01E-01	0.9679
rno-miR-434-3p	0.676	0.3187	rno-miR-337-5p	0.3783	0.9679
rno-miR-134-5p	1.73	0.3187	rno-miR-376c-3p	Inf	0.9679
rno-miR-1843-3p	1.14	0.3187	rno-miR-98-3p	0.2465	0.9679
rno-miR-378a-5p	0.7238	0.3187	rno-miR-324-5p	0.3242	0.9679
rno-miR-3068-3p	-8.69E-01	0.33	rno-miR-330-5p	-1.86E-01	0.9679
rno-miR-361-3p	-1.55E+00	0.33	rno-miR-488-3p	0.1727	0.9679
rno-miR-136-3p	0.8094	0.33	rno-mir-350*	-2.98E+00	0.9679
rno-miR-326-3p	0.8118	0.3426	rno-miR-140-5p	0.0688	0.9679
rno-miR-22-3p	-3.11E-01	0.3508	rno-miR-200a-5p	0.3778	0.9679
rno-miR-21-5p	0.4411	0.3508	rno-miR-449a-5p	-Inf	0.9679
rno-miR-15b-5p	-4.96E-01	0.3508	rno-miR-802-3p	Inf	0.9679
rno-miR-31a-5p	-6.88E-01	0.3544	rno-miR-181b-1-...	-Inf	0.9679
rno-miR-150-3p	-Inf	0.3544	rno-miR-30a-5p	0.1251	0.9679
rno-miR-34b-5p	-9.14E-01	0.4128	rno-miR-379-5p	Inf	0.9679
rno-miR-212-5p	0.3596	0.4128	rno-miR-361-5p	-2.52E-01	0.9679
rno-miR-192-3p	0.6619	0.4564	rno-miR-500-3p	0.2112	0.9679
rno-miR-345-3p	0.7995	0.4564	rno-miR-431	0.307	0.9679
rno-mir-126*	0.4047	0.4564	rno-miR-196c-3p	0.3314	0.9679
rno-miR-132-5p	-9.95E-01	0.4564	rno-miR-10a-3p	-2.16E-01	0.9679
rno-miR-221-3p	0.6355	0.4564	rno-miR-29b-3p	0.1357	0.9679
rno-miR-3585-5p	-8.98E-01	0.4564	rno-miR-429	0.0178	0.9679
rno-miR-151-5p	-3.82E-01	0.4564	rno-miR-362-3p	0.0066	0.9679
rno-miR-136-5p	0.8087	0.4564	rno-mir-421*	-5.09E-01	0.9679
rno-miR-133a-5p	-9.86E-01	0.4852	rno-miR-409a-3p	0.4536	0.9679
rno-miR-411-3p	-1.16E+00	0.5046	rno-miR-212-3p	0.4038	0.9679

rno-miR-339-3p	-8.76E-01	0.5046	rno-miR-1306-5p	-Inf	0.9679
rno-miR-3577	-8.93E-01	0.5046	rno-miR-153-3p	0.1801	0.9679
rno-miR-1-3p	-5.85E-01	0.5046	rno-miR-702-3p	-Inf	0.9679
rno-miR-181c-5p	-5.76E-01	0.5046	rno-miR-26b-3p	-3.42E-01	0.9679
rno-miR-382-5p	2.19	0.5385	rno-miR-532-3p	0.1383	0.9679
rno-miR-421-3p	-9.02E-01	0.5466	rno-miR-125a-3p	0.5053	0.9679
rno-miR-181b-5p	-5.85E-01	0.5466	rno-miR-216a-3p	Inf	0.9679
rno-miR-369-5p	-1.12E+00	0.5466	rno-miR-484	0.2519	0.9679
rno-miR-201-5p	-2.06E+00	0.5466	rno-miR-16-3p	-2.53E+00	0.9679
rno-miR-375-3p	-1.39E-01	0.5466	rno-miR-331-3p	-8.40E-02	0.9679
rno-let-7d-5p	-4.16E-01	0.5611	rno-let-7i-3p	0.228	0.9679
rno-mir-147*	2.55	0.5611	rno-miR-133a-3p	-7.48E-02	0.9679
rno-miR-16-5p	-3.00E-01	0.562	rno-miR-7a-1-3p	-3.21E-01	0.9679
rno-miR-222-3p	0.7154	0.562	rno-miR-490-3p	0.2278	0.9694
rno-miR-128-3p	-7.78E-01	0.5718	rno-miR-382-3p	Inf	0.9694
rno-miR-466b-2-...	-1.66E+00	0.5718	rno-miR-378b	0.7266	0.9694
rno-miR-423-3p	-4.29E-01	0.5718	rno-miR-26a-3p	-3.26E-02	0.9694
rno-miR-497-5p	-4.50E-01	0.583	rno-miR-30c-1-3...	0.2536	0.9694
rno-miR-99b-5p	-3.73E-01	0.5854	rno-miR-28-3p	0.0068	0.9796
rno-miR-497-3p	-1.35E+00	0.6445	rno-miR-182	-7.05E-03	0.9796
rno-let-7a-5p	-4.04E-01	0.6626	rno-miR-339-5p	0.112	0.9796
rno-miR-490-5p	1.52	0.6651	rno-miR-494-3p	Inf	0.9796
rno-miR-381-3p	0.5934	0.6651	rno-miR-132-3p	0.3688	0.9921
rno-miR-31a-3p	-8.44E-01	0.6651	rno-miR-187-3p	-Inf	1
rno-miR-203a-5p	0.2593	0.6651	rno-miR-34a-5p	-6.81E-02	1
rno-miR-27a-5p	0.7509	0.6651	rno-miR-879-5p	-9.05E-03	1
rno-miR-425-5p	-3.45E-01	0.6651	rno-miR-487b-3p	0.233	1
rno-miR-195-5p	-3.98E-01	0.6651	rno-miR-103-3p	0.0126	1
rno-miR-1249	-1.69E+00	0.6651	rno-miR-29a-5p	0.1931	1
rno-miR-384-5p	-1.36E+00	0.6651	rno-miR-99b-3p	0.2599	1
rno-miR-433-3p	-1.65E+00	0.6651	rno-miR-203b-3p	Inf	1
rno-miR-210-3p	0.5315	0.6651	rno-miR-223-5p	Inf	1
rno-miR-380-3p	-6.31E-01	0.6651	rno-miR-27b-3p	-9.12E-02	1
rno-miR-219-1-3...	1.13	0.6651	rno-miR-30d-5p	-1.93E-02	1

rno-miR-129-2-3...	1.44	0.6651	rno-miR-152-3p	0.028	1
rno-miR-195-3p	-7.58E-01	0.6928	rno-mir-194-1*	Inf	1
rno-miR-3559-3p	0.5625	0.6937	rno-miR-210-5p	-Inf	1
rno-miR-200c-5p	2.21	0.6937	rno-miR-218a-5p	0.18	1
rno-miR-125b-5p	-3.40E-01	0.7092	rno-mir-185*	Inf	1
rno-miR-205	-3.80E-01	0.7103	rno-miR-495	Inf	1
rno-miR-194-5p	0.0193	0.7103	rno-miR-3068-5p	-4.54E-01	1
rno-miR-18a-5p	0.7822	0.7103	rno-miR-130b-5p	0.1211	1
rno-miR-106b-5p	0.285	0.7103	rno-miR-335	-1.70E-01	1
rno-miR-708-5p	0.121	0.7106	rno-miR-192-5p	0.1142	1
rno-miR-196b-5p	0.1585	0.7106	rno-miR-320-3p	0.0106	1
rno-miR-1839-5p	0.3048	0.7106	rno-miR-708-3p	-3.11E-01	1
rno-miR-101a-5p	-1.17E+00	0.7106	rno-miR-130a-5p	Inf	1
rno-miR-3559-5p	0.4251	0.7106	rno-miR-301a-3p	0.0586	1
rno-miR-143-5p	-3.04E-01	0.7106	rno-miR-30e-5p	0.0272	1
rno-miR-24-2-5p	-3.51E-01	0.7106	rno-miR-10a-5p	-9.59E-02	1
rno-miR-671	-1.68E+00	0.7106	rno-miR-221-5p	-3.37E-01	1
rno-miR-23a-3p	-3.43E-01	0.7138	rno-miR-379-3p	Inf	1
rno-let-7a-1-3p...	0.3386	0.7222	rno-miR-547-3p	-Inf	1
rno-miR-181c-3p	-3.65E-01	0.7276	rno-miR-145-3p	0.048	1
rno-miR-215	0.1543	0.7335	rno-miR-1839-3p	-6.54E-01	1
rno-miR-3585-3p	-1.46E+00	0.7335	rno-miR-340-3p	0.2585	1
rno-miR-28-5p	-2.22E-01	0.7365	rno-miR-204-3p	Inf	1
rno-miR-21-3p	0.502	0.7365	rno-miR-450a-5p	-2.41E-01	1
rno-miR-100-5p	-4.47E-01	0.7365	rno-miR-126a-3p	-1.94E-02	1
rno-miR-20a-5p	0.3529	0.7478	rno-let-7b-5p	0.0288	1
rno-let-7f-5p	-3.75E-01	0.7478	rno-miR-130a-3p	0.0696	1
rno-miR-139-5p	0.4524	0.7491	rno-miR-664-2-5...	0.2505	1
rno-miR-181a-1-...	-5.11E-01	0.7491	rno-miR-122-5p	0.0998	1
rno-miR-872-3p	0.3315	0.755	rno-miR-140-3p	0.0174	1
rno-miR-191a-3p	-1.53E+00	0.755	rno-miR-30b-3p	0.2858	1
rno-miR-7a-5p	-9.22E-01	0.771	rno-miR-141-3p	-1.61E-01	1
rno-miR-10b-5p	-1.84E-01	0.771	rno-miR-342-5p	-Inf	1
rno-miR-674-5p	-3.04E+00	0.771	rno-miR-27b-5p	-1.19E-01	1

rno-miR-300-3p	0.4729	0.771	rno-miR-24-3p	-7.21E-02	1
rno-miR-124-3p	1.61	0.771	rno-miR-30c-5p	0.0412	1
rno-miR-350	0.2949	0.7719	rno-miR-30d-3p	-1.77E-01	1
rno-miR-101a-3p	0.0903	0.7719	rno-let-7d-3p	0.0413	1
rno-miR-378a-3p	0.333	0.7754	rno-miR-184	-Inf	1
rno-miR-6329	-9.49E-01	0.7819	rno-mir-425*	-2.01E-01	1
rno-miR-191a-5p	-2.14E-01	0.7828	rno-miR-15b-3p	0.0329	1
rno-let-7c-5p	0.2001	0.7828	rno-let-7b-3p	0.0821	1
rno-miR-146a-5p	0.3075	0.7828	rno-miR-96-5p	0.0279	1
rno-let-7e-3p	-9.28E-01	0.7828	rno-miR-874-3p	-Inf	1
rno-miR-341	0.5032	0.7828	rno-miR-188-5p	0.2322	1
rno-miR-24-1-5p	-2.58E+00	0.7828	rno-miR-186-5p	-1.21E-01	1
rno-miR-30a-3p	0.3053	0.7828	rno-miR-200b-3p	0.2165	1
rno-miR-25-5p	0.3744	0.7828	rno-miR-106b-3p	0.0443	1
rno-miR-30c-2-3...	0.3459	0.7828	rno-miR-128-1-5...	-Inf	1
rno-miR-27a-3p	-2.56E-01	0.7869	rno-miR-674-3p	-4.38E-02	1
rno-miR-141-5p	0.4316	0.7869	rno-miR-493-5p	Inf	1
rno-miR-540-3p	1.1	0.7869	rno-miR-652-5p	Inf	1
rno-miR-384-3p	-1.49E+00	0.7869	rno-let-7i-5p	-1.08E-01	1
rno-miR-322-5p	-3.73E-01	0.7869	rno-miR-23b-3p	0.0821	1
rno-mir-28*	-1.38E+00	0.7869	rno-miR-211-5p	-Inf	1
rno-miR-323-3p	0.6995	0.7869	rno-miR-3473	-9.13E-01	1
rno-miR-21*	-5.95E-01	0.7974	rno-miR-144-5p	-1.00E+00	1
rno-miR-223-3p	0.1874	0.7974	rno-miR-455-5p	-1.99E-01	1
rno-mir-21*	-5.95E-01	0.7974	rno-miR-200a-3p	0.0277	1
rno-miR-125b-2-...	-3.12E-01	0.7974	rno-miR-99a-3p	-6.29E-01	1
rno-miR-99a-5p	0.1955	0.7974	rno-miR-25-3p	-1.35E-02	1
rno-miR-582-5p	0.8088	0.8026	rno-miR-499-5p	0.5796	1
rno-miR-190a-5p	0.2552	0.8068	rno-miR-107-3p	0.1198	1
rno-miR-434-5p	0.6304	0.8068	rno-miR-17-1-3p	-3.16E-01	1
rno-miR-26a-5p	-3.21E-01	0.8068	rno-miR-374-3p	-1.42E-01	1
rno-miR-148b-3p	-1.88E-01	0.8068	rno-miR-144-3p	0.5315	1
rno-miR-301b-3p	0.7517	0.817	rno-miR-33-5p	-1.15E-02	1
rno-miR-26b-5p	-2.45E-01	0.8219	rno-miR-758-3p	Inf	1

rno-miR-200c-3p	0.3066	0.8328	rno-miR-127-3p	0.2209	1
rno-miR-93-5p	-2.19E-01	0.8404	rno-miR-193-3p	0.0573	1
rno-miR-340-5p	0.1755	0.8404	rno-miR-365-3p	-1.97E-01	1
rno-miR-338-3p	-3.51E-01	0.8404	rno-miR-376a-3p	Inf	1
rno-let-7e-5p	-3.01E-01	0.8404	rno-mir-455*	-Inf	1
rno-miR-652-3p	0.3143	0.8513	rno-miR-653-5p	-Inf	1
rno-miR-199a-3p	-5.52E-03	0.861	rno-let-7f-2-3p	-1.51E-01	1
rno-miR-9a-5p	0.1991	0.8644	rno-miR-148b-5p	-2.35E-01	1
rno-miR-147	0.475	0.8644	rno-miR-34c-5p	-2.54E-01	1
rno-miR-582-3p	0.4772	0.8683	rno-miR-93-3p	0.2916	1
rno-miR-130b-3p	0.5377	0.8712	rno-miR-151-3p	0.0061	1
rno-miR-328a-3p	0.2867	0.8712	rno-miR-33-3p	-1.60E-01	1
rno-miR-127-5p	1.47	0.8712	rno-miR-32-5p	-2.79E-01	1
rno-miR-190b-5p	0.3775	0.8857	rno-miR-29c-3p	-3.97E-02	1
rno-miR-216b-3p	Inf	0.8873	rno-miR-496-3p	Inf	1
rno-miR-129-5p	0.3019	0.9069	rno-miR-369-3p	-3.44E-01	1
rno-miR-92a-1-5...	-3.55E-01	0.9389	rno-miR-190a-3p	Inf	1
rno-miR-6324	-Inf	0.9495	rno-miR-146b-5p	0.0665	1
rno-miR-1843-5p	-4.17E-01	0.9495	rno-miR-183-5p	0.0556	1
rno-miR-18a-3p	-Inf	0.9495	rno-miR-511-3p	-5.61E-01	1
rno-miR-224-5p	-2.40E+00	0.9495	rno-miR-532-5p	-2.13E-01	1